Structural and Functional Analyses of Key

Mediators of Mammalian Immunity

Gareth Morrison

PhD Thesis

The University of Edinburgh

2009

Declaration

I, Gareth J Morrison, hereby certify that this thesis has been composed by myself, and it is a record of my work, and that it has not been accepted in partial or complete fulfilment of any other degree or professional qualification.

Acknowledgements

Firstly, I would like to express my gratitude to Dr Dominic Campopiano for allowing me the opportunity to carry out this PhD study in his laboratory. His enthusiastic approach to scientific research along with a plethora of research ideas provided the basis for a highly informative and enjoyable study. I would also like to thank Dr Perdita Barran not only for her intelligent scientific input but also her guidance and support during the difficult times.

At the MRC Human Genetics Unit, I would like to thank Dr Julia Dorin for the opportunity to carry out a large proportion of my research in her laboratory. I would like to thank every member of her research group – with special mention to Dr Karen Taylor, Fiona Kilanowski and Dr Uday Pathania for their constant help and expertise.

I would like to thank Dr David Clarke for his help with both mass spectrometry and general scientific input; Dr Lois Alexander and Dr Rosario Sanchez for their help with FACS; and Katherine Miles for her fearless extraction of human blood and expertise in monocyte culturing. I would also like to thank Dr Gerald Graham for allowing access to his laboratory and Clare McCulloch for her help in culturing L1.2 cells. I would also like to thank every member of Team Defensin for their intelligent scientific input and intense monthly meetings.

I would like to thank every member of Lab229 both past and present, foreign and domestic, both for their invaluable scientific input and for making work highly eventful everyday. Special mention has to be given to Dr Emily Seo, Scott Baxter and the enigmatic Thomas Vargues who without their help would have made this study much more difficult.

Most importantly, I would like to thank my mum and dad not only for their love and support throughout my studies but also for providing me with a roof over my head when needed; my sister Jane for providing me with my lovely niece, Eila, who has given so much joy in a difficult year; and finally to my girlfriend, Gillian, for her support and patience with this grumpy old man.

Abstract

Defensins are integral mediators of the immune system were they function at common sites of infection as direct killing agents and as chemical signals to amplify the cellular adaptive immune response. The dysregulation of defensin expression often manifests itself as chronic inflammatory diseases and in part results from increased infiltration of immune cells through specific peptide/GPCR interactions. Chemokine receptor 6 (CCR6), expressed on the outer surface of immature dendritic, memory T and B cells, is one such GPCR that various β-defensins can activate. However investigations into this interaction have been hampered by the difficulties in obtaining both β-defensins and CCR6 in the required quantities. In this study, optimization of both recombinant human β-defensins and human CCR6 purification has been performed in heterologous expression systems. Success in the production of human β-defensin 2 (HBD2) in milligram quantity subsequently allowed the functional importance of the HBD2 structural framework to be investigated.

Codon-optimized recombinant HBD2 was expressed in *E.coli* cells as an insoluble mutated ketosteroid isomerase (KSI) fusion protein. Efficient cyanogen bromide (CNBr) chemical cleavage released a soluble HBD2 peptide that upon RP-HPLC purification resulted in a highly pure reduced peptide. Oxidation using the redox partners cysteine/cystine resulted in a properly folded, functionally active HBD2 as assessed by both antimicrobial killing assay and chemotactic assay using CCR6 expressing human embryonic kidney (HEK) 293 cells. Subsequent purification of HBD1 and HBD2 single disulfide bond mutants revealed that this method could be used for the future production of other β-defensins.

Single disulfide mutant HBD2 peptides were analysed to investigate the effects that removing two disulfide bonds had on β-defensins functions. It was clearly shown that although still retaining antimicrobial activity in an *in vitro* assay the concentration of single disulfide mutants needed to kill an equivalent number of *E.coli* colonies was higher as

compared to wild-type HBD2. Comparison between the three individual mutants revealed little difference in their potency, although HBD2 with a disulfide bond between cysteines 2 and 4 did possess slightly increased activity. Unlike both HBD2 and N-terminally biotinylated HBD2, single disulfide mutants failed to chemoattract CCR6 expressing HEK293 cells. This indicates that all three structurally constraining disulfide bonds are necessary for full antimicrobial activity and chemotactic ability.

CCR6 was expressed in the HEK 293 cell line and expressed with an N-terminal FLAG tag and a C-terminal decahistidine tag. CCR6 expressed on the outer surface of these mammalian cells was solubilized in mild detergents, and its purification was optimized using various chromatographic techniques. The identity of purified CCR6 was subsequently confirmed by nanoelectrospray MS/MS analysis. Three separate peptide fragments were identified with identical sequences to the predicted fragments of an in-solution CNBr/trypsin digest. Sufficient quantity was purified to also analyze the receptors glycosylation state. A gel-shift western blot assay resulted in CCR6 being the third chemokine receptor in the family to be identified as N-glycosylated. N-terminal CCR6 truncation, resulting in removal of the first 27 amino acids (AA), was expressed in the same cell line. Although western blot analysis revealed transfection had been successful, surface expression of the mutated receptor could not be detected and as such the N-terminus has been implicated as necessary for cell surface trafficking.

Abbreviations

AA - Amino Acids

ACN - Acetonitrile

Ala - Alanine

AMPs - Antimicrobial peptides

AMV-RT - Avian Myeloblastosis Virus - Reverse transcriptase

ASL - Airway surface liquid

BNBD - Bovine neutrophil-derived β-defensin

bp - base pair

CCR6 - Chemokine receptor 6

CF - Cystic fibrosis

CFS - Carboxyfluorescein

CFU - Colony forming units

CHS - Cholesteryl hemisuccinate ester

CID - Collision-induced dissociation

CNBr - Cyanogen bromide

CNV - Copy number variations

COPD - Chronic obstructive pulmonary disease

CV - Column volume

Cys - Cysteine

Da - Daltons

DDM - n-dodecyl-β-maltoside

Defr1 - Defensin-related peptide 1

DEPC - Diethylpyrocarbonate

DMEM – Dulbecco's Modified Eagle Medium

DTT - Dithiothreitol

ECL - Extracellular loop

E.coli - Escherichia coli

EDTA - Ethylene diamine-tetraacetic acid

EGFR - Epithelial Growth Factor Receptor

EGTA – Ethylene glycol-tetraacetic acid

ELISA - Enzyme-linked Immunosorbent Assay

ESI - Electrospray ionization

FACS - Fluorescence-activated Cell Sorting

FCS - Fetal calf serum

FITC - Fluorescein isothiocyanate

FT-ICR - Fourier Transform Ion Cyclotron Resonance

GdnHCl - Guanidine hydrochloride

GPCR - G protein coupled receptor

HBD - Human β-defensin

HCT - High Capacity Trap

HEK - Human embryonic kidney

HEPES - N-(2-Hydroxyethyl)piperazine-N'-(2-ethanesulfonic acid)

HNP - Human neutrophil peptide

HRP - Horseradish peroxidase

ICL - Intracellular loop

iDC - immature dendritic cells

IGF-1 - Insulin-like growth factor 1

IL - Interleukin

IMAC - Immobilized metal affinity chromatography

IMDM - Iscove's Modified Dulbecco's Medium

IPTG - Isopropyl-1-thio-β-D-galactopyranoside

ISA - Isosensitest agar

ISB - Isosensitest broth

KSI - Ketosteroid isomerase

LB - Luria Bertani

LC-MS/MS - Liquid chromatography tandem mass spectrometry

LPS - Lipopolysaccharide

LTA - Lipoteichoic acid

mBD - Mouse β-defensin

Met - Methionine

MMP - Matrix metalloproteinase

NF - Nuclear factor

Ni^{2+}-NTA - Nickel-nitrilotriacetic acid

OVA - Ovalbumin

PAGE - Polyacrylamide gel electrophoresis

PAMPs - Pathogen-associated molecular patterns

PBS - Phosphate buffered saline

PGN - Peptidoglycan

PI3K - Phosphatidylinositol 3-kinase

PMA - Phorbol 12-myristate 13-acetate

PTH - Phenylthiohydantoin

PTMs - Post-translational modifications

RP-HPLC - Reverse Phase-High Pressure Liquid Chromatography

RTD - Rhesus Theta Defensin

RT-PCR - Reverse transcription Polymerase chain reaction

SDS - Sodium dodecylsulfate

SNP - Single nucleotide polymorphism

TAP - Tracheal antimicrobial peptide

TCEP - Tris carboxyethylphosphine

TFA - Trifluoroacetic acid

TGF-α - Transforming growth factor alpha

TLR - Toll-like receptor

TNF-α - Tumor necrosis factor alpha

Tris - Tris [hydroxymethyl] aminomethane

V - Volts

Vegf-A - Vascular endothelial growth factor-A

VREF - Vanomycin-resistant *Enterococcus faecium*

wt - Wild-type

Table of Contents

List of Figures

Chapter 3: Purification and Biochemical Analysis of Human Chemokine

Receptor 6

List of Tables

Chapter 1

Introduction

1.1 - Antimicrobial Peptides in Innate and Adaptive Immunity

Multicellular organisms are constantly bombarded by thousands of potentially pathogenic microorganisms, with intestinal epithelium alone exposed to more than 400 bacterial species and 10^{14} microbial cells [1]. Their survival depends initially on the physical barrier provided by skin keratinocytes and epithelial cells lining the exposed tissues such as intestines, lungs and urinary tract. The breach of this barrier initiates the beginning of the innate immune response, which in higher vertebrates can then interact with elements of the adaptive immune system if needed. Efficient detection of microbial invasion is via evolutionary-conserved pathogen-associated molecular patterns (PAMPs) [2]. These PAMPs are often major components of the bacterial outer membrane, such as lipopolysaccharide (LPS), or the bacterial cell wall such as peptidoglycan (PGN) or lipoteichoic acid (LTA) [3]. However these are not restricted to extracellular components, with both viral double-stranded RNA and CG dinucleotide DNA sequences being shown to act as PAMPs [4]. Binding of PAMPs to cell surface receptors, such as the Toll-like receptor family, initiates an inflammatory response consisting, in part, of increased synthesis and secretion of soluble antimicrobial peptides (AMPs) [5].

AMPs are found in a multitude of multicellular organisms ranging from bacteria to plants and from invertebrates to vertebrates. AMPs can be roughly grouped into four structural categories: (i) β-sheet structures stabilised by multiple disulfide bonds; (ii) linear α-helical peptides without disulfide bonds; (iii) extended peptides with an unusually high proportion of one or two amino acids; (iv) loop structures constrained with a single disulfide bond (Table 1.1) [6]. AMPs can be synthesized via both ribosomal and nonribosomal mechanisms, with the latter restricted to certain bacteria and fungi [7]. Gene-encoded, ribosomally-synthesized polypeptides typically consist of less than 100 AA which, when folded, form an amphipathic structure (distinct hydrophobic and cationic patches on the surface), and yield an overall charge of +2 - +11. This amphipathic structure has been shown to be extremely

important in their ability to perform as antimicrobial agents. Over 1000 AMPs have been identified to date and various databases have been established to categorize them (http://www.bbcm.units.it/~tossi/pag1.htm; http://aps.unmc.edu/AP/main.php) [8-10].
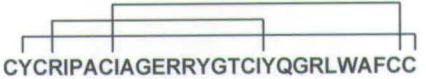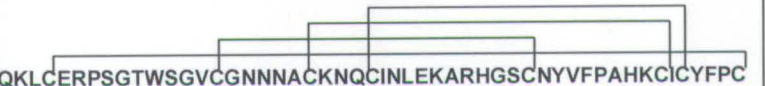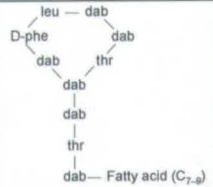
Family	Name	Secondary Structure	Primary structure	3D STRUCTURE
Human Cathelicidin	LL-37	α-helical	LLGDFFRKSKEKIGKEFKRIVQRIKDFLRNLVPRTES	
Bovine Cathelicidin	Indolicidin	Extended Structure -with major one type of AA.	ILPWKWPWWPWRR	
Human Defensin	HNP-3	β-sheet Multiple disulfide bonds	CYCRIPACIAGERRYGTCIYQGRLWAFCC	
Plant Defensin	Rs-AFP1	β-sheet Multiple disulfide bonds	QKLCERPSGTWSGVCGNNNACKNQCINLEKARHGSCNYVFPAHKCICYFPC	
Insect Thanatin	Thanatin	Loop Structures Single disulfide bonds	GSKKPVPIIYCNRRTGKCQRM	
Non-ribosomal	Polymyxin B	Cyclic	Cyclized isooctanyl BTBB(BF^{d}LBBT)	leu — dab / D-phe — dab / dab — thr / dab / dab / thr / dab— Fatty acid (C$_{7-9}$)

Table 1.1. Family Characterizatio n and Structure of Antimicrobial Peptides. Structures were downloaded from protein data bank; PBD accession numbers: LL-37:2K60, Indolicidin:1G89, HNP-3:1DFN, Rs-AFP1:1AYJ, Thanatin:8TFV. Disulfide bonds are indicated with connecting lines. Superscript ^{d} indicates a D-amino acid and dab represents 1-diamino-butyrate.

1.2 - Defensins

1.2.1 – Classification

A family of AMPs termed defensins have been identified in plants, invertebrates, birds and mammals and represent the only family of AMP conserved in all of these multicellular organisms [11-13]. A database dedicated to only defensins has been established to compile all the available defensin knowledge (http://defensins.bii.a-star.edu.sg/) [14]. Mammalian defensins constitute a major component of the antimicrobial armoury of granulocytic leukocytes, macrophages and epithelial tissues however further roles for defensins in the immune response are constantly being identified leading to them being renamed 'Host Defense Peptides' or 'Alarmins' in recent reviews [15, 16]. Despite low sequence homology, most mature mammalian defensin peptides share certain common properties. They are cationic, invariably arginine-rich, nonglycosylated peptides with a molecular mass of 3-5 kDa. However, more recently discovered defensins can be considerable larger in molecular mass with an extended C-terminus [17]. They contain six family conserved cysteines that form three intramolecular disulfide bonds and stabilise a triple-stranded antiparallel β-sheet. The distribution of cysteines, connectivity of disulfide bonds and overall molecular structure, allow defensins to be divided into three subfamilies: α-defensins, β-defensins, and θ-defensins (Figure 1.1).

α-Defensin

Cys1-Cys6

$$X_{(1\text{-}2)}C^1XC^2RX_{(2\text{-}3)}C^3XXXEXXXC^4XXXGXXXXXC^5C^6X_{(1\text{-}4)}$$

Cys2-Cys4   Cys3-Cys5

β-Defensin

Cys1-Cys5

$$X_{(2\text{-}10)}C^1X_{(5\text{-}6)}G/AXC^2X_{(3\text{-}4)}C^3X_{(9\text{-}13)}C^4X_{(4\text{-}7)}C^5C^6X_{(n)}$$

Cys2-Cys4   Cys3-Cys6
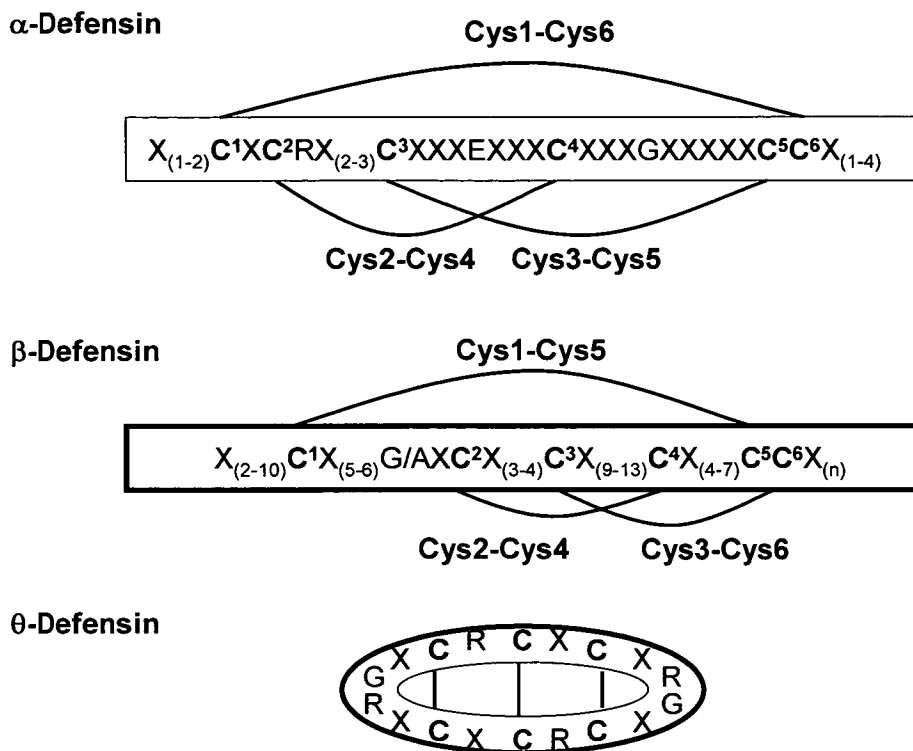
θ-Defensin

Figure 1.1. Differences in the Distribution of Cysteines and Connectivity of Disulfide Bonds between Defensin Families. X represents any amino acid except proline.

1.2.2 - α-Defensins

The first realization that granulocytes from polymorphonuclear leukocytes contained antimicrobial cationic peptides came in 1966 when Zeya and Spitznagel acid extracted a group of arginine and cysteine rich peptides that contained lysozyme-independent antimicrobial activity [18]. Surprisingly it wasn't until improvements in technical equipment in the mid 1980's that allowed subsequent characterisation of individual components responsible for this activity. Six individual rabbit antimicrobial peptides rich in cysteines and arginines were purified from peritoneal granulocytes and shown to be antimicrobial [19, 20]. Within a year three peptides, with homology to the previously isolated peptides from rabbit granulocytes, were purified and sequenced from the azurophil granules of normal human neutrophils [21, 22]. Based on their "oxygen-independent" antimicrobial activity and mobility they were named human neutrophil peptides 1-3 (HNP 1-3) and, for the first time in

the literature, referred to as "defensins" [21]. These three defensins have identical sequences except for the N-terminal amino acid (AA), which in HNP-2 is absent and HNP-3 is an aspartic acid compared to alanine in HNP-1. A fourth member of the human neutrophil peptide family called HNP-4 was isolated later and characterised [23]. Although more hydrophobic and having lower sequence homology as compared to the previously identified α-defensins, it still retained the "classical" cysteine motif and was highly cationic. It was found that HNP 1-3 constitute between 30-50% of the protein content in human azurophil granules and together with HNP-4 reach a concentration of >10 mg/ml [24].

The first human defensins shown to be expressed in cells other than neutrophils were HD-5 and HD-6 in Paneth cells [25, 26]. Conservation of the sequence encoding the 5' signal sequence of all α-defensins allowed the design of oligonucleotide probes to hybridize to these two novel defensin genes. Paneth cells, a specialised epithelial cell, are located at the base of crypts of Lieberkuhn throughout the small intestine and colon. They are granule-containing secretory cells that upon stimulation release various molecules involved in our defence system e.g. lysozyme, defensins and secretory phospholipase [27]. Using both ileal neobladder tissue and urine, mature HD-5 and HD-6 were later isolated and their sequences verified [28].

α-defensins contain between 29-35 AA and the six cysteines are disulfide-linked between residues Cys1-Cys6, Cys2-Cys4 and Cys3-Cys5. The genes encoding α-defensins are clustered on chromosome 8p23, except for HNP-2 which is thought to be a proteolytic product of HNP-1 or -3 rather than a separate gene-encoded peptide [29]. The myeloid α-defensin genes (three exons) are synthesised as 90-100 AA pre-pro-peptides. They contain ~20 AA signal sequence which is proteolytically cleaved to leave a 75-residue pro-defensin. A further pre-aspartate proteolytic cleavage results in an intermediate 56-residue antimicrobial inactive pro-defensin before the active mature 29 or 30 AA peptide is stored in the azurophil granules (Figure 1.2) [30]. The inactive pro-peptide is thought to be a

consequence of the anionic nature of the propiece which acts as a charge balance to the cationic mature peptide. Although it is now known that the posttranslational processing of myeloid defensins occurs, the identity of the enzymes responsible for the proteolytic cleavage to generate the mature peptides are still not known.

More success has been achieved in deciphering the enzymes involved in enteric defensin processing. Studies using the murine Paneth cell α-defensins (Cryptdins) showed that recombinant matrix metalloproteinase matrilysin (MMP7), which co-localizes with the cryptidins in Paneth cells, converts cryptdin into its mature form primed for secretion into the crypt lumen [31]. This finding was subsequently enforced in the same study when mice with a homozygous disruption of the matrilysin gene prevented cleavage of the propeptide and resulted in decreased antimicrobial activity [31]. Similar to the human myeloid defensins, HD-5 and -6 genes (two exons) are transcribed and translated as prepropeptides. Isolation of HD-5 from ileal neobladder tissue and in secreted urine revealed multiple N-terminally processed peptides, indicating that HD-5 is stored in its proform and subsequently posttranslationally processed upon degranulation [28]. The major identified forms had putative cleavage sites for trypsin and were hypothesized to be responsible for the processing. Further evidence for a role of trypsin in the maturation process came when *in vitro* studies showed partially purified trypsin from ileal tissue cleaved proHD-5 into the mature luminal form [32]. In the same study both α1-antitrypsin inhibitor and two isoforms of trypsin (meso and anionic) were found co-localized with HD-5 in secretory granules and therefore thought to regulate the process (Figure 1.2) [32].

```
                    1        Signal                              Propeptide                                                          Mature                        103
PreproHNP1 (1)  MRTLAILAAILLVALQAQAEPLQARADEVAAAPEQIAADIP------EVVVSLAWDESLAPKHPGSRKNMACYCRIPACIAGERRYGTCIYQGRLWAFCC----
                                                       ↑
     HNP2 (1)  ----------------------------------------------------------------------------------CYCRIPACIAGERRYGTCIYQGRLWAFCC----
                                                                                                                    ↑
PreproHNP3 (1)  MRTLAILAAILLVALQAQAEPLQARADEVAAAPEQIAADIP------EVVVSLAWDESLAPKHPGSRKNMDCYCRIPACIAGERRYGTCIYQGRLWAFCC----
                                                         ↑
PreproHNP4 (1)  MRIIALLAAILLVALQVRAGPLQARGDEAPGQEQRGPEDQD-------ISISFAWDKSSALQVSGSTRGMVCSCRLVFCRRTELRVGNCLIGGVSFTYCCTRV-
PreproHD-5 (1)  MRTIAILAAILLVALQAQAESLQERADEATTQKQSGEDNQD-------LAISFAGNGLSALRTSGSQARATCYCRTGRCATRESLSGVCEISGRLYRLCCR---
                                     ↑       ↑                               ↑
PreproHD-6 (1)  MRTLTILTAVLLVALQAKAEPLQAEDDPLQAKAYEADAQEQRGANDQDFAVSFAEDASSSLRALGSTRAFTCHCRR-SCYSTEYSYGTCTVMGINHRFCCL---
Cryptdin-1 (1)  MKKLVLLFALVLLGFQVQADPIQNTDEETKTEEQPGEEDQA-------VSVSFGDPEGTSLQEE-SLRDLVCYCRSRGCKGRERMNGTCRKGHLLYTLCCR---
```

Figure 1.2. Sequence Alignment Showing Cleavage Sites of Full-length Prepro α-Defensins. Cleavage sites are identified by a change in colour and arrows indicates the positions of intermediate cleavage sites. Conserved residues in the mature peptide are indicated in green.

1.2.3 - β-Defensins

The first realisation that other defensin families existed came in 1991 when extracts of bovine tracheal mucosa contained a 38 AA peptide with potent antimicrobial activity; hence being named tracheal antimicrobial peptide (TAP) [33]. However, it was not until 1993 that the term β-defensin was suggested when thirteen structurally similar peptides isolated from bovine blood neutrophils (BNBD) shared a consensus sequence with TAP [34]. Using the most abundant BNBD-12, Edman degradation analysis revealed the spacing and topology of their cysteine residues differed from previously analysed defensins [35]. These new defensins displayed a novel disulfide connectivity Cys1-Cys5, Cys2-Cys4, and Cys3-Cys6 and were called β-defensins with the original defensins now called α-defensins.

The first human β-defensin (HBD1) was purified from the human blood filtrate of renal disease patients [36]. This isolated, mature 36 AA peptide was named due to its homology to the previously identified TAP. Analysis of large volumes of urine found various HBD1 isoforms ranging in length from 36-47 AA [37]. In the same study multiple forms of HBD1 were also identified in kidney tissue, blood filtrate, vaginal and lavage fluid. The 47 AA isoform is suspected to be the pro-defensin with proteolytic N-terminal processing responsible for resultant variations in the mature peptides (which was also identified in HD-5). The second and third human β-defensins were first purified from patients suffering with psoriasis. Since psoriasis is a chronic inflammatory disease, psoriatic scales have been used as a rich source of various antimicrobial peptides including Psoriasin, LL-37 and Elafin [38]. Harder and Schroder have cleverly applied the antimicrobial activity of the β-defensins to produce an array of bacterial affinity columns which they used to isolate HBD2 and HBD3. Using an *E. coli* affinity column, a 41 AA antimicrobial peptide was recovered from psoriatic scales and termed HBD2 [39]. Unfortunately no experimental details of this purification procedure accompanied the publication. Later this same 41 AA peptide was isolated from immortalized lung epithelial cell supernatant using a *P.*

aeruginosa affinity column indicating, like other β-defensins, HBD2 is epithelia stored before being secreted [40]. Using Gram-positive *S. aureus* as the affinity "bait" a 45 AA antimicrobial peptide, termed HBD3, was purified from both psoriatic scales and human skin-derived stratum corneum [41]. Almost simultaneously HBD3 was also discovered using a BLASTp search based on the six cysteine β-defensin motif, a strategy also used to identify HBD4 [42, 43]. This was the beginning of a change in novel defensin identification with new bioinformatics methods being used to explore the recently published human and mouse genomes. Recently, a computational strategy utilizing both BLAST and HMMER programs identified five β-defensin clusters in total identifying 28 putative human β-defensin genes (Figure 1.3) [17]. Since this discovery various studies identifying transcripts for these genes have been successful, including the defensin genes on chromosome 20p13 (DEFB125-129) and 20q11.1 (DEFB118-23) [44, 45]. However, apart from HBD4, which was identified in the epithelial lining fluid of patients with chronic lower respiratory tract infection, and DEFB118, which was extracted from human sperm, no other newly-identified defensin peptides have been detected [46, 47].

```
                 1                                                                  100
HBD1    (1) ----------------DHYNCVS--SGGQCLYSACPIFTKIQ----GTCY-RGKAKCCK----------------------------
HBD2    (1) -------------GIGDPVTCLK--SGAICHPVFCPRRYKQI----GTCG-LPGTKCCKKP--------------------------
HBD3    (1) ----------GIINTLQKYYCRV--RGGRCAVLSCLPKEEQI----GKCS-TRGRKCCRRKK-------------------------
HBD4    (1) -------------EFELDRICG--YGTARCRK-KCRSQEYRI----GRC-PNTYACCLRKWD-ESLLNRTKP----------------
HBD5    (1) ---GLDFSQPFPSGEFAVCESCK--LGRGKCRK-ECLENEKPD----GNC-RLNFLCCRQRI-------------------------
HBD6    (1) ----------------FFDEKCNK--LKGTCKN-NCGKNEELI----ALC-QKSLKCCRTIQPCGSIID------------------
HBD7    (1) --------------AIHRALISKRMEGHCEA-ECLTFEVKI----GGCRAELAPFCCKNRKKH------------------------
HBD8    (1) ----------------KFKEICE--RPNGSCRD-FCLETEIHV----GRC-LNSQPCCLPLGHQPRIESTTPKKD-------------
HBD9    (1) -------------------GHCLN--LFGVCRTDVCNIVEDQI----GAC-RRRMKCCRAWWILMPIPTPLIMSDYQEPLKPNLK----
HBD11   (1) ------------------RECRI--GNGQCKN-QCHENEIRI----AYCI-RPGTHCCLQQ-------------------------
HBD12   (1) TEKISTARSEGHHITFSRWKSCTA--IGGRCKN-QCDDSEFRI----SYCA-RPTTHCCVTECDPTDPNNWIPKDSVGTQEWYPKDSRH-
HBD14   (1) --------------TLVNADRCT--KRYGRCKR-DCLESEKQI----DICS-LPRKICCTEKLYEEDDMF------------------
HBD18   (1) ---------------YSGEKKCWN--RSGHCRK-QCKDGEAVK----DTC-KNLRACCIPSNEDHRRVPATSPTPLSDSTPGIIDDILTVRFTTDYFEV
HBD19   (1) --------------KRHILRCMG--NSGICRA-SCKKNEQPY----LYC-RNCQSCCLQSYMRISISGKEENTDWSYEKQWPRLP----
HBD20   (1) -----------------VECWM---DGHCRL-LCKDGEDSI----IRC-RNRKRCCVPSRYLTIQPVTIHGILGWTTPQMSTTAPKMKTNITNR---
HBD21   (1) -----------------VMKCWG--KSGRCRT-TCKESEVYY----ILC-KTEAKCCVDPKYVPVKP---------------------
HBD23   (1) -----------------GTQRCWN--LYGKCRY-RCSKKERVY----VYC-INNKMCCVKPKYQPKERWWPF-----------------
HBD25   (1) ---------------SFEPQKCWK-NNVGHCRR-RCLDTERYI----LLC-RNKLSCCISIISHEYTRRPAFPVIHLEDITLDYSDVDSFTGSPVSMLN
HBD26   (1) ---------------NWYVKKCLN--DVGICKK-KCKPEEMHVKNGWAMC-GKQRDCCVPADRRANYPVFCVQTKTTRISTVTATTATTTLMMTTASMS
HBD27   (1) --------------EQLKKCWNNYVQGHCRK-ICRVNEVPE----ALC-ENGRYCCLNIKELEACKKITKPPRPKPATLALTLQDYVTIIENFPSLK
HBD28   (1) ---------------LKKCFN--KVTGYCRK-KCKVGERYE----IGC-LSGKLCCANDEEEKKHVSFKKPHQHSGEKLSVLQDYIILPTITIFTV-
HBD29   (1) --------------EFIGLRRCLM--GLGRCRD-HCNVDEKEI----QKC--KMKKCCVGPKVVKLIKNYLQYGTPNVLNEDVQEMLKPAKNSSAVIQR
HBD31   (1) ---------------FISNDECPS--EYYHCRL-KCNADEHAI----RYC--ADFSICCKLKIIEIDGQKKW----------------------
```

```
                 101                                                                        188  Charge
HBD1   (37)  ------------------------------------------------------------------------------      +4
HBD2   (42)  ------------------------------------------------------------------------------      +6
HBD3   (46)  ------------------------------------------------------------------------------      +11
HBD4   (51)  ------------------------------------------------------------------------------      +6
HBD5   (52)  ------------------------------------------------------------------------------      +2
HBD6   (46)  ------------------------------------------------------------------------------      +3
HBD7   (45)  ------------------------------------------------------------------------------      +4
HBD8   (52)  ------------------------------------------------------------------------------      +1
HBD9   (60)  ------------------------------------------------------------------------------      +3
HBD11  (36)  ------------------------------------------------------------------------------      +2
HBD12  (82)  ------------------------------------------------------------------------------      0
HBD14  (49)  ------------------------------------------------------------------------------      0
HBD18  (77)  SSKKDMVEESEAGRGTETSLPNVHHSS---------------------------------------------------      -1
HBD19  (64)  ------------------------------------------------------------------------------      +6
HBD20  (69)  ------------------------------------------------------------------------------      +6
HBD21  (43)  ------------------------------------------------------------------------------      +5
HBD23  (48)  ------------------------------------------------------------------------------      +10
HBD25  (78)  DLITFDTTKFGETMTPETNTPETTMPPSEATTPETTMPPSETATSETMPPPSQTALTHN-------------------      -7
HBD26  (81)  SMAPTPVSPTG------------------------------------------------------------------      +8
HBD27  (78)  TQST-------------------------------------------------------------------------      +5
HBD28  (74)  ------------------------------------------------------------------------------      +6
HBD29  (77)  KHILSVLPQIKSTSFFANTNFVIIPNATPMNSATISTMTPGQITYTATSTKSNTKESRDSATASPPPAPPPPNILPTPSLELEEAEEQ  +5
HBD31  (49)  ------------------------------------------------------------------------------      -1
```

Figure 1.3. Sequence Alignment Showing Conserved Residues and Charge of the β-Defensin Family. Sequences were aligned using AlignX before manual alignment of conserved cysteines was performed. Conserved cysteines are in red. Conserved glycines are in green. Charge is theoretical value at pH7.0. β-defensin peptide has been identified in defensins coloured blue.

β-defensins have been shown to be slightly larger than α-defensins, containing between 36 to 155 AA and a consensus sequence: $x_{2-10}Cx_{5-6}(G/A)xCx_{3-4}Cx_{3-4}Cx_{9-13}Cx_{4-7}CCx_n$ [48, 49]. With the exception of DEFB105, all β-defensin genes are composed of two exons and one intron. β-defensins genes encode a substantially smaller anionic pro-peptide compared with α-defensins which can either be cleaved once or multiple times to release the mature peptide (Figure 1.4). Enzymes responsible for these cleavages are currently unknown.
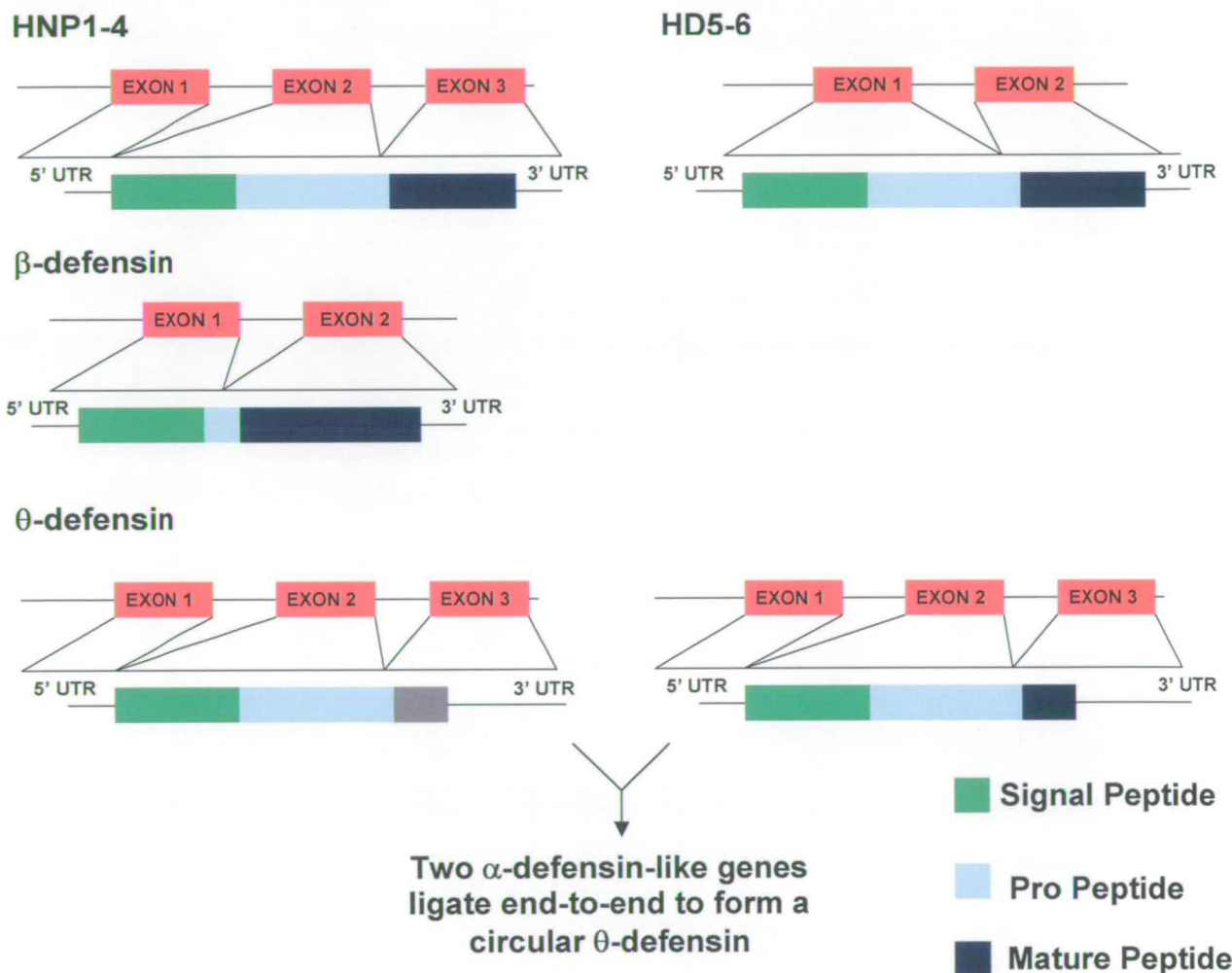
Figure 1.4. Differences in Gene Structure between Members of the Defensin Family. Signal peptide in green, pro peptide in pale blue and mature peptide in dark blue.

1.2.4 - θ-Defensins

The third family of defensins to be discovered were θ-defensins, first isolated from the leukocytes of rhesus macaque monkeys and termed Rhesus Theta Defensin 1 (RTD-1) [50]. RTD-1 is encoded by two different genes with high similarity to a α-defensin gene apart from a premature stop codon shortly after the third cysteine of the mature peptide. Both genes encode a 12 AA peptide, that upon cleavage of the first three N-terminal AA are ligated together to form a heterodimeric, 18 AA, cyclic peptide (Figure 1.4). This defensin is the first cyclic peptide discovered in vertebrates and like all mammalian defensins is stabilized by three intramolecular disulfide bonds. The ability of each gene product to form homodimeric cyclic peptides was later confirmed when RTD-2 and -3 were isolated first from the bone marrow and then the leukocytes of rhesus monkeys [50, 51].

The existence of θ-defensins in modern human leukocytes is unlikely despite the expression of human θ-defensin (DEFT) genes that are very similar to genes encoding RTDs. Identification of six human DEFT genes each with a premature stop codon at position 17 in the signal peptide identifies these genes as pseudogenes [52]. Despite the lack of human θ-defensin production, it has been shown recently that human promyelocytic cells still retain the ability to perform the novel post-translational ligation. Cotransfection of promyelocytic HL60 cells with constructs encoding both full length DEFT1 and DEFT1 (R70K), with the stop codon replaced with glutamine, resulted in the isolation of the 18 AA heterodimer [53]. In the same study addition of aminoglycosides to cervicovaginal tissue allowed Retrocyclin 1 to be identified indicating the suppression of stop codon termination in the signal peptide and allowing θ-defensins to perform their immune roles in these cells [53].

1.2.5 - Gene Regulation and Tissue Expression of β-Defensins

Although there are currently 32 putative β-defensins identified in the human genome, only four of these have been characterised in detail using structural and functional methods (HBD1-4). HBD1 mRNA is most abundant in the kidney and pancreas also being constitutively expressed in a plethora of epithelia cells including skin, intestinal, respiratory tracts and urogenital tissues [36, 37, 54]. However this "housekeeping" defensin has also been shown to be up-regulated upon epithelial stimulation with mononuclear blood leukocyte stimulated supernatants and cell wall components of *Mycobacterium tuberculosis* [55, 56]. Although the individual components responsible were not identified, in the latter case the transcription factor NF-IL6 was shown to be important.

In contrast to the predominant constitutive expression of HBD1, expression of the other defensins, HBD2-4 is tightly regulated and they are only highly expressed upon bacterial challenge or via a cytokine inflammatory response. This was unsurprising since both HBD2 and 3 were originally isolated from psoriatic (inflamed) scales and the identification of multiple transcription factor binding sites in the promoter region of HBD2 including nuclear factor (NF)-κB, AP-1, AP-2 and NF-IL6 [40]. Although HBD2 has a low basal expression in lung and trachea tissues, stimulation with proinflammatory cytokines including Interleukin-1α (IL-1α), IL-1β, IL-17 and Tumor Necrosis Factor-α (TNF-α) identified or upregulated HBD2 expression in epithelia cells of skin, respiratory and gastrointestinal tract origin [40, 57-59]. Gram-negative and Gram-positive bacteria challenges can also upregulate HBD2 expression through PAMPs such as LPS, LTA and PGN. These interact with specific Toll-like receptors (TLRs) to initiate signal transduction pathways culminating in transactivation of NF-κB and/or AP1 transcription factors [4]. Mutation, truncation or inhibitors of the two proximal NF-κB and AP1 binding sites in the HBD2 gene leads to reduced or loss of HBD2 expression identifying their role in regulating HBD2 expression [60, 61].

HBD3 has a low basal expression in both epithelial and non-epithelial cells and like HBD2, its expression can be up-regulated upon proinflammatory cytokine stimulation or bacterial challenge [41, 42]. However HBD3 expression can also be regulated via a different mechanism from HBD2. HBD3 is induced by Transforming Growth Factor alpha (TGF-α) and Insulin-like Growth Factor 1 via transactivation of Epithelial Growth Factor Receptor (EGFR) in a metalloprotease-directed process [56]. HBD4 is unique in only having a few sites of expression being highly expressed only in the testis and epididymis [43]. However, HBD4 expression in the lungs can be up regulated by phorbol 12-myristate 13-acetate, LPS and bacterial challenge [43]. Like HBD4, all the novel putative β-defensin genes are expressed predominantly in the testis and/or epididymis where DEFB118-123 expression is down-regulated after androgen removal [45].

1.2.6 - Role of β-Defensins in Innate and Adaptive Immunity

1.2.6.1 - Antimicrobial Activity

The β-defensin family of cationic peptides have potent broad-spectrum antimicrobial activity *in vitro*, with each defensin having differential activity against certain bacterial strains. Both HBD1 and HBD2 have salt-sensitive antimicrobial activities against a plethora of Gram-negative bacteria, fungi and some enveloped viruses [58, 62, 63]. These peptides have potent antimicrobial activity against only a limited number of Gram-positive bacteria but are only bacteriostatic against *Staphylococcus aureus*, a major cause of infections in atopic dermatitis [58]. However, HBD3 has potent salt-insensitive antimicrobial activity against various microbes, including the previous β-defensin resistant Gram-positive bacteria *S. aureus* and vanomycin-resistant *Enterococcus faecium* [41]. A limited number of the newly identified β-defensins have been functionally characterized and their antimicrobial activity determined. Of these, HBD4, HBD18 and HBD28 have all been shown to have at

least potent antimicrobial activity against *E. coli*, with only HBD27 failing to possess this activity [43, 64, 65].

Despite the increasing number of antimicrobial killing targets it was necessary to show defensins could kill *in vivo* under physiological conditions. α-defensins were first shown to have important antimicrobial activity *in vivo* when mice deficient in their processing enzyme matrilysin and therefore lacking mature cryptidins showed greater sensitivity to *S. typhimurium* and enhanced number of bacteria colonizing their small intestines compared to wild-type mice [31]. Further studies showing HD-5 had a protective effect on transgenic mice after *S. typhimurium* challenge compared to wild-type again highlighted defensins in vivo activity [66]. β-defensin killing *in vivo* was subsequently shown when *E. coli* injected into a HBD2 transfected tumour in immunodeficient mice resulted in less viable colonies upon harvesting [67]. This was an important finding as the HBD2 salt-sensitivity posed the question of whether HBD2 could kill under physiological conditions.

Despite the potent antimicrobial activity of defensins the mechanism of action of defensin killing is still speculative. Using negatively-charged artificial membranes, defensins were shown to associate to bacteria membranes primarily via electrostatic interactions [68]. However, although members of both α- and β-defensin families have been shown to perforate *E. coli* and *S. aureus* membranes the exact mechanism of membrane disruption is still the focus of much debate [69, 70]. One mechanism is the pore/channel hypothesis where the peptides self-associate in the outer and/or inner membrane(s) to form an ion-permeable hole [71]. A second mechanism is the 'carpet-like' model, which is a non-specific mechanism where high concentrations of defensins bind to the membrane and cause changes in membrane fluidity and polarisation [72]. Both mechanisms cause membrane disruption and leakage of intracellular components. Evidence suggests however that membrane permeabilization is just the first step of a cascade of events that lead to bacteria killing.

17

Following permeabilization defensins have been shown to inhibit DNA, RNA and protein synthesis as well as cell wall biosynthesis [69, 73].

1.2.6.2 - Chemotactic Activity

The focus on the functional role of defensins in immunity soon switched to adaptive immunity upon the seminal finding that an α-defensin rich extract from human neutrophils was able to chemoattract monocytes (Figure 1.5) [74]. Since this original discovery both α- and β-defensin have been shown to chemoattract a host of cell types at nanomolar concentrations. As well as monocytes, α-defensins migrate naïve T cells, macrophage and immature dendritic cells (iDC) but not memory T cells, mature dendritic cells or neutrophils [75, 76]. The first evidence that chemotaxis was mediated by a G protein coupled receptor (GPCR) came when HBD2 and, to a lesser extent, HBD1 were shown to chemoattract iDC and memory T cells. The chemokine receptor 6 (CCR6), expressed on the outer surface of iDC, was transfected into HEK293 cells and shown to migrate towards β-defensins in a concentration dependent way [77]. In combination with anti-CCR6 antibodies and pertussis toxin blocking iDC chemotaxis, CCR6 was identified as the chemokine receptor that β-defensins signal through [77]. Since this finding β-defensins have also been shown to possess CCR6-independent chemotactic activity. HBD-3 and -4 have been shown to chemoattract non-CCR6 expressing monocytes whereas HBD2-4 have been shown to chemoattract both rat and human mast cells that neither CCL20 (also known as MIP-3α, the natural chemokine for CCR6) nor HBD1 could block [43, 78-80]. In the latter cell type, α- and β-defensins have been shown to promote degranulation and therefore histamine and prostaglandin D_2 release, leading *in vivo* to increased vascular permeability in skin [79, 81]. Interestingly, β-defensin induced mast cell activation and chemotaxis were both mediated through a G protein-phospholipase C-dependent pathway [79, 80]. These salt-insensitive *in*

vitro chemotactic activities were thought to represent recruitment of circulating leukocytes and lymphocytes to sites of infections and this hypothesis was subsequently proven *in vivo* when subcutaneous injections of HNP1 and 2 in BALB/c mice resulted in the recruitment of T lymphocytes to the site of injection [82].

More recent work has shown that the chemotactic properties of defensins are not restricted to cells implicated directly in the immune response. Defensins have been shown to have a role in promoting wound repair through direct recruitment of human endothelial cells and epidermal keratinocytes. HBD2 was capable of reducing wound closure time through the promotion of endothelial recruitment, proliferation and capillary tube formation [83]. All three are essential for the formation of new blood vessels (angiogenesis) and hence wound repair. Defensins HBD2-4 were also shown to induce migration and proliferation of human keratinocytes leading to a decrease in wound closure time [84]. Moreover, inhibition of the β-defensin-induced phosphorylation of the signalling components EGFR, STAT-1 and STAT-3 resulted in suppression of wound closure highlighting their importance [84]. However the exact mechanism for cell migration is not well understood as CCR6 expression was either not identified or not tested on these cell types. Therefore this migrational effect could be through an alternative receptor like that found in mast cell- or monocyte-induced migration, or could be indirect effects were the β-defensins stimulate the release of other chemokines.
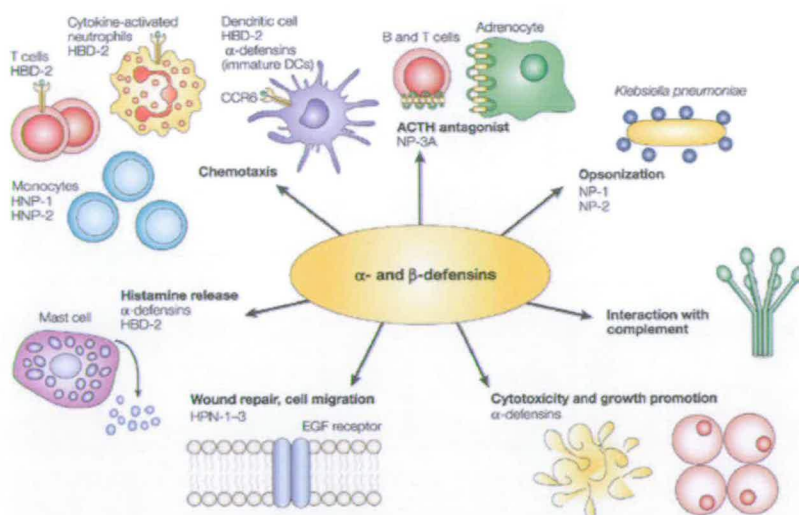
Figure 1.5. α- and β-Defensins Multiple Functional Roles [85].

1.2.6.3 - Defensin Induced Maturation of iDendritic Cells leading to *in vivo* Immunoenhancing Activity

Mouse BD2 (mBD2), but not mBD3, was shown to induce the maturation of murine iDC leading to a type 1 polarized adaptive immune response [86]. However this maturation process was negated when iDCs were isolated from TLR4 -/- mice which suggested that TLR4-dependent signalling as being responsible for this maturation [86]. Although CCR6 is not responsible for iDC maturation, it is responsible for the enhancement of the *in vivo* antigen (Ag) specific and antitumor activity. Fusion of both mBD2 and mBD3 to non-immunogenic tumor Ag rendered this species immunogenic via antigen presenting cell uptake and induced production of Ag specific antibodies [87]. The inability of non chemotactic promBD2 and mutated CCL20 to enhance the adaptive immune response implicates CCR6 signalling in this role. Despite the mBD3 fusion producing a greater humoral immune response, only mBD2 fusions were able to remove established tumors from infected mice showing that the enhanced antitumor activity is due not only to humoral immunity but also Ag specific cellular immunity [87]. This cellular activity was identified later when mBD2 was fused to the generic nonimmunogenic embryonic Ag, immature

laminin receptor, rendering it immunogenic and producing a T cell response [88]. Splenocytes from immunized mice were able to specifically lyse tumours expressing this epitope however upon CD8^{+} effecter cell depletion their tumour protective activity was lost [88]. Therefore the cellular response was determined to be tumor specific CD8^{+} T lymphocytes.

Both human α- and β-defensins have also been shown to have immune enhancing ("adjuvant") capabilities through simultaneous intranasal administration of ovalbumin (OVA) together with various defensins. Compared with OVA alone, HNP coadministration lead to increased OVA humoral response consisting of increased OVA specific IgG antibodies and cellular response from OVA specific CD4^{+} T cells leading to increased production of IFN-γ, IL-5,-6 and -10 [89]. HBD-1 and -2 were also able to increase OVA-specific IgG antibodies however there were significant differences in their cytokine production indicating differences in their immuno-enhancing roles [90].

Although defensin fusions have been shown to enhance antitumor activity, it has been shown that defensins can have detrimental effects through enhanced tumor progression. Intraperitoneal injection of ovarian cancer cells transfected with mBD29 and vascular endothelial growth factor-A (Vegf-A) into C57BL/6 mice lead to a decreased survival time and greater tumor growth [91]. Tumor recruitment of iDC by mBD29 via CCR6 was followed by Vegf-A promoted endothelial-like differentiation and promotion of angiogenesis and tumor survival [91]. Therefore, although defensins have been shown to enhance both innate and adaptive responses, in certain circumstances it could also have a detrimental effect on survival.

To summarize their functional role in immunity, defensins are expressed at sites of both tissue damage and infection and are therefore in an ideal location to act as modulators of both innate and adaptive immunity (Figure 1.6) [49]. Initially defensins are upregulated and secreted upon appropriate stimulation to act as non-specific antimicrobial peptides. Their

role becomes more specialized through attraction of both killer neutrophil/macrophage cells and iDC. Upon antigen uptake, mature DCs are free to interact with effector cells from the adaptive immune response including both B and T lymphocytes leading to a more specific immune response. In addition, defensins have also been found to play a role completing the healing process by promoting wound closure and restoration of the impermeable barrier.

Innate Immunity	Linking Innate and Adaptive Immunity	Adaptive Immunity	Wound Closure
IMMUNE RESPONSE			
Antimicrobial Killing	Attracts iDC – CCR6	Increased CD4+ T helper cell response	Promotes Angiogenesis
Attracts Neutrophils – CCR6	Stimulates DC maturation – TRL4	Increased CD8+ T cytotoxic cell response	Attracts Keratinocytes
Attracts Macrophages – independent of CCR6	Attracts Memory T cells –CCR6	Increased antigen specific Antibody production	
Attracts Mast cells – independent of CCR6			
Induces Mast cell degranulation			

Figure 1.6. Overview of the Role that β-Defensins have in the Immune Response.

1.2.7 - Structure of β-Defensins – 'Defensin-like' Fold

Comparison between amino acid sequences of α- and β-defensins revealed that only a few amino acids were conserved between the families (Figure 1.7 A). Therefore it was surprising when comparison of NMR and/or x-ray crystallographic structures of both defensin families revealed a structurally-conserved core motif now termed the 'Defensin-like' fold [72, 92-96]. With the exception of θ-defensins which are cyclic [97], defensins contain three β-strands constructed in an antiparallel sheet with the first β-strand disulfide bonded to the β-hairpin formed by the final two β-strands (Figure 1.7 B) [94]. Another conserved structural motif is a β-bulge, acting as a 'hinge' in the second β-sheet. This β-bulge is formed between a glycine in the highly conserved Gly-X-Cys motif and the previous amino acid [92, 93, 96]. Stabilization is via formation of hydrogen bonds of these two amino acids to the fifth cysteine. However a major difference between the structures of the two families exists at the N-terminus with β-defensins forming a α-helix which is held against the core structure by Cys1-Cys5 [72, 92, 93, 96].

A

```
              1                                              48
HNP-3   (1)   --------------DCYCRIPACIAGERRYGTCIYQGRLWAFCC----
HNP-4   (1)   -------------VCSCRLVFCRRTELRVGNCLIGGVSFTYCCTRVD
HD-5    (1)   ------------ATCYCRTGRCATRESLSGVCEISGRLYRLCCR---
HD-6    (1)   -----------AFTCHCRR-SCYSTEYSYGTCTVMGINHRFCCL---
HBD1    (1)   ------DHYNCVSSGGQCLYSACPIFTKIQGTCYRGK---AKCCK---
HBD2    (1)   ---GIGDPVTCLKSGAICHPVFCPRRYKQIGTCGLPG---TKCCKKP-
HBD3    (1)   GIINTLQKYYCRVRGGRCAVLSCLPKEEQIGKCSTRG---RKCCRRKK
```

B

α-defensins
- HNP-4
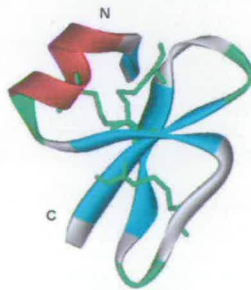
β-defensins
– HBD2
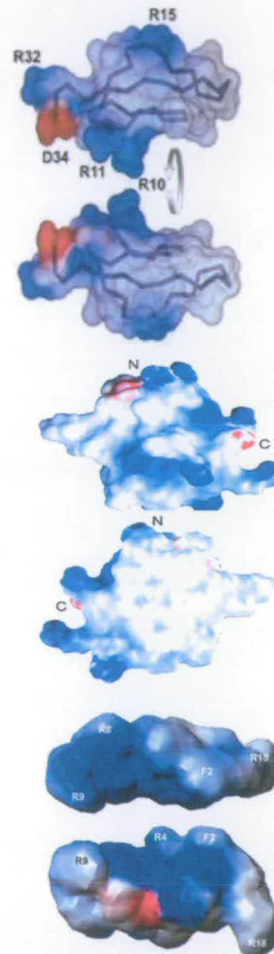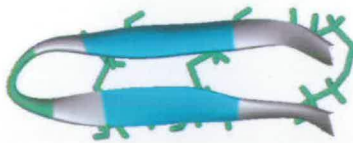
θ-defensins
– RTD-1

Figure 1.7. Structural Analysis of a Representative from each Defensin Family Showing both the 'Defensin-like' Fold and Amphipathic Nature. (A) Sequence alignment of structurally determined defensins showing the limited primary sequence homology between families, except for the six conserved cysteines and the glycine involved in β-bulge. **(B) (Left panel)** Ribbon diagrams of a representative from each defensin family. Structures were downloaded from the protein data bank; HNP-4: 1ZMM, HBD2: 1FD4, RTD-1: 1HVZ. Disulfide bonds are indicated in green. **(Right panel)** Electrostatic surface plots indicating defensins amphipathic nature were adapted from [92, 95, 97]. Blue residues are basic, red residues are acidic and white residues are hydrophobic.

When α- or β- defensins fold into their native state they form amphipathic structures with cationic residues on one face and hydrophobic on the other (Figure 1.7 B). All α-defensins have been shown to form topologically similar dimers with hydrogen bonding between residues in the second β-strand on each monomer responsible [94, 95]. This six-stranded β-sheet dimer was shown to have its hydrophobic face and cationic face at opposite ends and hence had the potential to form large pores in bacterial membranes [94, 95]. The capacity of β-defensins to dimerize and how the individual monomers interact differs from one member to the next. HBD2 was first shown to dimerize when crystal studies showed an oligomeric formation composed of four noncovalent dimers. Hydrogen bonding between the second Cys of each monomer stabilized this interaction while N-terminal helix interactions were shown to stabilize the oligomeric structure [72]. The consequence of this dimerization was a burying of the hydrophobic face leaving cationic residues solvent exposed and lead to the 'carpet-like' model being proposed as cationic residues have the potential at high enough concentration to disrupt the bacterial membrane [72]. However whether HBD2 or HBD1 actually dimerizes is controversial since neither NMR nor native gel electrophoresis found any evidence of dimerization in solution [92, 96]. It is thought that these structures could be artefacts and that the high peptide concentrations used in these studies may lead to formation of higher order multimers. HBD3 can form a dimer in solution when studied by native gel electrophoresis, light scattering and NMR diffusion experiments [92]. Unfortunately the exact interaction is unknown; although NMR studies did show that the dimer is symmetrical possibly interacting through the second β-strand. Replacement of a three amino acid stretch Lys-Glu-Glu with the equivalent part of HBD1 resulted in mutated HBD3 running as monomer on a native gel [70]. This was unsurprising since the second Glu had been proposed to form a dimer-strengthening salt-bridge with the Lys on the second β-strand of the opposing monomer but what was surprising was a lack of dimerization had little effect on its antimicrobial activity [70]. Therefore it was concluded that for HBD3, like HBD2, pore

formation was not necessary for killing and probably permeabilizes the bacterial membrane via the 'carpet-like' mode [70, 92]. However the importance of dimerisation has recently been highlighted by the finding that a β-defensin-related peptide (Defr1) forms a covalent bound dimer. Defr1 had enhanced microbial activity due to the presence of this intermolecular disulfide bond as compared to its six cysteine-containing analogue (Defr1 Y5C) that formed only non-covalent dimers [98].

1.2.8 - Structure and Functional Relationship between CCL20 and β-Defensins

CCL20 is the only chemokine ligand known for CCR6 which is unlike most other chemokine receptors that have multiple activating ligands. CCL20, also known as MIP3α, Liver and Activation-Regulated Chemokine (LARC) and EXODUS-1, has many similarities to the β-defensin family. CCL20 is synthesized with an N-terminal signal sequence which is subsequently cleaved leaving a 70 AA peptide, ~8 kDa soluble protein [99]. CCL20 is expressed constitutively in a wide range of tissues and cell types including skin, liver and the lung [99-101]. This constitutive expression can be significantly up-regulated e.g. CCL20 was upregulated in keratinocytes by proinflammatory cytokines and bacterial challenge [102]. Despite their similarities, the ability of β-defensins to signal through CCR6 was surprising since there is little sequence similarity between any β-defensin and CCL20 (Figure 1.8 A). However, the reasons for the functional overlap became clearer when both the NMR and crystal structures of HBD2 and human CCL20 were solved. Folded, mature CCL20 forms an amphipathic structure consisting of an antiparallel three strand β-sheet followed by a C-terminal helix [103-105]. The N-terminus is mostly random coil that has some constraints imposed by its two cysteines forming disulfide bonds with the core structure [103, 105]. Comparison between the defensin and chemokine structures revealed two main structural

motifs found to be similar in both structures (Figure 1.8 B). The first is a structurally restrained DCCL motif near the N-terminus of CCL20, which is a highly conserved motif in the CC chemokine family. A similar motif exists in HBD2, being DPV or DPVTCL, and is thought to be important in receptor activation and signalling [72, 103]. A second feature, which is reported to be important for the specificity of CCR6, is a groove in CCL20 formed by the N-loop and the β2-β3 hairpin [103, 104]. This groove is ~13 Å wide whereas HBD2, which shows a similar groove on its surface, is only ~9 Å wide [72, 103]. This narrower groove, combined with the more restrained N-terminus found in HBD2, have been proposed as reasons for the higher affinity and activity of CCL20.

It is of interest to note that chemotaxis is not the only functional overlap between β-defensins and CCL20. Recently CCL20 has been shown to possess equivalent salt-sensitive antimicrobial activity against certain Gram-negative and Gram positive bacteria as compared to β-defensins. In fact, CCL20 possess antimicrobial activity against *S. aureus*, a bacterial strain that shows high resistance to both HBD1 and HBD2 [103, 106]. The cationic patch on the CCL20 chemokine has been proposed for this antimicrobial activity and the C-terminal α-helix that constitutes a large proportion of this cationic patch possesses significant antimicrobial activity alone [104].

A


```
                                1                                                                    70
CCL20(1)ASNFDCCLGYTDRILHPKFIVGFTRQLANEGCDINAIIFHTKKKLSVCANPKQTWVKYIVRLLSKKVKNM


HBD2 (1)GIGDPVTCLKSGAICHPVFCPRRYKQIGTCGLPGTKCCKKP
```

B

HBD2   CCL20
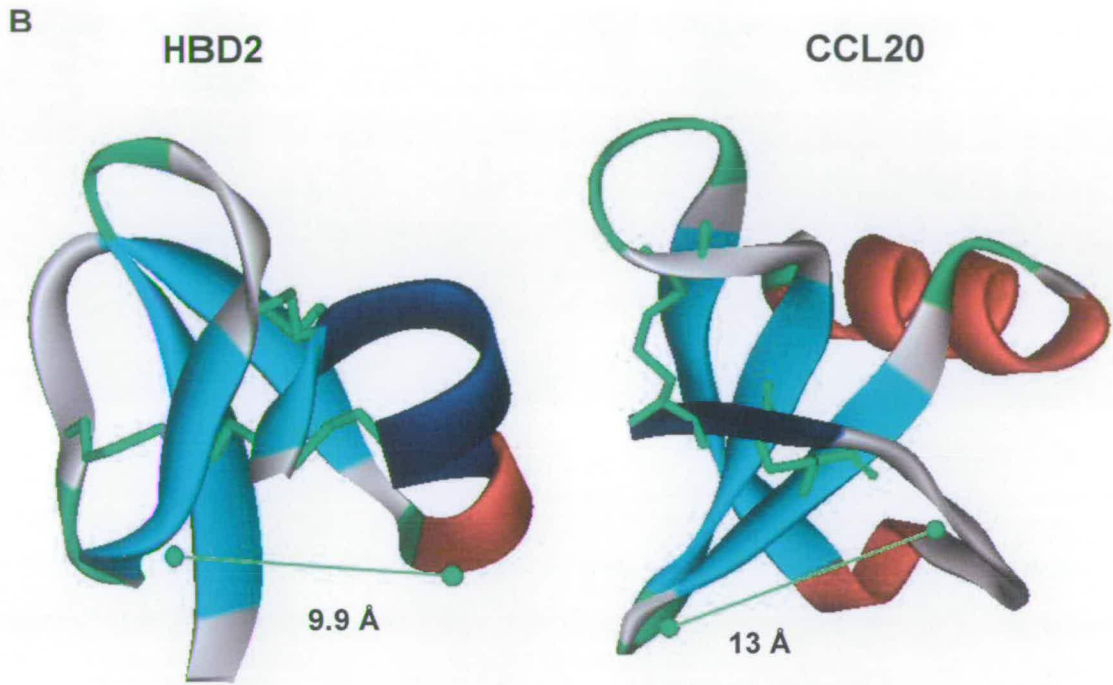
Figure 1.8. Structural Comparison between HBD2 and CCL20 – Highlighting Two Functionally Important Motifs. (A) Sequence alignment showing conserved residues in red. Secondary elements are indicated with blue a cylinder representing α-helix and red arrow representing β-sheet. **(B)** Ribbon diagrams comparing the structures of HBD2 (1FD4) and CCL20 (1M8A). The DPVTCL stretch of HBD2 and DCCL stretch of CCL20 are highlighted blue. The distance of the binding groove motif is also indicated. Disulfide bonds are highlighted in green.

1.2.9 - Role in Health and Disease

Defensins have been associated with various chronic inflammatory diseases where deficiencies or inactivation can lead to increased and recurring bacterial colonization. Two chronic inflammatory skin diseases highlight the role of defensins in human health, namely atopic dermatitis and psoriasis. Although both involve lesions in the skin barrier, atopic dermatitis is highly susceptible to *S. aureus* skin infection whereas psoriasis has significantly fewer infections [107, 108]. The inability to stimulate either HBD2 or HBD3 in atopic dermatitis is implicated in, and has been attributed to, the upregulation of Th2 cytokines that have been shown to block proinflammatory cytokine induced defensin up regulation [109]. Psoriatic skin however contains numerous proinflammatory cytokine induced peptides/proteins including defensins that act as a killing barrier to invading organisms [109].

Defensin deficiency has also been implicated in Crohn's disease with reduced α-defensin expression and lack of β-defensin induction linked to ileal and colonic Crohn's disease respectively [110, 111]. Both locations of Crohn's disease are associated with an increased number of colonizing adhesive and invading *E. coli* strains indicating that a breakdown in the antimicrobial protective layer could in part be responsible for this chronic inflammation [112].

An interesting point worth noting is that the β-defensin cluster on chromosome 8 containing DEFB4 and DEFB103-107 has been found to be repeated up to 12 times in humans and this copy number varies between individuals [113]. A case study investigating copy number variations (CNV) of the defensin cluster in psoriasis discovered that the addition of only one copy compared to the median 4 copies increased an individual's susceptibility to the disease [114]. Likewise a case study into a link between CNV and Crohn's disease discovered a loss of only one copy increased an individual's susceptibility to colonic Crohn's disease [115]. Whether predisposition to psoriasis and Crohn's disease is

related to β-defensin genomic copy number is still controversial and until gene expression and protein levels are shown to relate to increased copy number then this is an intriguing theory that merits further study.

A third defensin-associated inflammatory disease is Cystic fibrosis (CF). This is characterised by recurring and increased bacterial infection of the airways and is caused by various mutations in the Cystic Fibrosis Transmembrane conductance Regulator gene [116]. Despite intensive study it is still not clear how the defective chlorine channel is involved in chronic lung infection. The "high salt" or "salty lung" hypothesis was proposed when an impaired antimicrobial activity was detected in the higher salt environment of airway surface liquid (ASL) in CF patients [117]. The role of defensins in this impaired activity was postulated when HBD1 and -2 were shown to be present in the bronchoalveolar lavage fluid of CF patients and possessed salt-sensitive antimicrobial activity *in vitro* [62, 63, 118]. Furthermore an *ex vivo* human bronchial xenograft model highlighted HBD1 as an important component of ASL killing activity - antisense oligonucleotide inhibition of HBD1 expression in ASL resulted in significantly reduced *P. aeruginosa* killing activity [62]. Although difficulties in obtaining exact salt concentrations make this hypothesis controversial, it does further highlight the importance of defensins in the pathogenesis of chronic inflammatory diseases.

1.3 - G-Protein Coupled Receptors

1.3.1 - Introduction to G-Protein Coupled Receptors

G-protein coupled receptors (GPCRs) represent one of the largest and most important families of proteins in humans [119, 120]. Over 800 GPCRs are estimated to be present in the human genome [121], with over 30% of current drug targets acting on only a small percentage of these receptors [122]. The importance of GPCRs in human health and pharmacology is due to the variety of ligands which activate a plethora of physiological

processes. Both endo- and exogenous ligands act on these seven transmembrane helical receptors upon binding by transducing a signal across the cell membrane using heterotrimeric (α, β, γ) G proteins as intermediates. Exchange of GDP to GTP on the α-subunit causes dissociation from the dimer βγ. Both of these components are capable of activating or inhibiting several effectors in a signalling cascade which terminates with a cell response (Figure 1.9).
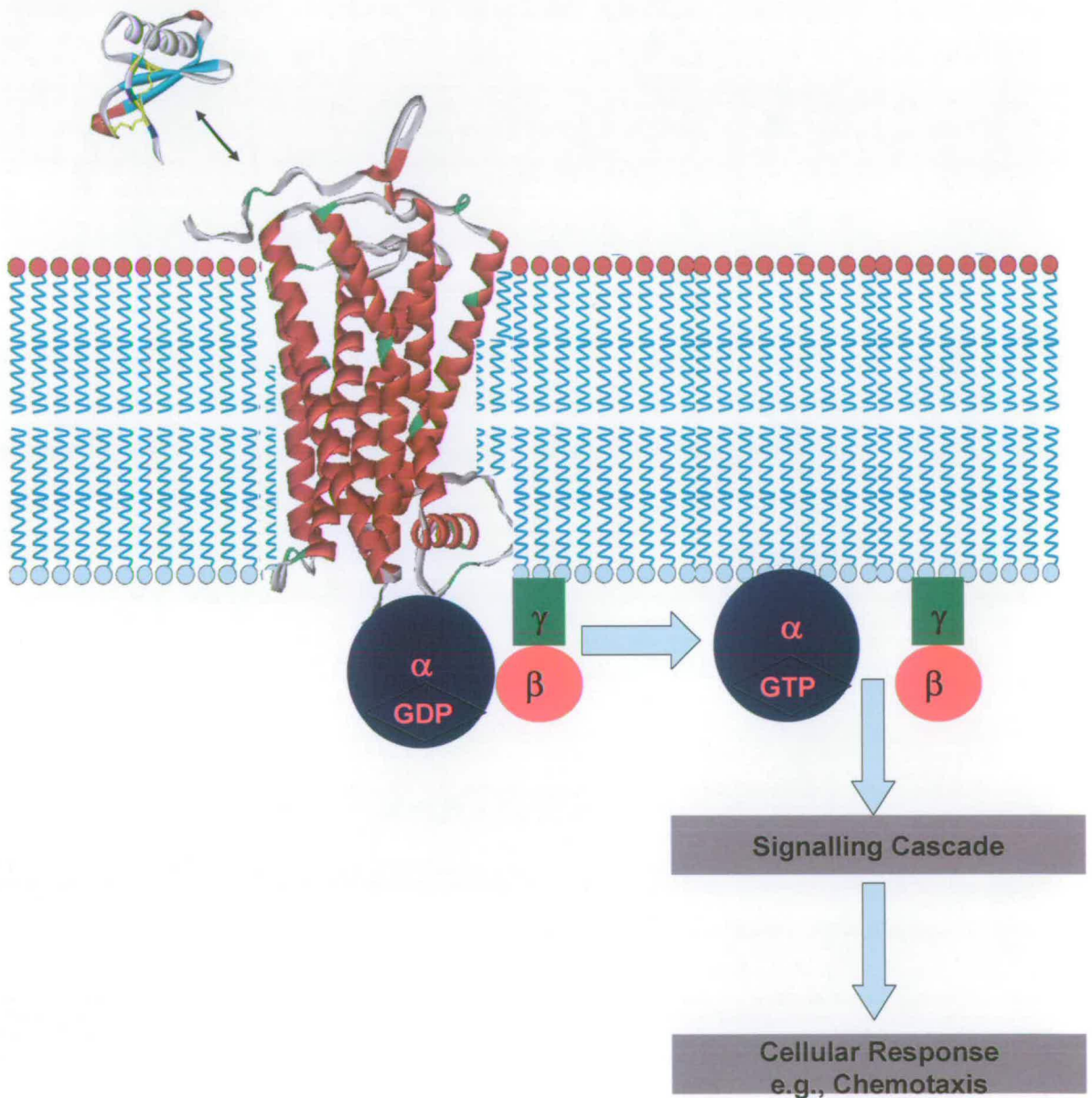
Figure 1.9. Schematic Representation of GPCR Signalling upon Agonist Binding.

The large numbers of diverse GPCRs identified by numerous studies from various scientific fields made it necessary for a classification system to be proposed. A commonly used system for both vertebrates and invertebrates was the A-F system [123, 124]. The largest family, family A, contains the classical rhodopsin receptor, adrenergic and chemokine receptors. Although these receptors have relatively low sequence homology, they have structurally-conserved motifs which can be used as indicators for family members. A classification specifically for human GPCRs was later proposed by Fredriksson in 2003. The GRAFS classification system, which is the acronym for the receptor families, reclassified human GPCRs [125, 126]. This system allowed distinctions to be made between the Secretin (S) and Adhesion (A) receptor families previously grouped in family B. Also, the large Rhodopsin family was subdivided into four main groups with 13 sub-groups [126]. Due to the different ligands that activate these receptors this was essential.

The quantity and complexity of GPCRs have been extensively reviewed by Jacoby et al., Pierce et al. and Kristiansen et al. [127-129]. Recently, various databases have been set up including the RINGdb and GPdb to help categorise the interactions between the GPCR, G proteins and their activating ligands [130, 131].

1.3.2 - Expression and Purification of GPCR's

Although GPCRs are major drug targets, structure-based drug design has been hampered by the lack of available structural information. This is a consequence of the difficulties involved in obtaining milligram quantities of homogenous protein for structural studies. Purification of native GPCRs from natural sources has been restricted to either highly abundant proteins, of which bovine Rhodopsin from rod outer segment membranes remains unique [132] or extreme up-scaling as exemplified by the need for 1200 porcine

brains to obtain a partial amino acid sequence coverage of neuropeptide Y2 [133]. Therefore it has been necessary to optimize heterologous expression of GPCRs. Prokaryotic systems such as *E. coli* have been used to express GPCRs either in low yields as maltose binding protein fusions [134, 135] or as inclusion bodies that require subsequent refolding to produce functional receptors [136, 137]. A major disadvantage of expression in *E. coli*, apart from the inefficient refolding, is an inability to perform functionally important post-translational modifications. To combat this, various eukaryotic expression systems such as yeast, baculovirus/insect, and mammalian cells have been optimized each with their own advantages and disadvantages. Fermentation of yeast, including *S. cerevisiae, Schizosaccharomyces pombe* and *Pichia pastoris* allows easy up-scale and this expression system can perform some of the essential post-translational modifications [138]. However, extraction of GPCRs from yeast is difficult due to the thick cell wall reducing the isolated protein yield [139]. Also the biosynthetic components of N-glycosylation in yeast are different than in mammalian systems potentially altering their structure [140]. Likewise insect cells infected with plasmid constructs encoding GPCRs within baculovirus have been successful in obtaining milligram quantities. However just as in yeast, insect-produced GPCRs have improper glycosylation modifications [139]. It must be stated that for crystal structure studies described later glycosylation modifications are often removed to improve the homogeneity of the receptor and therefore improve crystallisation [141]. Finally, mammalian expression systems obviously have the advantage of being capable of producing GPCRs fully post-translationally modified in a close to native membrane environment. However unlike the previous expression systems, up-scaling is extremely time-consuming and can produce only moderate yields. To improve both yield and up-scaling in mammalian expression systems a tetracycline inducible system combined with the suspension HEK293s cell line has been designed [142, 143]. This expression system has been applied to both rhodopsin and β2-adrenergic receptors, successfully producing milligram quantities [142,

144]. However a limitation of these cells is they lack N-acetylglucosaminyltransferase I activity leading to improper glycosylation modifications [142].

The emergence of various structural genomics consortiums, including MePNet and E-MeP, dedicated to GPCR expression, purification and structural characterization shows both the difficulties and importance of this family of receptors. Various high throughput studies have been performed investigating the expression levels of ~100 GPCRs in *E. coli*, Semliki Forest virus/mammalian and *P. pastoris* cell expression systems [145-147]. Coupled with the increasing success of GPCR crystal studies, this is an important step forward in structure-based drug design.

1.3.3 - Crystal Structure Studies

The crystal structure of the dark state of bovine rhodopsin was the first three dimensional structure determined for a GPCR [148]. This seminal study revealed the conserved seven-transmembrane helical topology as well as providing a structural relevance for the family A conserved motifs. One such motif, E/DRY motif, was shown to provide an 'ionic lock' between residues in TM3 and TM6 proposed to restrain the inactive state via reducing helical movements. Other conserved motifs such as the rotamer toggle switch tryptophan or the NPXXY motif were also shown to form important intramolecular interactions, with the former shown to interact with the 11-cis-retinal ligand [148]. The difficulties in obtaining GPCR crystal structures including low natural expression, heterogeneity, intrinsic flexibility and low numbers of surface accessible polar residues has forced groups to reengineer their respective GPCRs to compensate for these barriers to protein isolation and crystallization (Table 1.2). This effort has seen the number of GPCR structures in the protein databank (http://www.rcsb.org) rise rapidly over the last two years. Crystal structures for human A_{2A} adenosine, β2 adrenergic-Fab5, β2 adrenergic-T4L, and turkey β1 adrenergic receptors have all been determined in association with either an

antagonist or inverse agonist [141, 149-152]. Despite the overall topology being similar to bovine rhodopsin there were subtle differences between all known structures especially in the lack of an 'ionic lock'. In the structures of both the human A_{2A} adenosine and turkey $\beta 1$ adrenergic receptor the E/DRY motif restrains the short helix in ICLII via hydrogen bonding whereas in the $\beta 2$ adrenergic receptors this helix section does not exist [141, 149]. The resulting $\beta 2$ adrenergic receptor has a more open, less restrained structure and this is thought to be the reason for its higher basal activity [150-152].

Despite the recent successes in GPCR crystal structure determination, all of these previous structures have been determined in their inactive state. Recently the protein component of rhodopsin, apoprotein Opsin, was crystallised in its active state and, in a separate study, the crystal structure complexed with the C terminus of Transducin $G\alpha_t$ subunit was resolved [153, 154]. These active conformations differed predominantly at the cytoplasmic end of transmembrane helix 6 which turned at the toggle switch tryptophan and moved 6 Å away from the main helical structure [154]. This movement resulted in the E/DRY associated 'ionic lock' to be broken allowing a G protein accessible binding site to open up. The C-terminal of Transducin was then able to interact with the liberated Arg from the E/DRY motif and this open structure was further stabilized by the insertion of Tyr from NPXXY into the void left by TM6 [153]. In fact via a hydrogen bonded network the C-terminal of Transducin connects these two highly conserved motifs stabilizing the active site even further [153].
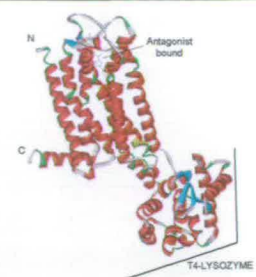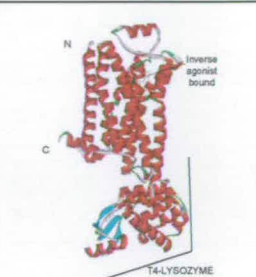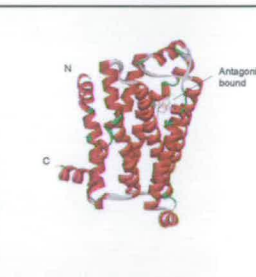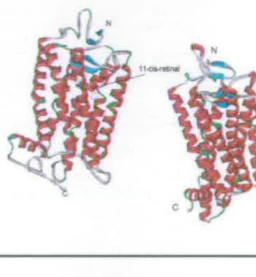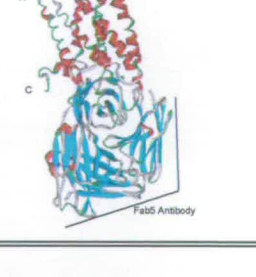
PDB FILE	NAME	RESOLUTION	PURIFICATION	ENGINEERING	STRUCTURE
3EML	Human A2a Adenosine Receptor	2.6 Å	Baculovirus/SF9 insect cells	ICL III replaced with T4 lysozyme. Antagonist bound (ZM24135). Acquired affinity tags. Removed glycosylation and phosphorylation sites. Purified in presence of NaCl.	
2RH1	Human β2-Adrenergic Receptor	2.4 Å	Baculovirus/SF9 insect cells	ICL III replaced with T4 lysozyme. Inverse agonist bound (Carazolol). Removed flexible C-terminus. (phosphorylation sites). Deglycosylated.	
2VT4	Turkey β1-adrenergic Receptor	2.7 Å	Baculovirus/High 5 insect cells	Truncation of N-terminal, ICLIII and C-terminal removing glycosylation and phosphorylation sites. 8 stabilzing point mutations including removal of palmitoylation site. Antagonist bound.	
1F88/ 3CAP	Bovine Rodopsin/ Opsin	2.8 Å/2.9 Å	Natural – bovine rod outer membranes	11-cis retinal covalently bound / none.	
2R4R	Human β2 adrenergic Receptor	3.4 Å	Baculovirus/Sf9 insect cells	Fab antibody bound to ICL III. Deglycosylated. C-terminal truncation removing phosphorylation sites. Inverse agonist bound.	

Table 1.2. GPCR Re-Engineering - Highlighting the Difficulties of GPCR Purification and Crystallization. GPCRs are intrinsically unstable receptors that, with the exception of Rhodopsin/ Opsin, require extensive engineering to remove both areas of flexibility and heterogeneity that are detrimental to structural studies. Furthermore a lack of surface accessible polar molecules for crystal contacts has made it necessary to increase this polar surface area with either an antibody bound (Fab) to ICL III or engineering the GPCR to express another protein in place of the ICL III [149-152]

Using these crystal structures as templates to model other family A receptors has to be treated with caution since even receptors with the same ligand can have subtle differences. Also the crystal structure of a representative of the family A receptors, which use peptides for activation, has yet to be solved. Therefore much more research needs to be performed on a wider range of receptors before GPCR signalling is fully understood.

1.3.4 - Chemokine Receptor Family

1.3.4.1 - Classification

Chemokine receptors are seven-transmembrane receptors that represent the family A rhodopsin like receptors (Figure 1.10). Currently there are ~20 signalling chemokine receptors known and their main role in immunity is the recruitment of leukocytes during both homeostatic and inflammatory trafficking [155, 156]. Chemokine receptors are classified as CC, CXC, CX3C or C depending on the number of residues between the first two cysteines of their chemokine ligand, with the exception of C receptor whose chemokine ligand only has two cysteines instead of the normal four [156]. Despite a low overall sequence homology between chemokine receptors they do contain highly conserved motifs, aside from the obvious seven-transmembrane topology; they have two highly conserved cysteines in the N-terminal and the putative ECLII, HCCXNP motif in TMVII and the DRY motif in cytoplasmic end of TMII. This latter motif has been shown to be very significant for chemokine receptor signalling as three identified chemokine receptors without this motif fail to signal and termed scavenger receptors [155, 157].

```
                1                                                                                               100
bRho    (1)     ---------MNGTEGPNFYVPFSNKTGVVRSPFEAPQYYLAEPWQFSMLAAYMFLLIMLGFPINFLTLYVTVQHKKLRTPLNYILLNLAVADLFMVFGGF
hCCR6   (1)     MSGESMNFSDVFDSSEDYFVSVNTSYYSVDSEMLLCSLQEVRQFSRLFVPIAYSLICVFGLLGNILVVITFAFYKKARSMTDVYLLNMAIADILFVLTLP
mCCR6   (1)     -----MNSTESYFGTDDYDN---TEYYSIPPDHGPCSLEEVRNFTKVFVPIAYSLICVFGLLGNIMVVMTFAFYKKARSMTDVYLLNMAITDILFVLTLP
hCCR5   (1)     --------MDYQVSSPIYDIN---YYTSEP-----CQKINVQIAARLLPPLYSLVFIFGFVGNMLVILILINCKRLKSMTDIYLLNLAISDLFFLLTVP
hCXCR4  (1)     -MSIPLPLLQIYTSDNYTEEMGSGDYDSMKEP---CFREENANFNKIFLPTIYSIIFLTGIVGNGLVILVMGYQKKLRSMTDKYRLHLSVADLLFVITLP

                101                                              E/DRY Motif                                    200
bRho    (92)    TTTLYTSLHGYFVFGPTGCNLEGFFATLGGEIALWSLVVLAIERYVVVCKPMSNFR---FGENHAIMGVAFTWVMALACAAPPLVGWSRYIPEGMQCSCG
hCCR6   (101)   FWAVS-HATGAWVFSNATCKLLKGIYAINFNCGMLLLTCISMDRYIAIVQATKSFRLRSRTLPRSKIICLVVWGLSVIISSSTFVFNQKYN-TQGSDVCE
mCCR6   (93)    FWAVT-HATNTWVFSDALCKLMKGTYAVNFNCGMLLLACISMDRYIAIVQATKSFRVRSRTLTHSKVICVAVWFISIIISSPTFIFNKKYE-LQDRDVCE
hCCR5   (85)    FWAH--YAAAQWDFGNTMCQLLTGLYFIGFFSGIFFIILLTIDRYLAVVHAVFALKARTVTFG--VVTSVITWVVAVFASLPGIIFTRSQK-EGLHYTCS
hCXCR4  (97)    FWAV--DAVANWYFGNFLCKAVHVIYTVNLYSSVLILAFISLDRYLAIVHATNSQ--RPRKLLAEKVVYVGVWIPALLLTIPDFIFANVSE-ADDRYICD

                201                                                                                             300
bRho    (189)   IDYYTP-HEETNNESFVIYMFVVHFIIPLIVIFFCYGQLVFTVKEAAAQQQESATTQKAEKEVTRMVIIMVIAFLICWLPYAGVAFYIFTHQGSDFGP--
hCCR6   (199)   PKYQTVSEPIRWKLLMLGLELLFGFFIPLMFMIFCYTFIVKTLVQAQNSK---------RHKAIRVIIAVVLVFLACQIPHNMVLLVTAANLGKMNRS-C
mCCR6   (191)   PRYRSVSEPITWKLLGMGLELFFGFFTPLLFMVFCYLFIIKTLVQAQNSK---------RHRAIRVVIAVVLVFLACQIPHNMVLLVTAVNTGKVGRS-C
hCCR5   (180)   SHFP-YSQYQFWKNFQTLKIVILGLVLPLLVMVICYSGILKTLLRCRNEKK--------RHRAVRLIFTIMIVYFLFWAPYNIVLLLNTFQEFFGLNN-C
hCXCR4  (192)   RFYP----NDLWVVVFQFQHIMVGLILPGIVILSCYCIIISKLSHSKGHQ---------KRKALKTTVILILAFFACWLPYYIGISIDSFILLEIIKQGC

                301                     NPXXY Motif                                                             389
bRho    (286)   ------IFMT-IPAFFAKTSAVYNPVIYIMMNKQFRNCMVTTLCCG-----------------KNPLGDDEASTTVSKTETSQVAPA-
hCCR6   (289)   QSEKLIGYTKTVTEVLAFLHCCLNPVLYAFIGQKFRNYFLKILKDLWCVRRKYKSSGFSCAGRYSEN-ISRQTSETADNDNASSFTM--
mCCR6   (281)   STEKVLAYTRNVAEVLAFLHCCLNPVLYAFIGQKFRNYFMKIMKDVWCMRRKNKMPGFLCARVYSESYISRQTSETVENDNASSFTM--
hCCR5   (270)   SSSNRLDQAMQVTETLGMTHCCINPIIYAFVGEKFRNYLLVFFQKHIAKR------FCKCCSIFQQEAPERASSVYTRSTGEQEISVGL
hCXCR4  (279)   EFENTVHKWISITEALAFFHCCLNPILYAFLGAKFKTSAQHALTSVSRGS---------SLKILSKGKRGGHSSVSTESESSSFHSS--
```

Figure 1.10. Sequence alignment showing family A conserved motifs and residues between Rhodopsin and chemokine receptors. X – NPXXY motif, X – DRY motif, X – Conserved residues in each TM, X – other conserved residues

1.3.4.2 - Human Chemokine Receptor 6

An orphan receptor termed CKR-L3 was discovered from genomic DNA using a degenerate PCR strategy [158]. Almost simultaneously STLR22 was discovered from both genomic DNA and a tumour-infiltrating lymphocyte cDNA library [159]. These two receptors were shown to be almost identical and although neither study could identify the ligand involved these receptors did have chemokine receptor characteristics. Identification of the ligand became possible later upon discovery of the chemokine now known as CCL20 (aliases are MIP-3α, LARC, and EXODUS) [99]. In the same year, four different groups showed CCL20 had the ability to chemoattract only cells transfected with this orphan receptor and its binding induced calcium mobilization characteristic of chemokine signalling [157, 160-162]. This was the sixth functional chemokine receptor identified and was hence named CCR6.

The CCR6 gene, also known in the literature as STRL22, CKR-L3, BN-1, DCCR2, GPR-CY4, is composed of two exons with a 96 bp intron between the third and fourth codons which was not identified in sequences obtained from genomic DNA and is uncommon for chemokine receptors [159]. The CCR6 gene was also identified on chromosome 6q27, removed from the main CC chemokine receptor cluster [159]. Together with the fact that neither CCR6 nor CCL20 can interact in any other chemokine or chemokine receptor combination, highlighting CCR6 as an intriguing chemokine receptor.

CCR6 has many conserved chemokine receptor characteristics including the DRY motif, serine/threonine rich C-terminal and four putative extracellular conserved cysteines (Figure 1.11). However, little information is known about which residues are important for ligand affinity and receptor activation of CCR6. A study mutating all four conserved cysteines individually or together to serine highlighted their functional importance. Mutation of extracellular loop (ECL) I and II cysteines both together and individually resulted in reduced receptor surface expression, whereas N-terminal and ECLIII cysteine mutants had

near wild-type receptor surface expression (Figure 1.12) [163]. Interestingly the cysteine residues found in ECLI and ECLII are connected via a disulfide bond and it is therefore implied that reduced surface expression is due to improper folding resulting in intracellular accumulation [163]. Although not necessary for receptor trafficking, mutation of both N-terminal and ECLIII cysteines did have a negative effect on receptor binding and as a consequence their chemotactic activity. However, at higher concentrations, these mutated receptors were still able to induce calcium flux indicating that they do not completely lose receptor function [163]. The first putative C-terminal cysteine of CCR6 has been proposed to enhance the stability of the receptor by post-translational modification of this cysteine with a palmitoyl fatty acid chain. Replacement of this cysteine with a serine resulted in both impaired surface expression and chemotactic ability but not to the same extent as the disulfide bonded cysteines on ECLI and II [163].

Further evidence for CCR6 specificity came from a domain swapping approach with CCR5. Replacement of the ECLs of CCR6 with CCR5 either individually or together resulted in a loss of chemotactic or calcium mobilization ability upon CCL20 stimulation despite similar surface expression [164]. Only the chimera CCR6/CCR5-ECLI could produce a reduced calcium response but was not chemotactic to CCL20 even at high concentrations. Interestingly a chimera was prepared were the mouse N-terminal CCR6 domain (41% identity compared with the human CCR6) was swapped with the human counterpart. This chimera showed no detrimental effects when both receptor expression and chemotaxis were tested [164]. Identical sites of interest included the two potential N-terminal glycosylation sites, N-terminal cysteine as well as the YY motif shown to be important for CCR5 ligand binding [165].
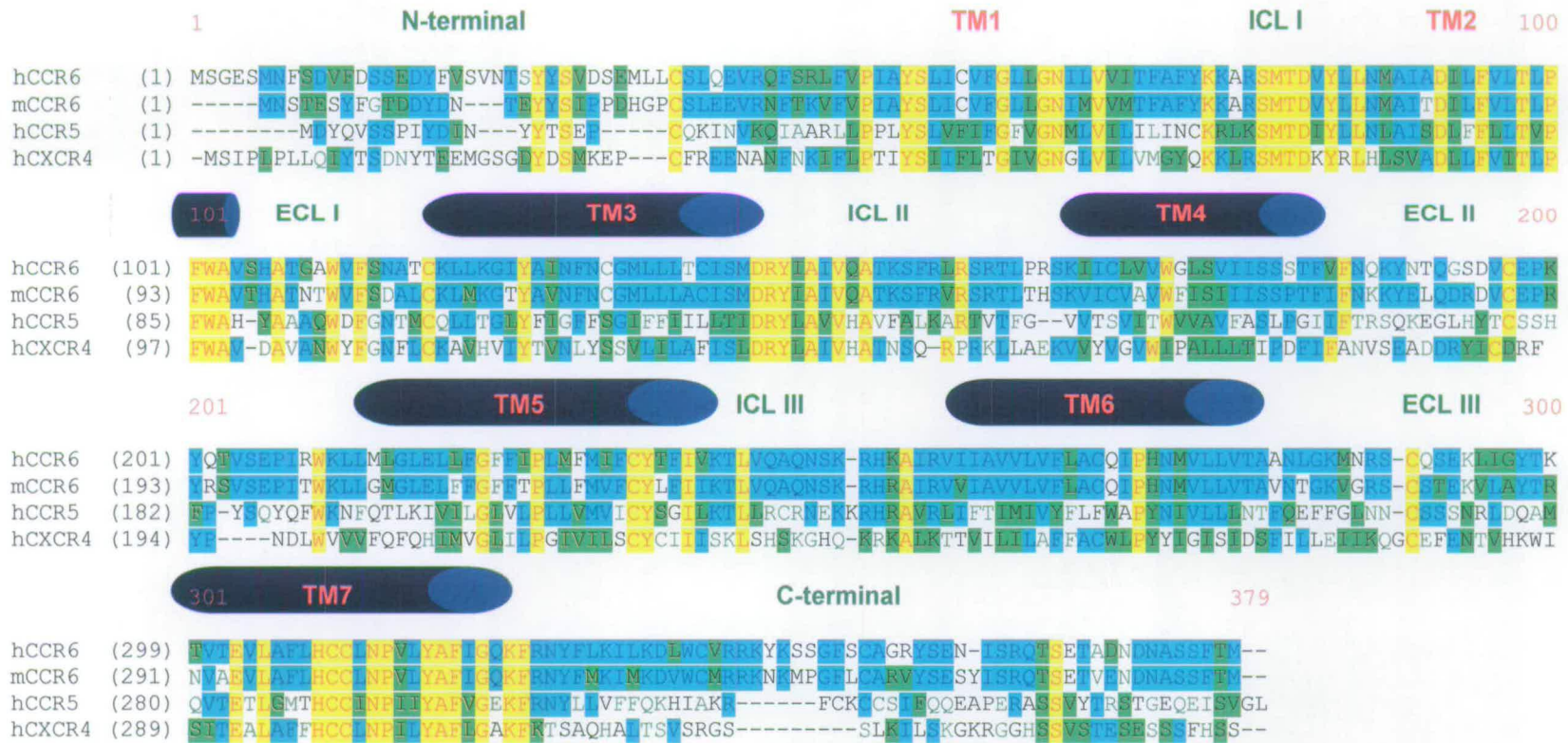
Figure 1.11. Sequence Alignment Showing the Conserved Residues Between Members of the Chemokine Receptor Family. The secondary motifs are highlighted with a blue cylinder representing transmembrane (TM) α-helices. X - Identical residues throughout, X -similar residue, X –identical residues in at least two out of the four cases.

CCR6, like most other chemokine receptors, signals through the $G\alpha_i$ G protein subunit, identified due to its sensitivity to the pertussis toxin [157]. A further indication of signalling through the $G\alpha_i$ pathway came when activation of CCR6 expressing human intestinal epithelial cells resulted in inhibition of forskolin-stimulated cAMP production [166]. However it is the $G\beta\gamma$ subunits that have been implicated in the signalling cascade resulting in chemotaxis due to their ability to signal through both phosphatidylinositol 3-kinase (PI3K) and phospholipase C effectors [166]. Early work on CCR6 signalling in leukocytes discovered that chemokine activation resulted in increased intracellular Ca^{2+} release which was reduced by a phospholipase C inhibitor (U-73122) [157]. Recently this $[Ca^{2+}]$ increase was also identified in CCR6-expressing intestinal epithelial cells and blocking Ca^{2+} release resulted in inhibition of cell migration in a wound assay [167]. This same in-depth study of CCR6 signalling also identified other important signalling mediators for migration. Both CCL20 and β-defensin stimulation resulted in the increased production of F-actin at the leading edge of the cell which is the driving force for chemotaxis [167]. At the tail of a polarised cell, actomyosin complexes can form that contract the cell from behind. Ligand stimulation of intestinal epithelial cells activated RhoA; this resulted in Rho-kinase dependent phosphorylation of myosin light chain that in turn has been shown to activate actomyosin contraction [167]. Finally both RhoA activation and subsequent cell migration was negated by PI3K inhibition [167]. This is unsurprising since PI3K signalling, like phospholipase C, has been implicated as a major pathway in chemokine receptor signalling [168]. This is a very limited review of a multitude of components involved in both *in vitro* and *in vivo* cell signalling however it does show that both CCL20 and β-defensins have the ability to activate multiple components of these pathways from an extracellular source finalizing in chemotaxis.

Top view

- ■ **Extracellular**
- ■ **Intracellular**
- ■ **Transmembrane**
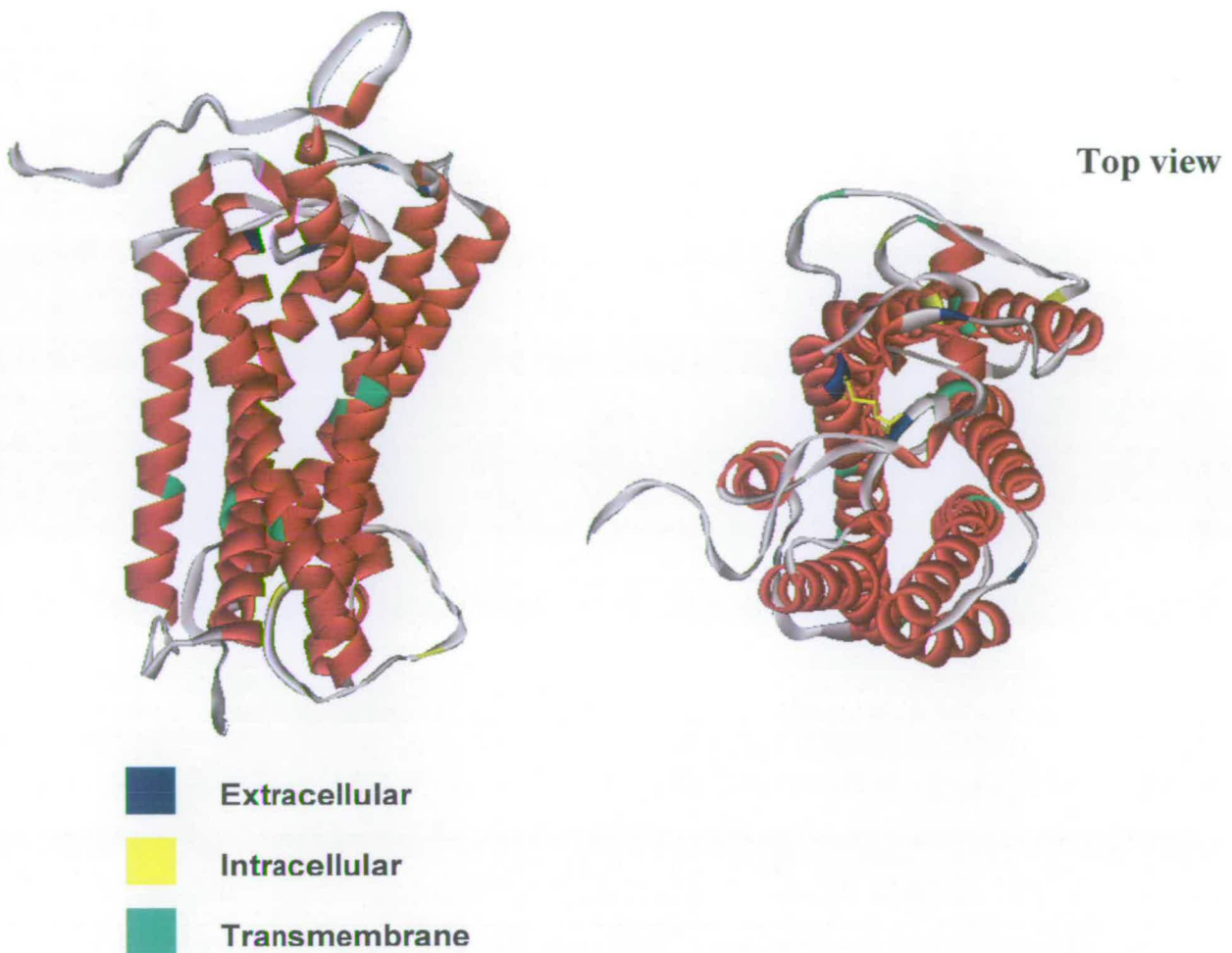
Figure 1.12. Ribbon Diagram representing a Theoretical Model of CCR6. CCR6 predicted structure was downloaded from http://cssb.biology.gatech.edu/skolnick/files/gpcr and ribbon diagrams generated using DS Viewer Pro [169]. Cysteines mutated as part of the CCR6 biochemical analyses are shown [164]. Extracellular cysteines are highlighted blue, Intracellular cysteines are highlighted yellow and transmembrane cysteines are highlight green. Disulfide bond between ECLI and ECLII cysteines is represented by a yellow bond in the top view structure (Right panel).

1.3.4.3 - Tissue and Immune Cell Expression

A number of studies have explored the tissues where CCR6 expression occurs. Northern blot analysis identified CCR6 mRNA transcripts mostly in secondary lymphoid tissues, with expression greatest in the spleen, lymph nodes, appendix and fetal liver [158, 160]. Furthermore CCR6 was shown initially to be expressed in various leukocytes including

lymphocytes instigating a role in immune cellular trafficking [158, 160]. However this expression pattern was further complicated upon the realization that subtle changes in cell maturation status and subtype effected this expression. Due to the low natural abundance of DCs, in vitro stimulation of CD34$^+$ hematopoietic progenitor cells or monocytes with an appropriate cytokine cocktail were used for immature DC expression studies. CCR6 has been shown to be expressed in both myeloid and lymphoid derived immature DCs as well as the skin-homing Langerhan cells [157, 170, 171]. Upon antigen uptake and their activation, iDCs undergo a maturation process which results in the down-regulation of CCR6 mRNA and upregulation of other chemokine receptors including CCR7 [172].

Both northern blot and RT-PCR analysis found CCR6 to be expressed on CD4$^+$ (Helper) and CD8$^+$ (Cytotoxic) T cells as well as CD19$^+$ B cells [173, 174]. Surface expression of CCR6 on T cells was identified later when FACS analysis identified CCR6 expression more predominantly on CD4$^+$ cells than CD8$^+$ cells [174]. The exact subtype of these CD4$^+$ cells were identified as memory T cells as CCR6 positive cells also expressed the memory specific surface marker CD45RO$^+$ [174]. Interestingly CCR6 expression is not restricted to one type of memory T cell. A recent study has shown both T_h1 and the recently identified T_h17 memory T cells express CCR6, and have implicated these CCR6 expressing T cells in the clearance of both intracellular pathogens and *C. albicans* [175]. In another study, surface expression analysis of CCR6 expressing CD8$^+$ cells also identified co expressing surface markers of the memory or effector memory subset [176]. These memory T cells were also found to express either skin or mucosa homing specific receptors, indicating their role in immunity where β-defensins and CCL20 are highly expressed upon pathogenic challenge [174]. With CCR6 also being expressed on mature memory B cells it has been proposed that CCR6 ligands direct these cells to the appropriate compartments so that they can efficiently interact to link the innate and adaptive immune response.

1.3.4.4 - Role of CCR6 in Normal and Diseased Immunity

The role that human CCR6 performs in immunity has been inferred by using either knockout or CCR6-GFP knock-in mice. CCR6 -/- mice do not display any developmental abnormalities in any major organ but specialised intestinal lymphoid structures such as Peyer's Patches, known to accumulate CCR6 expressing iDCs have been shown to be abnormal in size in some cases [177]. However, mice deficient in CCR6 do have differences in cellular recruitment under both homeostatic and inflammatory responses. Analysis of specific subsets of lymphocytes resulted in differences in concentration under homeostatic conditions and a reduced humoral response to both antigen and Rotavirus infection [178]. One reason for this defect could be a breakdown in antigen presentation because of defective accumulation of CCR6 expressing iDCs. This impaired iDC accumulation in CCR6 -/- mice has been identified in the three major areas of β-defensin or CCL20 expression being the lung BAL fluid, skin and intestinal associated Peyer's patches upon activation of the immune response [178-180]. In both the skin and Peyer's patches this resulted in a failure to activate pathogen-associated T lmphocytes as performed in the wt mice and as such provides direct *in vivo* evidence for a role of CCR6 in adaptive immunity [180, 181].

Identification of CCR6-mediated inflammatory diseases has also been inferred from CCR6 deficient mice. Chronic Obstructive Pulmonary Disease (COPD) is characterised by increased infiltration of DC, neutrophils and T lymphocytes [182]. Comparison of the accumulation of these leukocytes in the lungs of CCR6 -/- mice compared to wt upon cigarette smoke inhalation resulted in reduced numbers of both iDCs and T lymhocytes [183]. These CCR6 -/- mice were more protected against chronic smoke-induced emphysema [183]. The role for CCR6 in human COPD has subsequently been shown with increased accumulation of both CCL20 and DC in affected patients [182]. In fact as the disease gets progressively worse the accumulation of CCR6 expressing DCs increases [182]. This is just one of many inflammatory diseases CCR6 has been linked to. Mice deficient in

CCR6 have been shown to offer protection against experimental induced sepsis, onset of experimental autoimmune encephalomyelitis and allergic pulmonary inflammation [184-186]. Together these studies indicate the important role that the CCR6 and β-defensin/CCL20 interaction has in controlling the inflammatory response and the severe consequences of its dysfunction.

1.4 - Overall Aim

Difficulties in expressing and purifying both β-defensins and CCR6 have been a major bottleneck in the elucidation of their structural-functional relationship. Certain intrinsic properties of both β-defensins and CCR6 are responsible and these problems must be circumvented in order for their interaction to be investigated fully. Therefore the major aim of this thesis was to optimize the expression and purification of both these difficult targets so as to provide a platform for future structural-functional studies.

1.5 - Chapter 1 References

1. Muller, C.A., I.B. Autenrieth, and A. Peschel, *Innate defenses of the intestinal epithelial barrier.* Cell Mol Life Sci, 2005. **62**(12): p. 1297-307.
2. Janeway, C.A., Jr. and R. Medzhitov, *Innate immune recognition.* Annu Rev Immunol, 2002. **20**: p. 197-216.
3. Heine, H. and E. Lien, *Toll-like receptors and their function in innate and adaptive immunity.* Int Arch Allergy Immunol, 2003. **130**(3): p. 180-92.
4. Froy, O., *Regulation of mammalian defensin expression by Toll-like receptor-dependent and independent signalling pathways.* Cell Microbiol, 2005. **7**(10): p. 1387-97.
5. Miller, S.I., R.K. Ernst, and M.W. Bader, *LPS, TLR4 and infectious disease diversity.* Nat Rev Microbiol, 2005. **3**(1): p. 36-46.
6. Hancock, R.E., *Peptide antibiotics.* Lancet, 1997. **349**(9049): p. 418-22.
7. Hancock, R.E. and D.S. Chapple, *Peptide antibiotics.* Antimicrob Agents Chemother, 1999. **43**(6): p. 1317-23.
8. Wang, G., X. Li, and Z. Wang, *APD2: the updated antimicrobial peptide database and its application in peptide design.* Nucleic Acids Res, 2009. **37**(Database issue): p. D933-7.

9. Crovella, S., et al., *Primate beta-defensins--structure, function and evolution.* Curr Protein Pept Sci, 2005. **6**(1): p. 7-21.

10. Wang, Z. and G. Wang, *APD: the Antimicrobial Peptide Database.* Nucleic Acids Res, 2004. **32**(Database issue): p. D590-2.

11. Thomma, B.P., B.P. Cammue, and K. Thevissen, *Plant defensins.* Planta, 2002. **216**(2): p. 193-202.

12. van Dijk, A., E.J. Veldhuizen, and H.P. Haagsman, *Avian defensins.* Vet Immunol Immunopathol, 2008. **124**(1-2): p. 1-18.

13. Selsted, M.E. and A.J. Ouellette, *Mammalian defensins in the antimicrobial immune response.* Nat Immunol, 2005. **6**(6): p. 551-7.

14. Seebah, S., et al., *Defensins knowledgebase: a manually curated database and information source focused on the defensins family of antimicrobial peptides.* Nucleic Acids Res, 2007. **35**(Database issue): p. D265-8.

15. Jenssen, H., P. Hamill, and R.E. Hancock, *Peptide antimicrobial agents.* Clin Microbiol Rev, 2006. **19**(3): p. 491-511.

16. Oppenheim, J.J. and D. Yang, *Alarmins: chemotactic activators of immune responses.* Curr Opin Immunol, 2005. **17**(4): p. 359-65.

17. Schutte, B.C., et al., *Discovery of five conserved beta -defensin gene clusters using a computational search strategy.* Proc Natl Acad Sci U S A, 2002. **99**(4): p. 2129-33.

18. Zeya, H.I. and J.K. Spitznagel, *Cationic proteins of polymorphonuclear leukocyte lysosomes. II. Composition, properties, and mechanism of antibacterial action.* J Bacteriol, 1966. **91**(2): p. 755-62.

19. Selsted, M.E., et al., *Primary structures of six antimicrobial peptides of rabbit peritoneal neutrophils.* J Biol Chem, 1985. **260**(8): p. 4579-84.

20. Selsted, M.E., D. Szklarek, and R.I. Lehrer, *Purification and antibacterial activity of antimicrobial peptides of rabbit granulocytes.* Infect Immun, 1984. **45**(1): p. 150-4.

21. Selsted, M.E., et al., *Primary structures of three human neutrophil defensins.* J Clin Invest, 1985. **76**(4): p. 1436-9.

22. Ganz, T., et al., *Defensins. Natural peptide antibiotics of human neutrophils.* J Clin Invest, 1985. **76**(4): p. 1427-35.

23. Wilde, C.G., et al., *Purification and characterization of human neutrophil peptide 4, a novel member of the defensin family.* J Biol Chem, 1989. **264**(19): p. 11200-3.

24. Ganz, T., *Defensins: antimicrobial peptides of innate immunity.* Nat Rev Immunol, 2003. **3**(9): p. 710-20.

25. Jones, D.E. and C.L. Bevins, *Defensin-6 mRNA in human Paneth cells: implications for antimicrobial peptides in host defense of the human bowel.* FEBS Lett, 1993. **315**(2): p. 187-92.

26. Jones, D.E. and C.L. Bevins, *Paneth cells of the human small intestine express an antimicrobial peptide gene.* J Biol Chem, 1992. **267**(32): p. 23216-25.

27. Ayabe, T., et al., *Secretion of microbicidal alpha-defensins by intestinal Paneth cells in response to bacteria.* Nat Immunol, 2000. **1**(2): p. 113-8.

28. Porter, E.M., et al., *Isolation of human intestinal defensins from ileal neobladder urine.* FEBS Lett, 1998. **434**(3): p. 272-6.

29. Daher, K.A., et al., *Isolation and characterization of human defensin cDNA clones.* Proc Natl Acad Sci U S A, 1988. **85**(19): p. 7327-31.

30. Valore, E.V. and T. Ganz, *Posttranslational processing of defensins in immature human myeloid cells.* Blood, 1992. **79**(6): p. 1538-44.

31. Wilson, C.L., et al., *Regulation of intestinal alpha-defensin activation by the metalloproteinase matrilysin in innate host defense.* Science, 1999. **286**(5437): p. 113-7.

32. Ghosh, D., et al., *Paneth cell trypsin is the processing enzyme for human defensin-5.* Nat Immunol, 2002. **3**(6): p. 583-90.

33.   Diamond, G., et al., *Tracheal antimicrobial peptide, a cysteine-rich peptide from mammalian tracheal mucosa: peptide isolation and cloning of a cDNA.* Proc Natl Acad Sci U S A, 1991. **88**(9): p. 3952-6.

34.   Selsted, M.E., et al., *Purification, primary structures, and antibacterial activities of beta-defensins, a new family of antimicrobial peptides from bovine neutrophils.* J Biol Chem, 1993. **268**(9): p. 6641-8.

35.   Tang, Y.Q. and M.E. Selsted, *Characterization of the disulfide motif in BNBD-12, an antimicrobial beta-defensin peptide from bovine neutrophils.* J Biol Chem, 1993. **268**(9): p. 6649-53.

36.   Bensch, K.W., et al., *hBD-1: a novel beta-defensin from human plasma.* FEBS Lett, 1995. **368**(2): p. 331-5.

37.   Valore, E.V., et al., *Human beta-defensin-1: an antimicrobial peptide of urogenital tissues.* J Clin Invest, 1998. **101**(8): p. 1633-42.

38.   Harder, J. and J.M. Schroder, *Psoriatic scales: a promising source for the isolation of human skin-derived antimicrobial proteins.* J Leukoc Biol, 2005. **77**(4): p. 476-86.

39.   Harder, J., et al., *A peptide antibiotic from human skin.* Nature, 1997. **387**(6636): p. 861.

40.   Harder, J., et al., *Mucoid Pseudomonas aeruginosa, TNF-alpha, and IL-1beta, but not IL-6, induce human beta-defensin-2 in respiratory epithelia.* Am J Respir Cell Mol Biol, 2000. **22**(6): p. 714-21.

41.   Harder, J., et al., *Isolation and characterization of human beta -defensin-3, a novel human inducible peptide antibiotic.* J Biol Chem, 2001. **276**(8): p. 5707-13.

42.   Jia, H.P., et al., *Discovery of new human beta-defensins using a genomics-based approach.* Gene, 2001. **263**(1-2): p. 211-8.

43.   Garcia, J.R., et al., *Human beta-defensin 4: a novel inducible peptide with a specific salt-sensitive spectrum of antimicrobial activity.* Faseb J, 2001. **15**(10): p. 1819-21.

44.   Rodriguez-Jimenez, F.J., et al., *Distribution of new human beta-defensin genes clustered on chromosome 20 in functionally different segments of epididymis.* Genomics, 2003. **81**(2): p. 175-83.

45.   Radhakrishnan, Y., et al., *Identification, characterization, and evolution of a primate beta-defensin gene cluster.* Genes Immun, 2005. **6**(3): p. 203-10.

46.   Yanagi, S., et al., *Isolation of human beta-defensin-4 in lung tissue and its increase in lower respiratory tract infection.* Respir Res, 2005. **6**: p. 130.

47.   Liu, Q., et al., *Primate epididymis-specific proteins: characterization of ESC42, a novel protein containing a trefoil-like motif in monkey and human.* Endocrinology, 2001. **142**(10): p. 4529-39.

48.   Semple, C.A., et al., *The changing of the guard: Molecular diversity and rapid evolution of beta-defensins.* Mol Divers, 2006. **10**(4): p. 575-84.

49.   Yang, D., et al., *Multiple roles of antimicrobial defensins, cathelicidins, and eosinophil-derived neurotoxin in host defense.* Annu Rev Immunol, 2004. **22**: p. 181-215.

50.   Tang, Y.Q., et al., *A cyclic antimicrobial peptide produced in primate leukocytes by the ligation of two truncated alpha-defensins.* Science, 1999. **286**(5439): p. 498-502.

51.   Leonova, L., et al., *Circular minidefensins and posttranslational generation of molecular diversity.* J Leukoc Biol, 2001. **70**(3): p. 461-4.

52.   Nguyen, T.X., A.M. Cole, and R.I. Lehrer, *Evolution of primate theta-defensins: a serpentine path to a sweet tooth.* Peptides, 2003. **24**(11): p. 1647-54.

53.   Venkataraman, N., et al., *Reawakening Retrocyclins: Ancestral Human Defensins Active Against HIV-1.* PLoS Biol, 2009. **7**(4): p. e95.

54.   Zhao, C., I. Wang, and R.I. Lehrer, *Widespread expression of beta-defensin hBD-1 in human secretory glands and epithelial cells.* FEBS Lett, 1996. **396**(2-3): p. 319-22.

55. Zhu, B.D., et al., *Mycobacterium bovis bacille Calmette-Guerin (BCG) enhances human beta-defensin-1 gene transcription in human pulmonary gland epithelial cells.* Acta Pharmacol Sin, 2003. **24**(9): p. 907-12.

56. Sorensen, O.E., et al., *Differential regulation of beta-defensin expression in human skin by microbial stimuli.* J Immunol, 2005. **174**(8): p. 4870-9.

57. Kao, C.Y., et al., *IL-17 markedly up-regulates beta-defensin-2 expression in human airway epithelium via JAK and NF-kappaB signaling pathways.* J Immunol, 2004. **173**(5): p. 3482-91.

58. Schroder, J.M. and J. Harder, *Human beta-defensin-2.* Int J Biochem Cell Biol, 1999. **31**(6): p. 645-51.

59. O'Neil, D.A., *Regulation of expression of beta-defensins: endogenous enteric peptide antibiotics.* Mol Immunol, 2003. **40**(7): p. 445-50.

60. Wehkamp, J., et al., *NF-kappaB- and AP-1-mediated induction of human beta defensin-2 in intestinal epithelial cells by Escherichia coli Nissle 1917: a novel effect of a probiotic bacterium.* Infect Immun, 2004. **72**(10): p. 5750-8.

61. Tsutsumi-Ishii, Y. and I. Nagaoka, *NF-kappa B-mediated transcriptional regulation of human beta-defensin-2 gene following lipopolysaccharide stimulation.* J Leukoc Biol, 2002. **71**(1): p. 154-62.

62. Goldman, M.J., et al., *Human beta-defensin-1 is a salt-sensitive antibiotic in lung that is inactivated in cystic fibrosis.* Cell, 1997. **88**(4): p. 553-60.

63. Bals, R., et al., *Human beta-defensin 2 is a salt-sensitive peptide antibiotic expressed in human lung.* J Clin Invest, 1998. **102**(5): p. 874-80.

64. Schulz, A., et al., *Engineering disulfide bonds of the novel human beta-defensins hBD-27 and hBD-28: differences in disulfide formation and biological activity among human beta-defensins.* Biopolymers, 2005. **80**(1): p. 34-49.

65. Yenugu, S., et al., *The androgen-regulated epididymal sperm-binding protein, human beta-defensin 118 (DEFB118) (formerly ESC42), is an antimicrobial beta-defensin.* Endocrinology, 2004. **145**(7): p. 3165-73.

66. Salzman, N.H., et al., *Protection against enteric salmonellosis in transgenic mice expressing a human intestinal defensin.* Nature, 2003. **422**(6931): p. 522-6.

67. Huang, G.T., et al., *A model for antimicrobial gene therapy: demonstration of human beta-defensin 2 antimicrobial activities in vivo.* Hum Gene Ther, 2002. **13**(17): p. 2017-25.

68. Fujii, G., M.E. Selsted, and D. Eisenberg, *Defensins promote fusion and lysis of negatively charged membranes.* Protein Sci, 1993. **2**(8): p. 1301-12.

69. Lehrer, R.I., et al., *Interaction of human defensins with Escherichia coli. Mechanism of bactericidal activity.* J Clin Invest, 1989. **84**(2): p. 553-61.

70. Boniotto, M., et al., *A study of host defence peptide beta-defensin 3 in primates.* Biochem J, 2003. **374**(Pt 3): p. 707-14.

71. Kagan, B.L., et al., *Antimicrobial defensin peptides form voltage-dependent ion-permeable channels in planar lipid bilayer membranes.* Proc Natl Acad Sci U S A, 1990. **87**(1): p. 210-4.

72. Hoover, D.M., et al., *The structure of human beta-defensin-2 shows evidence of higher order oligomerization.* J Biol Chem, 2000. **275**(42): p. 32911-8.

73. Sass, V., et al., *Mode of action of human beta-defensin 3 against Staphylococcus aureus and transcriptional analysis of responses to defensin challenge.* Int J Med Microbiol, 2008. **298**(7-8): p. 619-33.

74. Territo, M.C., et al., *Monocyte-chemotactic activity of defensins from human neutrophils.* J Clin Invest, 1989. **84**(6): p. 2017-20.

75. Yang, D., et al., *Human neutrophil defensins selectively chemoattract naive T and immature dendritic cells.* J Leukoc Biol, 2000. **68**(1): p. 9-14.

76.   Grigat, J., et al., *Chemoattraction of macrophages, T lymphocytes, and mast cells is evolutionarily conserved within the human alpha-defensin family.* J Immunol, 2007. **179**(6): p. 3958-65.

77.   Yang, D., et al., *Beta-defensins: linking innate and adaptive immunity through dendritic and T cell CCR6.* Science, 1999. **286**(5439): p. 525-8.

78.   Wu, Z., et al., *Engineering disulfide bridges to dissect antimicrobial and chemotactic activities of human beta-defensin 3.* Proc Natl Acad Sci U S A, 2003. **100**(15): p. 8880-5.

79.   Chen, X., et al., *Antimicrobial peptides human beta-defensin (hBD)-3 and hBD-4 activate mast cells and increase skin vascular permeability.* Eur J Immunol, 2007. **37**(2): p. 434-44.

80.   Niyonsaba, F., et al., *Epithelial cell-derived human beta-defensin-2 acts as a chemotaxin for mast cells through a pertussis toxin-sensitive and phospholipase C-dependent pathway.* Int Immunol, 2002. **14**(4): p. 421-6.

81.   Befus, A.D., et al., *Neutrophil defensins induce histamine secretion from mast cells: mechanisms of action.* J Immunol, 1999. **163**(2): p. 947-53.

82.   Chertov, O., et al., *Identification of defensin-1, defensin-2, and CAP37/azurocidin as T-cell chemoattractant proteins released from interleukin-8-stimulated neutrophils.* J Biol Chem, 1996. **271**(6): p. 2935-40.

83.   Baroni, A., et al., *Antimicrobial human beta-defensin-2 stimulates migration, proliferation and tube formation of human umbilical vein endothelial cells.* Peptides, 2009. **30**(2): p. 267-72.

84.   Niyonsaba, F., et al., *Antimicrobial peptides human beta-defensins stimulate epidermal keratinocyte migration, proliferation and production of proinflammatory cytokines and chemokines.* J Invest Dermatol, 2007. **127**(3): p. 594-604.

85.   Lehrer, R.I., *Primate defensins.* Nat Rev Microbiol, 2004. **2**(9): p. 727-38.

86.   Biragyn, A., et al., *Toll-like receptor 4-dependent activation of dendritic cells by beta-defensin 2.* Science, 2002. **298**(5595): p. 1025-9.

87.   Biragyn, A., et al., *Mediators of innate immunity that target immature, but not mature, dendritic cells induce antitumor immunity when genetically fused with nonimmunogenic tumor antigens.* J Immunol, 2001. **167**(11): p. 6644-53.

88.   Biragyn, A., et al., *Tumor-associated embryonic antigen-expressing vaccines that target CCR6 elicit potent CD8+ T cell-mediated protective and therapeutic antitumor immunity.* J Immunol, 2007. **179**(2): p. 1381-8.

89.   Lillard, J.W., Jr., et al., *Mechanisms for induction of acquired host immunity by neutrophil peptide defensins.* Proc Natl Acad Sci U S A, 1999. **96**(2): p. 651-6.

90.   Brogden, K.A., et al., *Defensin-induced adaptive immunity in mice and its potential in preventing periodontal disease.* Oral Microbiol Immunol, 2003. **18**(2): p. 95-9.

91.   Conejo-Garcia, J.R., et al., *Tumor-infiltrating dendritic cell precursors recruited by a beta-defensin contribute to vasculogenesis under the influence of Vegf-A.* Nat Med, 2004. **10**(9): p. 950-8.

92.   Schibli, D.J., et al., *The solution structures of the human beta-defensins lead to a better understanding of the potent bactericidal activity of HBD3 against Staphylococcus aureus.* J Biol Chem, 2002. **277**(10): p. 8279-89.

93.   Hoover, D.M., O. Chertov, and J. Lubkowski, *The structure of human beta-defensin-1: new insights into structural properties of beta-defensins.* J Biol Chem, 2001. **276**(42): p. 39021-6.

94.   Hill, C.P., et al., *Crystal structure of defensin HNP-3, an amphiphilic dimer: mechanisms of membrane permeabilization.* Science, 1991. **251**(5000): p. 1481-5.

95.   Szyk, A., et al., *Crystal structures of human alpha-defensins HNP4, HD5, and HD6.* Protein Sci, 2006. **15**(12): p. 2749-60.

96.   Sawai, M.V., et al., *The NMR structure of human beta-defensin-2 reveals a novel alpha-helical segment.* Biochemistry, 2001. **40**(13): p. 3810-6.

97. Trabi, M., H.J. Schirra, and D.J. Craik, *Three-dimensional structure of RTD-1, a cyclic antimicrobial defensin from Rhesus macaque leukocytes.* Biochemistry, 2001. **40**(14): p. 4211-21.

98. Campopiano, D.J., et al., *Structure-activity relationships in defensin dimers: a novel link between beta-defensin tertiary structure and antimicrobial activity.* J Biol Chem, 2004. **279**(47): p. 48671-9.

99. Hieshima, K., et al., *Molecular cloning of a novel human CC chemokine liver and activation-regulated chemokine (LARC) expressed in liver. Chemotactic activity for lymphocytes and gene localization on chromosome 2.* J Biol Chem, 1997. **272**(9): p. 5846-53.

100. Hromas, R., et al., *Cloning and characterization of exodus, a novel beta-chemokine.* Blood, 1997. **89**(9): p. 3315-22.

101. Charbonnier, A.S., et al., *Macrophage inflammatory protein 3alpha is involved in the constitutive trafficking of epidermal langerhans cells.* J Exp Med, 1999. **190**(12): p. 1755-68.

102. Homey, B., et al., *Up-regulation of macrophage inflammatory protein-3 alpha/CCL20 and CC chemokine receptor 6 in psoriasis.* J Immunol, 2000. **164**(12): p. 6621-32.

103. Hoover, D.M., et al., *The structure of human macrophage inflammatory protein-3alpha /CCL20. Linking antimicrobial and CC chemokine receptor-6-binding activities with human beta-defensins.* J Biol Chem, 2002. **277**(40): p. 37647-54.

104. Chan, D.I., et al., *Human macrophage inflammatory protein 3alpha: protein and peptide nuclear magnetic resonance solution structures, dimerization, dynamics, and anti-infective properties.* Antimicrob Agents Chemother, 2008. **52**(3): p. 883-94.

105. Malik, Z.A. and B.F. Tack, *Structure of human MIP-3alpha chemokine.* Acta Crystallogr Sect F Struct Biol Cryst Commun, 2006. **62**(Pt 7): p. 631-4.

106. Yang, D., et al., *Many chemokines including CCL20/MIP-3alpha display antimicrobial activity.* J Leukoc Biol, 2003. **74**(3): p. 448-55.

107. Ong, P.Y., et al., *Endogenous antimicrobial peptides and skin infections in atopic dermatitis.* N Engl J Med, 2002. **347**(15): p. 1151-60.

108. Christophers, E. and T. Henseler, *Contrasting disease patterns in psoriasis and atopic dermatitis.* Arch Dermatol Res, 1987. **279 Suppl**: p. S48-51.

109. Nomura, I., et al., *Cytokine milieu of atopic dermatitis, as compared to psoriasis, skin prevents induction of innate immune response genes.* J Immunol, 2003. **171**(6): p. 3262-9.

110. Wehkamp, J., et al., *Inducible and constitutive beta-defensins are differentially expressed in Crohn's disease and ulcerative colitis.* Inflamm Bowel Dis, 2003. **9**(4): p. 215-23.

111. Wehkamp, J., et al., *Reduced Paneth cell alpha-defensins in ileal Crohn's disease.* Proc Natl Acad Sci U S A, 2005. **102**(50): p. 18129-34.

112. Wehkamp, J., et al., *Defensin deficiency, intestinal microbes, and the clinical phenotypes of Crohn's disease.* J Leukoc Biol, 2005. **77**(4): p. 460-5.

113. Hollox, E.J., J.A. Armour, and J.C. Barber, *Extensive normal copy number variation of a beta-defensin antimicrobial-gene cluster.* Am J Hum Genet, 2003. **73**(3): p. 591-600.

114. Hollox, E.J., et al., *Psoriasis is associated with increased beta-defensin genomic copy number.* Nat Genet, 2008. **40**(1): p. 23-5.

115. Fellermann, K., et al., *A chromosome 8 gene-cluster polymorphism with low human beta-defensin 2 gene copy number predisposes to Crohn disease of the colon.* Am J Hum Genet, 2006. **79**(3): p. 439-48.

116. O'Sullivan, B.P. and S.D. Freedman, *Cystic fibrosis.* Lancet, 2009. **373**(9678): p. 1891-904.

117.   Smith, J.J., et al., *Cystic fibrosis airway epithelia fail to kill bacteria because of abnormal airway surface fluid.* Cell, 1996. **85**(2): p. 229-36.

118.   Singh, P.K., et al., *Production of beta-defensins by human airway epithelia.* Proc Natl Acad Sci U S A, 1998. **95**(25): p. 14961-6.

119.   Venter, J.C., et al., *The sequence of the human genome.* Science, 2001. **291**(5507): p. 1304-51.

120.   Lander, E.S., et al., *Initial sequencing and analysis of the human genome.* Nature, 2001. **409**(6822): p. 860-921.

121.   Takeda, S., et al., *Identification of G protein-coupled receptor genes from the human genome sequence.* FEBS Lett, 2002. **520**(1-3): p. 97-101.

122.   Hopkins, A.L. and C.R. Groom, *The druggable genome.* Nat Rev Drug Discov, 2002. **1**(9): p. 727-30.

123.   Kolakowski, L.F., Jr., *GCRDb: a G-protein-coupled receptor database.* Receptors Channels, 1994. **2**(1): p. 1-7.

124.   Attwood, T.K. and J.B. Findlay, *Fingerprinting G-protein-coupled receptors.* Protein Eng, 1994. **7**(2): p. 195-203.

125.   Schioth, H.B. and R. Fredriksson, *The GRAFS classification system of G-protein coupled receptors in comparative perspective.* Gen Comp Endocrinol, 2005. **142**(1-2): p. 94-101.

126.   Fredriksson, R., et al., *The G-protein-coupled receptors in the human genome form five main families. Phylogenetic analysis, paralogon groups, and fingerprints.* Mol Pharmacol, 2003. **63**(6): p. 1256-72.

127.   Jacoby, E., et al., *The 7 TM G-protein-coupled receptor target family.* ChemMedChem, 2006. **1**(8): p. 761-82.

128.   Kristiansen, K., *Molecular mechanisms of ligand binding, signaling, and regulation within the superfamily of G-protein-coupled receptors: molecular modeling and mutagenesis approaches to receptor structure and function.* Pharmacol Ther, 2004. **103**(1): p. 21-80.

129.   Pierce, K.L., R.T. Premont, and R.J. Lefkowitz, *Seven-transmembrane receptors.* Nat Rev Mol Cell Biol, 2002. **3**(9): p. 639-50.

130.   Theodoropoulou, M.C., et al., *gpDB: a database of GPCRs, G-proteins, effectors and their interactions.* Bioinformatics, 2008. **24**(12): p. 1471-2.

131.   Fang, Y.C., et al., *RINGdb: an integrated database for G protein-coupled receptors and regulators of G protein signaling.* BMC Genomics, 2006. **7**: p. 317.

132.   Okada, T., K. Takeda, and T. Kouyama, *Highly selective separation of rhodopsin from bovine rod outer segment membranes using combination of divalent cation and alkyl(thio)glucoside.* Photochem Photobiol, 1998. **67**(5): p. 495-9.

133.   Wimalawansa, S.J., *Purification and biochemical characterization of neuropeptide Y2 receptor.* J Biol Chem, 1995. **270**(31): p. 18523-30.

134.   White, J.F., et al., *Automated large-scale purification of a G protein-coupled receptor for neurotensin.* FEBS Lett, 2004. **564**(3): p. 289-93.

135.   Weiss, H.M. and R. Grisshammer, *Purification and characterization of the human adenosine A(2a) receptor functionally expressed in Escherichia coli.* Eur J Biochem, 2002. **269**(1): p. 82-92.

136.   Baneres, J.L. and J. Parello, *Structure-based analysis of GPCR function: evidence for a novel pentameric assembly between the dimeric leukotriene B4 receptor BLT1 and the G-protein.* J Mol Biol, 2003. **329**(4): p. 815-29.

137.   Baneres, J.L., et al., *Structure-based analysis of GPCR function: conformational adaptation of both agonist and receptor upon leukotriene B4 binding to recombinant BLT1.* J Mol Biol, 2003. **329**(4): p. 801-14.

138.   Lundstrom, K., *Structural genomics for membrane proteins.* Cell Mol Life Sci, 2006. **63**(22): p. 2597-607.

139.   Sarramegna, V., et al., *Heterologous expression of G-protein-coupled receptors: comparison of expression systems fron the standpoint of large-scale production and purification.* Cell Mol Life Sci, 2003. **60**(8): p. 1529-46.

140.   Gemmill, T.R. and R.B. Trimble, *Overview of N- and O-linked oligosaccharide structures found in various yeast species.* Biochim Biophys Acta, 1999. **1426**(2): p. 227-37.

141.   Jaakola, V.P., et al., *The 2.6 angstrom crystal structure of a human A2A adenosine receptor bound to an antagonist.* Science, 2008. **322**(5905): p. 1211-7.

142.   Reeves, P.J., et al., *Structure and function in rhodopsin: high-level expression of rhodopsin with restricted and homogeneous N-glycosylation by a tetracycline-inducible N-acetylglucosaminyltransferase I-negative HEK293S stable mammalian cell line.* Proc Natl Acad Sci U S A, 2002. **99**(21): p. 13419-24.

143.   Reeves, P.J., J.M. Kim, and H.G. Khorana, *Structure and function in rhodopsin: a tetracycline-inducible system in stable mammalian cell lines for high-level expression of opsin mutants.* Proc Natl Acad Sci U S A, 2002. **99**(21): p. 13413-8.

144.   Chelikani, P., et al., *The synthesis and high-level expression of a beta2-adrenergic receptor gene in a tetracycline-inducible stable mammalian cell line.* Protein Sci, 2006. **15**(6): p. 1433-40.

145.   Hassaine, G., et al., *Semliki Forest virus vectors for overexpression of 101 G protein-coupled receptors in mammalian host cells.* Protein Expr Purif, 2006. **45**(2): p. 343-51.

146.   Lundstrom, K., et al., *Structural genomics on membrane proteins: comparison of more than 100 GPCRs in 3 expression systems.* J Struct Funct Genomics, 2006. **7**(2): p. 77-91.

147.   Michalke, K., et al., *Mammalian G-protein-coupled receptor expression in Escherichia coli: I. High-throughput large-scale production as inclusion bodies.* Anal Biochem, 2009. **386**(2): p. 147-55.

148.   Palczewski, K., et al., *Crystal structure of rhodopsin: A G protein-coupled receptor.* Science, 2000. **289**(5480): p. 739-45.

149.   Warne, T., et al., *Structure of a beta1-adrenergic G-protein-coupled receptor.* Nature, 2008. **454**(7203): p. 486-91.

150.   Rosenbaum, D.M., et al., *GPCR engineering yields high-resolution structural insights into beta2-adrenergic receptor function.* Science, 2007. **318**(5854): p. 1266-73.

151.   Cherezov, V., et al., *High-resolution crystal structure of an engineered human beta2-adrenergic G protein-coupled receptor.* Science, 2007. **318**(5854): p. 1258-65.

152.   Rasmussen, S.G., et al., *Crystal structure of the human beta2 adrenergic G-protein-coupled receptor.* Nature, 2007. **450**(7168): p. 383-7.

153.   Scheerer, P., et al., *Crystal structure of opsin in its G-protein-interacting conformation.* Nature, 2008. **455**(7212): p. 497-502.

154.   Park, J.H., et al., *Crystal structure of the ligand-free G-protein-coupled receptor opsin.* Nature, 2008. **454**(7201): p. 183-7.

155.   Allen, S.J., S.E. Crown, and T.M. Handel, *Chemokine: receptor structure, interactions, and antagonism.* Annu Rev Immunol, 2007. **25**: p. 787-820.

156.   *Chemokine/chemokine receptor nomenclature.* J Leukoc Biol, 2001. **70**(3): p. 465-6.

157.   Power, C.A., et al., *Cloning and characterization of a specific receptor for the novel CC chemokine MIP-3alpha from lung dendritic cells.* J Exp Med, 1997. **186**(6): p. 825-35.

158.   Zaballos, A., et al., *Molecular cloning and RNA expression of two new human chemokine receptor-like genes.* Biochem Biophys Res Commun, 1996. **227**(3): p. 846-53.

159. Liao, F., H.H. Lee, and J.M. Farber, *Cloning of STRL22, a new human gene encoding a G-protein-coupled receptor related to chemokine receptors and located on chromosome 6q27.* Genomics, 1997. **40**(1): p. 175-80.

160. Baba, M., et al., *Identification of CCR6, the specific receptor for a novel lymphocyte-directed CC chemokine LARC.* J Biol Chem, 1997. **272**(23): p. 14893-8.

161. Greaves, D.R., et al., *CCR6, a CC chemokine receptor that interacts with macrophage inflammatory protein 3alpha and is highly expressed in human dendritic cells.* J Exp Med, 1997. **186**(6): p. 837-44.

162. Liao, F., et al., *STRL22 is a receptor for the CC chemokine MIP-3alpha.* Biochem Biophys Res Commun, 1997. **236**(1): p. 212-7.

163. Ai, L.S. and F. Liao, *Mutating the four extracellular cysteines in the chemokine receptor CCR6 reveals their differing roles in receptor trafficking, ligand binding, and signaling.* Biochemistry, 2002. **41**(26): p. 8332-41.

164. Ai, L.S., et al., *Molecular characterization of CCR6: involvement of multiple domains in ligand binding and receptor signaling.* J Biomed Sci, 2004. **11**(6): p. 818-28.

165. Huang, C.C., et al., *Structures of the CCR5 N terminus and of a tyrosine-sulfated antibody with HIV-1 gp120 and CD4.* Science, 2007. **317**(5846): p. 1930-4.

166. Yang, C.C., et al., *Chemokine receptor CCR6 transduces signals that activate p130Cas and alter cAMP-stimulated ion transport in human intestinal epithelial cells.* Am J Physiol Cell Physiol, 2005. **288**(2): p. C321-8.

167. Vongsa, R.A., N.P. Zimmerman, and M.B. Dwinell, *CCR6 regulation of the actin cytoskeleton orchestrates human beta defensin-2- and CCL20-mediated restitution of colonic epithelial cells.* J Biol Chem, 2009. **284**(15): p. 10034-45.

168. Thelen, M., *Dancing to the tune of chemokines.* Nat Immunol, 2001. **2**(2): p. 129-34.

169. Zhang, Y., M.E. Devries, and J. Skolnick, *Structure modeling of all identified G protein-coupled receptors in the human genome.* PLoS Comput Biol, 2006. **2**(2): p. e13.

170. Yang, D., et al., *Cutting edge: immature dendritic cells generated from monocytes in the presence of TGF-beta 1 express functional C-C chemokine receptor 6.* J Immunol, 1999. **163**(4): p. 1737-41.

171. Dieu-Nosjean, M.C., et al., *Macrophage inflammatory protein 3alpha is expressed at inflamed epithelial surfaces and is the most potent chemokine known in attracting Langerhans cell precursors.* J Exp Med, 2000. **192**(5): p. 705-18.

172. Dieu, M.C., et al., *Selective recruitment of immature and mature dendritic cells by distinct chemokines expressed in different anatomic sites.* J Exp Med, 1998. **188**(2): p. 373-86.

173. Krzysiek, R., et al., *Regulation of CCR6 chemokine receptor expression and responsiveness to macrophage inflammatory protein-3alpha/CCL20 in human B cells.* Blood, 2000. **96**(7): p. 2338-45.

174. Liao, F., et al., *CC-chemokine receptor 6 is expressed on diverse memory subsets of T cells and determines responsiveness to macrophage inflammatory protein 3 alpha.* J Immunol, 1999. **162**(1): p. 186-94.

175. Acosta-Rodriguez, E.V., et al., *Surface phenotype and antigenic specificity of human interleukin 17-producing T helper memory cells.* Nat Immunol, 2007. **8**(6): p. 639-46.

176. Kondo, T., H. Takata, and M. Takiguchi, *Functional expression of chemokine receptor CCR6 on human effector memory CD8+ T cells.* Eur J Immunol, 2007. **37**(1): p. 54-65.

177. Lugering, A., et al., *Absence of CCR6 inhibits CD4+ regulatory T-cell development and M-cell formation inside Peyer's patches.* Am J Pathol, 2005. **166**(6): p. 1647-54.

178. Cook, D.N., et al., *CCR6 mediates dendritic cell localization, lymphocyte homeostasis, and immune responses in mucosal tissue.* Immunity, 2000. **12**(5): p. 495-503.

179. Osterholzer, J.J., et al., *CCR2 and CCR6, but not endothelial selectins, mediate the accumulation of immature dendritic cells within the lungs of mice in response to particulate antigen.* J Immunol, 2005. **175**(2): p. 874-83.

180. Le Borgne, M., et al., *Dendritic cells rapidly recruited into epithelial tissues via CCR6/CCL20 are responsible for CD8+ T cell crosspriming in vivo.* Immunity, 2006. **24**(2): p. 191-201.

181. Salazar-Gonzalez, R.M., et al., *CCR6-mediated dendritic cell activation of pathogen-specific T cells in Peyer's patches.* Immunity, 2006. **24**(5): p. 623-32.

182. Demedts, I.K., et al., *Accumulation of dendritic cells and increased CCL20 levels in the airways of patients with chronic obstructive pulmonary disease.* Am J Respir Crit Care Med, 2007. **175**(10): p. 998-1005.

183. Bracke, K.R., et al., *Cigarette smoke-induced pulmonary inflammation and emphysema are attenuated in CCR6-deficient mice.* J Immunol, 2006. **177**(7): p. 4350-9.

184. Wen, H., et al., *The chemokine receptor CCR6 is an important component of the innate immune response.* Eur J Immunol, 2007. **37**(9): p. 2487-98.

185. Lukacs, N.W., et al., *Requirement for the chemokine receptor CCR6 in allergic pulmonary inflammation.* J Exp Med, 2001. **194**(4): p. 551-5.

186. Reboldi, A., et al., *C-C chemokine receptor 6-regulated entry of TH-17 cells into the CNS through the choroid plexus is required for the initiation of EAE.* Nat Immunol, 2009. **10**(5): p. 514-23.

Chapter 2

Purification and Functional

Characterization of Human β-Defensins

2.1 - Production of Human β-Defensins

2.1.1 - Introduction

Although a number of defensins have been isolated from natural sources, the difficulty in obtaining the required amount of tissue or fluid, coupled with the labour-intensive, low-yielding isolation steps has led to the use of recombinant DNA technology to provide material for study. This bottleneck in studying the structure-function activity relationships of β-defensins has been overcome to an extent by the success of large scale solid-phase synthesis of both α- and β- defensins [1-3]. However, it has been discovered that due to their innate amphipathic properties defensins often form aggregates resulting in formation of both deletion and truncated products. As an alternative, extensive investigation into appropriate expression systems has been carried out. Early work centred around utilizing both *Escherichia coli* (*E.coli*) and Baculovirus/insect cells as suitable hosts in expression systems that have resulted in moderate expression of defensins [4-7]. The problems associated with recombinant production are the obvious toxicity of defensins and their low expression yields. These problems have been circumvented by using a fusion partner expression system. Both soluble fusion expression using thioredoxin and insoluble fusions using a portion of the *E. coli* tryptophan operon have been successful [8-10]. The former strategy has now been used to purify both wild-type (wt) and GFP-labelled HBD2-4 using either a batch or a continuous exchange *E. coli* cell-free system [9, 11, 12]. However this purification strategy only obtained moderate concentrations of fusion protein and concentrations of cleaved, functional active β-defensins were never revealed. Furthermore, neither the purity nor disulfide bond connectivity were addressed and whether it is possible to reduce and chemically oxidize β-defensins without affecting the functionality of the GFP is currently unknown.

To produce various defensins suitable for structural and functional analyses purification of HBD2 was optimized as part of this study. Prior to the studies discussed in this thesis, a codon-optimised, synthetic HBD2 gene had been cloned into the expression plasmid pET-31b (Helen Fielder, Masters student, Edinburgh University, 2005). However, this plasmid contained multiple copies of this gene including a mutated version. Therefore this plasmid is unsuitable for subsequent HBD2 mutational studies. Thus, the codon-optimized HBD2 gene was re-designed for expression in *E. coli* and amplified using overlapping primers by recursive PCR. The expression strategy combined a ketosteroid isomerase (KSI) fusion and poly-histidine tag. This allowed the protein to be expressed in an insoluble form within inclusion bodies and then be isolated using immobilized metal affinity chromatography (IMAC). Cost-effective chemical cleavage was achieved using cyanogen bromide (CNBr) and the mature peptide was further purified using RP-HPLC.

Our aim was to isolate purified forms of HBD1, HBD2 and three single disulfide HBD2 mutants – each was produced using this procedure allowing routine production of defensins for structure-function studies.

2.1.2 - Synthesis of HBD2 Gene

Six overlapping primers (see Materials and Methods) with codons optimized for expression in *E. coli* were designed to synthesize the HBD2 gene using a recursive PCR reaction [13]. The furthermost 5' and 3' primers coded for the restriction sites *Alw*NI, used for cloning into a linear expression vector pET31b thereby utilizing KSI as a fusion partner. To separate the mature HBD2 from the KSI fusion in a cost-effective way, a single methionine (Met) was engineered in between the 5'*Alw*NI site and the start of HBD2 gene, enabling chemical cleavage using CNBr. Cloning directly into pET-31b would have allowed us to utilize a C-terminal 6X His-tag. However, due to a C-terminal encoded Met, our

Chapter 2: Purification and Functional Characterization of Human β-defensins

released HBD2 would contain a C-terminal homoserine lactone [14]. Therefore a stop codon was incorporated upstream of the 6X His-tag.

Using high fidelity Herculase Hotstart DNA polymerase the recursive PCR generated a major band at 147 bp corresponding to the newly engineered HBD2 gene (Figure 2.1 A). The HBD2 gene was then subjected to a final PCR amplification reaction and 'A' overhangs were added to allow ligation into the linear cloning vector pGEM-T easy vector. Positive clones were sequenced to confirm the fidelity of the PCR reaction. Sequencing of the HBD2 gene revealed a single nucleotide had been mutated in the first position of glycine at position 34 (G34S). Consequently, megaprimer mutagenesis was undertaken to correct the mutation.
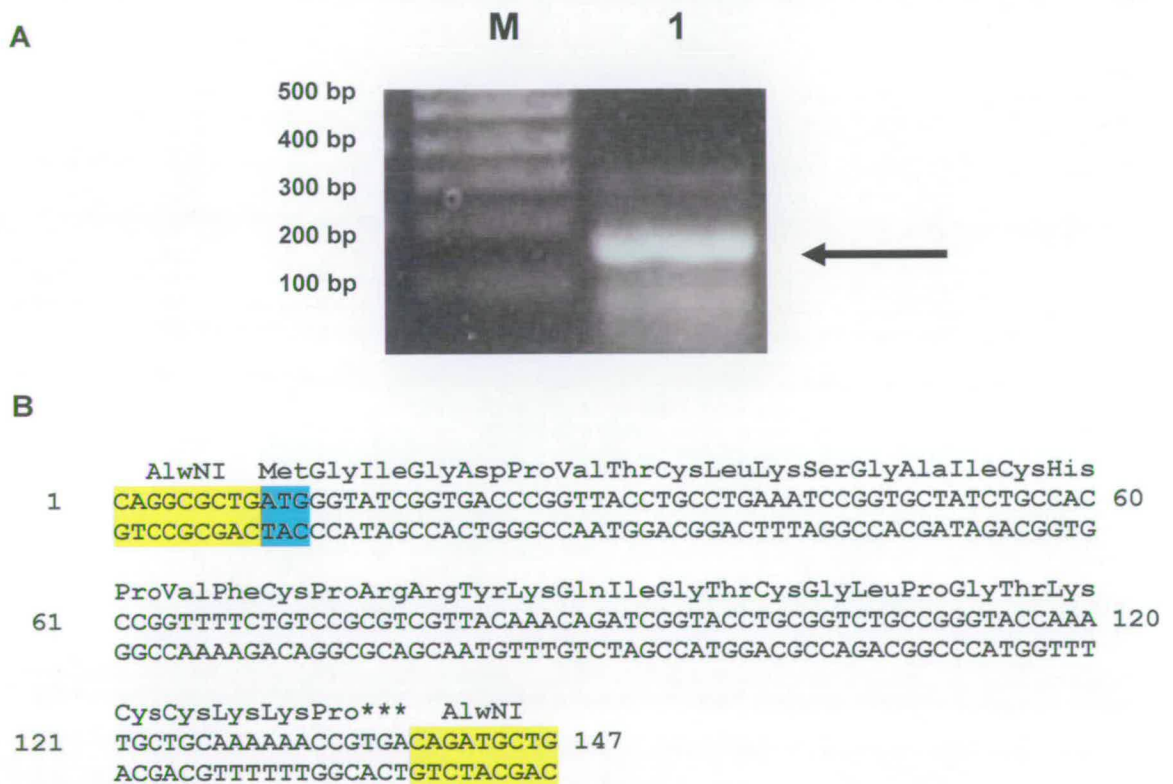
Figure 2.1. Cloning of Codon-Optimized Synthetic HBD2. (A) Synthesis of optimised HBD2 gene by recursive PCR. Lane M, 1 kb DNA Hyperladder I (Bioline); lane 1, recursive HBD2 PCR product. The band indicated by an arrow is synthesised 147 bp codon-optimised HBD2 gene. **(B)** Sequence of synthetic, codon-optimized HBD2 gene (147 bp) after mutational correction. 5' and 3' AlwNI restriction sites (yellow) allowed cloning into plasmid pET-31b and expression of HBD2 as a KSI-HBD2 fusion. The engineered Met (cyan) and stop (***) codons are indicated.

2.1.3 - Construction of the Expression Plasmid using Megaprimer Mutagenesis

Removal of the PCR-induced mutation in the gene-synthesized HBD2 gene was performed using the megaprimer mutagenesis method [15]. The first PCR reaction is responsible for the synthesis of the mega primer and involves the mutagenic primer and the plasmid specific primer on the complementary strand. This is subsequently used in a second PCR along with the opposite plasmid specific primer to the one used in the first reaction.

Using pGEM/HBD2 (G34S) as the template, the mutagenic primer (S34G primer For) and plasmid specific primer (pGEM Rev Mutagenesis) were used to synthesize the megaprimer, now incorporating the corrected nucleotide. A second PCR reaction including the megaprimer and plasmid specific primer (pGEM For Mutagenesis) generated the full length HBD2 gene still including the 5' and 3' *Alw*NI restriction sites. As before, this gene was cloned into pGEM and verified by DNA sequencing (Figure 2.1 B).

*Alw*NI restriction digested HBD2 was cloned into the expression plasmid pET31b. Furthermore, to replace the 6X His tag lost by inserting a stop codon, KSI-HBD2 fusion gene was cloned into the expression plasmid pET28a via *Nco*I and *Xho*I restriction sites. Thus, a 6X His tag was engineered upstream of the KSI gene producing a HISKSI-HBD2 fusion gene (Figure 2.2).
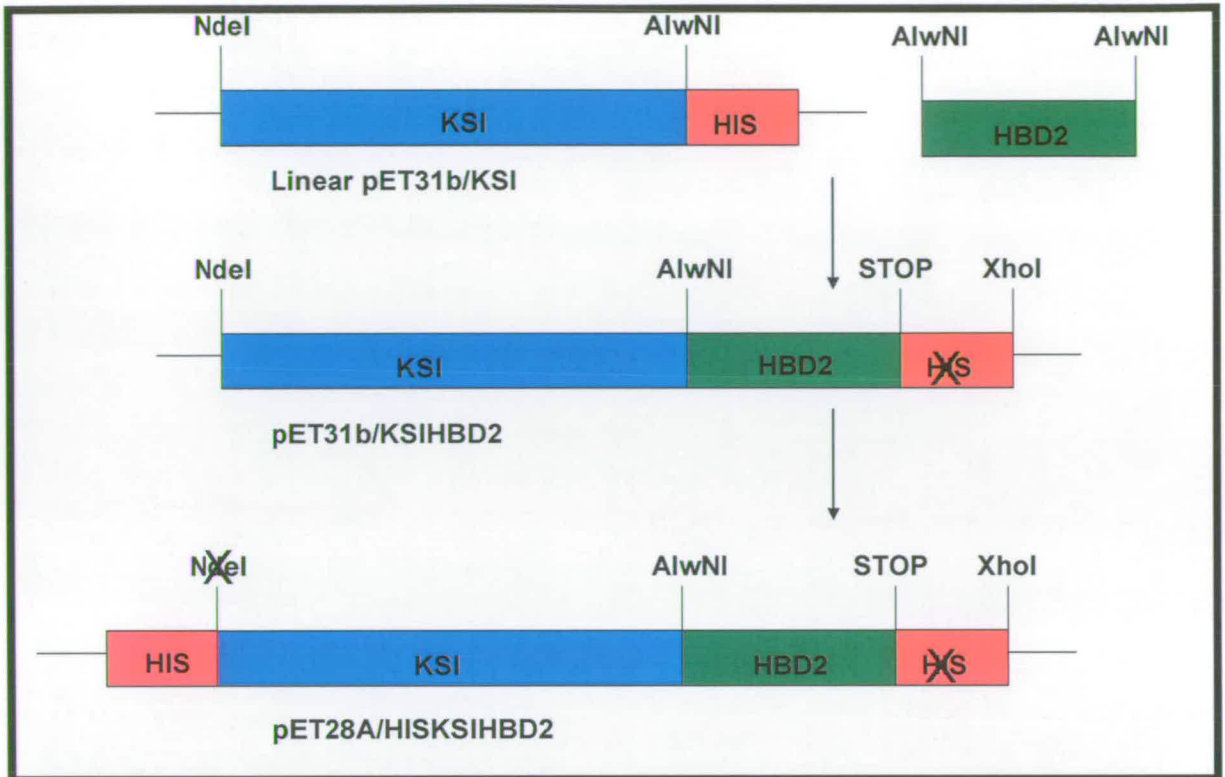
Figure 2.2. Schematic Representation of the Construction of the Expression Plasmid.

This fusion gene was then subjected to two site-directed mutagenesis steps. Both the 5' *Nde*I site and 3' *Alw*NI site flanking the fusion gene contain an ATG Met codon that will reduce the efficiency of CNBr cleavage. Therefore using megaprimer mutagenesis as before, Met was replaced with Alanine (Ala), removing the *Nde*I site but leaving the *Alw*NI restriction site intact for cloning different defensin genes (Figure 2.3 A).

The final expression plasmid pET28a/HISKSI-HBD2 was used for all further studies on HBD2 (Figure 2.3 B).

A

```
1     MGSSHHHHHH SSGLVPRGSH AHTPEHITAV VQRFVAALNA GDLDGIVALF
51    ADDATVEDPV GSEPRSGTAA IREFYANSLK LPLAVELTQE VRAVANEAAF
101   AFTVSFEYQG RKTVVAPIDH FRFNGAGKVV SIRALFGEKN IHACQALMGI
151   GDPVTCLKSG AICHPVFCPR RYKQIGTCGL PGTKCCKKP
```

B
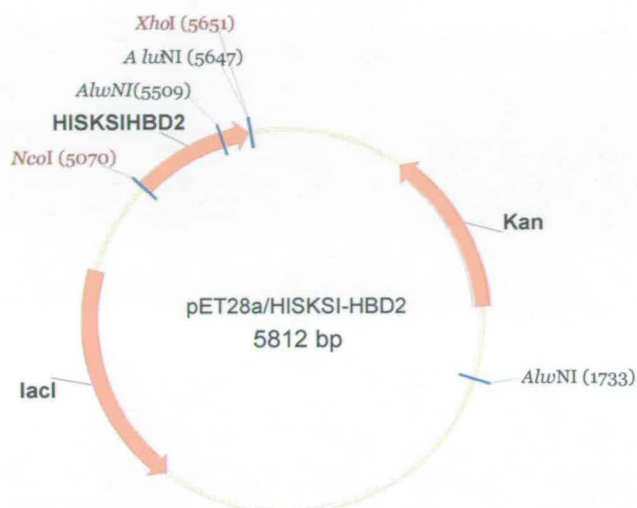
Figure 2.3. HISKSI-HBD2 Fusion Gene. (A) Sequence of HISKSI-HBD2 fusion gene (189 AA). Mature HBD2 peptide highlighted in bold. Met-Ala mutations in KSI (M1A and M126A) are underlined. **(B)** Schematic representation of expression vector pET28a HISKSI-HBD2.

2.1.4 - Over Expression of HBD2 Fusion Protein in *E.coli*

The ability of pET28a/HISKSI-HBD2 to express the fusion protein at high levels in *E. coli* was tested in the *E. coli* host strain BL21 (DE3) on a small scale (10 ml LB). Transformed *E. coli* was either induced with 1 mM IPTG or left to replicate un-induced for 6 hours. Protein analysis by SDS-PAGE clearly showed an induced protein band corresponding to a mass of ~23 kDa (Figure 2.4) indicating the fusion protein had been over expressed. Due to the high expression level of the induced protein band no further optimization of expression conditions were necessary. Therefore large scale expression studies were carried out to produce large quantities of fusion protein. Typically, six litre cultures produced large, creamy white cell pellets (~12 g) indicative of overexpression of

fusion proteins. Cell pellets were either stored at -20 °C until needed or lysed to isolate the

fusion protein.
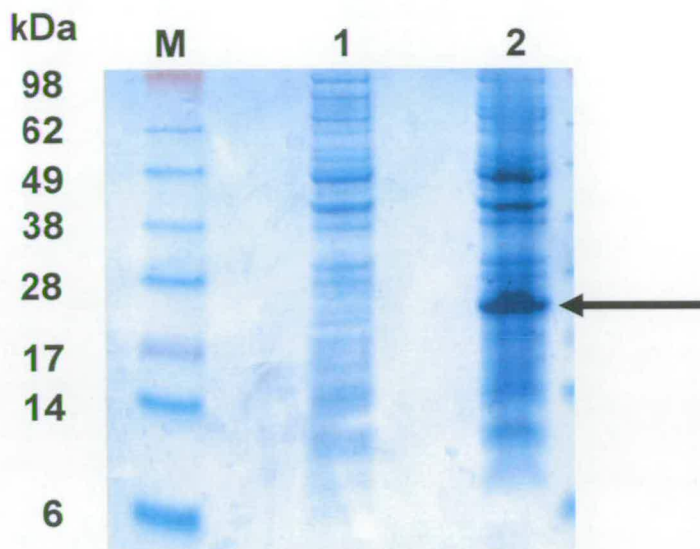
Figure 2.4. Expression of HISKSI-HBD2. 12% Bis-Tris acrylamide gel analysis before and after induction with IPTG. Lane M, SeeBlue 2 protein marker (Invitrogen); lane 1, total crude lysate before induction; lane 2, insoluble fraction after induction. The band indicated by arrow is expected mass of HISKSI-HBD2.

2.1.5 - Purification of Recombinant HBD2 Fusion Protein

Accumulation of insoluble HISKSI-HBD2 as inclusion bodies allowed

centrifugation to be used as a purification step. The resuspended cell pellet was subjected to

enzymatic, chemical and physical cell wall disruption before the pelleted inclusion bodies

were resuspended in denaturing Ni^{2+}-NTA binding buffer. Single step IMAC purification

using nickel resin yielded a highly pure fusion protein.

2.1.6 - CNBr Cleavage of Recombinant HBD2 Fusion Protein

Efficient cleavage of the mature recombinant HBD2 (rHBD2) from its hydrophobic

fusion partner requires an appropriate reaction buffer. The isolated fusion protein was either

dissolved in 70% formic acid or dissolved in acidified 6 M Guanidine HCl, 25 mM Tris-HCl

buffer and the efficiency of cleavage was investigated. Recently it has been shown that 70%

TFA cleavage efficiency is low for amphipathic peptides and was thus not tested [16].

Complete CNBr cleavage was observed in 18-22 hrs in both reaction mixtures. An advantage

of using 70% formic acid is that excess water and excess CNBr can be removed by rotor

evaporation and lyophilization. Mature rHBD2 was then extracted from the fusion mixture

using 0.01% acetic acid and analysed by ESI-MS. Unfortunately mass spectrometric analysis

showed evidence for the presence of mono- and bis-formylated peaks, in addition to the

expected m/z peaks for HBD2 (Appendix A1). Although formylation was partially reversed

by hydrolysis under basic conditions, due to the lowering of the overall yield using these

steps, 6 M GdnHCl was used for all future purifications. Again unreactive CNBr and

hydrogen cyanide, which are by-products in the presence of HCl, were removed by rotor

evaporation. Taking advantage of the inherent insolubility of KSI, dialysis against a slightly

basic reducing buffer caused the cleaved KSI to form a precipitate negating the need for a

chromatography step. Centrifugation allowed the cleaved, soluble, mature, rHBD2 to be

separated from its fusion partner and analysis by SDS-PAGE showed the majority of HBD2

had been cleaved (Figure 2.5).
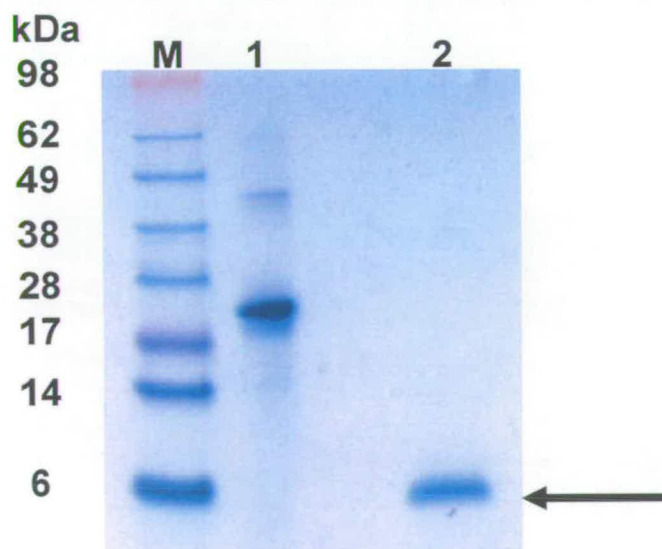
Figure 2.5. CNBr Chemical Cleavage of HBD2 Fusion Protein. 12% Bis-Tris acrylamide gel analysis of HISKSI-HBD2. Lane M, SeeBlue 2 protein marker (Invitrogen); lane 1, insoluble HISKSI-HBD2 before chemical cleavage; lane 2, soluble fraction after chemical cleavage. The band indicated by the arrow is the expected mass of mature rHBD2.

2.1.7 - Purification and Oxidation of Mature Recombinant HBD2

The original purification of reduced rHBD2 was carried out using a reverse phase Poros column attached directly to an AKTA Purifier. Unfortunately the peptide isolated from this step was not of high enough purity to allow for oxidative refolding to the three disulfide bond-containing form. Therefore subsequent purifications utilized a semi-preparative RP-HPLC strategy to purify both reduced and oxidized HBD2 to homogeneity.

A necessary step in production of both synthetic and recombinant defensins is the correct refolding of the peptide. Although the correct folding is problematic for defensins, there are established methods including DMSO oxidation and using redox partners [1, 3, 17]. To optimize refolding, small scale refolding experiments were performed on lyophilized reduced peptide under the following reaction conditions: (1) DMSO oxidation; (2) redox reagents GSH and GSSH; (3) cysteine and cystine in presence or absence of a denaturing agent (Figure 2.6). DMSO oxidation led to extensive precipitation of the peptide and subsequently only a low yield of oxidized HBD2 was recovered. Denaturing agent GdnHCl has been shown to assist in the oxidation process [3]. However using the redox pair cysteine/cystine under both denaturing and non denaturing conditions, the latter was found to be more efficient at producing oxidized HBD2. This is in agreement with Chino et al. who when optimizing the oxidation of HBD1-4 found GndHCl actually interfered with the folding process [17]. GSH/GSSH at a ratio of 1:100:10 (peptide:GSH:GSSG) was found to be as efficient as cysteine/cystine however due to the significant extra cost of glutathione the latter was chosen for all large scale oxidation reactions.
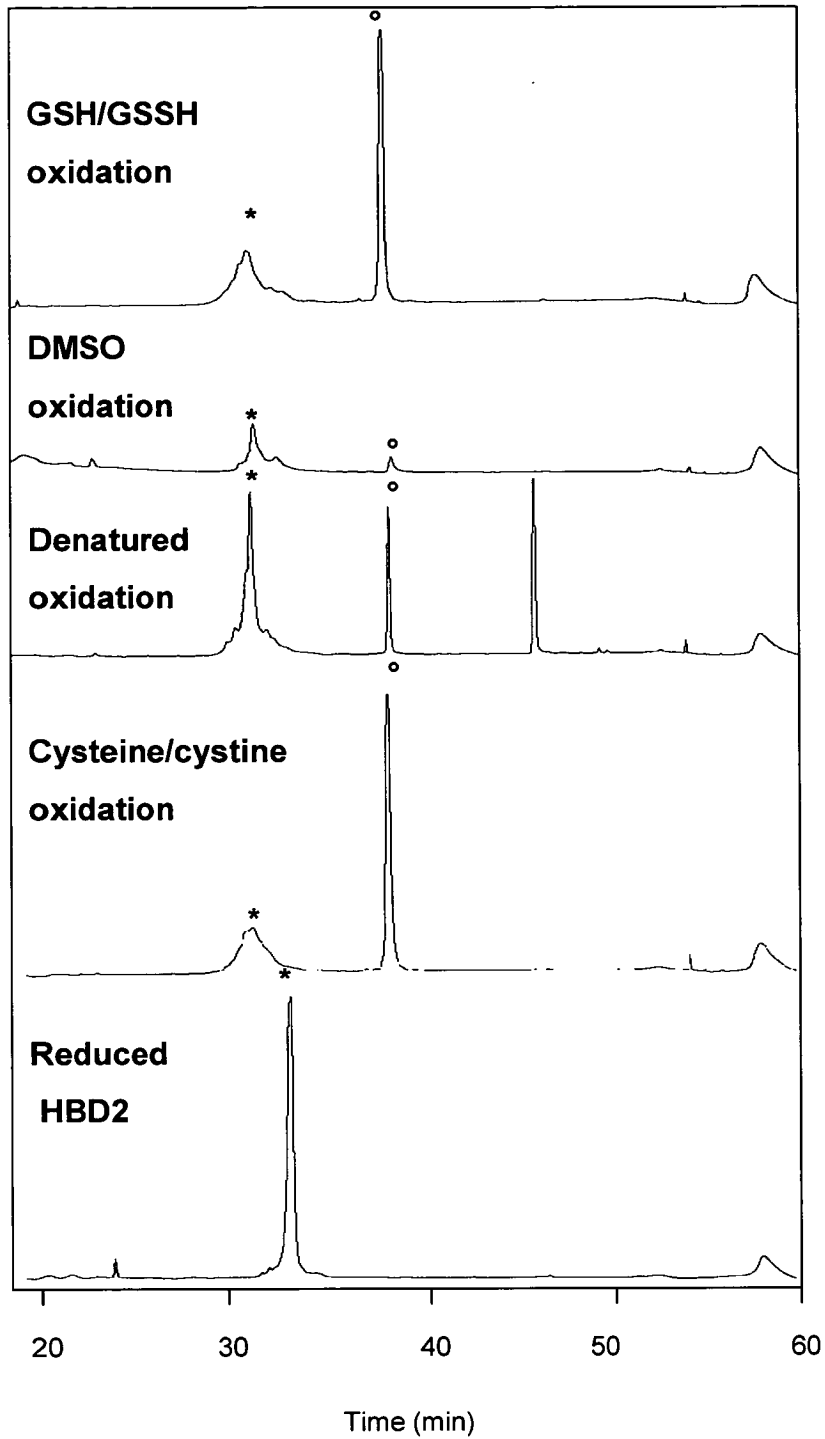
Figure 2.6. Oxidation Efficiency of HBD2 Analyzed by RP-HPLC. Reduced and oxidized HBD2 peaks labelled with * and ° respectively.

2.1.8 - Characterization of Oxidized Recombinant HBD2

Although there was clearly a shift to a longer retention time for oxidized HBD2 compared to the reduced form as previously described [3], an accurate mass of oxidized HBD2 was required to show all three disulfide bonds had formed. Using the HBD2 empirical formula (oxidized HBD2, $C_{188}H_{305}N_{55}O_{50}S_6$; reduced HBD2, $C_{188}H_{311}N_{55}O_{50}S_6$) the intensity and isotopic distribution can be predicted for both oxidized and reduced forms (Figure 2.7). High resolution FT-ICR mass spectrometry analysis of the $[M+4H]^{4+}$ charge state clearly shows the isotopic distribution and masses fit extremely well to that for oxidized HBD2.
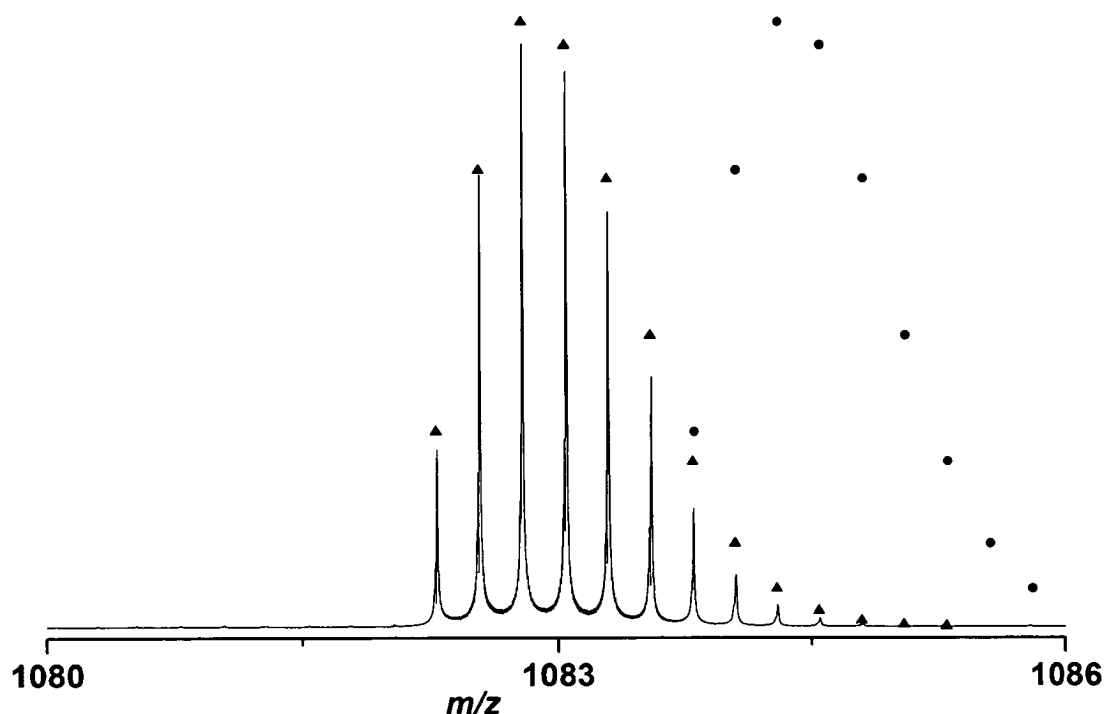
Figure 2.7. FT-ICR Isotopic Envelope of Oxidized rHBD2. Isotopic envelope of the $[M+4H]^{4+}$ charge state of oxidized rHBD2. Triangles represent the isotopic distribution expected for oxidized HBD2. Circles represent the isotopic distribution expected for reduced HBD2.

The crystal structure of HBD2 implicated the potential for HBD2 to form oligomeric structures [18]. Neither dimeric nor higher order oligomeric charge states were observed by

FT-ICR analysis, indicating HBD2 is in a monomeric state under these conditions (Appendix A2). This conclusion was supported by results from native gel electrophoresis analysis where both the reduced and oxidized forms of HBD2 migrated at the same monomeric mass as seen previously (Figure 2.8) [19].
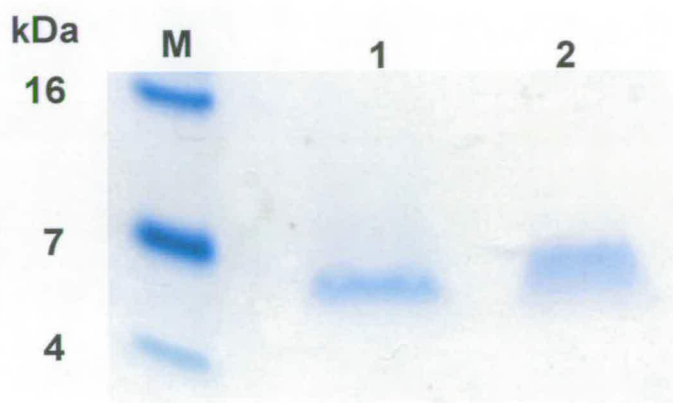
Figure 2.8. Native Gel Analysis of Monomeric HBD2. 16% Tricine gel analysis of HBD2. Lane M, SeeBlue 2 protein marker (Invitrogen); lane 1, HBD2 reduced; lane 2, HBD2 oxidized.

Before functional analysis, the disulfide bond connectivity and folded state were analyzed. Using one dimensional (1D) ^{1}H NMR spectroscopy, it was observed that rHBD2 displayed well dispersed chemical shifts in the amide region as compared to the unstructured Defb14 [20], suggesting the presence of secondary structures in the folded defensin. Although characterization of the disulfide connectivity for natural, isolated HBD2 was never carried out it is assumed that HBD2 possess the β-defensin disulfide connectivity Cys1-Cys5, Cys2-Cys4, Cys3-Cys6 based on studies with synthetic material [3, 18]. Along with the refolding process, determination of the correct disulfide connectivity is the most technically difficult step in production of active β-defensins. Since residues Cys5 and Cys6 are consecutive in the linear sequence, trypsin/chymotrypsin digest alone can not decipher between a disulfide bond connectivity linked to Cys5 or to Cys6. There are two methods used after enzymatic digest: (1) Edman degradation; (2) Collision-induced dissociation (CID). Using a synthetic biotinylated HBD2 (BioHBD2) as a test peptide,

trypsin/chymotrypsin digest yielded two major peptide fragments (Table 2.1). The first peptide fragment represented the peptide connected by the Cys2-Cys4 disulfide bond found in both α and β-defensins. The second peptide fragment contained two disulfide bonds with unknown connectivity. Separating these two fragments was achieved using LC-MS and on-line CID, using argon gas, was applied to the second fragment. A parent ion was fragmented by collision with the inert gas and fragment ions were analyzed. Unfortunately, although N-terminal sequencing was achieved, the fragment ion that we hoped to observe to enable us to decipher between the α– and β– connectivites could not be found. In parallel work carried out by Dr Emily Seo, Edman degradation was performed on the HPLC purified second fragment of the rHBD2. Phenylisothiocyanate reacted with uncharged N-terminal amino group of Cys5 to yield a final phenylthiohydantoin (PTH) Cys derivative which formed a disulfide bound with the Cys1 fragment and this was identified by mass spectrometry (Table 2.1).

Therefore the conclusion from these combined analyses was that the rHBD2 has the β-defensin disulfide pairings Cys1-Cys5, Cys2-Cys4, Cys3-Cys6.

EXPECTED FRAGMENTS FROM BIOHBD2 TRYPSIN/CHYMOTRYPSIN DIGEST	CALCULATED MASS (DA)	OBSERVED MASS (DA)
[SGAIC^{2}HPVF] [QIGTC^{4}GIPGTK]	2002.4	2002.5
[GIGDPVTC^{1}L] [C^{3}PR] [C^{5}C^{6}K]^a	1823.0	1823.5
Expected fragments from rHBD2 trypsin/chymotrypsin digest		
[SGAIC^{2}HPVF] [QIGTC^{4}GIPGTK]	2002.4	2002.5
[GIGDPVTC^{1}L] [C^{3}PR] [C^{5}C^{6}K]^b	1596.1	1596.4
Expected fragments from Collision Induced Dissociation		
[PVTC^{1}L] [C^{3}PR] [C^{5}C^{6}K]$^\ominus$	1255.9	1254.8
[VTC^{1}L] [C^{3}PR] [C^{5}C^{6}K]$^\ominus$	1158.5	1157.7
[TC^{1}L] [C^{3}PR] [C^{5}C^{6}K]$^\ominus$	1059.3	1058.7
[C^{1}L] [C^{3}PR] [C^{5}C^{6}K]$^\ominus$	958.2	957.6
[GIGD]$^\Delta$	569.2	569.5
[GIG]$^\Delta$	454.2	454.5
[GI]$^\Delta$	397.2	397.4
[G]$^\Delta$	284.1	284.2
Expected Fragments from Edman Degradation		
[IGDPVTC^{1}L] [^{PTH}C^5]	1054.0	1054.8
[IGDPVTC^{1}L] [C^{6}K]	1065.0	Not observed

Table 2.1. Analysis of Disulfide Connectivity using CID and Edman Degradation.
^{a} [M+3H]$^{3+}$ charge state of [GIGDPVTC^{1}L] [C^{3}PR] [C^{5}C^{6}K] (m/z 608.46) was subjected to CID.
^{b} [GIGDPVTC^{1}L] [C^{3}PR] [C^{5}C^{6}K] was subjected to Edman Degradation.
$^\ominus$ **y ions**
$^\Delta$ **b ions**
[G] Biotin modified Glycine (+226.3 Da)

2.1.9 - Antimicrobial Activity

β-defensins role in innate immunity involves the direct killing of invading pathogens. To test rHBD2 for this activity *in vitro*, an antimicrobial assay was performed using a method published previously by our group that was based on a procedure used by Prof. Bob Hancock and coworkers [21]. A wide range of microbes were tested incorporating Gram-negative bacteria, Gram-positive bacteria and fungal species. In brief, varying concentrations of rHBD2 were incubated with the test organism and the surviving organisms were allowed to grow on nutrient agar. The concentrations of peptide required to kill 50%, 90% and 99.99% (LD50, LD90 and MBC99.99 respectively) were calculated and compared to a control solution containing no peptide (Table 2.2).

ORGANISM	STRAIN	SOURCE	MBC^A/MIC^B	LD90^C	LD50^D
Gram-negative					
E. coli	MG1655	Thesis	<20 ^{A}	1.5-3.0	<1.5
	ML-35	24	17 ^{B}		
	Unspecified	23		~10	
	ML-35p	22		4.25-12.25 ^{F}	
P. aeruginosa	PA01	Thesis	<25 ^{A}	1.5-3.0	<1.5
	ATCC 27853	24	17 ^{B}		
	Unspecified	23		~10	
	ATCC 9027	22		4.25-12.25 ^{F}	
Gram-positive					
S. aureus	ATCC 25923	Thesis	>50 ^{A}	12.5-25	1.5-3.0
	710A	24	35-70 ^{B}		
	Unspecified	23	100 ^{E}		
	ATCC 6341	22	N.D ^{E}		
Yeast					
C. albicans	J2922	Thesis	>50 ^{A}	3.0-6.0	1.5-3.0
	Unspecified	24	70 ^{B}		
	Unspecified	23		25	
	820	22		4.25-12.25 ^{F}	

Table 2.2. Antimicrobial Activity of Oxidized rHBD2 Against a Panel of Micro-organisms. All values stated are in μg/ml.
^{A} MBC values are the minimum concentration required to kill 99.99% of initial inoculum.
^{B} MIC values are the lowest concentration required to inhibit microbial growth.
^{C} LD90 values are the minimum concentration required to kill 90% of initial inoculum.
^{D} LD50 values are the minimum concentration required to kill 50% of initial inoculum.
^{E} Bacteriostatic Effect
^{F} Bactericidal Effect

We found that rHBD2 exhibited MBCs against the Gram-negative bacteria *E. coli* and *P. aeruginosa* at <20 and <25 μg/ml respectively. rHBD2 displayed antifungal activity with an LD90 in the range 6-12.5 μg/ml, however the peptide is clearly not as potent an antimicrobial peptide against Gram-positive *S. aureus*. Direct comparison of the antimicrobial values found for our HBD2 preparation and previous literature values are difficult. Firstly, there is more than one type of antimicrobial assay being performed including radial diffusion assay and microbroth dilution assays making direct comparisons impossible [22, 23]. Even when the same method is used variations in micro-organism strains can have an effect on the concentration of peptide needed to kill efficiently (Table 2.2). However analysis of the literature values does reveal a trend that indicates that our rHBD2's antimicrobial specificity is similar to that of natural purified HBD2. Comparison of four separate studies, including this thesis, clearly identifies HBD2 as being a more potent antimicrobial agent against Gram-negative bacteria and *C.albicans* than against Gram-positive *S.aureus* [22-24]. Therefore in conclusion it was shown that the purification process has had no detrimental effects on rHBD2 antimicrobial properties.

2.1.10 - Chemotactic Activity

Another important role for β-defensins is the recruitment of cells involved in adaptive immunity to sites of infection via the chemokine receptor CCR6. Yang et al. were the first to show that both HBD1 and HBD2 were able to chemoattract immature dendritic, memory T cells and CCR6 transfected HEK293 cells [25]. Since this finding, CCR6 has been shown to be a promiscuous GPCR with various human and mouse β-defensins been shown to activate this receptor including certain linear analogues of these peptides [3, 20].

Using a previously published method, in collaboration with Julia Dorin, rHBD2 chemotactic activity was analysed using CCR6 transfected HEK293 cells and was found to chemoattract in a concentration dependent way with an optimal concentration of 100 ng/ml

(Figure 2.9). This is in good agreement with the optimal concentrations of 100 ng/ml and 1000 ng/ml for the natural CCR6 chemokine CCL20 (MIP-3α) and HBD2 respectively that were published previously [25]. The chemotaxis assay depends on the concentration dependent movement of CCR6 expressing cells to the under surface of a collagen coated polycarbonate filter. Any assay involving growing, living cells is difficult to reproduce because of differing surface expression of the ligand inducing functional receptor and each cells differing ability to bind to the filter. Therefore each peptide concentration was tested in triplicates in three separate experiments meaning a total of nine data points were collected for each peptide concentration. Each assay performed must also be carried out with both positive and negative control peptides to access the assays viability. To prove the results are statistically relevant a paired, two-tailed, student's t test must be carried out comparing the results to the number of cells migrated by media alone.
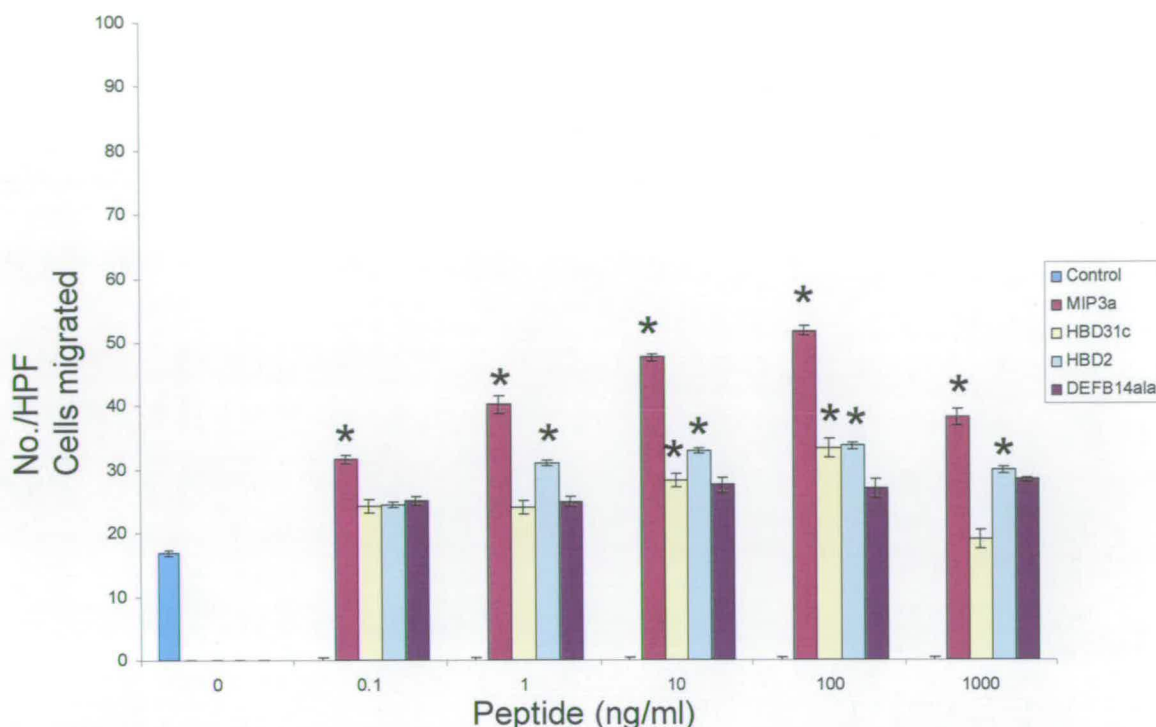
Figure 2.9. Chemotaxic Activities of Oxidized rHBD2 of CCR6 Transfected HEK293 cells. Migration by CCL20/MIP-3α (light purple) and HBD3 1C (yellow) were positive controls, DEFB14ala (dark purple) was negative control. The numerical data (number of cells per high power field) was recorded as an average of three separate experiments in triplicate and error bars indicate the Standard Error (SE). Statistical significance ($p < 0.05$) is indicated with a * as compared to the number of cells per HPF of culture media alone.

2.1.11 - Purification of Oxidized HBD1

Having prepared the rHBD2 by our new method we wanted to also apply it to the production of another defensin and the 'housekeeping' β-defensin HBD1 was chosen as a target. The HBD1 gene was synthesized in a similar manner as to that described for HBD2 with *Alw*NI sites flanking both the 5' and 3'ends of the gene. However, upon restriction analysis of the pET/HISKSI-HBD2 plasmid it was found that replacing the Met codon with an Ala codon in the *Alw*NI recognition site resulted in a Dcm methylase recognition site, resulting in blocking the cleavage site for the restriction enzyme [26]. Despite efforts to transform the methylase mutant *E. coli* K12 strain (ER2925) which is both Dcm⁻ and Dam⁻,

HBD2 gene could still not be isolated from the expressing plasmid. Therefore a fusion gene incorporating both KSI and HBD1 was purchased from Codon devices replacing the upstream *Alw*NI site with a *Hind*III restriction site. This change allowed all future defensin genes synthesized with flanking upstream *Hind*III and downstream *Alw*NI restrictions sites to be cloned into the pET28A expression plasmid. The expressing plasmid pET28a HISKSI-HBD1 was used to transform *E. coli* BL21 (DE3) cells and large scale purification was carried out. Purification of HBD1 was performed essentially as described for HBD2. One step Ni^{2+}-NTA chromatography was applied to isolate the HBD1 fusion protein prior to CNBr chemical cleavage in acidified 6 M GndHCl buffer. RP-HPLC was applied to isolate highly pure reduced rHBD1 before chemical oxidation using the cysteine/cystine redox pair in Tris-HCl buffer was performed. Following RP-HPLC purification of oxidized rHBD1, SDS-PAGE analysis clearly identifies a highly pure single band with the correct mass for oxidized rHBD1 (Figure 2.10). Furthermore, ESI-MS analysis revealed HBD1 had a deconvoluted mass of 3928.27 Da (theoretical mass 3928.56 Da) suggesting the presence of only oxidized HBD1 containing three disulfide bonds (Figure 2.11).

We did not carry out a full antimicrobial or chemotactic analysis of the rHBD1 because a paper was published which investigated >20 HBD1 site-directed mutants [27]. Instead the purified rHBD1 was gifted to Dr E. Seo within the group for structural studies with N^{15} labelled HBD2. Here, we wished to identify any possible interaction between HBD1 and HBD2 using NMR (E. Seo, personal communication).
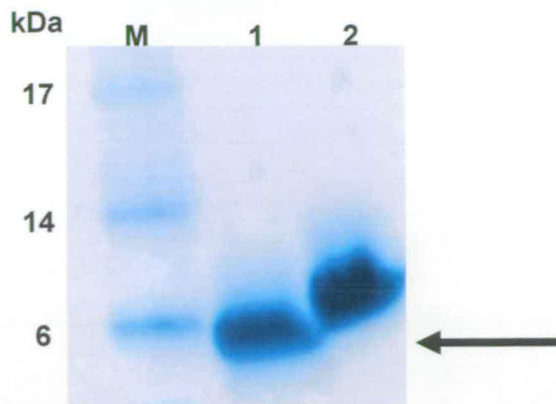
Figure 2.10. Purification of rHBD1. 12% Bis-Tris acrylamide gel analysis of rHBD1. Lane M, SeeBlue 2 protein marker (Invitrogen); lane 1, soluble rHBD1; lane 2, soluble rHBD2. The band indicated by arrow is expected mass of mature rHBD1.
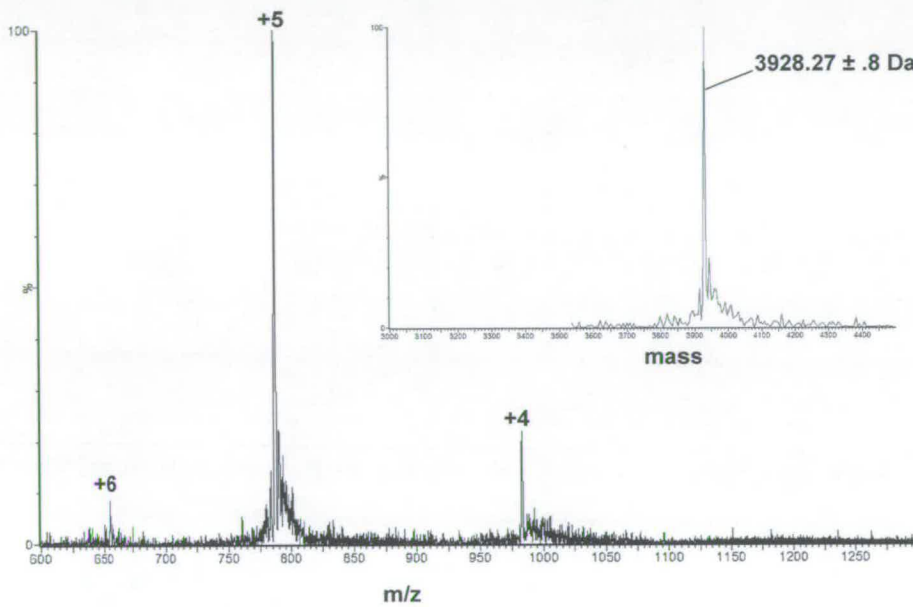
Figure 2.11. rHBD1 Analysis by ESI-MS. The spectrum shows the +4 to +6 charge states for HBD1. *Inset,* deconvoluted data resulting in a mass of 3928.27 ±0.8 Da (theoretical mass 3928.56 Da).

2.2 - Single Disulfide Bond Mutants of HBD2

2.2.1 - Introduction

Despite recent improvements in the production of defensins, in-depth structure/function relationships of specific peptides are lacking. Investigations have focused

mainly on the antimicrobial function of defensins, with chemotactic effects mostly ignored. Our collaborators, along with various other groups, have focused on HBD3 or its mouse ortholog Defb14 [3, 28, 29]. Disulfide connectivity, peptide length and charge have all been investigated with respect to its antimicrobial activity. Linearized HBD3, achieved by cysteine amino acid replacement or by carboxyaminomethyl derivitization, was found to be as potent as oxidized HBD3 containing three disulfide bonds [3]. Therefore the antimicrobial potency of a defensin (and AMPs in general) appears to be dependent on a combination of hydrophobicity and charge rather than the spatial arrangement of the charged and/or hydrophobic residues imposed by the disulfide bonded framework. This amphipathic nature of antimicrobial peptides has been used as a template to design novel "unnatural" peptides with potent activity [30].

However there is evidence that some defensins do require their structurally-constrained motifs to maintain their antimicrobial potency. For example, linear HBD2, in artificial lipid vesicle permeabilization experiments, was ineffective at releasing the intracellular marker when compared to the oxidized HBD2 indicating that disulfide bonds are indeed needed [18]. Addition of only a single disulfide bond between the third and sixth disulfide bond in a N-terminal truncated HBD2 did display antimicrobial activity against Gram-negative microbes, implicating a structurally restrained β-strand motif as playing an important role [31]. Although this conclusion was strengthened by the loss of antimicrobial activity upon deletion of this motif, a second structural motif, an N-terminal α-helix has also been implicated. Removal of the α-helix stabilizing Asp4 reduced the efficiency of (-D)HBD2 in permeabilizing *E. coli* cytoplasmic membranes [24, 32].

The role played by the structural constraint imparted by the conserved defensin disulfide motif is even less well understood with respect to chemotactic activity. However, it is not surprising that specific structural motifs are required for a peptide to be an active chemokine since this process requires a specific receptor/peptide ligand interaction. Using

solid phase peptide synthesis, coupled with an elegant orthogonal cysteine protection strategy, Wu et al. prepared a series of six HBD3 isoforms of known disulfide bond connectivity. Each isoform was tested for antimicrobial and chemotactic activity and a control, linear peptide was also prepared where each the of six cysteines were replaced with α-aminobutyric acid (abu) [3]. It was found that the six defensins with disulfide bonds and the abu-HBD3 were potent antimicrobial peptides but the chemotactic activity varied, with the cysteine-free peptide being inactive. Although this study appeared to confirm the essential nature of the disulfide bonds for a defensin to display chemotactic activity, a recent paper has challenged this view. Taylor et al. showed that not only does a linear HBD3 peptide with iodoacetamide treated cysteines display chemotactic activity but also a linear HBD3 peptide were the cysteines are replaced with alanines except for a single cysteine residue at position five (HBD3-1cys[5]) [20]. This latter peptide was shown to form a covalent dimer upon DMSO oxidation, however treatment of the free cysteine with iodoacetamide failed to inhibit this chemotactic ability revealing that dimerization is not essential for this activity. Furthermore neither a N-terminal truncated version of HBD3-1cys[5] nor a HBD3 peptide with only a single cysteine at position one (HBD3-1cys[1]) could display chemotactic activity [20]. Together this implies that HBD3 chemotactic ability is not dependent on the disulfide bonded structural framework imposing a certain spatial arrangement but rather on individual residues throughout the sequence that include the cysteine at position five. In the study of 26 site-directed mutants of HBD1, non cysteine residues were evaluated to discover the important residues for both antimicrobial and chemotactic activity [27]. Using charge swapping or neutralization mutations, C-terminal cationic residues were shown to be important for antimicrobial activity as previously seen with other defensins. Chemotactic data indicated that the N-terminal α-helix was important, as was hypothesized from structural comparisons between CCL20 and HBD2 [33]. This binding epitope was also

extended to include three residues (Lys22, Arg29, Lys33) which are spread out along the length of the peptide but are only adjacent in the folded β-defensin isoform of HBD1.

Although the pET28/HISKSI-HBD2 plasmid was ideal for a similar mutagenesis study on HBD2s structure-function activity, the conflicting results obtained with regard to the importance of disulfide bonds, especially with respect to chemotactic activity, highlighted the need for further investigation. Furthermore it was our groups understanding that a similar study on HBD2 had already been performed and was awaiting publication (personal communication). Therefore using the method optimized for rHBD2, three HBD2 mutants were prepared and purified with each containing a single, canonical disulfide bond with the other four cysteine residues replaced with alanines (HBD2 1-5, HBD2 2-4 and HBD2 3-6, Figure 2.12). The structure of each mutant was analyzed using 1D ^{1}H NMR and functional antimicrobial and chemotactic assays were also performed.

A

```
                    1                                         43
HBD2°               GIGDPVTCLKSGAICHPVFCPRRYKQIGTCGLPGTKCCKKP--
HBD2 1-5°           GIGDPVTCLKSGAIAHPVFAPRRYKQIGTAGLPGTKCAKKP--
HBD2 2-4°           GIGDPVTALKSGAICHPVFAPRRYKQIGTCGLPGTKAAKKP--
HBD2 3-6°           GIGDPVTALKSGAIAHPVFCPRRYKQIGTAGLPGTKACKKP--
HBD2 (-d)28,29      GIG-PVTCLKSGAICHPVFCPRRYKQIGTCGLPGTKCCKKP--
HBD2 5-41 29        ----PVTCLKSGAICHPVFCPRRYKQIGTCGLPGTKCCKKP--
HBD2 (-N)27         ------------------FCPRRYKQIGTG-LPGTKCK-----
HBD2 BREVI 29       GIGDPVTCLKSG-------------------LPGTKCARRKKP
```

B
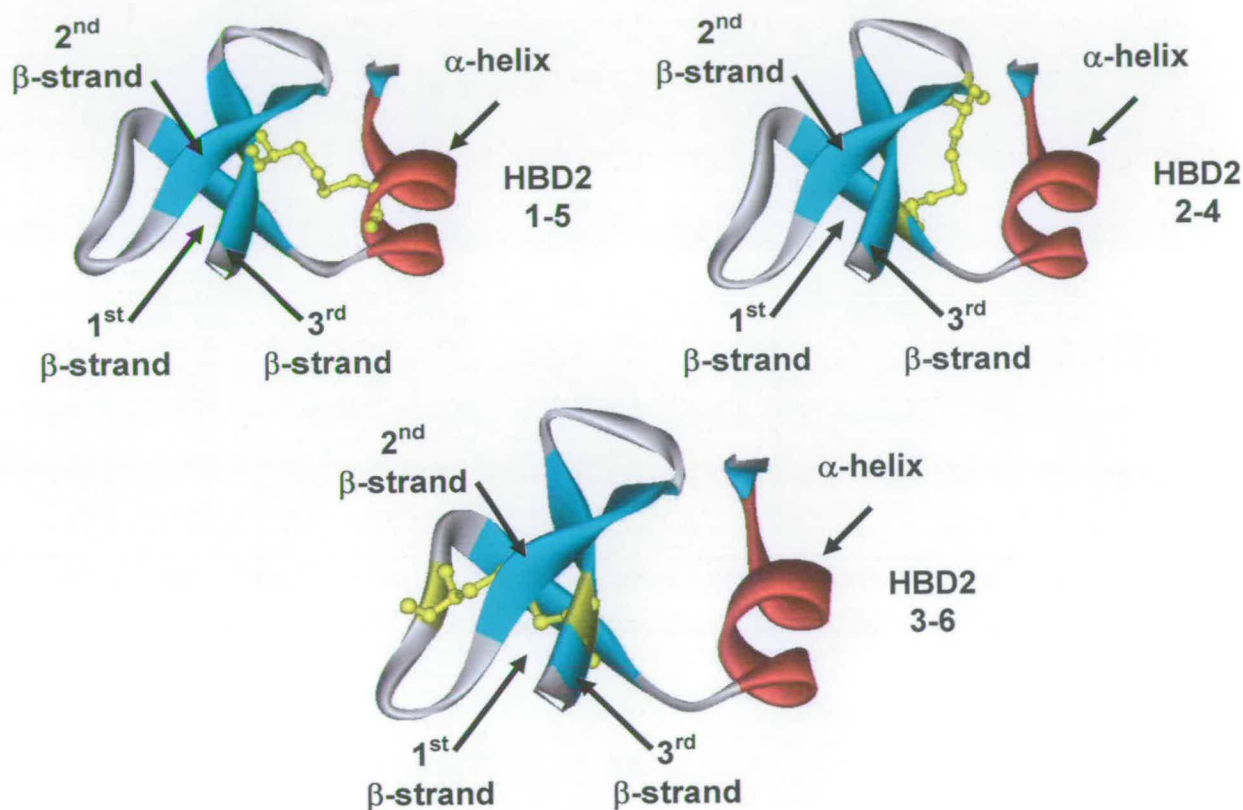
Figure 2.12. Single Disulfide Bond HBD2 Mutants. (A) Sequence Alignment of wt HBD2 and Mutated Peptides. ° indicates peptides purified as part of this study. **(B)** Ribbon Diagrams Representing the 3D Structure of HBD2 with each Individual Disulfide Bonds Indicated. Structure was downloaded from the protein data bank; HBD2: 1FD4. Structural motifs are labelled and the disulfide bonds are indicated in yellow.

2.2.2 - Construction and Purification of Single Disulfide Mutants

Single disulfide mutant genes were synthesized using the same procedure as described for rHBD2 except for the replacement of *Alw*NI restriction site at the 5' end of the

Chapter 2: Purification and Functional Characterization of Human β-defensins

gene for a *Hind*III restriction site. Mutant genes were then cloned into the expression

plasmid using the restriction sites *Hind*III and *Xho*I (pET28a/HISKSI-HBD2 1-5, 2-4, and 3-

6) (Figure 2.13). Following the same purification procedure as with both HBD1 and HBD2,

the three separate HBD2 mutants were over-expressed and reduced HBD2 mutants were

purified using RP-HPLC after CNBr cleavage of the fusion protein.
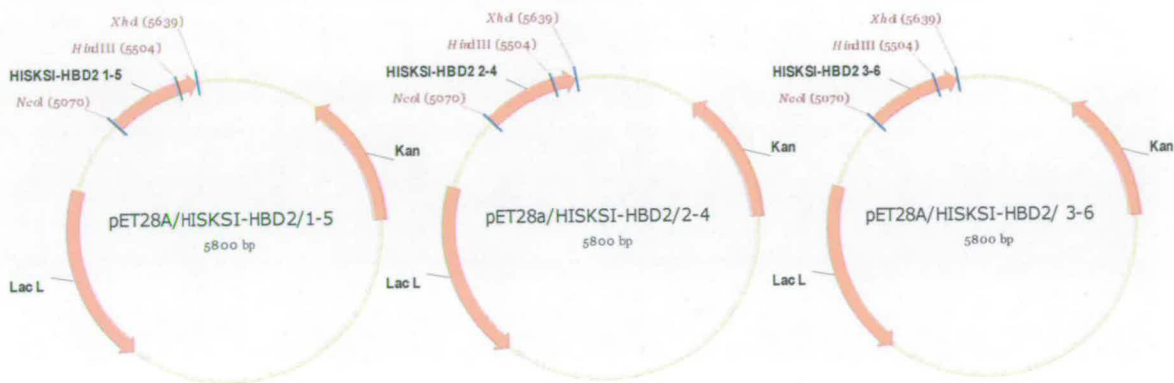
Figure 2.13. Schematic Representations of the Expression Vectors pET28a/HISKSI-HBD2/1-5, 2-4, and 3-6.

Single disulfide bond mutant β-defensins have been shown to oxidize efficiently in

20% DMSO [31]. Therefore instead of using the redox pairs (e.g. cysteine/cystine) as with

HBD2 and HBD1, the HBD2 mutants were oxidized using 20% DMSO and the reaction was

monitored by LC-ESI-MS. Oxidized HBD2 mutants were purified again using RP-HPLC

(Figure 2.14). Interestingly, from the UV trace the retention time for all three mutants was

less than that for wt HBD2 (HBD2 1-5, 26 min; HBD2 2-4, 31 min; HBD2 3-6, 27 min;

HBD2 38 min). This could be due to the hydrophobicity of the alanines replacing the normal

cysteines. However this can not explain the differences between the retention times for

HBD2 2-4 compared to the other two mutants (HBD2 1-5 and HBD2 3-6), ~ 3-4 minutes,

which all have the same charge and hydrophobic residues. This suggests that the HBD2 2-4

mutant has a different structure than the other two peptides and a possible explanation could

be that the folded conformation of HBD2 2-4 may have more hydrophobic residues exposed

to the surface.
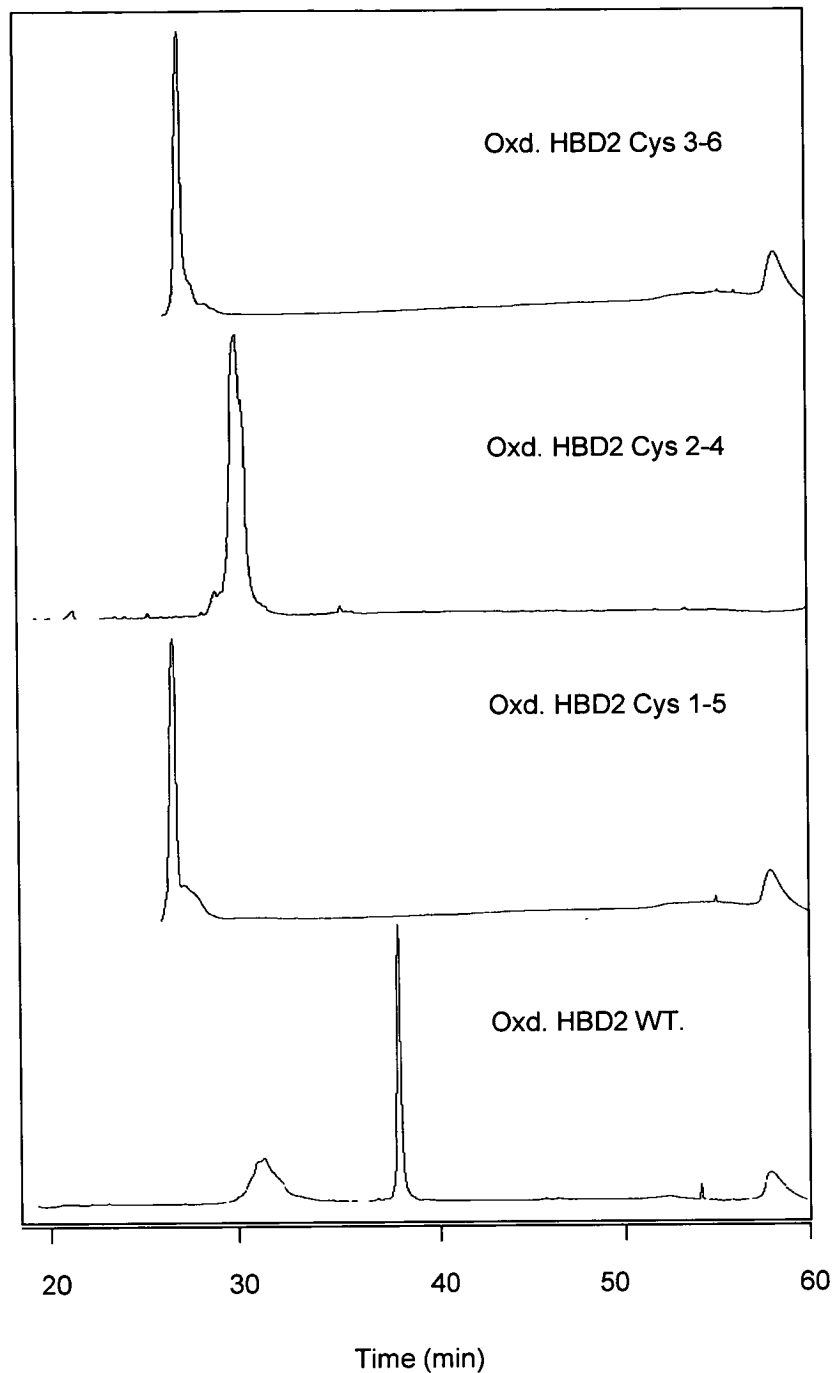
Figure 2.14. HPLC Analysis of Oxidized HBD2 and its Single Disulfide Bond Mutants.

Using SDS-PAGE analysis all three HBD2 mutants were shown to be pure and migrated with a mass of ~4 kDa in comparison to wt HBD2 (Figure 2.15). Due to their identical masses, trypsin digestion was performed on the oxidized HBD2 single disulfide bond mutants and analyzed by LC-ESI-MS. The peptide fragments identified were unique to

each individual peptide and corresponded to their predicted trypsin fragment masses (Table 2.3)
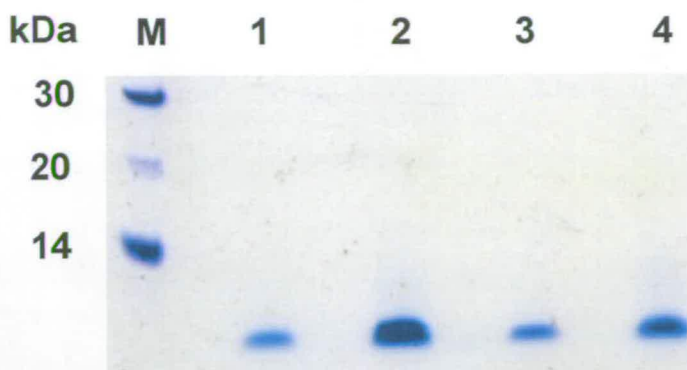
Figure 2.15. Purification of Oxidized HBD2 and its Single Disulfide Bond Mutants. 12% Bis-Tris acrylamide gel analysis of oxidized HBD2 and its single disulfide mutants. Lane M, SeeBlue 2 protein marker (Invitrogen); lane 1, purified oxidized HBD2; lane 2, purified oxidized HBD2 1-5; lane 3, purified oxidized HBD2 2-4; lane 4, purified oxidized HBD2 3-6.

PEPTIDE	TRYPTIC FRAGMENTS	EXPECTED MASS (DA)	OBSERVED MASS (DA)
HBD2 1-5	[GIGDPVTC^{1}LK] [C^{5}AK]	1320.6	Not Observed
HBD2 1-5	[SGAIAHPVFAPR]	1222.4	1221.12 ± 3.89
HBD2 2-4	[SGAIC^{2}HPVFAPR] [QIGTC^{4}GLPGTK]	2326.8	2326.19 ± 0.48
HBD2 2-4	[GIGDPVTALK]	970.1	969.92 ± 0.14
HBD2 3-6	[SGAIAHPVFC^{3}PR] [AC^{6}K]	1572.9	Not observed
HBD2 3-6	[GIGDPVTALK]	970.1	970.34 ± 0.45
HBD2 3-6	[QIGTAGLPGTK]	1042.2	1041.77 ±1.08

Table 2.3. Protease Digestion and Peptide Analysis by Electrospray Mass Spectrometry. Oxidized HBD2 single disulfide bond mutants were digested with trypsin and identified peptides are shown. Expected masses from a tryptic derived digest were compiled using PAWS software.

2.2.3 - Characterization of HBD2 Mutants

The oxidization and oligomeric state were analysed using high resolution FT-ICR mass spectrometry. Due to the small mass difference between the reduced ($C_{188}H_{311}N_{55}O_{50}S_2$, Avg. mass 4206.01 Da) and oxidized state ($C_{188}H_{309}N_{55}O_{50}S_2$, Avg. mass 4204.00 Da), high resolution mass spectrometry was needed to confirm the extent and efficiency of the oxidization reaction. Clearly, in all three cases, the HBD2 mutants had been converted into the oxidized form (Figure 2.16). A second observation from the ion envelopes was a lack of dimerization or higher order oligmerization, suggesting that each peptide contained a single intramolecular disulfide bond.
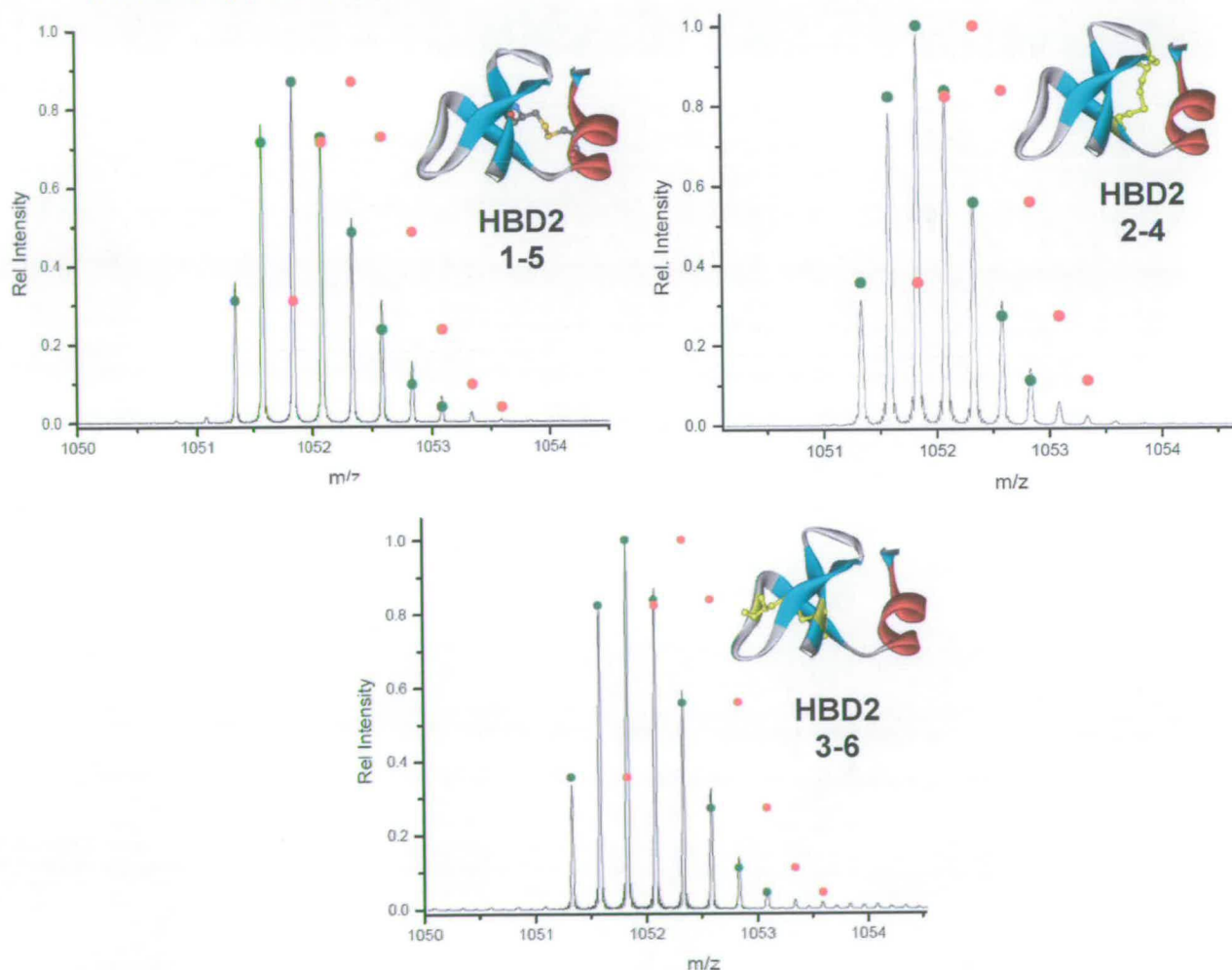
Figure 2.16. FT-ICR Isotopic Envelope of Oxidized HBD2 Single Disulfide Bond Mutants. Isotopic envelope of the [M+4H]$^{4+}$ charge state of oxidized HBD2 mutants. Green circles represent the isotopic distribution expected for oxidized HBD2 mutants. Red circles represent the isotopic distribution expected for reduced HBD2 mutants.

1D ^{1}H 600 MHz NMR was used to compare the structure of the HBD2 mutants to that of the wt HBD2. The wt HBD2 has highly resolved, well dispersed resonances in the amide region indicating a folded state. Resolution of HBD2 mutants are not as well dispersed indicating a less structured peptide (Figure 2.17). Based on the resonances resolution both HBD2 1-5 and 2-4 are slightly more structured compared to HBD2 3-6. This could be a consequence of the different secondary structural elements imposed by each disulfide bond. Analysis of both the crystal and solution structures of wt HBD2 (PDB accession no: 1E4Q, 1FQQ, 1FD4) revealed that the N-terminal α-helix is connected to the third β-sheet by the disulfide bond 1-5 and results in the α-helix being held against the β-sheet in a rigid structure (Figure 2.12B) [18, 34]. Residue Cys5 not only forms a disulfide bond with Cys1 but is also involved in multiple hydrogen bonds with the second β-sheet forming a conserved β-bulge which appears to be a signature structural motif in the β-defensin family. The disulfide bond Cys2-Cys4 is involved in stabilizing the anti-parallel β-sheets through bonding between the first β-sheet and the start of the β-hairpin. Residue Cys4 is also involved in a hydrogen bond holding the β-hairpin in a rigid structure and bringing the third β-sheet closer [34]. Disulfide bond 3-6 holds the third β-sheet to the first type IV turn after the first β-sheet. This β-turn between the first two β-sheets was shown to be highly flexible indicating the possible reason for the lack of structure in HBD2 3-6 [18].
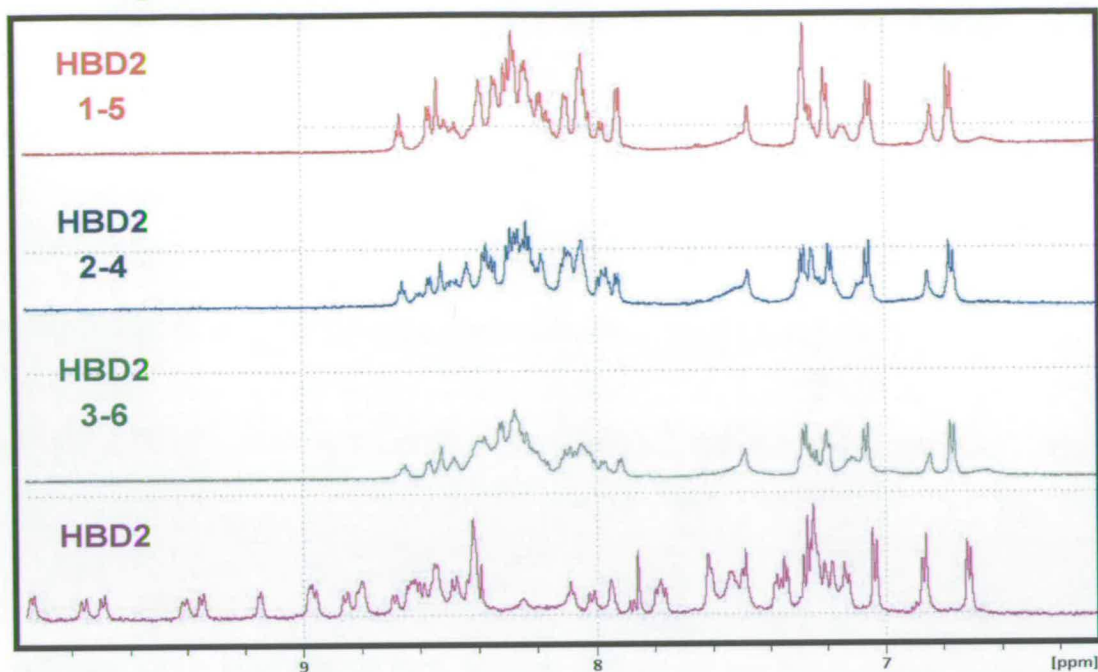
Figure 2.17. 1D ^{1}H NMR Spectrum of Oxidized HBD2 and its Single Disulfide Mutants. Amide region of the proton NMR spectrum of HBD2 1-5 (red), HBD2 2-4 (blue), HBD2 3-6 (green), wt HBD2 (purple).

2.2.4 - Antimicrobial Activity

It was shown in Section 2.1.9 that wt HBD2 possessed antimicrobial activity against Gram-negative bacteria at micromolar concentrations. Using the same protocol as before HBD2 single disulfide mutants were tested against this standard *E. coli* strain (MG1655) (Table 2.4). HBD2 single disulfide bond mutant concentrations as high as 100 µg/ml were not able to kill 99.99% of bacteria. Clearly the canonically folded HBD2 is more potent an antimicrobial peptide with an MBC of <20 µg/ml.

PEPTIDE	MBC [A]	LD90 [B]	LD50 [C]
HBD2	<20	1.5-3.0	<1.5
HBD2 1-5	>100	50-100	12.5-25
HBD2 2-4	>100	25-50	6-12.5
HBD2 3-6	>100	50-100	12.5-25

Table 2.4. Antimicrobial Activity of Oxidized wt HBD2 and its Single Disulfide Bond Mutants Against a Gram-negative *E. coli* (MG1655) strain. All values stated are in μg/ml.
[A] MBC values are the minimum concentration required to kill 99.99% of initial inoculum.
[B] LD90 values are the minimum concentration required to kill 90% of initial inoculum.
[C] LD50 values are the minimum concentration required to kill 50% of initial inoculum.

Inclusion of a single disulfide does however recover antimicrobial activity found to be lost by Hoover et al. when HBD2 was reduced [18]. All three mutants can kill 90% of *E. coli* with LD90 values of 25-50 μg/ml for HBD2 2-4 and 50-100 μg/ml for HBD2 1-5 and 3-6. The difference in potency for HBD2 2-4 could be a consequence of a non-native fold causing more solvent exposed hydrophobic residues as could be implicated from the extended retention time by HPLC. A further discovery of note was the recovery of antimicrobial activity that was lost in studies with Brevi HBD2. Brevi HBD2 is HBD2 1-5 with most of the antiparallel β-sheet removed (Figure 2.12A). Morgera et al. found that removing a stretch of 19 amino acids containing Cys2, Cys3 and Cys4 inactivated its antimicrobial activity against a reference *E.coli* ML-35 strain [32]. However antimicrobial activity of the full length peptide with only the single disulfide bond Cys1-Cys5 was never tested. In this present study the inclusion of this antiparallel β-sheet has resulted in partial antimicrobial activity as compared to wt HBD2. Furthermore, Nagaraj et al tested an N-terminal truncated HBD2 peptide that contained the defensin conserved β-hairpin motif constrained with disulfide bond Cys3-Cys6 (Figure 2.12A) [31]. This peptide displayed antimicrobial activity against an *E.coli* (W 160-37) strain; unfortunately comparisons with

87

wt HBD2 were not tested. These results together, indicate that the highly-conserved, antiparallel β-sheet "platform", as well as charge and hydrophobicity, are important in generating a β-defensin with potent antimicrobial activity and a single disulfide bond is not sufficient to provide this specific structural framework.

2.2.5- Chemotactic Activity

It was important that wt HBD2 had been previously shown to be able to chemoattract HEK293 cells transfected with the chemokine receptor CCR6 (Figure 2.9). To determine the role of the disulfide bonds on the ability of HBD2 to act as a chemokine we performed chemotactic assays with each of the single disulfide bond HBD2 mutants (Figure 2.18). The lack of a classical bell-shaped curve indicates that the three single disulfide mutants are not chemoattractants for CCR6 transfected HEK293 cells. In fact, in the concentration range tested the three disulfide mutants are never significantly better chemoattractants than the control medium alone.
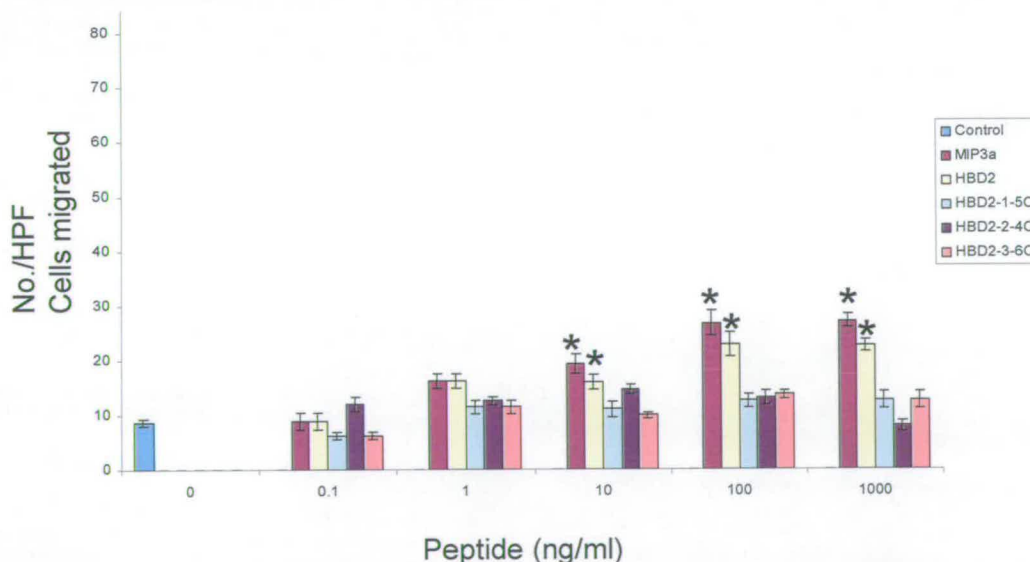
Figure 2.18. Chemotactic Activities of Oxidized wt HBD2 and Single Disulfide Bond Mutants for CCR6 Transfected HEK293 Cells. Migration by MIP-3α (light purple) and wt HBD2 (yellow) were positive controls. Migration by HBD2 1-5 (light green), HBD2 2-4 (dark purple) and HBD2 3-6 (pink) are indicated. The numerical data (number of cells per high power field) was recorded as an average of three separate experiments in triplicate and error bars indicate the SE. Statistical significance ($p < 0.05$) is indicated with a * as compared to the number of cells per HPF of culture media alone.

Chapter 2: Purification and Functional Characterization of Human β-defensins
Comparisons of the crystal and solution structures of human β-defensins with the chemokine MIP-3α/CCL20 indicated that two structural motifs are conserved and implicated as being important (Figure 2.19) [33, 35-37]. The N-terminal motif DCCL and DPVTCL in CCL20 and HBD2 respectively, are thought to be held in a rigid conformation and required for receptor activation. This structural rigidity was proposed to be conserved in HBD2 1-5. Its inability to chemoattract could imply that either this is not the case or that both structural motifs are essential. The wide, shallow groove formed between the N-terminal α-helix, loop connecting β1-β2 strands and C-terminal residues of HBD2 is also implicated in receptor recognition [33, 37]. Positioning of this loop towards the C-terminus is conferred in part by the disulfide bond Cys3-Cys6. However, the inability of HBD2 3-6 to chemoattract suggests that without the disulfide bond Cys1-Cys5 this groove is not maintained and this peptide is not recognized or cannot activate the receptor. It appears that the structural requirements for HBD2 to be a potent chemoattractant are defined by its rigid structure imposed by its disulfide bonds. Such structural requirements appear to depend on the individual defensin since a linear Defb14 with no disulfide bonds acts as a potent chemokine [20].
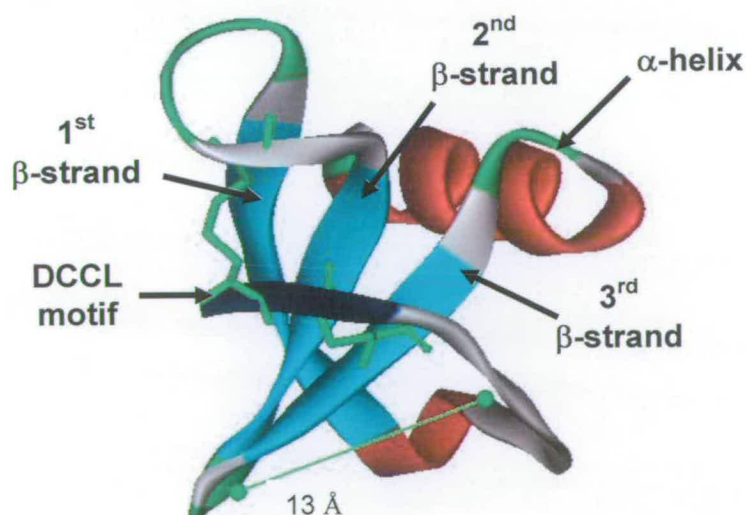
Figure 2.19. Ribbon Diagram Highlighting the Structural Important Motifs of CCL20. Structure was downloaded from the protein data bank; CCL20: 1M8A. Structural motifs are labelled and the disulfide bonds are indicated in green. DCCL motif is highlighted in blue and the distance of the putative binding groove is also indicated.

89

2.3 - Production of Human β-defensins in Mammalian Cell Lines

2.3.1 - Introduction

Many mammalian cell lines have been used to dissect the complicated issue of defensin expression. These cell lines, for example CaCo2 cells and primary keratinocytes, have the potential to be used for defensin isolation. CaCo2 cells are human caucasian colon adenocarcinoma epithelial cells and have been used as models for intestinal epithelial cells in cell culture [38, 39]. O'Neil et al. has shown that it is possible to isolate HBD1 and HBD2 from these intestinal epithelial cells [38]. Using one step, weak cationic exchange chromatography, two HBD1 isoforms and a HBD2 isoform (migrated slower than a standard rHBD2 on acetic acid urea gel) were purified [38, 39]. Although the relative concentrations of the two isoforms were low, HBD1 (~15 ng/ml) and HBD2 (5 ng/ml), more stringent chromatography should increase the concentration to a more workable level. Therefore initial experiments were performed on these cells to isolate sufficient levels of HBD2 for proteomic and sequencing analysis.

2.3.2 - Expression, Cloning and Attempted Isolation of β-defensins

To determine whether unstimulated CaCo2 cells constitutively express HBD1, cells were grown until they were confluent and RNA was extracted for analyses by RT-PCR and gel electrophoresis (Figure 2.20). A DNA band at 204 bp is representative of the full length transcript of signal-pro-HBD1 – the HBD1 gene containing the signal sequence and pro-sequence. The lack of a distinct band in the reactions without reverse transcriptase (-RT) indicates that this positive result is due to gene expression rather than DNA contamination.

Using the same protocol we found that full length signal-pro-HBD2 was not expressed. As expected HBD2 expression is regulated and requires transcriptional induction.

Figure 2.20. Expression of HBD1 in Unstimulated CaCo2 Cells. Defensin gene expression was analysed by RT-PCR using primers specific for HBD-1 and -2. Lane 1-6, extracted RNA subjected to RT-PCR analysis - RT. Lane 7, H_2O subjected to RT-PCR analysis - RT. Lane 8-13, RNA subjected to RT-PCR analysis +RT. Lane 14, H_2O subjected to RT-PCR analysis +RT. Lane 15, H_2O subjected to PCR analysis. β-Actin was used as house-keeping gene.
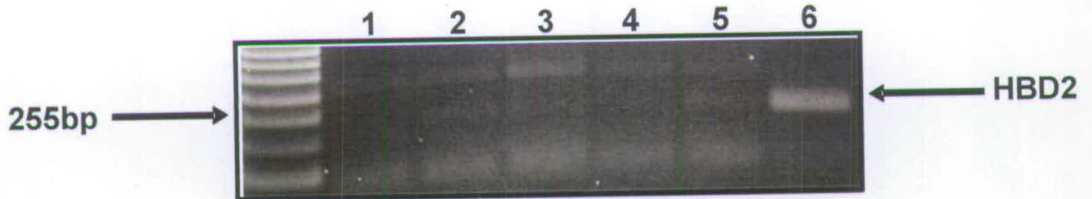
Figure 2.21. Expression Analysis of HBD2 from Stimulated CaCo2 Cells. Expression was analysed by RT-PCR using primers specific for HBD-2. Lane 1-6, extracted RNA stimulated for 0, 0 (with H_2O), 15, 30, 60 and 360 min with IL-1β were subjected to RT-PCR analysis.

We added the pro-inflammatory cytokine, interleukin-1β (IL-1β) to the CaCo2 cells and RT-PCR analysis was carried out at different time points for up to 6 hrs. Clearly, after 6 hrs induction with IL-1β, a RT-PCR product at 255 bp is observed, consistent with the size predicted for the signal-pro-HBD2 (Figure 2.21). Despite the correct size being observed for both defensin genes, confirmation was required by gene sequencing the RT-PCR product. Cloning of both products into the plasmid pGEM followed by transformation into *E. coli* JM109 generated a number of colonies. A number of plasmids were isolated and the insert

sequenced. Both HBD1 and HBD2 wt sequences were identified. Interestingly, half of the HBD2 clones contained a single nucleotide polymorphism (SNP), resulting in the substitution of a lysine residue with a glutamic acid in the mature HBD2 peptide (K25E) (Appendix A3). This SNP could result from a PCR induced mutation; however a high fidelity polymerase was used in the RT-PCR reaction suggesting that this was not the case. Rather, it appears that CaCo2 cells may express two different HBD2 isoforms. The CaCo2 cells have undergone an unknown number of replications so it is not clear whether this mutation was present when these cells were originally immortalized. It would be interesting to prepare the HBD2 K25E mutant and analyse its antimicrobial and chemotactic activity – this was outwith the scope of this study. This is not the first SNP identified in β-defensin genes, with multiple SNPs in both the DEFB1 and DEFB4 genes been identified throughout the gene including the 5'UTR, 3'UTR, promoter region, exon 1 and exon 2 [40, 41]. These SNPs have been found to have an effect on transcriptional activity. A SNP in the NF-IL6 consensus sequence of the DEFB4 promoter region increased its transcriptional activity and it was hypothesized that it could have an effect on disease susceptibility [42]. An association between SNP and disease susceptibility has now been shown with DEFB1. The C-G SNP at position -44 in the 5'UTR of DEFB1 has been shown to provide protection against Candida oral infection, Chronic Obstructive Pulmonary Disease and Crohn's Disease [43-45]. A number of recent studies have begun to analyse the impact of defensin copy number variations and their linkage to disease susceptibility. For example, both α- and β- defensins are thought to play a role in chronic inflammatory diseases such as Crohn's disease and inflammatory bowl disease [46]. However, it is important that the defensin sequence, and not simply copy number variation, be analyzed to fully understand these issues.

Preliminary work on the purification of mature HBD2 from CaCo2 cells was carried out as part of this study. CaCo2 cells were initially grown in serum medium before undergoing differentiation in ITS serum free media for 21 days. Cell supernatant was

collected 6 hrs post IL-1β induction and cationic exchange used for purification. Western

blot analysis using an HBD2 antibody was unable to detect any mature peptide. The lack of

detectable levels could be due to a combination of factors: (1) low expression; (2) salt levels

in media (although diluted) interfered with chromatography; (3) the excreted HBD2 in the

cell supernatant was not extractable possibly because it was bound to other proteins, lipids

etc. Optimization of these factors could result in detectable levels of HBD2 and allow for

sequence analysis of mature HBD2 peptide using high-resolution mass spectrometry.

2.4 - Functional Analysis of Synthetic Biotinylated HBD2

A major technical difficulty in the identification of any possible interacting partners

of a defensin is an inability to "fish-out" the peptide efficiently before, during or after they

perform their important role. An N-terminal biotinylated HBD2 (BioHBD2), which could be

used in streptavidin pull-down experiments, was synthesized (AlbaChem) and its ability to

perform the same functional roles as unmodified HBD2 was tested.

The chemotactic activity of BioHBD2 was analysed using CCR6 transfected

HEK293 cells and was found to chemoattract in a concentration dependent way with an

optimal concentration at 1 ng/ml (Figure 2.22). This indicates that the biotin tag does not

interfere with the functionally important N-terminus of HBD2.
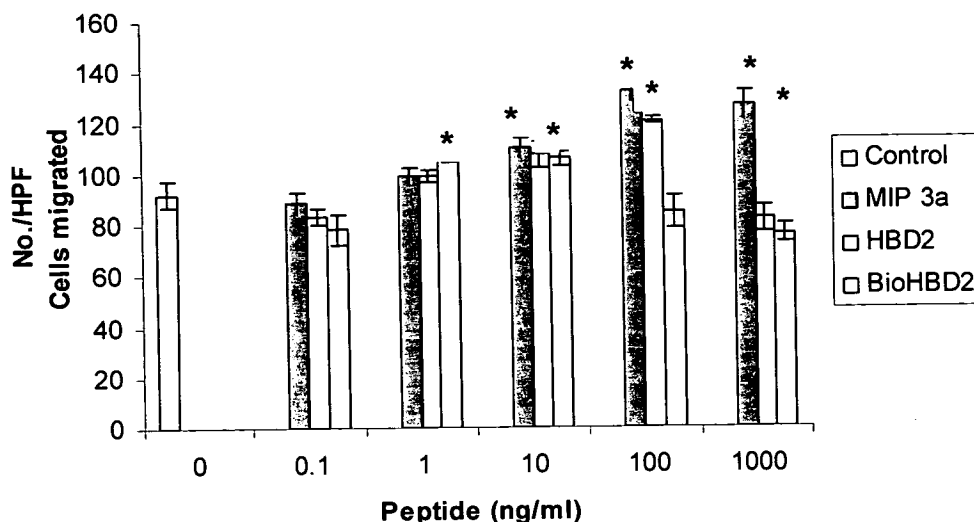
Figure 2.22. Chemotaxic Activity of BioHBD2 for CCR6 Transfected HEK293 Cells. Migration by MIP-3α (light purple) and sHBD2 (yellow) were positive controls. The numerical data (number of cells per high power field) was recorded as an average of three separate experiments in triplicate and error bars indicate the SE. Statistical significance ($p < 0.05$) is indicated with a * as compared to the number of cells per HPF of culture media alone.

A second functional role recently proposed for β-defensins is its anti-inflammatory properties [47, 48]. An important part of the mammalian innate immune system is the ability to detect and react to virulence factors. One of the most important activators is the bacterial outer membrane component lipopolysaccharide (LPS), also known as endotoxin. The important receptor that recognises LPS/endotoxin is the Toll-like receptor 4 (TLR4); a member of a the large family of receptors involved in recognition of virulence factors [49]. A working model of this recognition and activation involves the lipid A domain of bacterial LPS, along with LPS binding protein and CD14, interacting with TLR4 to trigger a complicated signalling transduction pathway within a number of cells in the immune system [49]. Up-regulation of the pro-inflammatory cytokine Tumor-Necrosis Factor-α (TNF-α) is one consequence of this interaction and HBD2 was shown previously to block LPS-induced TNF-α production by macrophages [47]. We tested the ability of BioHBD2 to block TNF-α production by primary human monocyte cells after stimulation using Kdo$_2$-lipid A, a chemically defined truncated LPS, isolated from a deep-rough strain of *E. coli* [50] (Figure

2.23). The results clearly show an increase in TNF-α production upon stimulation with

Kdo$_2$-lipid A as compared with media alone. A mixture of BioHBD2 (50 μg/ml) with Kdo$_2$-

lipid A (10 ng/ml) resulted in a decrease in TNF-α production compared to Kdo$_2$-lipid A

stimulation only. However there was no significant difference between the TNF-α levels

when the Kdo$_2$-lipid A concentration was increased (100 ng/ml). It has been previously

shown that stimulation of TNF-α production in macrophages with Kdo$_2$-lipid A in the range

of 50-100 μg/ml results in very similar TNF-α levels [50]. This lack of significant reduction

in TNF-α production after addition of BioHBD2 could be a result of a high concentration of

uncomplexed Kdo$_2$-lipid A. Subsequently an increase in concentration of BioHBD2 (100

μg/ml) mixed with Kdo$_2$-lipid A resulted in a significant decrease in TNF-α production as

compared to Kdo$_2$-lipid A alone and reveals that BioHBD2, like unmodified HBD2, has anti-

inflammatory properties. Together with its chemotactic properties, this indicates the addition

of a N-terminal biotin tag does not have a negative effect on HBD2 function and therefore is

an ideal peptide to use in searching for novel interacting partners within a range of tissues.
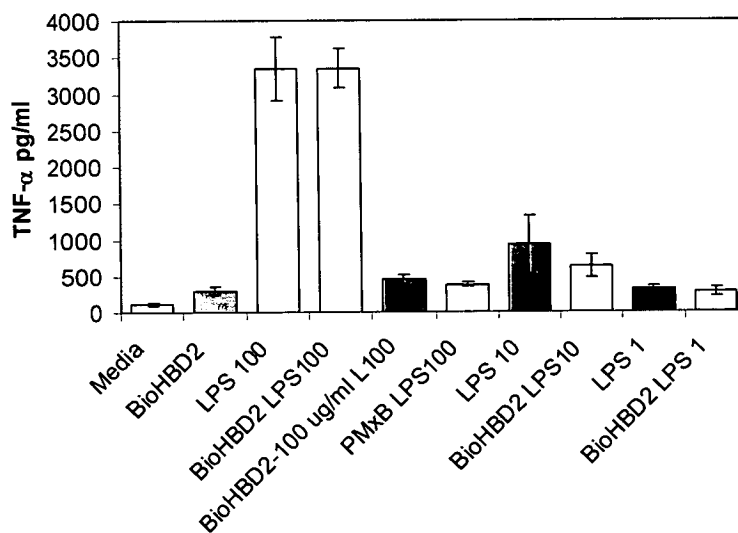
Figure 2.23. Inhibition of LPS-induced TNF-α Production by BioHBD2. Varying concentrations of BioHBD2 (μg/ml) and Kdo$_2$-lipid A (ng/ml) were mixed for 30 min prior to stimulation of primary human monocyte cells and production of TNF-α measured by ELISA. Data represent the mean and standard error of two independent experiments performed in triplicate, except stimulation with the BioHBD2 (100 μg/ml) and Kdo$_2$-Lipid A (100 ng/ml) mixture was only performed once in triplicate.

2.5 - Chapter 2 References

1. Kluver, E., K. Adermann, and A. Schulz, *Synthesis and structure-activity relationship of beta-defensins, multi-functional peptides of the immune system.* J Pept Sci, 2006. **12**(4): p. 243-57.

2. Raj, P.A., K.J. Antonyraj, and T. Karunakaran, *Large-scale synthesis and functional elements for the antimicrobial activity of defensins.* Biochem J, 2000. **347 Pt 3**: p. 633-41.

3. Wu, Z., et al., *Engineering disulfide bridges to dissect antimicrobial and chemotactic activities of human beta-defensin 3.* Proc Natl Acad Sci U S A, 2003. **100**(15): p. 8880-5.

4. Fang, X., et al., *Cloning and expression of human beta-defensin-2 gene in Escherichia coli.* Protein Pept Lett, 2002. **9**(1): p. 31-7.

5. Valore, E.V., et al., *Human beta-defensin-1: an antimicrobial peptide of urogenital tissues.* J Clin Invest, 1998. **101**(8): p. 1633-42.

6. Bals, R., et al., *Human beta-defensin 2 is a salt-sensitive peptide antibiotic expressed in human lung.* J Clin Invest, 1998. **102**(5): p. 874-80.

7. Harder, J., et al., *Isolation and characterization of human beta -defensin-3, a novel human inducible peptide antibiotic.* J Biol Chem, 2001. **276**(8): p. 5707-13.

8. Xu, Z., et al., *High-level expression of a soluble functional antimicrobial peptide, human beta-defensin 2, in Escherichia coli.* Biotechnol Prog, 2006. **22**(2): p. 382-6.

9. Xu, Z., et al., *High-level expression of soluble human beta-defensin-2 fused with green fluorescent protein in Escherichia coli cell-free system.* Appl Biochem Biotechnol, 2005. **127**(1): p. 53-62.

10. Pazgier, M. and J. Lubkowski, *Expression and purification of recombinant human alpha-defensins in Escherichia coli.* Protein Expr Purif, 2006. **49**(1): p. 1-8.

11. Chen, H., et al., *Efficient production of a soluble fusion protein containing human beta-defensin-2 in E. coli cell-free system.* J Biotechnol, 2005. **115**(3): p. 307-15.

12. Haiqin Chen, L.F., Zhinan Xu, Xiufei Yin, Peilin Cen, *Efficient production of soluble human beta-defensin-3–4 fusion proteins in Escherichia coli cell-free system.* Process Biochemistry, 2007. **42** p. 423-428.

13. Prodromou, C. and L.H. Pearl, *Recursive PCR: a novel technique for total gene synthesis.* Protein Eng, 1992. **5**(8): p. 827-9.

14. Kuliopulos, A. and C. Walsh, *Production, purification, and Cleavage of Tandem Repeats of Recombinant Peptides.* Journal of the American Chemical Society, 1994. **116**: p. 4599-4607.

15. Sarker, G. and S. Sommers, *The "Megaprimer" Method of Site-Directed Mutagenesis.* BioTechniques 1990. **8**(4): p. 404-407.

16. Rodriguez, J.C., L. Wong, and P.A. Jennings, *The solvent in CNBr cleavage reactions determines the fragmentation efficiency of ketosteroid isomerase fusion proteins used in the production of recombinant peptides.* Protein Expr Purif, 2003. **28**(2): p. 224-31.

17. Chino, N., et al., *Chemical Synthesis of Human β-Defensin (hBD)-1, -2, -3 and -4: Optimization of the Oxidative Folding Reaction.* International Journal of Peptide Research and Therapeutics, 2006. **12**(3): p. 203-209.

18. Hoover, D.M., et al., *The structure of human beta-defensin-2 shows evidence of higher order oligomerization.* J Biol Chem, 2000. **275**(42): p. 32911-8.

19. Crovella, S., et al., *Primate beta-defensins--structure, function and evolution.* Curr Protein Pept Sci, 2005. **6**(1): p. 7-21.

20.   Taylor, K., et al., *Analysis and separation of residues important for the chemoattractant and antimicrobial activities of beta-defensin 3*. J Biol Chem, 2008. **283**(11): p. 6631-9.

21.   Campopiano, D.J., et al., *Structure-activity relationships in defensin dimers: a novel link between beta-defensin tertiary structure and antimicrobial activity*. J Biol Chem, 2004. **279**(47): p. 48671-9.

22.   Harder, J., et al., *A peptide antibiotic from human skin*. Nature, 1997. **387**(6636): p. 861.

23.   Liu, A.Y., et al., *Human beta-defensin-2 production in keratinocytes is regulated by interleukin-1, bacteria, and the state of differentiation*. J Invest Dermatol, 2002. **118**(2): p. 275-81.

24.   Antcheva, N., et al., *Effects of positively selected sequence variations in human and Macaca fascicularis beta-defensins 2 on antimicrobial activity*. Antimicrob Agents Chemother, 2004. **48**(2): p. 685-8.

25.   Yang, D., et al., *Beta-defensins: linking innate and adaptive immunity through dendritic and T cell CCR6*. Science, 1999. **286**(5439): p. 525-8.

26.   Bourbonniere, M. and J. Nalbantoglu, *The restriction enzyme AlwNI is blocked by overlapping methylation*. Nucleic Acids Res, 1991. **19**(17): p. 4774.

27.   Pazgier, M., et al., *Studies of the biological properties of human beta-defensin 1*. J Biol Chem, 2007. **282**(3): p. 1819-29.

28.   Taylor, K., P.E. Barran, and J.R. Dorin, *Structure-activity relationships in beta-defensin peptides*. Biopolymers, 2008. **90**(1): p. 1-7.

29.   Kluver, E., et al., *Structure-activity relation of human beta-defensin 3: influence of disulfide bonds and cysteine substitution on antimicrobial activity and cytotoxicity*. Biochemistry, 2005. **44**(28): p. 9804-16.

30.   Hancock, R.E. and D.S. Chapple, *Peptide antibiotics*. Antimicrob Agents Chemother, 1999. **43**(6): p. 1317-23.

31.   Krishnakumari, V., S. Singh, and R. Nagaraj, *Antibacterial activities of synthetic peptides corresponding to the carboxy-terminal region of human beta-defensins 1-3*. Peptides, 2006. **27**(11): p. 2607-13.

32.   Morgera, F., et al., *Structuring and interactions of human beta-defensins 2 and 3 with model membranes*. J Pept Sci, 2008. **14**(4): p. 518-23.

33.   Hoover, D.M., et al., *The structure of human macrophage inflammatory protein-3alpha /CCL20. Linking antimicrobial and CC chemokine receptor-6-binding activities with human beta-defensins*. J Biol Chem, 2002. **277**(40): p. 37647-54.

34.   Sawai, M.V., et al., *The NMR structure of human beta-defensin-2 reveals a novel alpha-helical segment*. Biochemistry, 2001. **40**(13): p. 3810-6.

35.   Malik, Z.A. and B.F. Tack, *Structure of human MIP-3alpha chemokine*. Acta Crystallogr Sect F Struct Biol Cryst Commun, 2006. **62**(Pt 7): p. 631-4.

36.   Chan, D.I., et al., *Human macrophage inflammatory protein 3alpha: protein and peptide nuclear magnetic resonance solution structures, dimerization, dynamics, and anti-infective properties*. Antimicrob Agents Chemother, 2008. **52**(3): p. 883-94.

37.   Perez-Canadillas, J.M., et al., *NMR solution structure of murine CCL20/MIP-3alpha, a chemokine that specifically chemoattracts immature dendritic cells and lymphocytes through its highly specific interaction with the beta-chemokine receptor CCR6*. J Biol Chem, 2001. **276**(30): p. 28372-9.

38.   O'Neil, D.A., et al., *Expression and regulation of the human beta-defensins hBD-1 and hBD-2 in intestinal epithelium*. J Immunol, 1999. **163**(12): p. 6718-24.

39.   Witthoft, T., et al., *Enhanced human beta-defensin-2 (hBD-2) expression by corticosteroids is independent of NF-kappaB in colonic epithelial cells (CaCo2)*. Dig Dis Sci, 2005. **50**(7): p. 1252-9.

40.   Jurevic, R.J., et al., *Single-nucleotide polymorphisms and haplotype analysis in beta-defensin genes in different ethnic populations*. Genet Test, 2002. **6**(4): p. 261-9.

41.   Vatta, S., et al., *Human beta defensin 1 gene: six new variants.* Hum Mutat, 2000. **15**(6): p. 582-3.

42.   Kusano, K., Abiko, Y., Nishimura, M., Arakawa, T., Takeshima, M., Fugimoto, A., Takuma, T., Kuku, T., *Single-Nucleotide Polymorphism (SNP) in beta-defensin 2 in a Japanese Population and an Effect of -1029 SNP on Promoter Activity.* Oral Science International, 2005. **2**(2): p. 80-84.

43.   Jurevic, R.J., et al., *Single-nucleotide polymorphisms (SNPs) in human beta-defensin 1: high-throughput SNP assays and association with Candida carriage in type I diabetics and nondiabetic controls.* J Clin Microbiol, 2003. **41**(1): p. 90-6.

44.   Matsushita, I., et al., *Genetic variants of human beta-defensin-1 and chronic obstructive pulmonary disease.* Biochem Biophys Res Commun, 2002. **291**(1): p. 17-22.

45.   Kocsis, A.K., et al., *Association of beta-defensin 1 single nucleotide polymorphisms with Crohn's disease.* Scand J Gastroenterol, 2008. **43**(3): p. 299-307.

46.   Ramasundara, M., et al., *Defensins and inflammation: the role of defensins in inflammatory bowel disease.* J Gastroenterol Hepatol, 2009. **24**(2): p. 202-8.

47.   Scott, M.G., et al., *Cutting edge: cationic antimicrobial peptides block the binding of lipopolysaccharide (LPS) to LPS binding protein.* J Immunol, 2000. **164**(2): p. 549-53.

48.   Motzkus, D., et al., *The novel beta-defensin DEFB123 prevents lipopolysaccharide-mediated effects in vitro and in vivo.* Faseb J, 2006. **20**(10): p. 1701-2.

49.   Miller, S.I., R.K. Ernst, and M.W. Bader, *LPS, TLR4 and infectious disease diversity.* Nat Rev Microbiol, 2005. **3**(1): p. 36-46.

50.   Raetz, C.R., et al., *Kdo2-Lipid A of Escherichia coli, a defined endotoxin that activates macrophages via TLR-4.* J Lipid Res, 2006. **47**(5): p. 1097-111.

Chapter 3

Purification and Biochemical Analysis of

Human Chemokine Receptor 6 (CCR6)

3.1 - Production of Human Chemokine Receptor 6 (CCR6)

3.1.1 - Introduction

Despite the increasing number of heterologous expression systems available for chemokine receptor production, relatively few receptors have been purified to homogeneity and/or analyzed biochemically. The two HIV-1 coreceptors, CCR5 and CXCR4, along with the decoy chemokine receptor D6, are the most extensively analyzed receptors and purification has been achieved using both *E. coli* and/or mammalian cell systems [1-4].

The goal of this project was to optimize the purification of CCR6 to produce sufficient quantities of the protein for proteomic and biochemical analysis. Despite the low yields and time-consuming methods, mammalian cells were chosen as the expression system because of their closeness to the native environment and ability to perform post-translational modifications (PTMs). Furthermore, cells expressing CCR6 were available in our laboratory to assay the activity of various defensin peptides. The CCR6 gene was engineered with both N-terminal and C-terminal specific tags to aid both solubilization and purification before generation of a stable cell line expressing CCR6 was obtained. Successful solubilization followed by optimization of purification yielded sufficiently pure CCR6 to allow for both mass spectrometry and biochemical analysis. Although further optimization is required to increase the yield and purity, this is the first occasion that CCR6 has been purified and provides a platform for further characterization.

3.1.2 - Expression of Epitope-Tagged CCR6 in Mammalian Cell Lines

The CCR6 transfected HEK293 cells used in all previous chemotactic assays was an ideal expression system for initial purification studies. The expression plasmid

pcDNA3.1/CCR6, used to transfect the original HEK293 cells, was obtained from Dr De

Yang. Although the CCR6 gene had an enterokinase cleavable N-terminal FLAG tag, to

increase stability and facilitate purification of CCR6, the addition of a C-terminal tag was

deemed necessary. Using the original vector as a template, mega-primer mutagenesis was

carried out to add a C-terminal HIS10 tag. Although mutagenesis was successful, as revealed

by DNA sequencing, subsequent cloning back into pcDNA3.1 was unsuccessful because

large-scale restriction digestion of pcDNA3.1 resulted in multiple non-specific cleavages.

Therefore a CCR6 gene incorporating the C-terminal HIS10 tag was designed and purchased

from Codon devices (Figure 3.1 A). This epitope-tagged CCR6 gene was cloned into

pcDNA3.1 and was used as an expression plasmid for transfection of mammalian cells

(Figure 3.1 B).

A

```
1    MDSKGSSQKG SRLLLLLVVS NLLLCQGVVS DYKDDDDKLN FSDVFDSSED
51   YFVSVNTSYY SVDSEMLLCS LQEVRQFSRL FVPIAYSLIC VFGLLGNILV
101  VITFAFYKKA RSMTDVYLLN MAIADILFVL TLPFWAVSHA TGAWVFSNAT
151  CKLLKGIYAI NFNCGMLLLT CISMDRYIAI VQATKSFRLR SRTLPRSKII
201  CLVVWGLSVI ISSSTFVFNQ KYNTQGSDVC EPKYQTVSEP IRWKLLMLGL
251  ELLFGFFIPL MFMIFCYTFI VKTLVQAQNS KRHKAIRVII AVVLVFLACQ
301  IPHNMVLLVT AANLGKMNRS CQSEKLIGYT KTVTEVLAFL HCCLNPVLYA
351  FIGQKFRNYF LKILKDLWCV RRKYKSSGFS CAGRYSENIS RQTSETADND
401  NASSFTMHHH HHHHHHH
```

B
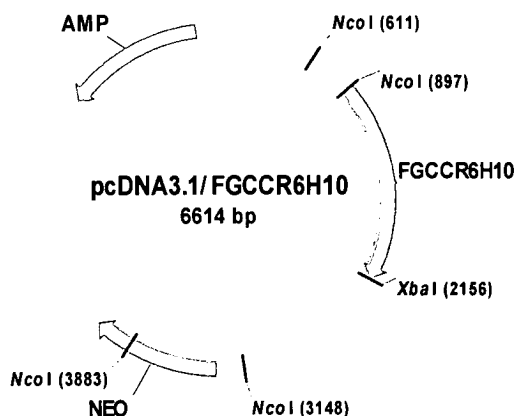
Figure 3.1. Epitope-Tagged CCR6 (A) Full Length Sequence of CCR6 (417 AA). Histidine tag (Red) and FLAG tag (Blue) is indicated. **(B)** Schematic Representation of Expression plasmid pcDNA3.1/FGCCR6H10.

Expression plasmid pcDNA3.1/FGCCR6H10 was transfected into two different mammalian cell lines, Human Embryonic Kidney (HEK) 293 and L1.2 murine pre-B cells. The HEK293 cells had been shown to express active CCR6 and insert the protein into its membrane in an orientation that allowed it to be chemoattracted by its natural ligands, CCL20 (also known as MIP3-α) and β-defensins [5]. Unfortunately, HEK293 cells are adherent cells and scaling-up the cell culture to facilitate purification of large amounts of protein is expensive and time-consuming. As an alternative, L1.2 cells are suspension cells and therefore scaling-up in large bioreactors was an attractive alternative. Although L1.2 cells had not been tested for CCR6, another receptor in the same GPCR family, the non-signalling chemokine receptor D6, had previously been shown to express high levels upon sodium butyrate treatment [1]. We used the same plasmid, pcDNA3.1/FGCCR6H10, to transfect the L1.2 cells but unfortunately, despite growth of transfected L1.2 cells in killing media, flow cytometric analysis determined there was no surface expression of the receptor even after sodium butyrate treatment (Figure 3.2 A-D). The difference between surface expression of D6 and CCR6 could be due to the lack of a N-terminal hemagglutinin (HA) tag present in D6. This signal peptide from influenza HA has been shown to increase the surface expression of GPCRs [6].
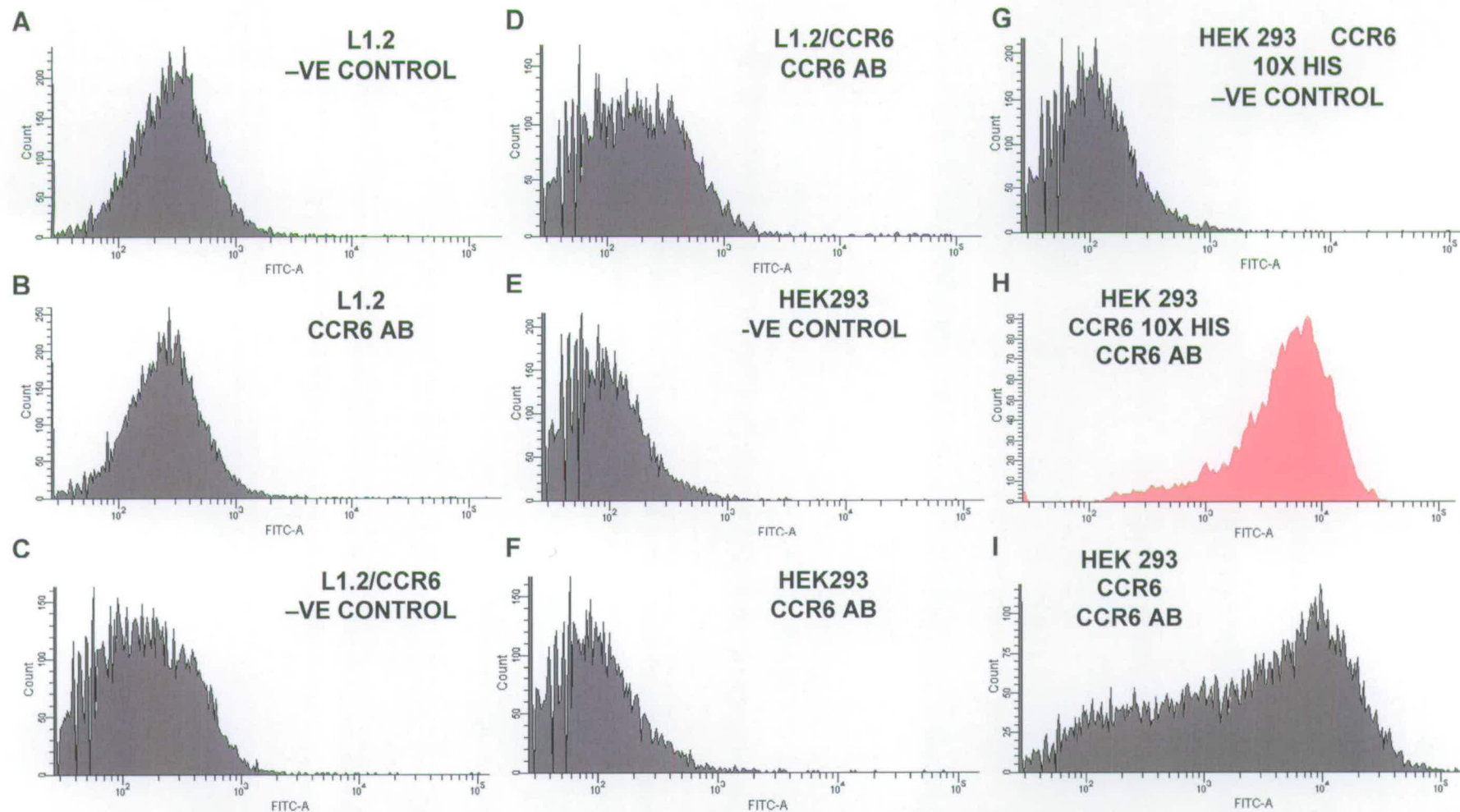
Figure 3.2. CCR6 Expression in Transfected Mammalian Cells. L1.2 control cells (A and B) or Epitope-tagged Human CCR6 transfected L1.2 cells (C and D) were examined for specific binding by flow cytometry after sodium butyrate treatment using either IgG2b-FITC negative control antibody (A and C) or an anti-CCR6-FITC antibody (B and D).

HEK293 control cells (E and F) or Epitope-tagged Human CCR6-expressing HEK293 cells (G and H) were examined for specific binding by flow cytometry using either IgG2b-FITC negative control antibody (E and G) or an anti-CCR6-FITC antibody (F and H). Previously confirmed CCR6 expressing HEK293 cells were used as positive control (I) [5].

Highly-expressing stable transformants of CCR6 in HEK293 cells were confirmed using both RT-PCR and FACS analysis. Using CCR6 specific primers, RNA extracted from both HEK293 control and HEK293 transfected cells underwent RT-PCR analysis. CCR6 gene expression was confirmed in only transfected HEK293 cells were reverse transcriptase had been added to the reaction (Figure 3.3, Lane 8). The lack of a CCR6 band in the reaction without reverse transcriptase indicated that this gene expression was not due to DNA contamination. It was also found that this CCR6 expression could not be detected in the control HEK293 cells. This result was confirmed by the identification of β-Actin expression indicating that both RNA extraction and RT-PCR analysis had been performed correctly. This result agrees with a previous microarray profiling study of HEK293 cells that revealed CCR6 was not expressed in this cell line and as such HEK293 cells could be used as a negative control for future investigations [7]. RT-PCR analysis only detects gene expression and does not reveal whether the CCR6 protein was being properly trafficked to the cell surface therefore FACS analysis was performed. FACS analysis using an anti-CCR6-FITC conjugated antibody was performed on both HEK293 control and HEK293 transfected cells. Comparison between the relative fluorescence of HEK293 control and HEK293 transfected cells confirms the RT-PCR analysis that only HEK293 transfected cells are expressing CCR6. Furthermore this shows that CCR6 was successfully inserted in the outer membrane in a topologically correct orientation (Figure 3.2 E-I). Comparison of the relative fluorescence between CCR6 expressing cells with and without a C-terminal HIS10 tag suggested that the affinity tag had no detrimental effect on surface expression (Figure 3.2 H and I).
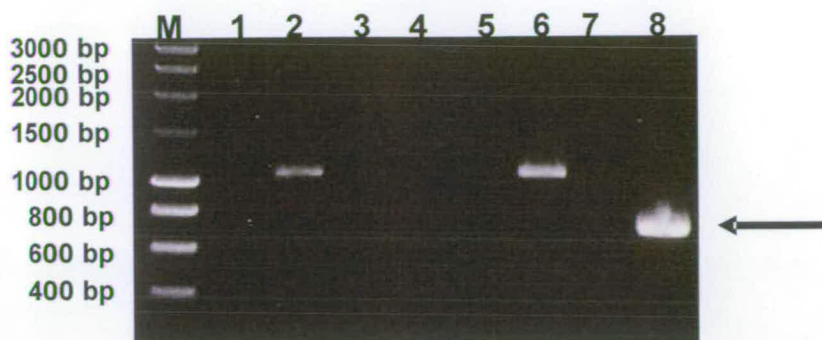
Figure 3.3. Expression of CCR6 in Transfected HEK293 Cells. CCR6 gene expression was analyzed by RT-PCR with β-Actin acting as house-keeping gene. Lanes 1-2, β-Actin expression in HEK293 cells, without and with reverse transcriptase. Lanes 3-4, CCR6 expression in HEK293 cells, without and with reverse transcriptase. Lanes 5-6, β-Actin expression in CCR6 transfected HEK293 cells, without and with reverse transcriptase. Lanes 7-8, CCR6 expression in CCR6 transfected HEK293 cells, without and with reverse transcriptase. The band indicated by arrow is correct size for CCR6 gene fragment.

Initial protein analysis of epitope-tagged CCR6 was performed on a small scale. The intrinsic hydrophobic properties of membrane proteins, along with their association with membrane lipids make visualization by SDS-PAGE analysis difficult due to their tendency to aggregate [8]. Therefore a temperature dependent SDS/DTT solubilization step was carried out prior to SDS-PAGE separation. Using anti-CCR6 antibody western blot analysis, epitope-tagged CCR6 was identified predominately as a dimeric species at temperatures above 50 °C (Figure 3.4). Below this temperature there was a slight increase in the monomeric form and reduction in the dimeric form. Reducing the temperature even further to 4 °C at the same time as increasing solubilization time allowed predominately monomeric epitope-tagged CCR6 to be visualized by western blot analysis and these conditions were therefore used in all future analysis. The effect of sodium butyrate treatment on CCR6 expressing HEK293 cells was also tested. Unfortunately treatment of these cells resulted in increased cell toxicity revealed by cell detachment from the culture flask and less CCR6 expression identified by anti-CCR6 antibody western blots analysis (Figure 3.5).
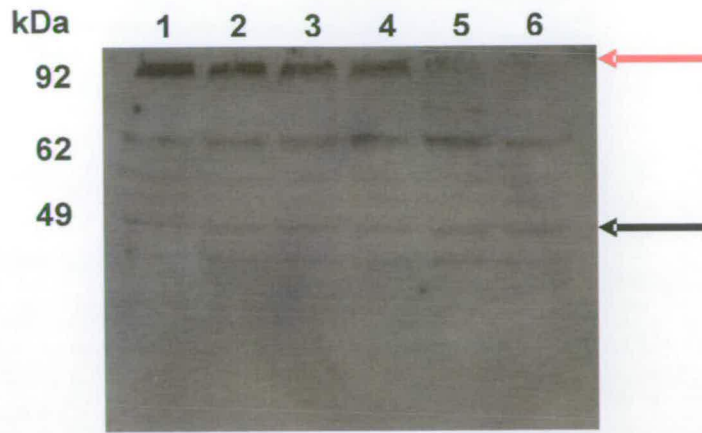
Figure 3.4. Western Blot Analysis Revealing the Effects of Temperature on CCR6 Protein Expression. Lane 1, 90 °C, Lane 2, 80 °C, Lane 3, 70 °C, Lane 4, 60 °C, Lanes 5, 50 °C, Lane 6, room temp. The black and red arrows indicate monomeric CCR6 and dimeric CCR6 respectively.
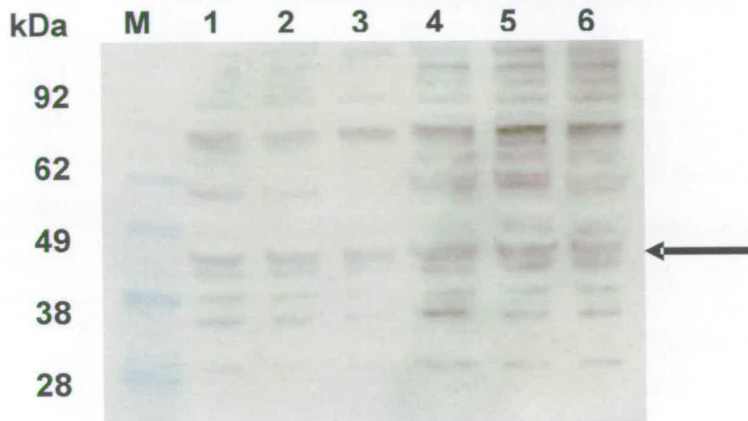
Figure 3.5. Western Blot Analysis Revealing the Effects of Sodium Butyrate on CCR6 Protein Expression. Lane M, SeeBlue 2 protein marker; Lanes 1-3, CCR6 transfected HEK293 cells with 10 mM sodium butyrate treatment; Lanes 4-6, CCR6 transfected HEK293 cells without sodium butyrate treatment. The arrow indicates monomeric CCR6.

3.1.3 - Solubilization of Epitope-Tagged CCR6

Removal of membrane proteins from their natural environment is both a necessary and problematic step in their purification. Instability and insolubility in aqueous buffers necessitates the use of either mild detergent extraction or, if the proteins have been expressed in a bacterial system, isolation from inclusion bodies and subsequent refolding. Due to the additional problems associated with refolding functional membrane proteins, epitope-tagged

CCR6 was extracted using mild, non-ionic detergents. Studies where chemokine receptors were subjected to systematic detergent screens have highlighted that a general method cannot be applied and even GPCRs from the same family require individual assessment and optimization [2, 3, 9]. Therefore initial solubilization of epitope-tagged CCR6 from HEK293 crude membrane extracts were performed using a combination of n-dodecyl-β-maltoside (DDM) and cholesteryl hemisuccinate ester (CHS), previously shown to be effective in solubilization of chemokine receptor CXCR4 [10]. A mixture of solubilizied epitope-tagged CCR6, other membrane proteins and mixed micelles of phospholipids and detergents were then subjected to various chromatographic techniques to optimize CCR6 purification.

3.1.4 - Immobilised Metal-Affinity Chromatography Purification of Epitope-Tagged CCR6

Solubilized epitope-tagged CCR6 was purified using two-step immobilized metal-affinity chromatography (IMAC) using resin as opposed to a packed column. SDS-PAGE and western blot analysis after Ni^{2+}-NTA purification revealed that epitope-tagged CCR6 was indeed soluble and that the deca-HIS tag was accessible to bind the affinity resin efficiently. In fact, anti-HIS antibody western blot analysis revealed the possible presence of proteolyzed, monomeric and higher-order forms of CCR6 (Figure 3.6 A). Whether proteolysis and aggregation is a result of the extended purification protocol and/or excessive incubation time in the denaturing SDS-PAGE loading buffer is unclear. This does however emphasize the natural instability of membrane proteins once they are removed from their native environment.

Although single-step IMAC chromatography had been previously shown to result in the purification of other GPCRs to near homogeneity, SDS-PAGE analysis clearly showed the presence of multiple non-CCR6 proteins necessitating another purification step. Fractions

containing proteins that were anti-HIS antibody positive were pooled, diluted and applied to pre-equilibrated cobalt affinity resin (Talon). SDS-PAGE analysis after Talon purification showed that this step led to increased purity of epitope-tagged CCR6. However western blot analysis shows an increasing number of cleavage products at ~24 and ~30 kDa with a loss of the ~47 kDa band thought to represent the full length monomeric epitope-tagged CCR6 (Figure 3.6 B) (47475.42 Da). Comparison of both SDS-PAGE and western blot analysis also reveals protein bands non-reactive to the anti-HIS antibody. These could represent C-terminal cleavage products of epitope-tagged CCR6 and also membrane associated proteins that bind non-specifically to either CCR6 or lipids still associated in the micelle. However, purification using only one affinity tag increases the probability that these protein bands are non-specifically bound contaminants. Therefore the second step using Talon resin was replaced with a size-exclusion chromatography step.

Identification of monomeric, full length, epitope-tagged CCR6 is also problematic by SDS-PAGE analysis alone. Using molecular mass estimates based on amino acid sequence is difficult since membrane proteins migrate faster than the soluble low molecular weight calibration proteins, however addition of purification tags and post-translational modifications, e.g., glycosylation, can retard this migration [11]. Therefore SDS-PAGE analysis alone can not used to identify full length CCR6. Moreover, anti-HIS antibody western blot analysis alone is also unable to identify full length CCR6 but together with an anti-FLAG antibody, full length CCR6 would be identifiable. Therefore all future purification analysis was performed using both antibodies.
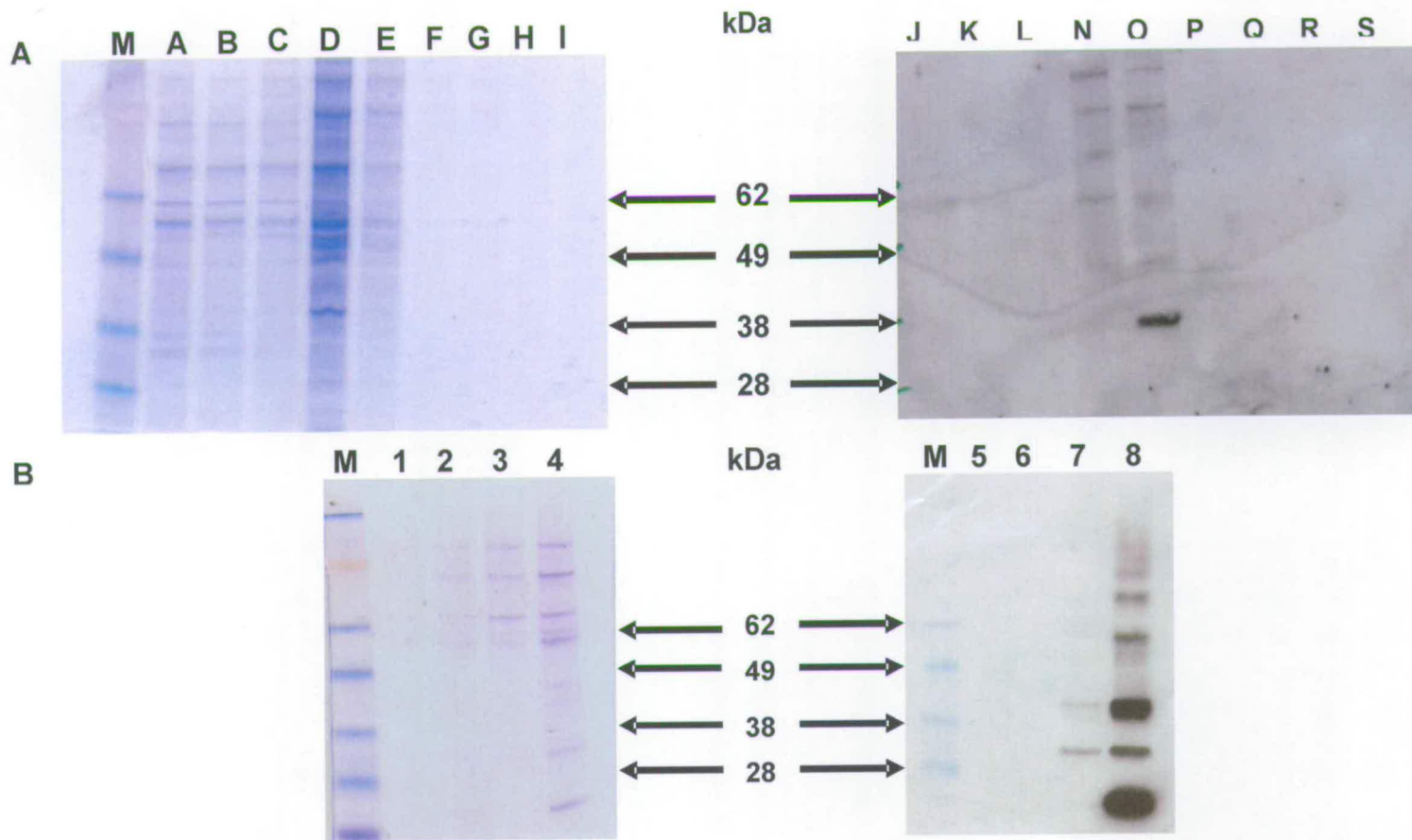
Figure 3.6. IMAC Purification of Epitope-Tagged Human CCR6 from HEK293 Cells. (A). Left hand side; SDS-PAGE of Ni^{2+}-NTA purification of FLAG-CCR6-HIS10. Lanes A - I, 10 mM imidazole wash, 300 mM imidazole elution and 500 mM imidazole elution fractions in triplicates. Right-hand side, western blot analysis of Ni^{2+}-NTA purification of FLAG-CCR6-HIS10. Lanes J - S, 10 mM imidazole wash, 300 mM imidazole elution and 500 mM imidazole elution fractions in triplicates analyzed with anti-HIS antibody. **(B)** SDS-PAGE and western blot analysis of Talon resin purification of FLAG-CCR6-HIS10. Left hand side, lane 1-4, 500 mM imidazole elution fractions and concentrated 500 mM imidazole elution fractions in duplicate analyzed by SDS-PAGE. Right hand side lane 5, flow through fraction; lane 6, 10 mM imidazole wash fraction; lanes 7-8, concentrated 500 mM imidazole elution fractions analyzed with anti-HIS antibody.

3.1.5 - Metal-Affinity followed by Size Exclusion Purification of Epitope-

Tagged CCR6

Size exclusion chromatography is often used as a final purification step, useful in removing small molecules used as elutants or large non-specific binders in affinity chromatography. Its capability of resolving monomeric and dimeric chemokine receptors also emphasized its usefulness in the purification of epitope-tagged CCR5 [4]. Ni^{2+}-NTA purification again yielded multiple HIS-containing proteins revealing proteolytic cleavage products as well as possible full length epitope-tagged CCR6 but no higher-order structures (Figure 3.7).
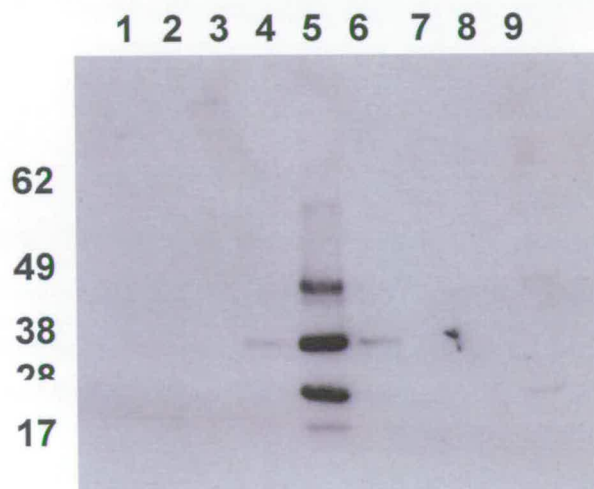
Figure 3.7. Western Blot Analysis of Ni^{2+}-NTA Purification of FLAG-CCR6-HIS10. Lanes 1-3, 10 mM imidazole wash; lanes 4-6, 300 mM imidazole elution fraction; lanes 7-9, 500 mM imidazole elution fraction. FLAG-CCR6-HIS10 was separated by SDS-PAGE and identified using an anti-HIS antibody.

Separation of cleavage products was attempted using a calibrated Superdex 200 size exclusion column. The elution profile was monitored at 280 nm and clearly shows separation of protein peaks (Figure 3.8 A). Unfortunately, anti-HIS antibody western blot analysis shows that separation of full-length CCR6 from cleavage products was not successful (Figure 3.9). Interestingly, anti-FLAG western blot analysis indicates the presence of two FLAG containing proteins. These two proteins also reacted with the anti-HIS antibody indicating the presence of full-length epitope-tagged CCR6. The difference in their migration

suggests a possible difference in their patterns of PTMs, although these differences are not known at present. Intriguingly, cleavage products of CCR6 did not react with the anti-FLAG antibody suggesting that it is the N-terminal section of CCR6 that is more sensitive to proteolytic cleavage.

A

B
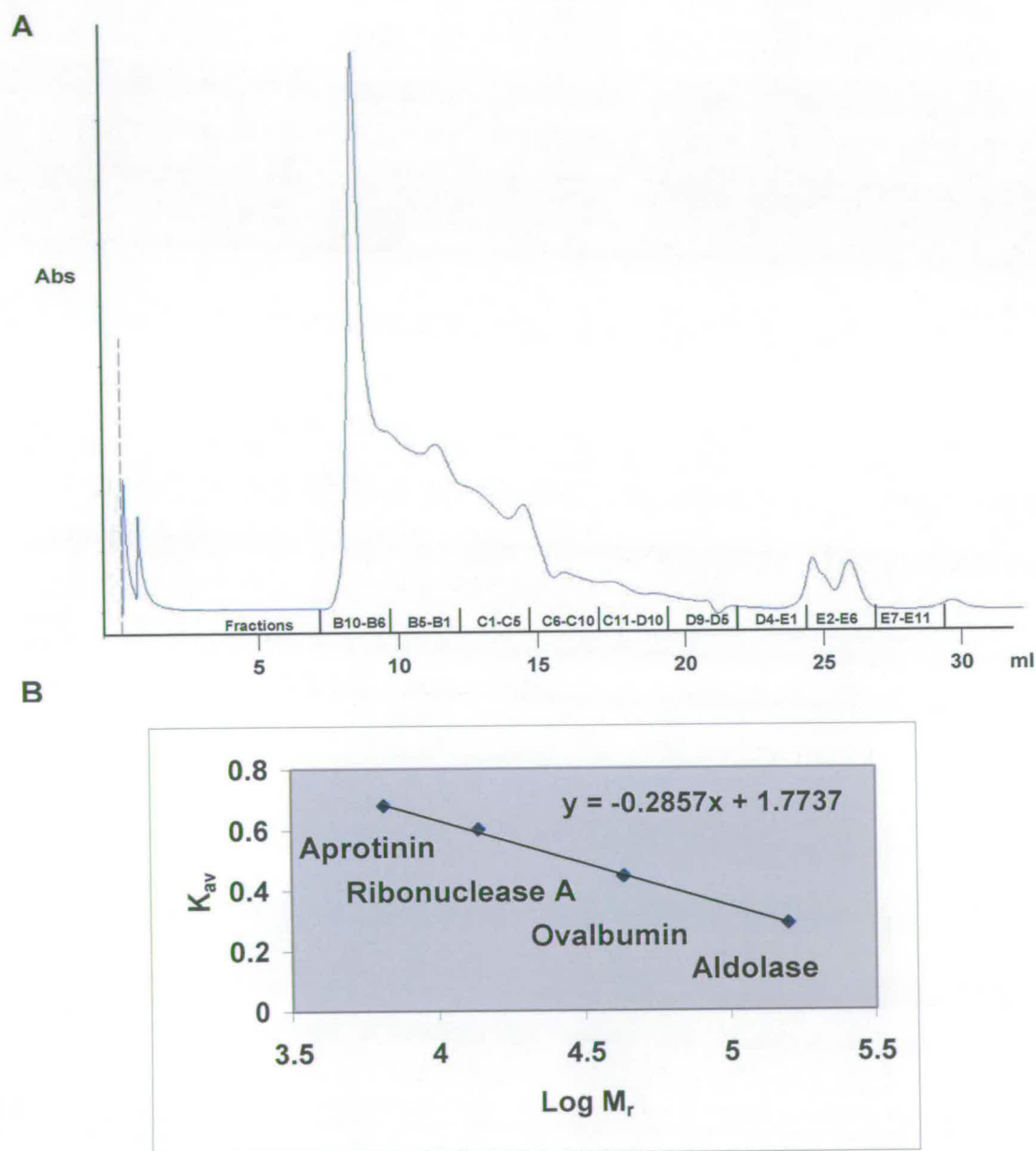
Figure 3.8. Size Exclusion purification of epitope-tagged CCR6. (A) FLAG-CCR6-HIS10 elution profile from Superdex 200 size exclusion column analyzed at wavelength 280 nm. **(B)** Calibration curve for column.

Using the calibration curve (Figure 3.8 B), it was estimated that CCR6 solubilized in the detergent DDM migrated with a mass > 230 kDa. This increase in mass is a consequence of the CCR6 being incorporated into a detergent micelle and as such the fractionation range of the column was not optimal for ideal separation. Future purifications should use Superdex 300 size exclusion chromatography which has higher resolution for large proteins. Furthermore, more stringent chromatography prior to size exclusion would be needed as SDS-PAGE analysis showed a mixture of proteins eluting together with the CCR6. Consequently a third purification was performed taking advantage of the N-terminal FLAG tag.
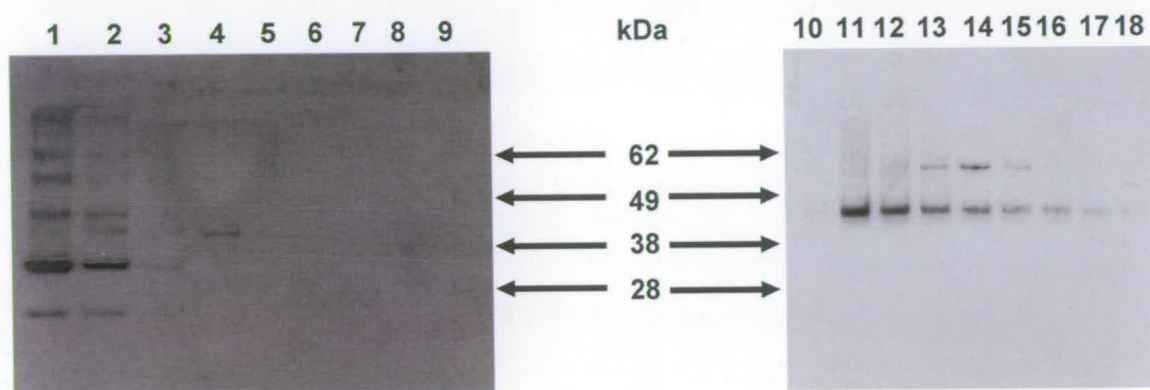
Figure 3.9. Western Blot Analysis of Superdex 200 Purification of FLAG-CCR6-HIS10. Lane 1, elution fractions B10-B6; lane 2, elution fractions B5-B1; lane3, elution fractions C1-C5; lane 4, elution fractions C6-C10; lane 5, elution fractions C11-D10; lane 6, elution fractions D9-D5; lane 7, elution fractions D4-E1; lane 8, elution fractions E2-E6; lane 9, elution fractions E7-E11. FLAG-CCR6-HIS10 was separated by SDS-PAGE and identified using an anti-HIS antibody. Lanes 10-18, elution fractions B9-B1 analyzed with an anti-FLAG antibody.

3.1.6 - Metal-Affinity followed by Immuno-Affinity Purification of Epitope-Tagged CCR6

Purification utilizing both the N-terminal and C-terminal tags is advantageous in isolating full-length CCR6 because only proteins with both tags will be isolated. In an attempt to avoid proteolysis of CCR6 which we observed with the methods described above, batch purification using loose Ni^{2+}-NTA resin was replaced with IMAC chromatography on a packed column attached to an AKTA Purifier. In addition, purification of CCR6 was performed without a previous freeze-thawing step between solubilization and metal-affinity chromatography.
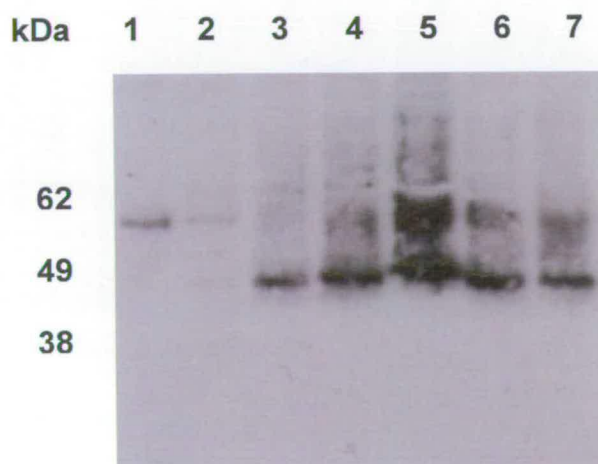
Figure 3.10. Western Blot Analysis of His-trap Ni^{2+} Purification of FLAG-CCR6-HIS10. Lane 1, elution fractions 14-20; lane 2, elution fractions 21-27; lane 3, elution fractions 28-34; lane 4, elution fractions 35-41; lane 5, elution fractions 42-48; lane 6, elution fractions 49-56; lane 7, elutions fractions 57-62. Proteins were eluted with an increasing imidazole gradient ranging from 30 mM to 500 mM and identified using an anti-FLAG antibody.

Analysis of the IMAC chromatography elution profile of purified epitope-tagged CCR6 was complicated by the inherent spectroscopic properties of imidazole. Imidazole absorbance at 280 nM increased the possibility of eluted CCR6 fractions being concealed especially at the higher concentrations. Therefore elution fractions were combined and anti-FLAG antibody western blot analysis was performed (Figure 3.10). Clearly this revealed the

existence of two proteins that reacted with the N-terminal epitope specific antibody. This would indicate two different forms of full-length CCR6, migrating at ~47 kDa and ~56 kDa respectively. These two proteins are identical in size to that previously isolated using size-exclusion chromatography (Figure 3.9). Further purification using immuno-affinity chromatography specific to the FLAG peptide tag resulted in a significant improvement in the purity of full-length CCR6. SDS-PAGE analysis with the extremely sensitive silver stain reveals a strong band at ~47 kDa with a major contaminating protein at ~62 kDa (Figure 3.11). Subsequent mass spectrometric analysis of the 62 kDa band following in-gel tryptic digestion revealed this contaminating band to be the heavy chain of monoclonal anti-FLAG antibody. The protein migrating at ~47 kDa clearly reacts strongly with both anti-HIS and anti-FLAG antibodies suggesting that it is the full length epitope-tagged CCR6 (predicted mass 47,475 Da, Figure 3.11). The protein migrating at ~56 kDa reacts with the anti-HIS antibody but only reacts weakly with the anti-FLAG antibody indicating that if it is an alternatively modified form of CCR6 then this it is less abundant. However another explanation could be that CCR6 is not fully denatured and/or reduced and therefore SDS binding is affected which alters its migration pattern for the same protein. Again this highlights the problems associated with GPCRs and their analysis by SDS-PAGE.
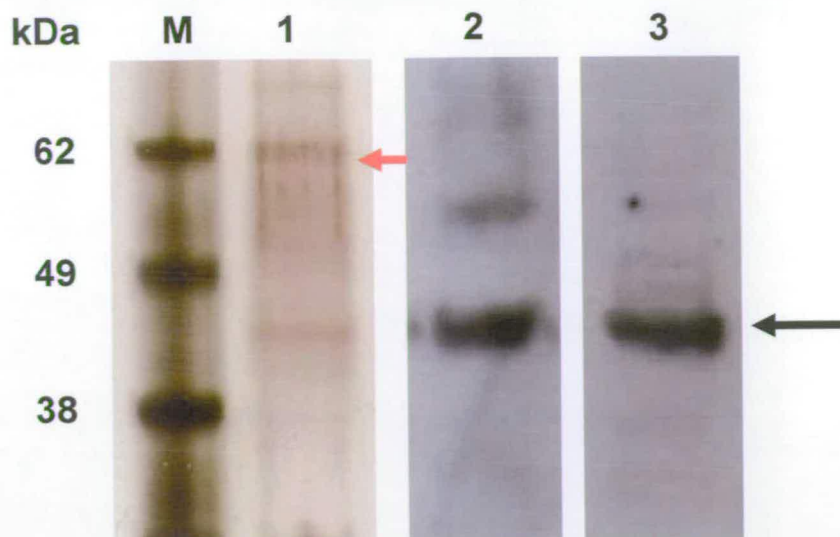
Figure 3.11. Anti-FLAG Affinity Purification of FLAG-CCR6-HIS10. Lane 1, silver stained SDS-PAGE gel of purified FLAG-CCR6-HIS10. Lane 2, purified FLAG-CCR6-HIS10 analyzed with anti-HIS antibody and lane 3, anti-FLAG antibody. The band indicated by a black arrow is the correct size for full length FLAG-CCR6-HIS10 (47,475 Da). The band indicated with a red arrow was subsequently identified as the heavy chain of the monoclonal anti-FLAG antibody.

3.2 - Characterization of Purified Epitope-Tagged CCR6

3.2.1 - Nanospray LC-MS/MS Analysis of Epitope-Tagged CCR6

To confirm the identity and further characterize the purified CCR6 isolated by the metal-affinity steps, nanospray (nano) LC-MS/MS analysis was performed on peptide fragments from proteolysis of CCR6. Detergents necessary for GPCR purification have detrimental effects on the quality of MS analysis through: 1) sample ionization suppression; 2) adduct formation; 3) detergent ionization signals concealing sample signals [12]. Two methods were performed to circumvent the detrimental effects of detergents. First, in-gel tryptic digestion of CCR6 separated by SDS-PAGE was performed. Extraction of peptide fragments into a MS-compatible buffer was attempted before nanospray LC-MS/MS analysis. Unfortunately no tryptic peptide fragments corresponding to CCR6 were identified. Successful trypsin digestion of CCR6 would yield two types of fragments. The first type is insoluble in mass spectrometry compatible buffers and hence could not be detected. This

group is composed of large, hydrophobic transmembrane helical domains of CCR6 and is a result of a low number of arginines and/or lysines present. In contrast, it was hoped that the hydrophilic N- and C-terminal regions, in addition to the loop regions, constituting the soluble MS-detectable fragments would be detected. The inability to detect the latter fragments is likely a result of inefficient enzymatic cleavage of CCR6, resulting in large, hydrophobic peptides which were extracted from the gel matrix in an extremely low yield.

The second method used to remove detrimental detergents was to precipitate CCR6 prior to in-solution chemical and enzymatic cleavage, with the detergents remaining in the organic solvent. It was found that precipitated CCR6 subsequently dissolved more readily in acidic conditions necessary for chemical cleavage. CNBr cleaves peptide bonds C-terminal to methionine residues often found in hydrophobic helical domains. Together with tryptic digestion, peptide fragments are shorter, more soluble and therefore more conducive to better mass spectrometry analysis after both chemical and enzymatic digestion. To further improve the efficiency of trypsin cleavage, chemically-digested fragments were dissolved in RapiGest (Waters), a MS-compatible detergent shown previously to improve enzymatic digestion and mass spectrometry analysis of neurotensin [13].

Gratifyingly, nanoLC-MS/MS analysis of CCR6 subjected to this procedure yielded a total of three sequenced peptide fragments corresponding to CCR6 (Table 3.1). Sequences from MS/MS analysis include peptides derived from N-terminal extracellular domain, intracellular loop 2 and extracellular loop 3 connected to part of transmembrane helix 6. A representative tandem mass spectrum reveals the sequencing of intracellular loop 2 (Figure 3.12). Although sequence coverage is <10%, this provides a good basis for further, more comprehensive MS analysis. Improvements in optimization of protein purification would undoubtedly improve sequence coverage as a contaminating protein, Cytoskeleton-associated protein 4 (63 kDa membrane protein) was identified and likely suppressed CCR6 peptide fragment ionization.

PEPTIDE	SEQUENCE	POSITION IN CCR6
1	$_{34}$ LLCSLQEVR $_{42}$	N-terminal to first transmembrane helix
2	$_{144}$ YIAIVQATK $_{152}$	Intracellular loop 2 (ICL2)
3	$_{273}$ VLLVTAANLGK $_{283}$	Part of transmembrane helix 6 connected to extracellular loop 3 (ECL 3)

Table 3.1 CCR6 Peptide Fragments Resulting from Both Chemical and Enzymatic Cleavage. Numbers indicated are the positions of the fragments in the context of the mature full-length hCCR6 sequence starting at the N-terminal. The MS/MS data for peptide 2 is shown in Figure 3.12 below.

A major reason for expressing CCR6 in the heterologous mammalian expression system was their ability to correctly post-translationally modify the protein of interest. Mass spectrometry has been successfully shown to identify previously putative post-translational modifications of GPCRs [14, 15]. NanoLC-MS/MS analysis of trypsin digested purified Histamine H_1 receptor not only identified an N-linked glycosylation site but also the individual components that constituted this modification [14]. Phosphorylation sites have also been identified using a similar strategy in the V2 Vasopressin receptor (V2R). NanoLC-MS/MS analysis of IMAC enriched trypsin digested V2R revealed a novel intracellular phophorylation site [15]. However even complete sequence coverage can not guarantee their identification, therefore a biochemical analysis of CCR6 PTMs was carried out in conjunction with MS analysis.
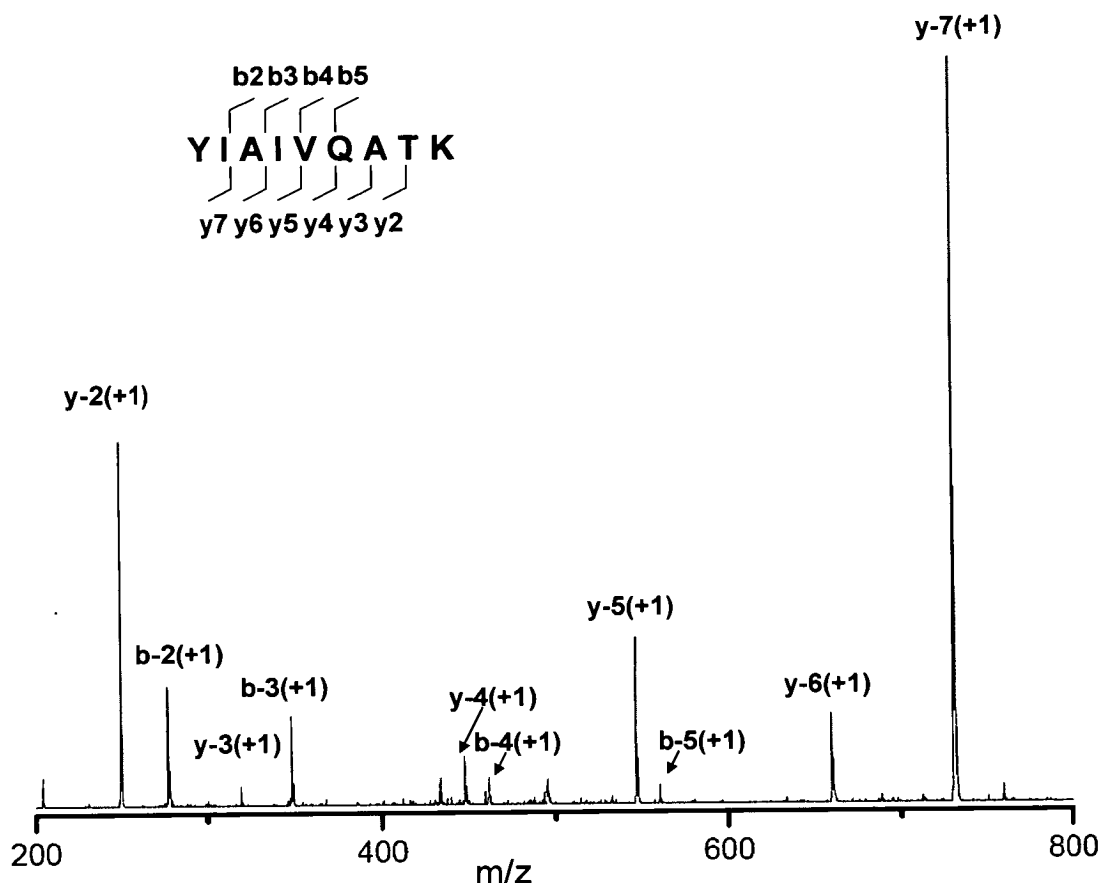
Figure 3.12. MS/MS Spectrum of a Peptide Fragment of Purified CCR6. *Inset,* Peptide sequence corresponding to a section of ICL 2. Observed monoisotopic mass was 1005.55 Da and calculated monoisotopic mass was 1005.59 Da.

3.2.2 - Post-translational Modification Analysis of CCR6

Biochemical methods have been used to identify a range of post-translational modifications (PTMs) in numerous chemokine receptors [16-18]. In general, proper intracellular trafficking (N-linked glycosylation), improved ligand binding (tyrosine sulfation and O-linked glycosylation), receptor stability (palmitoylation), and receptor densensitization and internalization (phosphorylation) are just some of the roles PTMs play in proper chemokine receptor functioning.

Due to a lack of CCR6 biochemical analysis, preliminary bioinformatic sequence analysis was performed to identify putative PTM sites. Results obtained using PROSITE; a

database of functional motifs [19], revealed CCR6 has five putative N-glycosylation sites (Figure 3.13). Only three are predicted to be extracellular with one being on the N-terminus. Results obtained using a combination of PROSITE and NetPhos revealed a plethora of putative phosphorylation sites for multiple GPCR kinases throughout the CCR6 sequence [20]. In general it is accepted that phosphorylation of the C-terminus is a first step in densensitization followed by internalization of the receptor, however the cluster of putative tyrosine and serine phosphorylation sites in the N-terminus could have a role in attracting positively-charged ligands, such as defensins, to CCR6. A similar role has already been shown for tyrosine sulfation in CCR5, CCR2b and CXCR4 [17, 21, 22]. Although an exact functional motif has not been identified for tyrosine sulfation it is implied that a tyrosine followed or preceded by a negatively charged amino acid could be sulfated [23]. Although the CCR6 N-terminal contains a conserved YY motif at position 26-27, in which the 1st tyrosine is sulfated in the corresponding residues in both hCCR5 and mCCR8 [16, 21], and a tyrosine at position 18 preceded by an aspartic acid, these residues are both putative sites for phosphorylation and further analysis is needed to confirm the PTM. Finally, putative sites for covalent modifications of cysteine residues with fatty acids were revealed with a N-myristoylation site on ECL2 and two palmitoylation sites bordering the putative extracellular side of transmembrane helix 7.
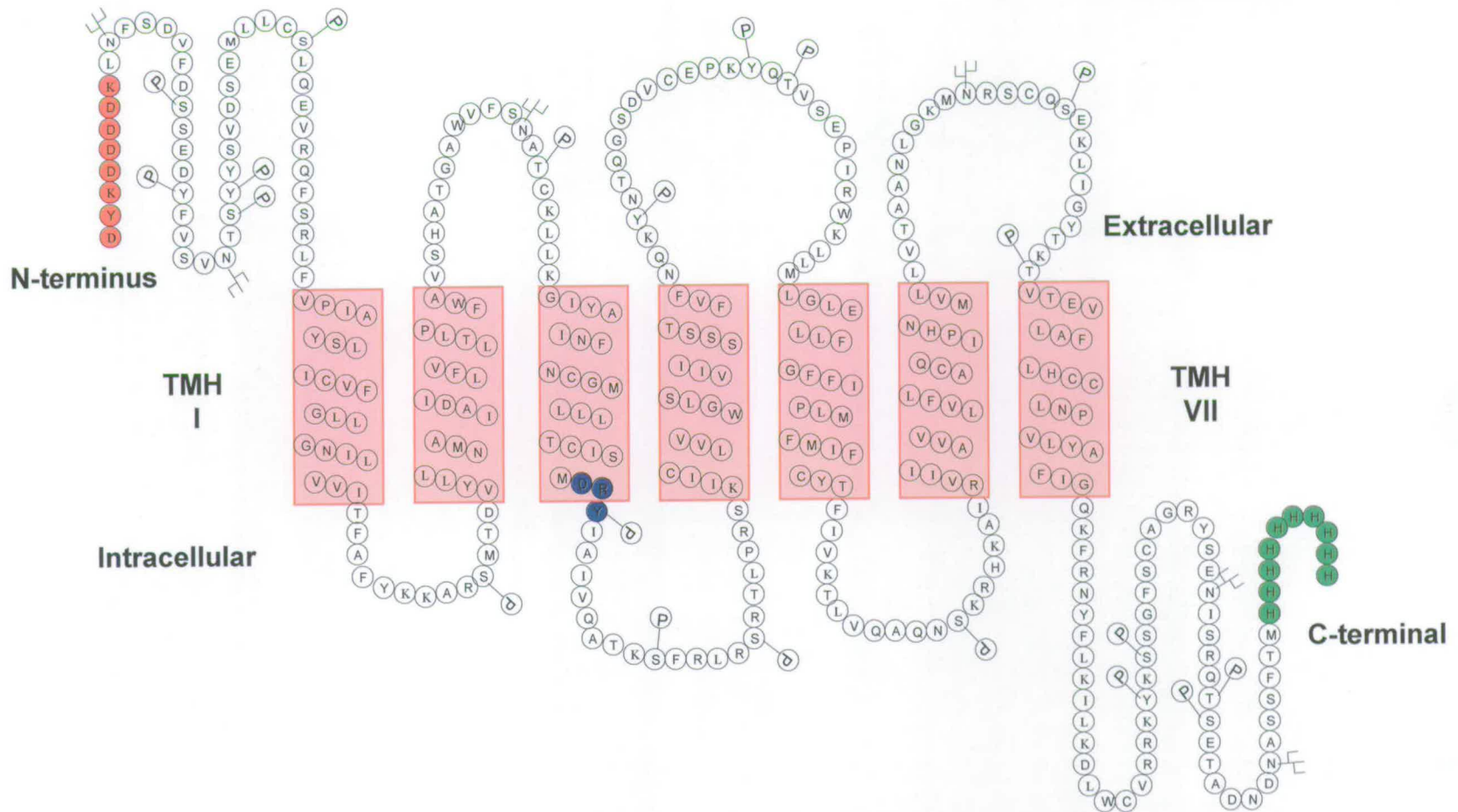
Figure 3.13. Snake-like Diagram Representing the Possible Topology and Post-Translational Modifications for Epitope-Tagged CCR6. Deca-HIS tag (Green) and FLAG tag (Red) are indicated. Putative glycosylation and phosphorylation sites are labeled ⊔ and Ⓟ respectively. Highly conserved DRY motif in signaling GPCRs (Blue) is indicated.

PTM analysis by comparative metabolic labeling is routinely carried with great success [1, 17]. Unfortunately this method of analysis was not available; therefore analysis was performed using a combination of enzymatic methods and fluorescent staining. Metal- and immuno-affinity purified epitope-tagged CCR6 was analyzed for both N- and O-linked glycosylation. Initially purified CCR6 was purified on a SDS-PAGE gel and stained with a glycosylation-specific stain, however although CCR6 has five putative N-linked glycosylations sites no band was observed. This was probably a consequence of low concentrations of epitope-tagged CCR6 in the gel matrix. Therefore a gel-shift assay followed by anti-FLAG western blot probing was carried out. Purified CCR6, denatured in SDS, was subjected to both N- and O- specific deglycosylation enzymes. N-glycosidase F digestion of purified CCR6 resulted in an increase in electrophoresis mobility with CCR6 shifting from ~47 kDa to ~38 kDa (Figure 3.14). This suggests that N-linked oligosaccharides were contributing greatly to the mass of CCR6. Although this method cannot specify which asparagines are glycosylated, a shift of 9 kDa is strong evidence that more than one amino acid is glycosylated. Digestion of purified CCR6 with O-linked deglycosylating enzymes did not result in a band shift. Although O-linked oligosaccharides are smaller in size removal of sialic acid by α2-3, 6, 8, 9-Neuraminidase would still result in an observable mass shift. Being the third CC chemokine receptor identified as being N-glycosylated indicates that this modification is common in the family and most likely has a functional role.
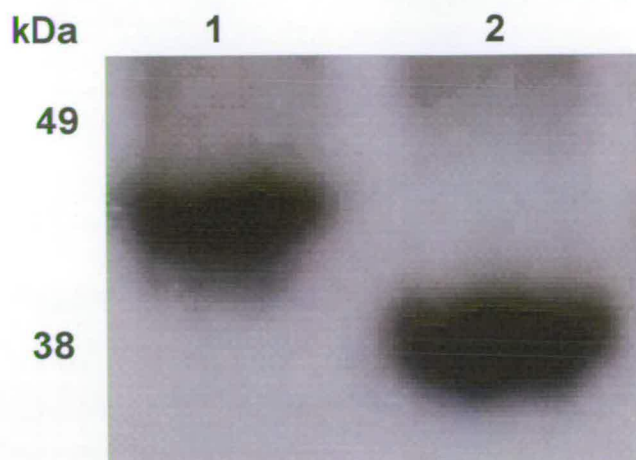
Figure 3.14 Glycosylation Analysis of Purified Epitope-Tagged CCR6. Epitope-tagged CCR6 without (lane 1) and with (lane 2) N-Glycosidase F.

Phosphorylation analysis of purified CCR6 was performed using a phosphoprotein specific fluorescent stain. Prior to gel staining, western blot analysis performed with both anti-tyrosine and anti-serine specific antibodies revealed a lack of reactivity with purified CCR6. Although at a basal level chemokine receptors are phosphorylated, it has been shown that they become hyper-phosphorylated upon stimulation with their natural ligand [24]. Since purified CCR6 was isolated without ligand stimulation it is possible that not enough of the putative sites were phosphorylated and therefore would not reactive with the antibodies. Purified CCR6 was separated on a SDS-PAGE gel and stained with a phosphoprotein specific fluorescent stain resulted in a faint band corresponding to the correct mass of CCR6 (Figure 3.15). An intrinsic problem associated with this method was the low abundance of purified CCR6 in the gel matrix. Consequently over-exposure was required to identify the fluorescent CCR6 band leading to proteins that are not known to be phosphorylated being identified. Therefore it is impossible to determine whether CCR6 is phosphorylated at a basal level.
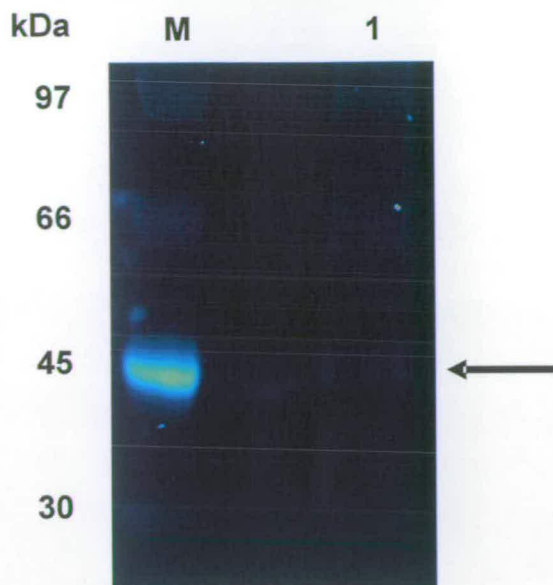
Figure 3.15 SDS-PAGE Analysis of Purified CCR6 Stained with Phosphoprotein Gel Stain. Lane M, protein marker, Lane 1, purified CCR6. The band indicated by a black arrow is the correct size for full length FLAG-CCR6-HIS10

3.3 - N-terminal Truncation of Epitope-Tagged CCR6

To begin to elucidate the functional role of the N-terminal domain of CCR6, site-directed mutagenesis on the wild-type expressing plasmid was performed to remove the first 27 AA from the N-terminal while keeping the N-terminal FLAG-tag for FACS analysis (Figure 3.16). Truncation of the first 27 AA removes putative phosphorylation, glycosylation and possible sulfation sites. In a similar study, removal of the corresponding section of CCR5 resulted in impairment of ligand binding but still enabled cell surface expression [2].

```
  1 MDSKGSSQKG SRLLLLLVVS NLLLCQGVVS DYKDDDDKLS VDSEMLLCSL
 51 QEVRQFSRLF VPIAYSLICV FGLLGNILVV ITFAFYKKAR SMTDVYLLNM
101 AIADILFVLT LPFWAVSHAT GAWVFSNATC KLLKGIYAIN FNCGMLLLTC
151 ISMDRYIAIV QATKSFRLRS RTLPRSKIIC LVVWGLSVII SSSTFVFNQK
201 YNTQGSDVCE PKYQTVSEPI RWKLLMLGLE LLFGFFIPLM FMIFCYTFIV
251 KTLVQAQNSK RHKAIRVIIA VVLVFLACQI PHNMVLLVTA ANLGKMNRSC
301 QSEKLIGYTK TVTEVLAFLH CCLNPVLYAF IGQKFRNYFL KILKDLWCVR
351 RKYKSSGFSC AGRYSENISR QTSETADNDN ASSFTMHHHH HHHHHH
```

Figure 3.16. Sequence of N-terminal Truncated CCR6 (396 AA). HIS tag (Red) and FLAG tag (Blue) are indicated.

HEK293 cells were transfected with pcDNA3.1/N-trunc/CCR6 and surface expression was analyzed by FACS analysis using anti-FLAG-FITC conjugated antibody. FACS analysis revealed there was no surface expression of the N-truncated receptor when compared to the full length CCR6 transfected HEK293 cells (Figure 3.17). To confirm that the N-trunc CCR6 had been successfully transfected; HEK293 cells were lysed before running the crude extract on a SDS-PAGE gel and western blotting with an anti-HIS antibody. Analysis of this data revealed the presence of both monomeric and dimeric N-trunc CCR6 reacting with the antibody and indicated that N-trunc CCR6 was being expressed but not properly trafficked to the cell surface (Figure 3.18).
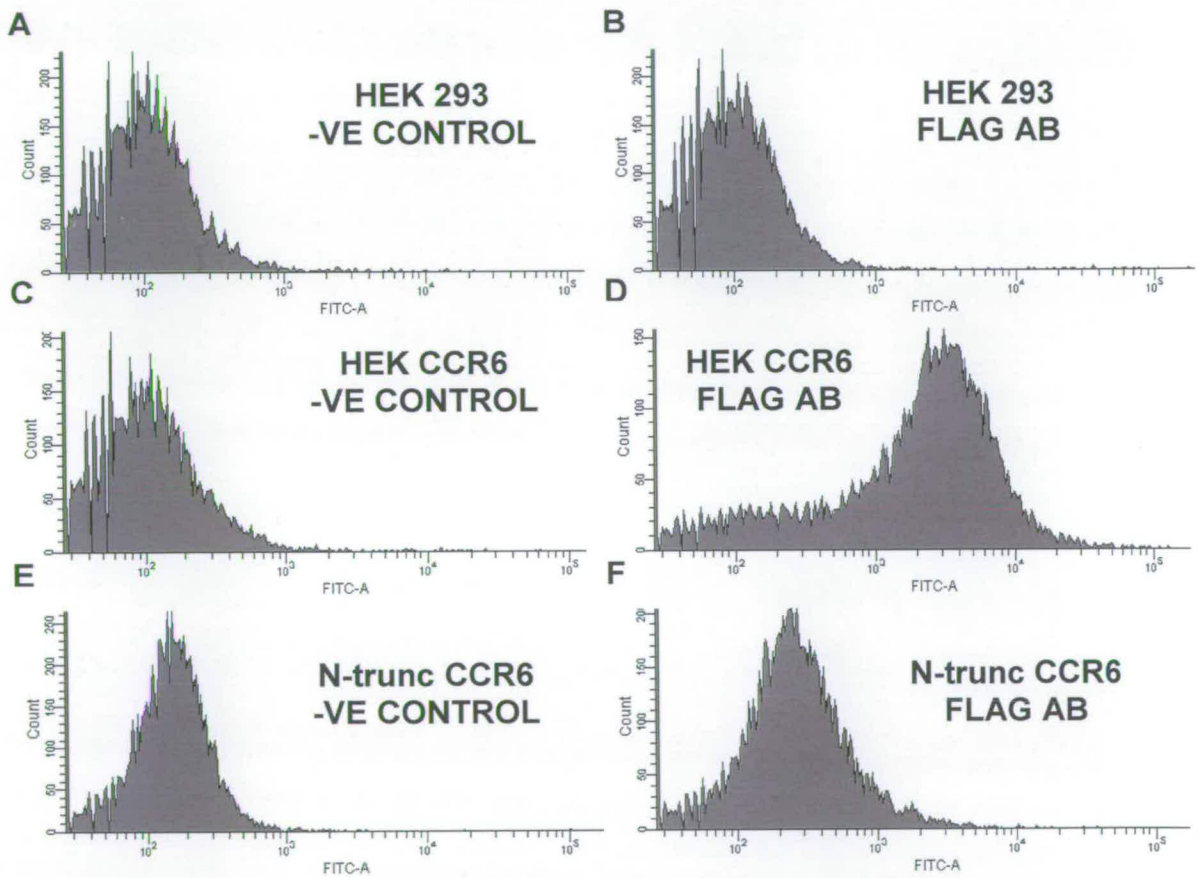
Figure 3.17. N-terminal Truncated CCR6 Expression in Transfected HEK293 cells.
HEK293 control cells (A and B) or Epitope-tagged Human CCR6-expressing HEK293 cells (C and D) were examined for specific binding by flow cytometry using either IgG$_1$-CFS negative control antibody (A and C) or an anti-FLAG-FITC antibody (B and D). N-terminal truncated CCR6-expressing HEK293 cells (E and F) were examined for specific binding by flow cytometry using either IgG$_1$-CFS negative control antibody (E) or an anti-FLAG-FITC antibody (F).

The differences in cell surface expression between N-terminal truncated CCR6 and a similar CCR5 mutant could be a result of CCR6 having a N-terminal putative N-glycosylation site, which has been shown to be important for surface expression of some GPCRs and irrelevant for others [25]. Additionally, a YS motif has been shown to be important in intracellular trafficking for α2-ARs which has been removed in the N-truncated CCR6 [26]. Removal of this motif retains the receptor in the Golgi apparatus. The exact intracellular location and N-terminal motif responsible for surface expression of CCR6 remains to be identified but these results indicate the importance of the N-terminus and are a good starting point for further analysis.
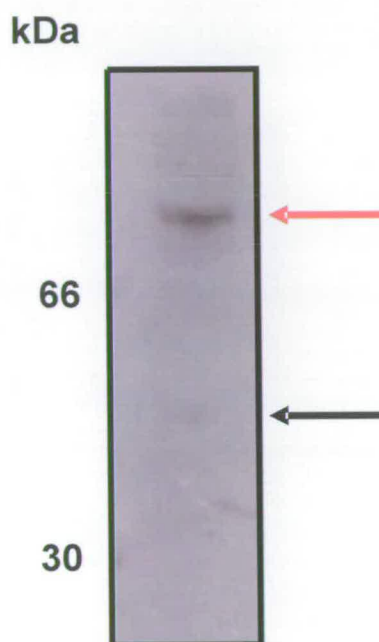
Figure 3.18. Western Blot Analysis of N-terminal Truncated CCR6. The feint band indicated by the black arrow is the correct size for N-terminal truncated epitope-tagged CCR6 (45,008 Da). The band indicated by the red arrow is possibly dimeric N-terminal truncated epitope-tagged CCR6.

3.4 - Chapter 3 References

1. Blackburn, P.E., et al., *Purification and biochemical characterization of the D6 chemokine receptor.* Biochem J, 2004. **379**(Pt 2): p. 263-72.

2. Mirzabekov, T., et al., *Enhanced expression, native purification, and characterization of CCR5, a principal HIV-1 coreceptor.* J Biol Chem, 1999. **274**(40): p. 28745-50.

3. Ren, H., et al., *High-level production, solubilization and purification of synthetic human GPCR chemokine receptors CCR5, CCR3, CXCR4 and CX3CR1.* PLoS ONE, 2009. **4**(2): p. e4509.

4. Nisius, L., et al., *Large-scale expression and purification of the major HIV-1 coreceptor CCR5 and characterization of its interaction with RANTES.* Protein Expr Purif, 2008. **61**(2): p. 155-62.

5. Yang, D., et al., *Beta-defensins: linking innate and adaptive immunity through dendritic and T cell CCR6.* Science, 1999. **286**(5439): p. 525-8.

6. Guan, X.M., T.S. Kobilka, and B.K. Kobilka, *Enhancement of membrane insertion and function in a type IIIb membrane protein following introduction of a cleavable signal peptide.* J Biol Chem, 1992. **267**(31): p. 21995-8.

7. Shaw, G., et al., *Preferential transformation of human neuronal cells by human adenoviruses and the origin of HEK 293 cells.* Faseb J, 2002. **16**(8): p. 869-71.

8. le Maire, M., P. Champeil, and J.V. Moller, *Interaction of membrane proteins and lipids with solubilizing detergents.* Biochim Biophys Acta, 2000. **1508**(1-2): p. 86-111.

9. Navratilova, I., J. Sodroski, and D.G. Myszka, *Solubilization, stabilization, and purification of chemokine receptors using biosensor technology.* Anal Biochem, 2005. **339**(2): p. 271-81.

10. Staudinger, R. and J.C. Bandres, *Solubilization of the chemokine receptor CXCR4.* Biochem Biophys Res Commun, 2000. **274**(1): p. 153-6.

11. Ratnala, V.R., et al., *Large-scale overproduction, functional purification and ligand affinities of the His-tagged human histamine H1 receptor.* Eur J Biochem, 2004. **271**(13): p. 2636-46.

12. Mirza, S.P., et al., *Improved method for the analysis of membrane proteins by mass spectrometry.* Physiol Genomics, 2007. **30**(1): p. 89-94.

13. Ho, J.T., et al., *Analysis of a G protein-coupled receptor for neurotensin by liquid chromatography-electrospray ionization-mass spectrometry.* Anal Biochem, 2008. **376**(1): p. 13-24.

14. Kamonchanok, S., et al., *GPCR proteomics: mass spectrometric and functional analysis of histamine H1 receptor after baculovirus-driven and in vitro cell free expression.* J Proteome Res, 2008. **7**(2): p. 621-9.

15. Wu, S., M. Birnbaumer, and Z. Guan, *Phosphorylation analysis of G protein-coupled receptor by mass spectrometry: identification of a phosphorylation site in V2 vasopressin receptor.* Anal Chem, 2008. **80**(15): p. 6034-7.

16. Gutierrez, J., et al., *Analysis of post-translational CCR8 modifications and their influence on receptor activity.* J Biol Chem, 2004. **279**(15): p. 14726-33.

17. Preobrazhensky, A.A., et al., *Monocyte chemotactic protein-1 receptor CCR2B is a glycoprotein that has tyrosine sulfation in a conserved extracellular N-terminal region.* J Immunol, 2000. **165**(9): p. 5295-303.

18. Allen, S.J., et al., *Expression, purification and in vitro functional reconstitution of the chemokine receptor CCR1.* Protein Expr Purif, 2009.

19. Bairoch, A., P. Bucher, and K. Hofmann, *The PROSITE database, its status in 1997.* Nucleic Acids Res, 1997. **25**(1): p. 217-21.

20. Blom, N., S. Gammeltoft, and S. Brunak, *Sequence and structure-based prediction of eukaryotic protein phosphorylation sites.* J Mol Biol, 1999. **294**(5): p. 1351-62.

21. Farzan, M., et al., *Tyrosine sulfation of the amino terminus of CCR5 facilitates HIV-1 entry.* Cell, 1999. **96**(5): p. 667-76.

22. Farzan, M., et al., *The role of post-translational modifications of the CXCR4 amino terminus in stromal-derived factor 1 alpha association and HIV-1 entry.* J Biol Chem, 2002. **277**(33): p. 29484-9.

23. Liu, J., et al., *Tyrosine sulfation is prevalent in human chemokine receptors important in lung disease.* Am J Respir Cell Mol Biol, 2008. **38**(6): p. 738-43.

24. Olbrich, H., A.E. Proudfoot, and M. Oppermann, *Chemokine-induced phosphorylation of CC chemokine receptor 5 (CCR5).* J Leukoc Biol, 1999. **65**(3): p. 281-5.

25. Dong, C., et al., *Regulation of G protein-coupled receptor export trafficking.* Biochim Biophys Acta, 2007. **1768**(4): p. 853-70.

26. Dong, C. and G. Wu, *Regulation of anterograde transport of alpha2-adrenergic receptors by the N termini at multiple intracellular compartments.* J Biol Chem, 2006. **281**(50): p. 38543-54.

Chapter 4

Materials and Methods

4.1 – Materials

4.1.1 - General Reagents

All chemicals and solvents were of the appropriate quality and unless stated were purchased from Bio-Rad, Fisher, GE Healthcare, Gibco BRL, Invitrogen and Promega. Synthetic Biotinylated (Bio) HBD2 was purchased from Albachem as a custom synthetic peptide. Synthetic genes HBD1 and CCR6 were purchased from Codon Devices, Inc.

Human embryonic kidney (HEK) 293 and CCR6 transfected HEK293 cell lines were a kind gift from Dr De Yang (National Cancer Institute, Frederick). Murine L1.2 pre-B cells were a kind gift from Prof. G Graham (Glasgow Biomedical Research Centre, University of Glasgow).

4.1.2 - General Buffers

TAE buffer - Tris-HCl (40 mM), acetic acid (20 mM), EDTA (1 mM), pH 8.3.

SDS sample buffer - Tris-HCl (0.5 M), 30% glycerol, 10% SDS, 2-β-mercaptoethanol, 0.05% bromophenol blue, pH 6.8.

SDS running buffer - Tris-HCl (25 mM), glycine (192 mM), 1% SDS, pH 8.3 or 20 x MES buffer was diluted to 1 x with deionised water.

Western blot transfer buffer - Tris-HCl (25 mM), glycine (150 mM), 10% methanol, pH 8.3.

Western blot washing buffer - Dissolved 10 PBS tablets in 1 litre of deionised water and autoclaved at 121 °C for 20 min. Upon cooling, 0.1% tween was added.

Digestion buffer - Tris-HCl (50 mM), $CaCl_2$ (20 mM), 0.005% triton X-100, pH 8.3.

4.1.3 - Bacterial Growth Media and Antibiotics

All media was autoclaved for 20 min at 121 °C and all antibiotics were sterile filtered through 0.22 μM filters.

2YT - Bacto-tryptone (16 g), bacto-yeast extract (10 g) and NaCl (5 g) were dissolved in 1 litre of deionised water and adjusted to pH 7.5.

SOC - Bacto-tryptone (20 g), bacto-yeast extract (5 g), NaCl (0.5 g), $MgCl_2$ (5 g) and glucose (3.2 g) were dissolved in 1 litre of deionised water and adjusted to pH 7.5.

Luria Bertani (LB) - Bacto-tryptone (10 g), bacto-yeast extract (5 g) and NaCl (10 g) were dissolved in 1 litre of deionised water and adjusted to pH 7.5.

Ampicillin - a stock solution (100 mg/ml) is filtered (0.2 μM) and used at a final concentration (100 μg/ml) in various media.

Kanamycin - a stock solution (30 mg/ml) is filtered (0.2 μM) and used at a final concentration (30 μg/ml) in various media.

LB Agar plates - Bacto-agar (15 g) was dissolved in 1 litre of LB to prepare agar plates.

S-Gal/LB/amp plates - a sachet of S-Gal ™/LB Agar Blend without IPTG was dissolved in deionised water (500 ml) and autoclaved for 20 min at 121 °C. Once cooled ampilicillin (final conc. 100 μg/ml) was added to the solution to prepare plates.

4.2 - DNA Manipulation

4.2.1 - Oligonucleotide Primers

The following oligonucleotide primers have been used in the various aspects of the study.

NAME	SEQUENCE (5' - 3')
pGEM For	TAATACGACTCACTATAGGG
pGEM Rev	ATTTAGGTGACACTATAGAA
pET For	CCCCTATAGTGAGTCGTATTA
pET Rev	GGATATAGTTCCTCCTTTCAGC
pcDNA3.1 For	CGACTCACTATAGGGAGACCCAAG
pcDNA3.1 Rev	TAGAAGGCACAGTCGAGG
HBD2 Primer 1	CAGATGCTGATGGGTATCGGTGACCCGGTTACCTGCCTGAAA TCC
HBD2 Primer 2	CGGACAGAAAACCGGGTGGCAGATAGCACCGGATTTCAGGC AGGT
HBD2 Primer 3	CCGGTTTTCTGTCCGCGTCGTTACAAACAGATCGGTACCTGCG GT
HBD2 Primer 4	GCAGCATTTGGTACCCGGCAGACCGCAGGTACCGAT
HBD2 Primer 5	ACCAAATGCTGCAAAAAATGACAGATGCTG
HBD2 Primer 6	CAGCATCTGTCACGGTTTTTTGCAGCATTTGGTACCCGG
pGem For Mutagenesis	AGTGAATTGTAATACGACTCACTATAGGGCG
pGem Rev Mutagenesis	CGCCAAGCTATTTAGGTGACACTATAG
HBD2 Met *Alw*NI For	CTGCAAAAAACCGTGAGTGATGCTGCTCGAGCAC
HBD2 Met *Alw*NI Rev	GTGCTCGAGCAGCATCACTCACGGTTTTTTGCAG
HBD2 Met *Nde*I For	GCGGCAGCCATGCGCATACCCCAGAACACATC
HBD2 Met *Nde*I Rev	GATGTGTTCTGGGGTATGCGCATGGCTGCCGC
CCR6 For	GTTTTCAGCAATGCCACGTGCAAG
CCR6 Rev	AAAGAAACCAAAGAGTAGCTCAAG

Internal CCR6 Rev	GGCTGCAAATTTGGGTAAAA
HBD2 S34G For	CTGCGGTCTGCCGGGTACCAAATGCTG
HBD2 S34G Rev	CAGCATTTGGTACCCGGCAGACCGCAG
Human β-Actin For	TGCAAGGCCGGCTTCGCGGGCGAC
Human β-Actin Rev	GAAGCATTTGCGGTGGACGATGGA
Mutant HBD2 Primer	AAGCTTATGGGTATCGGTGACCG
HBD2 1-5 Primer 2	CGCGGAGCGAAAACCGGGTGAGCGATAGCACCGGATTTCAG GCAGGTAAC
HBD2 1-5 Primer 3	CGGTTTTCGCTCCGCGTCGTTACAAACAGATCGGTACCGCTGG TCTGCCG
HBD2 1-5 Primer 4	CTCGAGTTCACGGTTTTTTAGCGCATTTGGTACCCGGCAGACC AGCGGTA
HBD2 2-4 Primer 2	CGCGGAGCGAAAACCGGGTGGCAGATAGCACCGGATTTCAG AGCGGTAAC
HBD2 2-4 Primer 3	CGGTTTTCGCTCCGCGTCGTTACAAACAGATCGGTACCTGCGG TCTGCCG
HBD2 2-4 Primer 4	CTCGAGTTCACGGTTTTTTAGCAGCTTTGGTACCCGGCAGACC GCAGGTA
HBD2 3-6 Primer 2	ACGACGCGGACAGAAAACCGGGTGAGCGATAGCACCGGATT TCAGAGCGG
HBD2 3-6 Primer 3	GTTTTCTGTCCGCGTCGTTACAAACAGATCGGTACCGCTGGTC TGCCGGG
HBD2 3-6 Primer 4	CTCGAGTTCACGGTTTTTTGCAAGCTTTGGTACCCGGCAGACC AGCG
HBD1 For	ATGAGAACTTCCTACCTTCTGCTG
HBD1 Rev	CTTGCAGCACTTGGCCTTCCCTCT
HBD2 For	CCAGCCATCAGCCATGAGGGTCTT
HBD2 Rev	GGAGCCCTTTCTGAATCCGCATCA

Table 4.1. Oligonucleotide Primer Sequences used in this Study.

4.2.2 - Electrophoresis of DNA

Agarose (1-2% w/v) was dissolved in 1 x TAE buffer upon heating (100 °C). Upon cooling (~50-60 °C), ethidium bromide (0.5 μg/ml) or GelRed ™ (Cambridge BioScience) was added, mixed and immediately poured into the casting mould. After solidifying at room

temperature, DNA samples were mixed with 5 x loading buffer (Bioline) and electrophersed at 100 volts (V) until good resolution was observed between the bands.

4.2.3 - Purification of DNA from Agarose Gel

The appropriate DNA band was excised using a clean scalpel identified by UV illumination. Excess agarose was removed prior to purification of the DNA using QIAquick® Gel Extraction Kit (Qiagen) carried out in accordance with the manufacturer's instructions. DNA was eluted in a final volume of 20 µl deionised water.

4.2.4 - Ligation into pGEM Cloning Vector

T4 DNA ligase (1 µl) was added to a mixture already including purified DNA (3 µl), pGEM®-T Easy Vector (1 µl) and 2 x T4 ligation buffer (5 µl). Ligations were incubated either for an hour (hr) at room temperature or overnight at 4 °C. Subsequently an aliquot (2 µl) of the ligation reaction was used to transform JM109 *E.coli* competent cells as described in section 4.2.6.

4.2.5 - Ligation into Expression Vector

Generally, T4 DNA ligase (1 µl) was added to a mixture already including purified DNA cut with appropriate restriction enzymes (13 µl), expression plasmid cut with appropriate restriction enzymes (4 µl) and 10 x T4 ligation buffer (2 µl). Ligations were incubated overnight at 4 °C and an aliquot (2 µl) of the ligation mixture was used to transform Top10 *E.coli* competent cells as described in section 4.2.6.

4.2.6 - Transformation of Competent Cells with Plasmid DNA

Competent cells were thawed at 4 °C for 5 minutes (min) before 2 µl of plasmid DNA (~40 ng) was added and gently mixed. Incubation proceeded at 4 °C for 30 min before being subjected to heat shock for 30 seconds (sec) at 42 °C. Cells were then returned to 4 °C for 2 min. SOC (250 µl) was added under sterile conditions and shaken at 200 rpm for 1.5 hrs at 37 °C. Subsequently, the cell suspension was spread to dryness on selective agar and incubated overnight at 37 °C.

4.2.7 - Purification of Plasmid DNA

Plasmid DNA was purified using the QIAprep® Spin Miniprep Kit (Qiagen) following the manufacturer's instructions and DNA was eluted in a final volume of 100 µl deionised water. Plasmid DNA was identified by restriction endonuclease analysis as described in section 4.2.8.

4.2.8 - Small Scale Restriction Enzyme Digestion of DNA

Generally, 8 µl purified plasmid DNA (~1 µg) was treated with the appropriate 10 x buffer (1 µl) and restriction endonucleases (1 µl) (New England Biolabs). After incubation for 2 hrs at 37 °C, loading dye was added to stop the reaction and was analysed by agarose gel electrophoresis. Agarose gels were viewed by trans illumination using UV-light.

4.2.9 - Large Scale Restriction Enzyme Digestion of DNA

Generally, 43 µl purified plasmid DNA (~4 µg) was treated with the appropriate 10 x buffer (5 µl) and restriction endonucleases (1 µl of each). After incubation for 2 hrs at 37

°C, loading dye was added to stop the reaction and was analysed by agarose gel electrophoresis. Agarose gels were viewed by trans illumination using UV-light.

4.2.10 - General PCR Reaction

Normally PCR reactions were carried out using a Perkin Elmer 480 Thermal Cycler. Template DNA (3 µl) was added to a PCR tube already containing 2 x puRe Taq Ready-To-Go PCR beads, deionised water (37 µl), forward primer (5 µl, of a 10 µM stock, to give a final concentration of 1 µM) and reverse primer (5 µl of a 10 µM stock) and covered with nujol oil. After a hot start (5 min, 94 °C) the reaction was generally subjected to 30 cycles:

PROCESS	TEMPERATURE (°C)	TIME (SEC)
Denaturation	94	60
Annealing	60	30
Elongation	72	60

A further elongation step (72 °C, 10 min) was included for addition of A-overhangs to produce a product which can be ligated into the linear pGEM cloning plasmid with 'T' overhangs. The PCR reactions are then prepared and electrophoresed as described in section 4.2.2. Generally the annealing temperature is set to ~5 °C less than the primer's melting temperature.

4.2.11 - Gene Synthesis

Recombinant defensin genes were constructed using recursive PCR performed on an eppendorf ® Mastercycler Personal. Using HBD2 as a typical reaction, six overlapping

primers with codons optimized for expression in *E. coli* were designed using the mature

HBD2 amino acid (AA) sequence. The reaction contained in a final volume of 100 μl; 10 μl

(100 pmol) of the outermost 5' primers (HBD2 Primer 1 and HBD2 Primer 6) of each strand,

10 μl (10 pmol) of the internal primers (HBD2 Primer 2 – HBD2 Primer 5), 4 μl DMSO, 10

μl 10 x Herculase reaction buffer (Stratagene), 4 μl 25 mM dNTPs, 21 μl dH$_2$O and finally 1

μl Herculase Hotstart DNA polymerase (Stratagene). This reaction mixture was subjected to

30 PCR cycles of 95 °C for 2 min, 40 °C for 3 min and 72 °C for 30 sec. A general PCR

reaction was performed to confirm annealing of all six primers in a final volume of 50 μl; 5

μl HBD2 Primer 1 (50 pmol), 5 μl HBD2 Primer 6 (50 pmol), 2 μl template, 38 μl dH$_2$O and

2 puRe Taq Ready-To-Go PCR beads were subjected to 30 PCR cycles of 95 °C for 2 min,

40 °C for 3 min, 72 °C for 30 sec and a final extension of 72 °C for 10 min to add 'A'

overhangs. The PCR product containing the codon optimized gene preceded by a methionine

(Met) and flanking *Alw*NI recognition sites was purified by agarose gel electrophoresis,

extracted and ligated into pGem T Easy vector as described previously. Each of the HBD2

single disulfide mutant genes were also synthesized using this method.

Dr David Clarke constructed HBD2 1-5 and HBD2 3-6.

4.2.12 - Megaprimer Mutagenesis

The megaprimer mutagenesis method used was adapted from a method previously

described [1]. A standard PCR reaction was performed as described in section 4.2.10,

including a forward mutagenic primer (5 μl, of a 10 μM stock) and reverse plasmid primer (5

μl of a 10 μM stock). The PCR products were separated by 1% agarose gel electrophoresis

and the DNA band representing the 'megaprimer' was excised, purified and 5 μl was used in

a second PCR reaction using forward plasmid primer (5 μl of a 10 μM stock).

4.2.13 - Site-Directed Mutagenesis PCR

Site-directed mutagenesis was performed using the Quickchange Site-Directed Mutagenesis kit (Stratagene) and was performed as described in the manufacturer's instructions. *Dpn*I treated PCR product was transformed into Top10 *E.coli* competent cells as described in section 4.2.6.

4.2.14 - DNA Sequencing

Sequencing reactions contained the following: DNA template (5 µl); primer (1 µl); 5 x Big Dye Sequencing buffer v3.1 (2 µl); and Big Dye v3.1 (2 µl). All sequencing reactions were carried out on an Eppendorf® Mastercycler Personal and the program consisted of:

STEP	TEMPERATURE (°C)	TIME
Step 1	94	30 sec
Step 2	94	30 sec
Step 3	45	30 sec
Step 4	60	4 min
Steps 2-4 x 30 cycles		

All sequencing was performed on an ABI prism 377 DNA sequencer using the Sanger dideoxy chain termination method.

4.3 - Cell Culture

4.3.1 - Culture of CaCo2 Cells

The human colonic epithelial cell line, CaCo2, were grown to confluency in Dulbecco modified Eagle's medium (DMEM), supplemented initially with 2% fetal calf serum (FCS), and 1% antibiotic agent (Penicillin/streptomycin). Since cells did not attach directly to the 75 cm^2 flasks when seeded with ITS (insulin, selenium and transferrin) supplemented media, 2% FCS was used initially and then replace with ITS once CaCo2 cells had attached. Cells were maintained at 37 °C in a water saturated incubator with 5% CO_2 and media changed every 3 days. Once confluent, cells were washed twice with PBS (5 ml) and incubated at 37 °C with trypsin (3 ml, 0.075%) until cells detached from the surface. The reaction was stopped with addition of media (9 ml) and cells were centrifuged (5,000 rpm, 5 min). The pellet was subsequently resuspended in 1 ml media and transferred (250 µl) to a new culture vessel. Alternatively cells were grown for up to 3 weeks, with media replaced every 3 days. The harvested supernatants were subsequently stored at -20 °C for future protein analysis.

4.3.2 - Stimulation Protocols

Confluent CaCo2 cells in six well tissue culture plates (Gibco BRL) were stimulated at time points up to 6 hrs with IL-1β (10 ng/ml) (Peprotech [EC]). Afterwards, supernatants were removed and the cells were used for RNA extraction and RT-PCR analysis as described below. CaCo2 cells grown in 75 cm^2 culture flasks were stimulated with IL-1β for 6 hrs and supernatants were harvested and stored at -20 °C prior to HBD2 purification.

4.3.3 - Purification of Mature HBD2 from CaCo2 Cells

IL-1β stimulated CaCo2 supernatants were diluted 4-fold in 10 mM HEPES buffer (pH 8.1) to reduce the salt concentrations before being incubated with 1 ml Fractogel EMD SO_3^--650 (Merck), pre-equilibrated with 10 mM HEPES, 50 mM NaCl (pH 8.1), for 2 hrs at 4 °C. The Fractogel resin was then centrifuged (500 x g, 5 min), and washed with 5 column volumes (CV) of pre-equilibration buffer. Fractions were then eluted with 1 CV of 10 mM HEPES containing 125 mM, 250 mM, 500 mM, and 1 M NaCl. Elution fractions were analyzed for HBD2 production using SDS-PAGE and anti-HBD2 western blot analysis.

4.3.4 - Culture of HEK 293 and HEK 293 CCR6 Cells

Both HEK293 and CCR6 transfected HEK293 cells were maintained in DMEM, supplemented with 10% FCS, 1% antibiotic agent (Penicillin/streptomycin) and sodium pyruvate (1 mM). HEK293/ CCR6 cells were also supplemented with G418 Geneticin. Cells were maintained at 37 °C in a water saturated incubator with 5% CO_2 and media changed every 3 days until cells needed.

4.3.5 - Culture of Murine L1.2 pre-B Cells

Both murine L1.2 pre-B control and transfected cells were maintained in RPMI 1640, supplemented with 10% FCS, 1% antibiotic agent, β-mercaptoethanol (50 μM) and glutamine (5 mM). Transfected L1.2 pre-B cells were also supplemented with G418 Geneticin. Cells were maintained at 37 °C in a water saturated incubator with 5% CO_2 and media changed every 3 days until cells needed.

4.3.6 - Linearization and Purification of pcDNA3.1/CCR6

The vector pcDNA3.1/CCR6 was linearized prior to transfection into HEK293 cells. Large scale digestion was performed, as described in section 4.2.9, using the unique *Pvu*I restriction site in pcDNA3.1/CCR6. DNA was purified by gel extraction after separation by agarose gel electrophoresis. An equal volume of phenol/chloroform/isoamyl alcohol (25:24:1) was added to the purified DNA, vortexed and centrifuged (13,000 rpm, 1 min). In a new eppendorf, the upper phase was added and mixed with an equal volume of chloroform/isoamyl alcohol (24:1), vortexed and centrifuged (13,000 rpm, 1 min). Upper phase was moved to a fresh tube were sodium acetate (3 M, 10% v/v) and ethanol (200% v/v) were added before precipitating at -20 °C. Precipitated DNA was centrifuged (13,000 rpm, 15 min), washed twice with 75% ethanol and resuspended in an appropriate volume of dH$_2$O.

4.3.7 - Transfection into Mammalian Cells

Plasmid DNA transfection was carried out according to the Lipofectamine 2000 (Invitrogen) or Superfect (Qiagen) manufacturer's instructions. In brief, DNA transfection into HEK293 mammalian cells was carried out in 24 well plates at a ratio of DNA to Lipofectamine™ 2000 of 1:2.5. Linearized DNA (0.8 µg) was diluted in Opti-MEM Reduced Serum Medium (50 µl) with no additional FCS added and mixed gently. Lipofectamine (2 µl) was diluted in the same media and incubated at room temperature for 5 min. Both components were then incubated together for 20 min at room temperature before being added to the confluent cells which one day before transfection were subcultured and plated at 1 x 10^6 cells in growth media without antibiotics. Cells were incubated at 37 °C, 5% CO$_2$ for 24 hrs before being passaged into fresh media at 1:10. 24 hrs later reduced serum

medium was replaced with selective media and cells were cultured as before until control cells without linearized plasmid DNA were killed.

DNA transfection into murine L1.2 preB-cells was carried out in 60 mm cell culture dishes at a ratio of DNA to Superfect of 1:4. DNA (5 μg) was diluted in serum free media (150 μl) with no additional FCS or antibiotics added, and mixed gently. Superfect (20 μl) was incubated with the DNA for 10 min at room temperature before being added to L1.2 cells which one day before transfection were subcultured and seeded in growth media without selective antibiotics. 48 hrs later, L1.2 cells were passaged and grown in selective media in 96 well plates until control cells were killed.

4.3.8 - Isolation of Monocytes

Monocytes were isolated from human donor blood preparations. Freshly extracted blood was added to sodium citrate (3.8%) before centrifugation (12,000 rpm, 20 min, brake off). Supernatent (Supernatent A) was removed with an aliquot (25 ml) centrifuged (3,000 rpm, 15 min) and this supernatant collected (Supernatent B) and stored till needed. 10 ml aliquots of supernatant A were placed in glass tubes containing $CaCl_2$ (1 M) and incubated at 37 °C until blood clot formed. Dextran (6%) was added to the remaining cells and made up to a final volume of 50 ml with NaCl (0.9%) and allowed to mix for 15-30 min until red blood cells settled. Supernatent was subsequently centrifuged (1000 rpm, 6 min) and the pellet resuspended in 2 ml supernatant B. White blood cells were then separated using 42% - 51 % Percoll gradients. Carefully 42% Percoll gradient (840 μl 90% Percoll and 1160 μl supernatant B) was added to resuspended the pellet followed by the addition of 51% Percoll gradient mixture (1020 μl 90% Percoll and 980 μl supernatant B), mixed and centrifuged (1000 rpm, 10 min, brake off). Monocytes (upper layer) were removed and resuspended in IMDM serum free media (PAA) before centrifugation (12,000 rpm, 5 min). This step was

repeated twice more until monocytes were resuspended at a concentration of 4×10^6/ml and

seeded in a 96 well plate. After 2 hrs IMDM serum free media was replaced with 10%

autologous serum supplemented media and monocytes were allowed to age for 7 days before

LPS stimulation experiments.

Method was optimized and performed by Katherine Miles.

4.3.9 - LPS Solubilization

Kdo$_2$-lipid A (1 mg/ml) was dissolved in sterile PBS and sonicated for 5 min in a

bath sonicator. After centrifugation (13,000 rpm, 1 min) the stock solution was transferred to

a clean eppendorf and stored at -20 °C until needed.

4.3.10 - LPS Stimulation

24 hrs before LPS stimulation IMDM media with 10% autologous serum was

replaced with serum free IMDM media. Kdo$_2$-lipid A was incubated for 30 min at room

temperature either alone or in combination with different concentrations of BioHBD2 or

polymyxin B (final volume of 200 µl made up with IMDM serum free media). 24 hrs after

stimulation supernatant was removed and used directly for TNF-α ELISA analysis.

4.3.11 - RNA Extraction from Mammalian Cells

Total cellular RNA was extracted from confluent cells in six well plates using

RNAzol B (1 ml, Biogenesis). Lysed cells we transferred to a screw-cap tube containing

chloroform (10% w/v), shaken vigorously (15 sec) and placed on ice for 5 min. After

centrifugation (15,000 rpm, 15 min, 4 °C), the upper phase containing RNA was transferred

to a sterile tube. The RNA was precipitated with an equal volume of isopropanol and incubated for 15 min at 4 °C. After centrifugation (15,000 rpm, 15 min, 4 °C), the pellet was washed with 75% ethanol (2 ml) and centrifuged again (15,000 rpm, 5 min, 4 °C). This step was repeated before the pellet was dried and finally resuspended in diethylpyrocarbonate (DEPC) treated water. The quantity and purity of RNA was assessed by spectrophotometry.

4.3.12 – Reverse Transcription Polymerase Chain Reaction (RT-PCR)

First strand cDNA synthesis was accomplished using a first-strand cDNA synthesis kit for RT-PCR (Roche). RNA (2 µg) resuspended in 7.8 µl DEPC-treated water was used as the template. RNA samples were denatured for 15 min at 65 °C, before being returned to ice. A reaction mixture containing 2 µl 10 x PCR buffer, 4 µl MgCl$_2$ (5 mM final concentration), 2 µl dNTPs (1 mM final concentration), 0.4 µl Gelatin (0.01 mg/ml final concentration), 2 µl random p(dN)6 primer (3.2 µg), 1 µl RNase inhibitor (50 units final concentration), and 0.8 µl Avian Myeloblastosis Virus - reverse transcriptase (AMV-RT) (20 units final concentration) was then added to denatured RNA. Duplicate samples were prepared without AMV-reverse transcriptase. Samples were incubated at room temperature to allow primers to anneal before incubating for 60 min at 42 °C. To deactivate, the RT samples were incubated for 5 min at 95 °C before being returned to ice. These samples were then used as the template for second strand synthesis.

4.3.13 - Chemotaxis Assay

Chemotaxis assays were carried out as previously described [2]. Multiwell Chemotaxis Chamber assays were performed using HEK 293 cells overexpressing CCR6 and synthetic CCL20 (PeproTech) used as a positive control. Chemotactic index value was

calculated for the optimal chemotactic concentration. All experiments were performed in triplicate and each experiment repeated three times. The number of cells per high power field (HPF) were counted for each concentration of peptide and the mean calculated for all three experiments. A sample data set is shown below. To assure the results are statistical relevant a paired, two tailed Student's t-test is performed using the t test statistical program on Microsoft Excel (=TTEST(data set 1, data set 2,2,1). When performing the t test, data set 2 was always the media control values. With the statistical significance set at $p < 0.05$, any value less than this can be identified as statistically relevant. In the example below this is every value except in the BioHBD2 100 ng/ml experiment.

BIOHBD2 CONC (NG/ML) / EXPT. NO.	0.1	1	10	100	1000	MEDIA CONTROL
1	60	103	99	61	65	73
2	64	117	119	52	89	80
3	57	88	93	96	59	76
4	70	118	109	109	84	108
5	75	105	113	91	65	87
6	102	113	100	97	84	108
7	106	118	98	75	87	80
8	93	97	113	79	78	111
9	76	111	110	104	76	107
Mean	78.11111	107.7778	106	84.88889	76.33333	92.22222
S.D.	6.035645	3.475221	2.910708	6.496675	3.636237	5.306646
pvalue	0.046115	0.025906	0.026494	0.205606	0.014765	

Method was optimized and performed by Uday Pathania and Fiona Kilanowski.

4.4 - Protein Expression and Purification

4.4.1 - Defensin Purification

All wild-type and single disulfide bond mutant β-defensins were expressed and purified using identical protocols until the chemical oxidation step. HBD2 expression and purification method will be described below as an example.

4.4.1.1 – Defensin Purification Buffers

Resuspension buffer - Tris-HCl (50 mM), 25% sucrose, EDTA (1 mM), 0.1% sodium azide, DTT (10 mM), pH 8.0.

Lysis buffer - Tris-HCl (50 mM), 1% triton X-100, NaCl (100 mM), 0.1% sodium azide, DTT (10 mM), pH 8.0.

Wash buffer - Tris-HCl (50 mM), 1% triton X-100, NaCl (100 mM), EDTA (1 mM), 0.1% sodium azide, DTT (1 mM), pH 8.0.

1 M Guanidine HCl buffer - GdnHCl (1 M), Tris-HCL (50 mM), 1% triton X-100, NaCl (100 mM), EDTA (1 mM), 0.1% sodium azide, DTT (1 mM), pH 8.0.

6 M Guanidine HCl buffer - GdnHCl (6 M), Tris-HCl (50 mM), imidazole (10 mM), NaCl (500 mM), β-Mercaptoethanol (5 mM), pH 8.0.

Elution Buffer - GdnHCl (6 M), Tris-HCl (50 mM), imidazole (120 mM), NaCl (500 mM), β-mercaptoethanol (5 mM), pH 8.0.

Reducing buffer – Tris-HCl (25 mM), TCEP (20 mM), pH 8.0.

Wild type oxidation buffer - Tris-HCl (50 mM), cysteine (3 mM), cystine (0.3 mM), pH 8.0.

Mutant oxidation buffer - Sodium phosphate (50 mM), 20% DMSO, pH 8.0.

4.4.1.2 – Ketosteroid Isomerase (KSI)-β-defensin Expression in *E.coli*

One freshly transformed BL21 (DE3) colony containing the pET-28a/HISKSI-HBD2 plasmid was used to inoculate 250 ml of 2YT medium, containing 30 μg/ml kanamycin. This was grown at 37 °C on an orbital shaker for 12 hrs and then an appropriate volume was added to 3 litres of 2YT, containing 30 μg/ml kanamycin to give a final OD_{600} of 0.1 and divided equally into six one litre flasks, with approximately 500 ml in each flask. Cells were grown at 37 °C until an OD_{600} of 0.5, induced with a final concentration of 1 mM isopropyl-1-thio-β-D-galactopyranoside (IPTG), and incubated for a further 6 hrs. Cells were subsequently harvested by centrifugation (8000 x g, 10 min, 4 °C). The cell pellet was stored at -20 °C until needed for protein extraction.

4.4.1.3 - Isolation of KSI-β-defensin Inclusion Bodies

All centrifugation steps were carried out for 20 min at 11000 x g and 4 °C. The cell pellet was suspended in 5 mL resuspension buffer per gram of wet pellet, before addition of 50 mg/ml lysozyme, 500 mM $MgCl_2$ and 10 μl DNase. After incubation for 30 min at room temperature, 5 ml/g wet weight pellet of lysis buffer was added and incubated for 45 min at room temperature. To this extract, 1 mM EDTA (500 mM stock) was added and the sample was snap-frozen in liquid N_2, before being thawed for 30 min in a 37 °C water bath. To this extract 1 mM $MgCl_2$ (500 mM stock) was added and the sample left at room temperature for 1 hr to allow a decrease in viscosity before another 1 mM EDTA was added and immediately centrifuged. The pellet was washed in an appropriate volume of wash buffer, sonicated for 4 x 30 sec blasts on ice and centrifuged. The pellet was then washed in 1 M Guanidine HCl buffer, sonicated for 4 x 30 second blasts on ice and centrifuged. The resultant pellet was resuspended in 6 M GdnHCl buffer and added to pre-equilibrated nickel-nitrilotriacetic acid

(Ni-NTA) agarose affinity chromatography (Qiagen). Mixture was incubated for 1 hr at 4 °C in an end-over-end rotator, before being washed 3 x with 5 column volumes of 6M GdnHCl buffer. Protein was eluted 3 x with 5 column volumes of elution buffer and subsequently dialyzed against 25 mM Tris buffer, pH 8.0 overnight at 4 °C which formed a precipitate of partially pure KSI-HBD2.

4.4.1.4 – Cyanogen Bromide (CNBr) Cleavage of KSI-β-defensin Fusion Protein

Precipitated fusion protein was centrifuged and the pellet resuspended in either degassed 6 M GdnHCl, 25 mM Tris-HCl buffer pH 8.0 and acidified with droplet additions of HCl (5 M) until pH ~1 or resuspended in degassed 70% formic acid. Solid CNBr (final concentration 250 mM) was added and cleavage proceeded for 24 hrs in the absence of light and under nitrogen. The cleaved mixture was evaporated at 42 °C using a rotary evaporator to remove any unreacted CNBr, and the concentrated sample was either precipitated by dialysis against 25 mM Tris-HCl buffer, pH 8.0 overnight at 4 °C (GndHCl cleavage) or freeze-dried (70% Formic acid cleavage). Precipitated KSI was removed by centrifugation (11000 x g, 20 min, 4 °C) and the aqueous phase containing impure HBD2 was filtered and purified by RP-HPLC as described in section 4.4.1.6. HBD2 was extracted from the freeze-dried mixture of KSI and HBD2 with 0.01% acetic acid. HBD2 formylation was partially reversed upon dialysis against 25 mM Ammonium acetate, pH 9.5, overnight at 4 °C and was monitored using positive electrospray ionisation mass spectrometry (ESI-MS) described in section 4.8.5.

4.4.1.5 - Reverse phase-High Pressure Liquid Chromatography (RP-HPLC) Purification of β-defensins

RP-HPLC on a Jupiter™ Proteo column was performed on a Waters 600 control pump with a photo diode array 996 detector instrument using Millenium 32 software. Impure HBD2 was loaded into a 5 ml loop and injected onto the Jupiter™ Proteo column at a flow rate of 3 ml/min. The proteins were eluted using a gradient of 5-55% acetonitrile over 50 min at a flow rate of 3 ml/min. Protein fractions containing β-defensin were identified by SDS-PAGE and positive ESI-MS. A mixture of partially reduced and oxidized peptides identified were pooled together and freeze-dried. Freeze-dried peptides were resuspended in reducing buffer and purified on RP-HPLC as described above. Fractions containing only reduced β-defensins were identified as before and were freeze-dried prior to chemical oxidation.

4.4.1.6 – Chemical Oxidation of β-defensins

All reactions were carried in sealed containers under N_2 and using degassed buffers. Freeze-dried, reduced, wild-type peptides (400 μg) were dissolved in wild-type oxidation buffer and stirred for 4 hrs at room temperature. All reduced single disulfide mutant HBD2s (400 μg) were dissolved in mutant oxidation buffer and the reaction was allowed to proceed for 3 days at room temperature with gentle stirring. The reactions were followed by RP-HPLC and analyzed by positive ESI-MS, to confirm the completion of the oxidation reaction.

In addition, freeze-dried, reduced HBD2 (400 μg) was dissolved in three additional oxidation buffers to identify the optimal HBD2 oxidation conditions: Sodium phosphate (50 mM), 20% DMSO, pH 8.1; GdnHCl (1 M), NaHCO$_3$ (100 mM), cysteine (3 mM), cystine (0.3 mM), pH 8.1; Tris-HCl (25 mM), ammonium acetate (100 mM), GSH (100 mM),GSSG (10

mM), pH 7.8. Reactions were allowed to proceed for 4 hrs at room temperature and reactions were monitored as before.

4.4.2 - Chemokine Receptor 6 (CCR6) Purification

4.4.2.1 - Crude Protein Extraction from CCR6 Expressing HEK293 Mammalian Cells

CCR6 expressing HEK293 cells were maintained as described above in six well tissue culture plates (Gibco BRL) and cells were grown until confluent. Cells were lysed using CelLytic™-M (Sigma-Aldrich) with protease inhibitor cocktail (Sigma-Aldrich) added. Mammalian cell lysis was performed according to the manufacturer's instructions and was carried out at 4 °C to reduced proteolysis. Protein containing supernatants were either stored at -80 °C or analyzed by SDS-PAGE and western blot.

CCR6 expressing HEK293 cells were treated with sodium butyrate (10 mM) at ~80% confluency for 18 hrs prior to cell lysis and analyzed as described previously.

4.4.2.2 - Buffers used in CCR6 Purification

Buffer A - HEPES (20 mM), EGTA (1 mM), pH 7.4.

Buffer B - HEPES (20 mM), EGTA (1 mM), $MgCl_2$ (5 mM), 20% glycerol (v/v), 2% DDM (w/v) and 0.25% CHS (w/v), pH 7.4.

Buffer C - HEPES (20 mM), $MgCl_2$ (5 mM), NaCl (300 mM), imidazole (20 mM), 20% glycerol, 2% DDM (w/v) and 0.25% CHS (w/v), pH7.4.

Buffer D - HEPES (20 mM), NaCl (150 mM), imidazole (10 mM), 20% glycerol, 2% DDM (w/v) and 0.025% CHS (w/v), pH 7.4.

Buffer E - HEPES (20 mM), NaCl (150 mM), imidazole (300 mM), 20% glycerol, 0.2% DDM (w/v) and 0.025% CHS (w/v), pH 7.4.

Buffer F - HEPES (20 mM), NaCl (150 mM), imidazole (500 mM), 20% glycerol, 0.2% DDM (w/v) and 0.025% CHS (w/v), pH 7.4.

Buffer G - HEPES (20 mM), NaCl (150 mM), 20% glycerol, 0.2% DDM (w/v) and 0.025% CHS (w/v), pH 7.4.

Buffer H - HEPES (20 mM), NaCl (150 mM), imidazole (30 mM), 20% glycerol, 0.2% DDM (w/v) and 0.025% CHS (w/v), pH 7.4.

Buffer I - HEPES (20 mM), NaCl (150 mM), imidazole (500 mM), 20% glycerol, 0.2% DDM (w/v) and 0.025% CHS (w/v), pH 7.4.

Buffer J - HEPES (20 mM), NaCl (150 mM), 3 x FLAG ® peptide, 20% glycerol, 0.2% DDM (w/v) and 0.025% CHS (w/v), pH 7.4.

4.4.2.3 – HEK293/CCR6 Membrane Isolation

Membranes were prepared as previously described for the human T-cell line, CEM cells [3]. Briefly, cells were scrapped into ice cold PBS and centrifuged (1000 rpm, 5 min, 4 °C) to collect all unbroken cells. Cell pellet was washed twice more before being resuspended in buffer A containing an EDTA-free protease inhibitor cocktail (Roche). Cells were lysed by physical disruption using 40 strokes of a tight pestle in a Dounce homogeniser. Cell lysate was firstly, centrifuged (1000 rpm, 10 min at 4 °C) before being ultracentrifuged (30,000 rpm, 30 min, 4 °C) to form the crude membrane pellet. Crude membrane was then washed by resuspension in buffer A and then ultracentrifuged (30,000 rpm, 30 min, 4 °C). Finally the HEK293/CCR6 membrane preparation was resuspended in buffer A and either frozen in liquid N_2, and stored at -80 °C or solubilized as described below.

4.4.2.4 - Solubilization Protocol

HEK293 membrane preparations were solubilized in buffer B containing an EDTA-free protease inhibitor cocktail. Membranes were incubated in solubilization buffer B for 2 hrs at 4 °C in an end-over-end rotator. Insoluble material was removed by ultracentrifugation (30,000 rpm, 30 min, 4 °C).

4.4.2.5 - HIS Tag Purification of CCR6

All purification steps were carried out at 4 °C unless stated otherwise. Solubilized membranes were diluted 2-fold in buffer C and incubated with buffer D pre-equilibrated Ni-NTA resin overnight in an end-over end rotator. Resin was poured into a 5 ml disposable column and allowed to settle under gravity. Resin was washed (1 CV, 3 x) in buffer C before being first eluted (1 CV, 3 x) with buffer E, then eluted (1 CV, 3 x) with buffer F. Fractions containing CCR6, identified by western blot were pooled together and diluted in buffer G till a final buffer concentration of 20 mM imidazole was obtained. CCR6 was further purified using 1ml pre-equilibrated Talon Cobalt resin (BD Clonetech, Oxford, UK) and eluted using buffer F. 1ml fractions were collected and analyzed for CCR6 using SDS-PAGE and western blot.

4.4.2.6 - HIS Tag followed by Gel Filtration Chromatography Purification of CCR6

Purification was carried out exactly as above except the Talon Cobalt resin step was replaced with a calibrated Prepacked Tricorn™ Superdex 200 10/300 GL (GE Healthcare) gel filtration step. Fractions containing CCR6 after Ni-NTA purification were identified as

above and were concentrated by ultrafiltration (VivaSpin concentrator, 30 kDa molecular weight cut-off). Filtered (0.45 µm) CCR6 samples were loaded into a 1 ml sample loop and injected onto a pre-equilibrated Superdex 200 10/300 GL gel filtration column using FPLC (ÄKTAexplorer 10, GE Healthcare). Column was run at an isocratic flow rate of 0.4 ml/min using buffer G as the mobile phase. Fractions containing CCR6 were identified as before.

4.4.2.7 - Gel Filtration Calibration

Prepacked Tricorn™ Superdex 200 10/300 GL was calibrated using a protein mixture consisting of Aldolase, Ovalbumin, Ribonuclease A, and Aprotinin dissolved in buffer E. A sample volume of 0.5% total column volume (TCV) was loaded onto a 100 µl loop and injected onto the preequilibrated column. Column was run at an isocratic flow rate of 0.4 ml/min using buffer G as the mobile phase and calibration curve was calculated according to the manufacturer's instructions. Void volume had previously been calculated using Blue Dextran (1 mg/ml, 0.5% TCV).

4.4.2.8 - HIS Tag followed by FLAG Immuno-Affinity Purification of CCR6

All purification steps were carried out at 4 °C unless stated otherwise. Filtered (0.45 µm) solubilized membranes were diluted 2-fold in buffer C and loaded into a 10 ml superloop and injected onto a pre-equilibrated 5 ml HisTrap ™ column (GE Healthcare) using FPLC (ÄKTABasic 100, GE Healthcare). Protein fractions were eluted with a linear imidazole gradient (100% buffer H to 100% buffer I) over 20 CV and eluted proteins were monitored at A_{280}. CCR6 containing fractions were determined by SDS-PAGE and western blot analysis as described before. CCR6 containing fractions were concentrated by

ultrafiltration (VivaSpin concentrator, 30 kDa molecular weight cut-off) and were incubated with washed and pre-equilibrated Anti-Flag M2 affinity gel (Sigma-Aldrich) for 2 hrs at 4 °C. The affinity gel had previously been washed 3 x with 0.1 M glycine HCl, pH 3.5, 3 x with PBS and pre-equilibrated with 3 washes of buffer G. Resin was then poured into a 1 ml disposable column and allowed to settle under gravity. After 5 x 1 CV washes with buffer G, the protein was eluted using buffer J. 1 ml fractions were collected and analyzed for CCR6 using SDS-PAGE and western blot.

4.5 - Enzymatic Digestion of Proteins

4.5.1 - Protease Digestion of β-defensins

Enzymatic digestion of peptides (1 mg/ml) with chymotrypsin (500 μg/ml) and/or trypsin (500 μg/ml) and was performed at 37 °C in digestion buffer and allowed to proceed overnight. After addition of 0.05% TFA to terminate reaction, cleavage products were analyzed by Liquid chromatography (LC)-ESI-MS as described in section 4.8.6.

4.5.2 - In-Gel Digestion

Excised protein gel bands were placed in sterile 1.5 ml eppendorf tubes and dried in a GyroVap for 30 min prior to treatment. Dried gel pieces were washed with 50% acetonitrile (ACN) twice and dried in GyroVap for 15 min. Protein disulfide bonds were then reduced with DTT/EDTA (100 mM Ammonium Bicarbonate, 10 mM DTT, 0.2% EDTA) for 30 min at 56 °C and cysteines alkylated, upon cooling to room temperature, with iodoacetamide (100 mM Ammonium Bicarbonate, 50 mM iodoacetamide) in the dark for 30 min at room temperature. Gel pieces underwent three cycles of washing (100 mM

Ammonium Bicarbonate) for 10 min at room temperature and dehydration (50% ACN) for 10 min at room temperature before being GyroVap for 15 min. Trypsin was added directly to the gel piece until completely absorbed before ammonium bicarbonate (50 mM) was added and incubated for 12-16 hrs on an orbital shaker at 37 °C. Alternatively, prior to trypsin digest, the gel piece was incubated with CNBr (5 M, 5 µl). Digested peptide solution was evaporated in the GyroVap and stored at -20 °C.

4.5.3 - Protein Precipitation

Purified CCR6 was precipitated with a mixture of chloroform, methanol and TFA. Methanol (150 µl) and chloroform (100 µl) were added to the protein solution (50 µl at 0.88 mg/ml) and vortexed. Addition of 10% TFA (100 µl) was followed by centrifugation (13,000 rpm, 20 min) to separate the two phases. Protein precipitated at the interface was carefully isolated and the methanol (150 µl) was added. Protein was pelleted and methanol removed using a pipette. Protein pellet was then air dried prior to chemical or enzymatic digestion.

4.5.4 – In-solution Digestion of CCR6

Protein was initially chemically cleaved using CNBr before undergoing trypsinization. Initially the protein was resuspended in 90% formic acid. CNBr (5 M, 5 µl) was added and mixed for 2 hrs at room temperature in the dark. The cleaved mixture was freeze-dried to remove any unreacted CNBr, and the protein mixture was acidified overnight in 0.5% TFA (500 µl). After another freeze-drying step, peptides were dissolved in 0.2% RapiGest (Waters) and incubated with DTT (4 mM) for 30 min at 55 °C. Reduced peptides were alkylated with iodoacetamide (10 mM) for 30 min in the dark before being digested further with Trypsin Gold (promega) at a ratio of 1:5 trypsin:CCR6 overnight at 37 °C. Prior

to mass spectrometric analysis RapiGest was hydrolysed by addition of formic acid (30%) for 30 min at 37 °C. Peptides were centrifuged (13,000 rpm, 10 min) and supernatant transferred to clean microcentrifuge tube. Digested peptides were stored at -20 °C until needed for mass spectrometric analysis.

4.6 - Molecular Immunology

4.6.1 - Antibodies

TYPE	NAME	COMPANY
Primary	Biotinylated Anti-HBD-2	Autogen Bioclear
Primary/ Secondary	Streptavidin-HRP	BD Biosciences, Pharmingen
Primary	Mouse Anti-His	GE Healthcare
Secondary	Goat anti-mouse-HRP	Cell Signalling
Primary	Anti-human CCR6-FITC	R & D systems
Control	Mouse IgG_1-CFS	R & D systems
Primary	ANTI-FLAG M2-FITC	Sigma
Primary	Mouse ANTI-FLAG M2	Sigma
Control	Mouse IgG_{2b}-FITC	BD Biosciences, Pharmingen
Primary	Rabbit Anti-human CCR6	AbCam
Secondary	Goat Anti-rabbit-HRP	AbCam

Table 4.2. Antibodies used in this Study.

4.6.2 – Fluorescence-Activated Cell Sorting (FACS) Analysis

Adherent mammalian cells were either trypsinized or scrapped into PBS and centrifuged (500 x g, 5 min). Cells were resuspended in PBS and washed (3 x) to remove any residual growth factors from the culture media. Washed cells (1 x 10^5) were transferred to a

new tube and blocked with human IgG (1 µg) for 15 min at room temperature. Fluorescein-labelled monoclonal antibodies (0.5 µg/ml) were incubated in the dark with the blocked cells for 45 min at 4 °C. Cells were washed (3 x) in PBS to remove any unbound antibody and finally resuspended in PBS for FACS analysis. FACS analysis was performed on a BD FACS Aria ™ System using a 488 nM excitation laser and 530/30 bandpass filter. Analysis was performed using FACS Diva software.

FACS analysis was performed by Dr Lois Alexander.

4.6.3 - Western Blot

Proteins separated on SDS-PAGE were equilibrated in transfer buffer for 20 min along with an equal sized Hybond-ECL nitrocellulose membrane (0.2 µm, Amersham). Proteins were then transferred and immobilized onto the equilibrated membrane by electroblotting at 15 V for 30 min using a Trans blot SD Semi-Dry Transfer cell. Membranes were blocked to avoid non-specific antibody binding. Membranes were shaken overnight at 4 °C in either 5% non-fat milk or Super Block (Pierce). Excess blocking solution was then removed by washing with PBS-T (0.1%). All washing steps were carried out at room temperature and consisted of 3 x 10 min washes unless stated. Blocked membranes were then incubated in primary antibody with blocking solution for 60 min at room temperature. Excess antibody was then removed with washings before being incubated with a secondary peroxidase conjugated antibody in blocking solution. A final wash was performed, before the membranes were dried and immuno-labelled proteins detected using the ECL^+ chemiluminescence detection system in accordance with the manufacturer's instructions. Proteins were visualised on BioMax XAR film (Kodak) and developed using a Compact X4 Automatic X-ray Film processor (Xograph).

4.6.4 – Enzyme-linked Immunosorbent Assay (ELISA)

Human TNF-α ELISA was carried out in accordance with the manufacturer protocol (R &D Systems). In brief, a 96-well plate was coated with the capture antibody (4 μg/ml) and incubated overnight at room temperature. Each well was washed (3 x) with a wash buffer (PBS with 0.05% Tween, pH 7.2) before blocking solution (PBS with 1% BSA, pH 7.2) was added for 1hr at room temperature. Again each well was washed (3 x) with wash buffer. Either standards or LPS stimulated supernatants (100 μl) were added to individual wells and incubated for 2 hrs at room temperature. After washing again (3 x), the detection antibody (goat anti-human TNF-α biotin conjugated antibody, 100 μl) was applied for 2 hrs at room temperature. After three more washes, streptavidin-HRP was applied and incubated in the dark for 20 min at room temperature. After three more washes, a substrate solution (1:1 mixture of H_2O_2 and Tetramethylbenzidine) was added and incubated in the dark for 20 min at room temperature. Finally a stop solution (2N H_2SO_4) was added and OD measured using a microplate reader set to 450 nm.

4.7 - Microbiology

4.7.1 - Bacterial Strains

All bacteria strains used were a kind gift from Prof. John Govan from the Edinburgh Cystic Fibrosis Microbiology Laboratory.

ORGANISM	STRAIN	DESCRIPTION
Gram-negative		
E.coli	MG1655	Type strain
P.aeruginosa	PAO1	Type strain
Gram-positive		
S.aureus	ATCC 25923	Type strain
Fungi		
C.albicans	J2922	Clinical Isolate

Table 4.3. Bacterial Strains used in this Study.

4.7.2 - Antimicrobial Assay

Antimicrobial assays were performed as previously described [4]. Bacterial strains were initially spread on nutrient agar (Oxoid). 10 ml isosensitest broth (ISB) was inoculated with a single colony and incubated overnight at 37 °C on an orbital incubator (150 rpm). Cells were subcultured into fresh ISB and further incubated for 4 hrs or until an OD_{600} of 1 was obtained. Bacteria were washed (3 x) in sodium phosphate buffer (10 mM, pH7.4) + 1% ISB to remove any residual NaCl from the ISB. The mid-logarithmic culture was diluted in 10-fold increments in sodium phosphate buffer (10 mM, pH 7.4) + 1% ISB until an optimal concentration was achieved.

Varying concentrations of peptides (1.5 µg/ml – 50 µg/ml) were added to the bacterial suspension and incubated for 2 hrs. Concentrated and 100-fold dilutions, in

duplicate, were spread onto isosensitest agar (ISA) and incubated overnight at 37 °C. Colony

forming units (CFU) were counted the next day and LD_{50}, LD_{90} and MBC were calculated.

All experiments were repeated three times and values were obtained by taking the mean of

all three experiments.

4.8 - Protein Analysis

4.8.1 - Polyacrylamide Gel Electrophoresis (PAGE)

SDS-PAGE was used to analyse proteins on the basis of their molecular mass. The

technique used was the discontinuous buffer system of Laemmli [5]. Denatured proteins

were analysed on precast 12% Bis-Tris Nu-Page gels (Invitrogen) according to

manufacturer's instructions. Alternatively, native proteins were analyzed on precast 16%

Tricine gels (Invitrogen) according to the manufacturer's instructions. Protein gels were

generally visualised using comassie blue stain or in cases of low concentration,

ProteoSilver™ Silver Staining kit (Sigma-Aldrich) was used and performed according to the

manufacturer's instructions.

4.8.2 - Deglycosylation Gel-Shift Assay

Deglycosylation was carried out in accordance with the manufacturer's instructions

(Calbiochem). In brief, 10 μl of reaction buffer (250 mM sodium phosphate buffer, pH 7.0)

and 2.5 μl denaturation solution (2% SDS, 1 M β-mercaptoethanol) of 30 μl of CCR6 (5 μg)

and mixed gently. 2.5 μl triton X-100 was added before 1 μl of each deglycosylating enzyme

was added to separate CCR6 aliquots and incubated for 24 hrs at room temperature to avoid

aggregation. Samples were analyzed by SDS-PAGE and western blot as described above.

4.8.3 - Phosphoprotein Gel Analysis

Phosphoprotein staining was performed using Pro-Q ® Diamond Phosphoprotein gel stain and carried out in accordance with the manufacturer's instructions (Invitrogen). Proteins were separated by SDS-PAGE and fixed (10% acetic acid, 50% methanol) overnight at room temperature to remove all the SDS. After one wash step (100% H_2O), gel was stained in the dark with Pro-Q ® Diamond gel stain for 90 min. Gel was destained (200 ml ACN, 50 ml 1 M sodium acetate, pH 4.0, 750 ml H_2O) for 30 min. This step was repeated another 2 times before two more washing steps. Fluorescent gel images were obtained using the Cy3 filter on a BioAnalyzer 4F/4S (LaVision BioTech).

4.8.4 - 1D ^{1}H NMR Spectrum

1 mg of oxidized HBD2 was dissolved in 20 mM sodium acetate buffer, pH 4.0 at 25 °C and 10% D_2O (v:v) was added to give to a final peptide concentration of 0.46 mM. The 1D ^{1}H NMR spectrum was recorded on a Bruker AVANCE spectrometer equipped with a cryoprobe operating at 600 MHz and 25 °C. 128 scans were taken with a sweep width (sw) of 15 ppm and 8000 complex points. For water suppression double-pulsed gradient spin echo was used. Oxidized HBD2 mutants were dissolved in 20 mM sodium acetate buffer, pH 4.0 and 10% D_2O (v:v) was added. The 1D ^{1}H NMR was recorded on a Brucker AVANCE spectrometer operating at 600 MHz and 25 °C. 32 scans were taken with a sweep width of 8k Hz and 9000 complex points. NMR data acquisition and processing was carried out using TopSpin software (Brucker BioSpin).

Method was optimized and carried out by Dr Emily Seo.

4.8.5 – Positive ESI-MS

Direct infusion mass spectrometry was performed on a Micromass ZMD mass spectrometer equipped with an electrospray ion source. Samples purified from HPLC were filtered (0.22 µM) and directly infused at a flow rate of 10 µl/min. Source parameters were kept constant except for the cone voltage and desolvation temperature. Cone voltage was typically set at 40-60 V and desolvation temperature set at 200 °C. All electrospray ionization was in positive mode and data acquired in continuum mode. Scans were accumulated, spectra combined and molecular mass calculated using the transform algorithm of the Mass Lynx 3.5 software (Micromass).

4.8.6 - LC-ESI-MS

ESI-MS was performed on a Micromass Platform equipped with an electrospray ion source. Protein samples were separated on a Waters HPLC 2795 using a Phenomenex Jupiter 4u Proteo column (250 x 2.0 mm) directly attached to the mass spectrometer. Peptides were eluted using a 10-95% ACN gradient over 45 min at a flow rate of 200 µl/min. The tune parameters were kept constant with only cone voltage and source temperature fluctuating depending on sample. Cone voltage was typically set at 40 V and source temperature was set at 110 °C. Total ion current was measured from 500-1900 m/z. All electrospray ionization was in positive mode and data acquired in continuum mode. Scans were accumulated, spectra combined and molecular mass calculated using the transform algorithm of the Mass Lynx 4.0 software (Micromass).

4.8.7 - LC-ESI-tandem Mass Spectrometry (MS/MS) using Q-TOF Mass Spectrometry

Positive LC-ESI-MS/MS was used for the characterisation of BioHBD2. Trypsin/chymotrypsin digested protein samples were separated using a C18 reverse phase column (Waters) on a CapLC system (Waters) connected directly to a Q-TOF Ultima (Micromass) mass spectrometer. Digested peptides were eluted using a 5-20% ACN with 0.1% formic acid gradient over 60 min at a flow rate of 240 μl/min. Q-TOF was run in data directed analysis mode and switch from MS to MS/MS mode when a double or triple charge state ion exceeded a threshold of 10 counts/sec. Argon was used as fragmentation gas and data was acquired from 100-2000 m/z.

4.8.8 - Fourier Transform Ion Cyclotron Resonance (FT-ICR)

High resolution mass spectrometry was performed on either a 9.4 Tesla or 12 Tesla Apex Qe FT-ICR (Brucker Daltonics, Billerica,MA). Both were equipped with mass resolving quadrupole, coupled to a nano-electrospray ionization enabled TriVersa Namomate (Advion Bioscience, Ithaca,NY). FT-ICR data was acquired using an AQS console and the acquisition rate was typically ~1 scan/2 sec. Lyophilized peptides were dissolved in 50% methanol with 0.2% formic acid and directly infused at a flow rate of 50 nl/min. Fast Fourier Transforms and analysis were performed using Data Analysis (Bruker Daltonics, Billerica,MA).

FT-ICR analysis was optimized and performed by Dr D Clarke.

4.8.9 - Nanospray LC-MS/MS using the HCT Mass Spectrometer

Following CCR6 receptor purification and either trypsin and/or CNBr digestion, samples were analyzed by nanoLC-MS/MS using a High Capacity Trap (HCT) quadrupole ion trap mass spectrometer (Brucker Daltonics). 10 µl injections were loaded onto a trap column (PepMap500 trap column) using an Ultimate 3000 LC in NanoHPLC mode at 20 µl/min of mobile phase A. Mobile phase A consisted of 95% H_2O, 5% ACN and 0.1% Formic Acid. Mobile phase B consisted of 100% ACN and 0.1% Formic Acid. Separation gradient was carried out on a PepMap100 3 µM Column (LC Packings, Dionex) at 20 µl/min. A linear gradient from 5% B to 55% B over 45 min was used. Eluted peaks were injected into the mass spectrometer in positive ionisation mode and peptides were analyzed using DataAnalysis. Acquired MS/MS spectra were exported as .MGF files and searched against a locally installed Mascot database.

HCT-MS analysis was optimized and performed by Dr D Clarke

4.8.10 - Edman Degradation

Oxidized HBD2 was digested with a mixture of trypsin/chymotrypsin as described in section 4.5.1 and both fragments were purified using RP-HPLC. Freeze-dried HBD2 fragment containing Cys1, Cys3, Cys5 and Cys6 was resuspended in a 1:1 mixture pyridine:water and incubated for 30 min at 60 °C upon addition of phenylthiohydantoin (PTH, 100 µl). After removal of the solvent under vacuum, the modified peptide fragment was incubated for 15 min at 60 °C with TFA (100 µl). After removal of TFA under vacuum, the peptide fragment without the N-terminal residue was resuspended in water (100 µl), washed with 4:1 mixture hexane:ethyl acetate and the aqueous phase analysed by ESI-MS.

Edman degradation was optimized and carried out by Dr Emily Seo.

4.9 - Chapter 4 References

1. Sarker, G. and S. Sommers, *The "Megaprimer" Method of Site-Directed Mutagenesis.* BioTechniques 1990. **8**(4): p. 404-407.
2. Taylor, K., et al., *Analysis and separation of residues important for the chemoattractant and antimicrobial activities of beta-defensin 3.* J Biol Chem, 2008. **283**(11): p. 6631-9.
3. Staudinger, R. and J.C. Bandres, *Solubilization of the chemokine receptor CXCR4.* Biochem Biophys Res Commun, 2000. **274**(1): p. 153-6.
4. Campopiano, D.J., et al., *Structure-activity relationships in defensin dimers: a novel link between beta-defensin tertiary structure and antimicrobial activity.* J Biol Chem, 2004. **279**(47): p. 48671-9.
5. Laemmli, U.K., *Cleavage of structural proteins during the assembly of the head of bacteriophage T4.* Nature, 1970. **227**(5259): p. 680-5.

Chapter 5

Conclusion and Future Work

5.1 - Conclusion

This study has achieved its aim of designing an efficient and reproducible method for production of functionally-active recombinant β-defensin peptides (HBD1 and HBD2). This was made possible due to the mutation of the KSI fusion protein to leave only a single CNBr cleavable methionine residue and manipulation of the pET-28a plasmid to allow expression as a N-terminal His-tagged KSI-fusion protein. Expression as inclusion bodies offered the host *E.coli* strain protection against the innate antimicrobial activity of β-defensins which if over expressed as a soluble protein would ultimately lead to the killing of the host. Functionally active rHBD2 was confirmed when both antimicrobial activity and chemotactic values were identified as comparable to other recombinantly produced or naturally purified HBD2 preparations [1-3]. Not only is the rHBD2 functionally active, but results from 1D ^{1}H NMR, high-resolution mass spectrometry and Edman degradation analysis indicate that the HBD2 peptide purified using this method is of the highest purity, fully oxidized and correctly folded. Careful construction of the expression plasmid allowed for the insertion of only one correctly orientated HBD2 gene. This provides a template for all future site-directed mutagenesis studies on HBD2. In fact this plasmid has now also been used to produce radioisotope ^{15}N-labelled HBD2 suitable for ligand-binding studies by NMR [4]. Unfortunately this expression plasmid is restricted to investigations of HBD2 due to the inability to remove the HBD2 gene. However this problem was solved by re-engineering the plasmid with a *Hind*III restriction site directly upstream of the CNBr cleavage site. Originally this expression plasmid was used to purify rHBD1, confirming that the purification method is applicable to other β-defensins and later replacement of the HBD1

gene with HBD2 mutants containing single disulfide bonds confirmed that this expression plasmid can be used for all future studies on recombinant β-defensins.

This study is the first to investigate the different effects that each individual canonical disulfide bond has on HBD2's function. None of the three single disulfide mutant HBD2 forms appeared to have the typical defensin β-sheet topology in the oxidized form. Removal of two structurally constraining disulfide bonds resulted in a reduced antimicrobial activity against an *E.coli* strain in all cases as compared to wt HBD2. Differences in activity between the single disulfide mutants are minimal although the disulfide bond Cys2-Cys4 constrained HBD2 was able to kill *E.coli* at lower concentrations. In conclusion, HBD2 with only one structurally constraining disulfide bond still retains antimicrobial activity albeit at a higher concentration. This was not the case for the chemotactic activity of HBD2, with all three mutants failing to chemoattract CCR6 expressing HEK293 cells.

The finding that synthetic HBD2 with biotinylated N-terminus (BioHBD2) retains the ability to chemoattract CCR6 expressing cells was extremely important as there is a dogma in the chemokine society that the N-terminus should not be altered. This indicates that biotinylated HBD2 can still bind to CCR6, therefore providing a useful tool for both pull-down and binding experiments. Its ability to also act as an anti-inflammatory mediator agrees with a previous study that showed HBD2 could inhibit LPS induced TNF-α release from a murine RAW 264.7 macrophage cell line [5]. Although the mechanism of this inhibition was not investigated in this study, it is the first time to my knowledge, that kdo_2-lipid A-induced TNF-α release has been reduced by a human β-defensin in matured human monocytes. Again this raises the possibility of using BioHBD2 as 'bait' in the pull-down of interacting partners.

Although the difficulties in purifying GPCRs are well documented, this study has shown for the first time the purification of CCR6 from transfected HEK293 mammalian cells. Identification of both complementary N and C-terminal tags by western blot analysis

provided evidence for the full-length chemokine receptor being isolated. The identity of CCR6 was confirmed by nanoelectrospray LC-MS/MS analysis which identified three separate peptides that corresponded to the sequence of CNBr and trypsin digested CCR6, including the highly conserved GPCR motif DRY. N-glycosylation modifications are conserved in the chemokine receptor family and CCR6 was predicted to contain five putative N-glycosylation sites. This modification was confirmed when enzymatic deglycosylation resulted in increased mobility by SDS-PAGE analysis indicative of a loss of the carbohydrate modification. Furthermore using the same expression system in which CCR6 was purified, an N-terminal deletion of CCR6 was expressed. The mutated receptor was identified by western blot analysis; however surface expression could not be detected. Therefore although original designed to investigate residues important in binding, this N-terminal section seems to be critical for cell surface trafficking.

5.2 - Future Work

Recent success in the purification and crystallization of a range of GPCRs has given renewed optimism that determination of the crystal structure of CCR6 is an achievable target. However what is clear is that using the current expression system of the wild-type receptor sequence would not produce the sufficient quantity required of a stable form of the protein to allow crystallization trails to begin. With the alternative heterologous expression systems now available the expression of CCR6 could be optimized to higher levels. To exploit a mammalian expression systems, the combination of a tetracycline inducible vector coupled with a suspension HEK293 cell line that resulted in high-level expression of rhodopsin could be investigated [6]. Very recently, CCR1 was expressed and purified using this expression system showing that it is applicable to chemokine receptors [7]. Furthermore, with the exception of glycosylation, this method would still allow full proteomics analysis of the recombinant protein to be performed. Recent success in crystallization of recombinant

GPCRs has come from extensive engineering of the native receptor. This same process would need to be applied to CCR6, however great care must be taken so as to avoid altering the core structure and inactivating the receptor. Furthermore, any results on ligand binding or downstream signaling derived from mutant receptors would subsequently have to be verified with the wild-type receptor using various biochemical and biophysical techniques to confirm that the activity was not a consequence of engineered tags or domains. Recent crystal studies have highlighted a family A conserved tryptophan in TMVI that is an integral part of a rotamer "toggle-switch" where it acts as a pivot point upon receptor activation [8, 9]. This tryptophan is conserved in the CC chemokine receptor family except for CCR6, CCR7 and CCR9 where the tryptophan is replaced with a glutamine. Interestingly these latter receptors are also less promiscuous [10]. A crystal structure of CCR6 in both its inactive and active states would reveal how this glutamine affects the rotamer "toggle-switch" and as such could reveal differences in these receptors activation mechanism.

The functional study of 26 single amino acid HBD1 mutants has set the standard for site-directed mutagenesis studies of defensins [11]. The expression plasmid constructed in this study could be used as a template for a similar study on HBD2. However a limitation in the defensin field is a lack of a reproducible binding assay for these mutants since radiolabeled ligands are not available and are no longer used in many laboratories. A method for production of fluorescently labeled defensins in *E. coli* or by solid phase peptide synthesis would be a great addition to the field and would allow for direct visualization of receptor binding both in vitro and in cells. Removal of the premature stop codon in our expression plasmid would allow for an additional methionine to be expressed as well as a C-terminal 6 x His tag. CNBr cleavage of the fusion protein would then leave a highly reactive C-terminal homoserine lactone. This can be used to conjugate various useful labels such as fluorescein to the C-terminal as has been shown with the yeast α-mating factor [12]. This would facilitate each mutant defensin purified to be fluorescently tagged and therefore using

flow cytometry analysis or fluorescent microscopy one could identify receptor binding on CCR6 expressing cells.

Finally, taking advantage of ^{15}N (and ^{13}C) labeled rHBD2; one could chemically synthesize the N-terminus of CCR6 and identify residues that interact during binding. The tactic of using N-terminal fragments rather than the full-length receptor has been successful in characterizing the interaction between various chemokine/chemokine receptors e.g., CXCL8/ CXCR1 [13]. This would also provide a framework for studying the effects of post-translational modifications on binding by modifying the N-terminus with recombinant glycotransferases or sulfotransferases. Although the CCR6 N-terminus is unlikely to be the only extracellular motif that binds defensins it would be an excellent starting point to elucidate the binding interactions of this important receptor.

5.3 - Chapter 5 References

1. Yang, D., et al., *Beta-defensins: linking innate and adaptive immunity through dendritic and T cell CCR6*. Science, 1999. **286**(5439): p. 525-8.
2. Harder, J., et al., *A peptide antibiotic from human skin*. Nature, 1997. **387**(6636): p. 861.
3. Antcheva, N., et al., *Effects of positively selected sequence variations in human and Macaca fascicularis beta-defensins 2 on antimicrobial activity*. Antimicrob Agents Chemother, 2004. **48**(2): p. 685-8.
4. Seo, E.S., et al., *Preparation of isotopically labelled recombinant beta-defensin for NMR studies*. Protein Expr Purif, 2009. **65**(2): p. 179-84.
5. Scott, M.G., et al., *Cutting edge: cationic antimicrobial peptides block the binding of lipopolysaccharide (LPS) to LPS binding protein*. J Immunol, 2000. **164**(2): p. 549-53.
6. Reeves, P.J., J.M. Kim, and H.G. Khorana, *Structure and function in rhodopsin: a tetracycline-inducible system in stable mammalian cell lines for high-level expression of opsin mutants*. Proc Natl Acad Sci U S A, 2002. **99**(21): p. 13413-8.
7. Allen, S.J., et al., *Expression, purification and in vitro functional reconstitution of the chemokine receptor CCR1*. Protein Expr Purif, 2009. **66**(1): p. 73-81.
8. Park, J.H., et al., *Crystal structure of the ligand-free G-protein-coupled receptor opsin*. Nature, 2008. **454**(7201): p. 183-7.
9. Shi, L., et al., *Beta2 adrenergic receptor activation. Modulation of the proline kink in transmembrane 6 by a rotamer toggle switch*. J Biol Chem, 2002. **277**(43): p. 40989-96.
10. Allen, S.J., S.E. Crown, and T.M. Handel, *Chemokine: receptor structure, interactions, and antagonism*. Annu Rev Immunol, 2007. **25**: p. 787-820.

11.   Pazgier, M., et al., *Studies of the biological properties of human beta-defensin 1*. J Biol Chem, 2007. **282**(3): p. 1819-29.

12.   Kuliopulos, A. and C. Walsh, *Production, purification, and Cleavage of Tandem Repeats of Recombinant Peptides*. Journal of the American Chemical Society, 1994. **116**: p. 4599-4607.

13.   Skelton, N.J., et al., *Structure of a CXC chemokine-receptor fragment in complex with interleukin-8*. Structure, 1999. **7**(2): p. 157-68.

Appendix
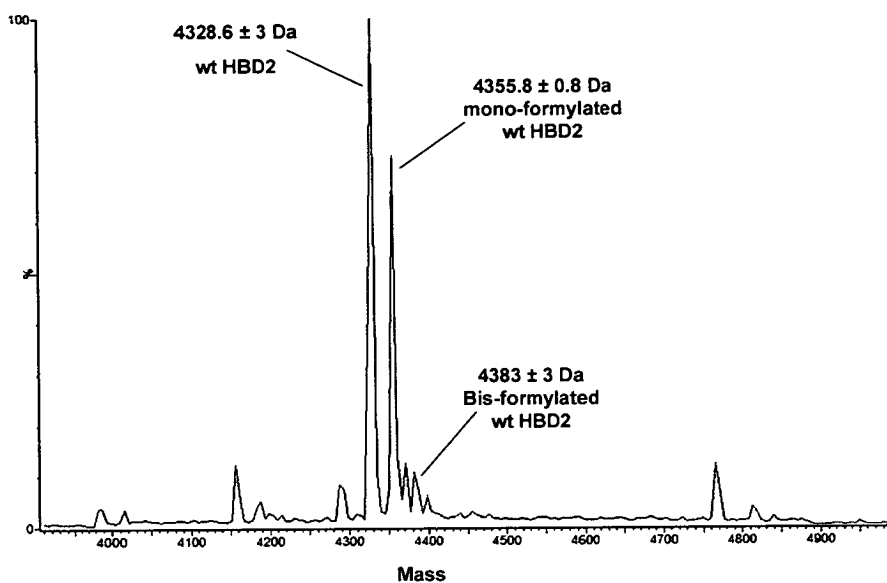
(A1) Deconvoluted Mass Data showing the effect of Formylation on Oxidized HBD2.
Masses indicated: oxidized HBD2 4328 ± 3 Da (theoretical mass 4328.2 Da); Mono-formylated oxidized HBD2 4355 ± 0.8 Da (theorectical mass 4356.2 Da); Bis-formylated oxidized HBD2 4383 ± 3 Da (theoretical mass 4384.3 Da).
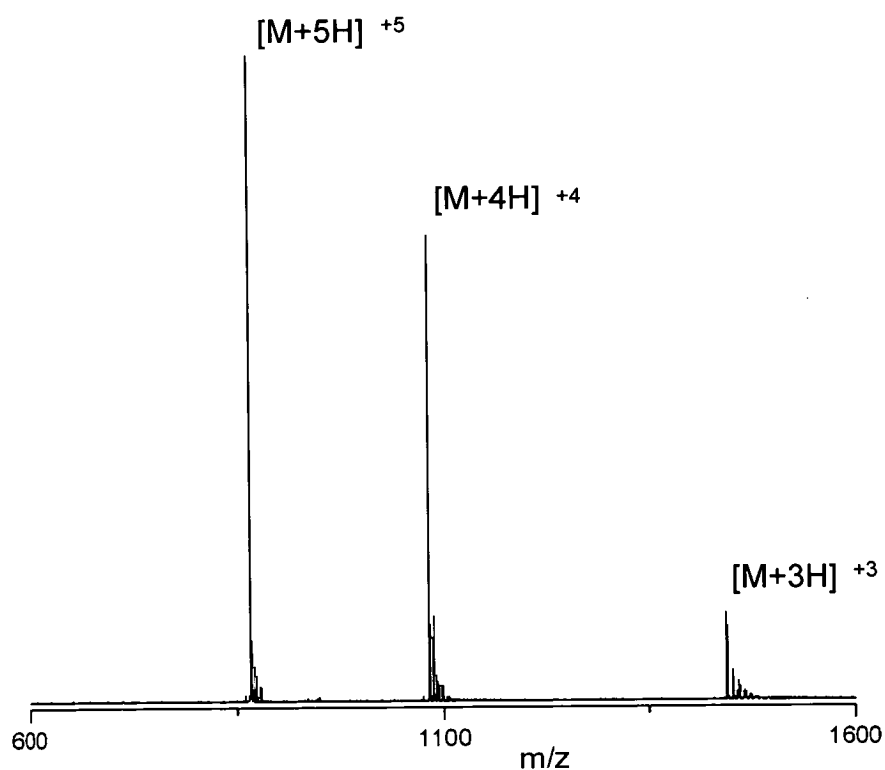
(A2) FT-ICR analysis showing the +3 to +5 charge state distribution for monomeric oxidized HBD2.

173

```
                               1                                                    50
Human beta-defensin 2    (1)  --------------ATGAGGGTCTTGTATCTCCTCTTCTCGTTCCTCTTC
Isolated HBD2 sequence   (1)  TCCAGCCATCAGCCATGAGGGTCTTGTATCTCCTCTTCTCGTTCCTCTTC

                               51                                                   100
Human beta-defensin 2   (37)  ATATTCCTGATGCCTCTTCCAGGTGTTTTTGGTGGTATAGGCGATCCTGT
Isolated HBD2 sequence  (51)  ATATTCCTGATGCCTCTTCCAGGTGTTTTTGGTGGTATAGGCGATCCTGT

                               101                                                  150
Human beta-defensin 2   (87)  TACCTGCCTTAAGAGTGGAGCCATATGTCATCCAGTCTTTTGCCCTAGAA
Isolated HBD2 sequence (101)  TACCTGCCTTAAGAGTGGAGCCATATGTCATCCAGTCTTTTGCCCTAGAA

                               151                                                  200
Human beta-defensin 2  (137)  GGTATAAACAAATTGGCACCTGTGGTCTCCCTGGAACAAAATGCTGCAAA
Isolated HBD2 sequence (151)  GGTATGAACAAATTGGCACCTGTGGTCTCCCTGGAACAAAATGCTGCAAA

                               201                                                  250
Human beta-defensin 2  (187)  AAGCCATGA-----------------------------------------
Isolated HBD2 sequence (201)  AAGCCATGAGGAGGCCAAGAAGCTGCTGTGGCTNATGCGGATTCAGAAAG
```

(A3) Sequence alignment showing the SNP in the HBD2 gene identified in CaCo2 cells. The signal and mature peptide sequences are marked with blue and green lines respectively. Residue highlighted in green is SNP and if translated the HBD2 mature peptide would have a K25E mutation.

Efficient Production of Human β-Defensin 2 (HBD2) in *Escherichia coli*

Thomas Vargues[1,#], Gareth J. Morrison[1,#], Emily S. Seo[1], David J. Clarke[1], Helen L. Fielder[1], Julien Bennani[1], Uday Pathania[2], Fiona Kilanowski[2], Julia R. Dorin[2], John R. W. Govan[3], C. Logan Mackay[1], Dušan Uhrín[1] and Dominic J. Campopiano[1,*]

[1]*School of Chemistry, EastChem, University of Edinburgh, Edinburgh, Scotland, EH9 3JJ, Scotland, United Kingdom;* [2]*Medical Research Council Human Genetics Unit, Edinburgh, EH4 2XU, Scotland, United Kingdom;* [3]*Centre for Infectious Diseases, University of Edinburgh, Edinburgh EH16 4SB, United Kingdom*

Abstract: Human β-defensin 2 (HBD2) has been shown to interact with pathogenic bacteria and components of the mammalian innate and adaptive immune response. We describe a quick and reliable method for the production of HBD2 in *Escherichia coli*. HBD2 was expressed as an insoluble fusion, chemically cleaved and oxidised to give a single, folded HBD2 β-isoform. The purified peptide was analysed by high resolution mass spectrometry, displayed a well-dispersed ^{1}H NMR spectrum, was a chemoattractant to HEK293 cells expressing CCR6 and acted as an antimicrobial agent against *E. coli*, *P. aeruginosa*, *C. albicans* and *S. aureus*.

Keywords: HBD2, Defensin, Peptide, *E. coli*, Chemotaxis, Antimicrobial activity.

INTRODUCTION

Antimicrobial peptides (AMPs) are essential components of the innate immune response and act as the first line of defence against invading pathogens [1]. The AMP family displays enormous sequence, structural and functional diversity and over 900 different eukaryotic peptides have been characterized to date (sequences are available in the Antimicrobial Sequences Database (AMSDb), http://www.bbcm.univ.trieste.it/). Defensins are a subset of the AMP family and are small (3-5 kDa), cationic peptides that play roles in both innate and adaptive immunity [2-7]. They are characterised by 6 conserved cysteine residues that form 3 disulfide bonds and are divided into two main subfamilies; alpha (α-) and beta (β-) are defined by their cysteine spacing, disulfide bond connectivity and genomic organisation. The α-defensins display Cys_1–Cys_6, Cys_2–Cys_4, Cys_3–Cys_5 S-S connectivity and contain 29-35 residues, whereas the β-defensins display a S-S connectivity of Cys_1-Cys_5, Cys_2-Cys_4, Cys_3-Cys_6 and consist of 40-50 residues. A third sub-family, the θ-defensins also contain 3 S-S bonds but are cyclic peptides, fused at the N- and C-termini, and have only been found in rhesus monkeys.

Analysis of the human genome revealed the presence of considerably more β-defensin genes than previously thought [8]. In contrast, only 6 human α-defensins have been identified [9] and elegant studies of the structures and properties of these peptides (HNP1-4 and HD5 and HD6) by a number of research groups have begun to provide a better understanding of their role in the immune response [7,10-14]. The high resolution structures of a few of the known mammalian β-

defensins have been determined by NMR spectroscopy and x-ray crystallography and include bovine neutrophil defensin (BNBD-12), penguin spheniscin (Sphe-2) and the human β-defensins (HBD1, HBD2, HBD3) [15-22], but more work is needed to explore the structure/functional relationship of this sub-family. We have chosen HBD2 as a target; it was shown that this defensin is expressed in epithelial cells and in the epidermis, and was originally isolated from human psoriatic scales [23]. It is expressed as a 64 amino acid precursor peptide and the mature form consists of 41 residues with a net positive charge of +7. The 3D structure of mature HBD2 revealed an amphipathic molecule with distinct patches of positively-charged and hydrophobic residues [17,19,20]. It is thought that this topology allows the defensin to interact with the outer cell components of bacterial membranes and act as a potent antimicrobial peptide against a range of pathogens [24]. Recent studies have shown that a number of defensins and their related peptide fragments, can act also as potent stimulators of the adaptive immune response, e.g. HBD2 acts as a chemoattractant for CD4 memory T cells and immature (but not mature) dendritic cells, by acting through the chemokine receptor CCR6, a member of the G-protein coupled receptor (GPCR) family [25,26].

To study the molecular details of the interaction of HBD2 with its various targets we required a robust method for the production of single isoform material. The production of defensins suitable for structural and functional studies has been achieved by solid-phase peptide synthesis but the inherent amphiphilic nature of the peptide, protection strategies and losses upon oxidation have caused associated problems [27,28]. As an alternative, recombinant methods have also been developed, e.g., Ganz and colleagues have used a baculovirus/insect cell system to produce active human peptides HNP-1, HD-5, HBD1 HBD2 [29-32]. As well as this method others have employed the common, easy-to-use host *E. coli* [33-36]. Here however, there is the inevitable prob-

lem of toxicity of the defensins towards the host expression system but this has been overcome by expressing the peptide fused to a protein partner within inclusion bodies. This introduces a further cleavage step to release the mature peptide and results in low overall yield. The use of expensive proteases such as enterokinase also increases the cost of the overall production of sufficient quantities of peptide. New strategies such as using the yeast *Saccharomyces cerevisiae* as a host organism or production by a cell-free system have also emerged recently [37,38]. These combined methods have allowed researchers to begin to explore the structure and activity of certain defensins [22,39-42].

To prepare defensins for a range of structural and functional studies, we describe a method for the production of recombinant, active, single isoform β-HBD2 from an *Escherichia coli* host. We designed a codon-optimised HBD2 gene for bacterial expression and synthesised this gene by recursive PCR [43] (Fig. **1**). and developed a protocol to isolate mature HBD2. This peptide was characterised by a range of structural techniques and was active in functional assays.

MATERIALS AND METHODS

Materials

E. coli strains Top10 (Invitrogen) and BL21 (DE3) (Novagen) were used for construction of plasmids and expression of proteins respectively. Polymerase chain reaction (PCR) was carried out using Hercules polymerase (Stratagene) and puRe Taq Ready-To-Go PCR beads (GE Healthcare). PCR products were cloned initially in pGEM-T easy (Promega), then re-cloned into pET plasmids (Novagen). Site-directed mutagenesis used the Quick-change kit (Stratagene). Nickel-nitrilotriacetic acid (Ni-NTA) affinity resin was from Qiagen. Snakeskin dialysis tubing was from Pierce (3 kDa cut-off). Oligonucleotide primers were purchased from SigmaGenosys. All restriction enzymes and T4 DNA ligase were from New England Biolabs. Nu-PAGE 12% Bis-Tris pre-cast gels were from Invitrogen. HPLC columns were purchased from Phenomenex, synthetic human β-defensin 2 (bHBD2, biotinylated at the N-terminus) was purchased from Albachem and Polymyxin B (PMB) was obtained from Calbiochem and tris(2-carboxyethyl)phosphine (TCEP) and CNBr were from Sigma.

Synthesis and Cloning of Codon-Optimized HBD2

Six overlapping primers (Table 1) with codons optimized for expression in *E. coli* were designed using the mature HBD2 amino acid sequence (also known as DEFB4, Genbank accession number, NM_004942). The reaction contained in a final volume of 100 μl: 10 μl (100 pmol) of the outermost 5' primers (P1 and P6) of each strand, 10 μl (10 pmol) of the internal primers (P2 – P5), 4 μl DMSO, 10 μl 10 x Herculase reaction buffer (Stratagene), 1 μl Herculase Hotstart DNA polymerase (Stratagene), 4 μl 25 mM dNTPs, 21 μl dH$_2$O and was subjected to 30 PCR cycles of 95 °C for 2 minutes, 40°C for 3 minutes and 72°C for 30 seconds. A second amplification was performed to confirm annealing of all six primers in a final volume of 50 μl: 5 μl primer P1 (50 pmol), 5 μl primer P6 (50 pmol), 2 μl template, 38 μl dH$_2$O and 2 puRe Taq Ready-To-Go PCR beads were subjected to

30 PCR cycles of 95°C for 2 minutes, 40°C for 3 minutes, 72 °C for 30 seconds and a final extension of 72°C for 10 minutes to add A overhangs. The PCR product (Fig. **2A**) containing the codon-optimized gene preceded by Met and flanking *Alw*N1 recognition sites was purified, cloned into pGEM-T Easy plasmid and a positive clone sequenced to confirm the fidelity of the insert. The target gene was then cut and ligated into the expression plasmid pET-31b (Novagen) to give pET-31b/HBD2. To incorporate a N-terminal His(6)-tag sequence, both pET-31b/HBD2 and pET-28a(+) vectors were cleaved by restriction enzymes *Nde*I and *Xho*I and the HBD2 fragment now containing the ketosteroid isomerase (KSI)-fused gene was cloned into pET-28a (Fig. **1A**). To avoid CNBr cleavage at unwanted sites within the fusion residues Met 1 and 126 of KSI were replaced with Ala by site-directed mutagenesis to give plasmid pET-28a/His-KSI-HBD2 (Fig. **1C**). The fidelity of this clone was confirmed by DNA sequencing.

Expression of KSI-HBD2 in *E. coli*

The freshly transformed BL21 (DE3) colony containing the pET-28a/His-KSI-HBD2 plasmid was used to inoculate 250 mL of 2YT medium at 37°C, with shaking containing 30 μg/mL kanamycin. This was grown for 12 hours and then added to 3 litres of 2YT, containing 30 μg/mL kanamycin to give an OD$_{600}$ 0.1 and divided into six one litre flasks, with approximately 500 mL in each flask. Cells were grown at 37 °C until an OD$_{600}$ = 0.5, induced with a final concentration of 1 mM isopropyl-β-D-1-thiogalactopyranoside (IPTG), and incubated for a further 6 h. Cells were subsequently harvested by centrifugation (6000 rpm for 10 minutes, 4°C).

Isolation of KSI-HBD2 Inclusion Bodies and Production of HBD2

All centrifugation steps were carried out for 20 minutes at 11000 rpm and 4 °C. The cell pellet containing highly expressed HisKSI-HBD2 was suspended in 5 mL/g in resuspension buffer (50 mM Tris, 25% sucrose, 1 mM EDTA, 0.1% sodium azide, 10 mM DTT, pH 8.0), before addition of 50 mg/mL lysozyme, 500 mM MgCl$_2$ and 10μl DNase. After incubation for 30 minutes at room temperature, lysis buffer (50 mM Tris, 1% Triton X-100, 100 mM NaCl, 0.1% sodium azide, 10 mM DTT, pH 8.0) was added (5 mL/g wet weight original pellet) and incubated for 45 minutes at room temperature. To this cloudy suspension, EDTA (500 mM) was added to give a final concentration of 1 mM, and the sample was snap-frozen in liquid N$_2$ before immediately thawing for 30 minutes in a 37°C water bath. To this thawed extract, MgCl$_2$ (500 mM) was added to give a 1mM final concentration and the sample was incubated at room temperature for 1 h to allow the viscosity to decrease before centrifugation. The supernatant was discarded and the pellet from this step was resuspended in an appropriate volume of buffer (50 mM Tris, 1% Triton X-100, 100 mM NaCl, 1 mM EDTA, 0.1% NaAzide, 1 mM DTT, pH 8.0), sonicated for 4 x 30 second blasts and centrifuged. The resulting pellet was then washed in 1 M Guanidine HCl buffer (1 M GuHCl, 50 mM Tris, 1% Triton X-100, 100 mM NaCl, 1 mM EDTA, 0.1% sodium azide, 1 mM DTT, pH 8.0), sonicated with 4 x 30 second bursts and centrifuged. The resulting pellet (inclusion bodies containing highly enriched KSI-HBD2) was resuspended in

A

B
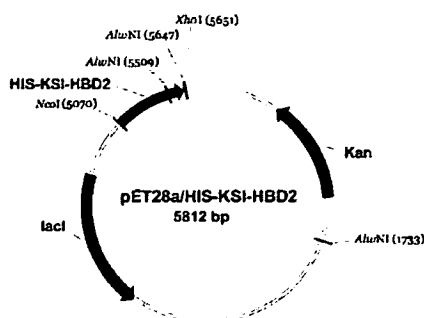
```
       AlwNI  MetGlyIleGlyAspProValThrCysLeuLysSerGlyAlaIleCysHis
   1   CAGGCGCTGATGGGTATCGGTGACCCGGTTACCTGCCTGAAATCCGGTGCTATCTGCCAC   60
       GTCCGCGACTACCCATAGCCACTGGGCCAATGGACGGACTTTAGGCCACGATAGACGGTG


       ProValPheCysProArgArgTyrLysGlnIleGlyThrCysGlyLeuProGlyThrLys
  61   CCGGTTTTCTGTCCGCGTCGTTACAAACAGATCGGTACCTGCGGTCTGCCGGGGTACCAAA   120
       GGCCAAAAGACAGGCGCAGCAATGTTTGTCTAGCCATGGACGCCAGACGGCCCATGGTTT


       CysCysLysLysPro***  AlwNI
 121   TGCTGCAAAAAACCGTGACAGATGCTG  147
       ACGACGTTTTTTGGCACTGTCTACGAC
```

C

```
   1   MGSSHHHHHH SSGLVPRGSH AHTPEHITAV VQRFVAALNA GDLDGIVALF
  51   ADDATVEDPV GSEPRSGTAA IREFYANSLK LPLAVELTQE VRAVANEAAF
 101   AFTVSFEYQG RKTVVAPIDH FRFNGAGKVV SIRALFGEKN IHACQALMGI
 151   GDPVTCLKSG AICHPVFCPR RYKQIGTCGL PGTKCCKKP
```

Figure 1. A. Schematic representation of expression vector pET-28a/HIS-KSI-HBD2.
B. Design of synthetic, codon-optimized HBD2 gene (147 bp) for *E. coli* expression. Primers were designed for overlapping recursive PCR (see Table 1). The 5' and 3' primers incorporated *Alw*N1 restriction sites (bold) to allow cloning of KSI-HBD2 fusion into pET28a. **C.** The full-length His-KSI-HBD2 fusion sequence (189 aa) with mature HBD2 (41 aa) produced by CNBr cleavage after the Met residue highlighted in bold. The Met-Ala mutations in KSI (M1A and Met126A) are underlined.

Table 1.   Primers Used in Synthesis of Codon-Optimised HBD2

Primer	Sequence (5'-3')
P1	CAGATGCTGATGGGTATCGGTGACCCGGTTACCTGCCTGAAATCC
P2	CGGACAGAAAACCGGGTGGCAGATAGCACCGGATTTCAGGCAGGT
P3	CCGGTTTTCTGTCCGCGTCGTTACAAACAGATCGGTACCTGCGGT
P4	GCAGCATTTGGTACCCGGCAGACCGCAGGTACCGAT
P5	ACCAAATGCTGCAAAAAATGACAGATGCTG
P6	CAGCATCTGTCACGGTTTTTTGCAGCATTTGGTACCCGG
M1A For	GCGGCAGCCATGCGCATACCCCAGAACACATC
M1A Rev	GATGTGTTCTGGGGTATGCGCATGGCTGCCGC
M126A For	GAATATTCACGCATGCCAGGCGCTGATGGGTATCGGTGAC
M126A Rev	GTCACCGATACCCATCAGCGCCTGGCATGCGTGAATATTC

~ 50ml 6 M GuHCl binding buffer (6 M GuHCl, 50 mM Tris, 10 mM imidazole, 500 mM NaCl, 5 mM β-mercaptoethanol, pH 8.0). These inclusion bodies were added to 10 ml pre-equilibrated nickel-nitrilotriacetic acid (Ni-NTA, Qiagen) agarose affinity resin, mixed by rotation for 1 h at 4°C, then decanted into an empty 25 ml column reservoir. The packed resin was washed with 6 M GuHCl binding buffer (50 ml) and then eluted with 25 ml of elution buffer (6 M GuHCl, 50 mM Tris, 120 mM imidazole, 500 mM NaCl, 5 mM β-mercaptoethanol, pH 8.0). This elution step with

120 mM imidazole was then repeated to give 50 ml of purified HisKSI-HBD2. The eluted fusion protein was dialyzed against 25 mM Tris buffer, pH 8.0 overnight at 4°C which caused precipitation of the fusion protein.

The fusion was recovered by centrifugation and the pellet was resuspended in 6 M GuHCl, 25 mM Tris buffer, pH 8.0. To this HCl (5 M stock) was added until the pH was ~1.0. Solid Cyanogen Bromide (CNBr) was added to give a final concentration of 250 mM and cleavage was allowed to proceed for 24 h in the absence of light and under nitrogen. The cleaved mixture was evaporated at 42°C using a rotary evaporator to remove any unreacted CNBr, and the concentrated sample was dialyzed against 25 mM Tris buffer, pH 8.0 overnight at 4°C to cause precipitation of the KSI. The precipitate was removed by centrifugation and the supernatant containing HBD2 was filtered (0. 45 μM) and purified by RP-HPLC as described below.

Purification of HBD2

Preparative RP-HPLC on a Jupiter™ Proteo column was performed with a Waters 600 control pump fitted with a photodiode array 996 detector using Millenium 32 software. The HBD2 isolated from the Cynogen Bromide (CNBr) cleavage step was applied to the column in 3-4 ml batches, the column was washed with 5% acetonitrile then a linear gradient of 5-55% acetonitrile over 50 minutes at a flow rate of 3 mL/minute was used to elute the HBD2. Fractions were analysed by SDS-PAGE and those containing HBD2 were pooled and shown to be a mixture of partially reduced and oxidized peptides (by ESI-mass spectrometry).

Oxidation of Recombinant HBD2

The HBD2 recovered by prep-HPLC was freeze-dried then reconstituted in 25 mM Tris, pH 8.0, with 20 mM (TCEP) added to convert the peptide to the fully reduced form before re-purification by prep-HPLC using identical conditions as above. Fractions containing HBD2 were freeze-dried then dissolved in 50 mM Tris, pH 8.0, 3 mM cysteine, 0.3 mM cystine and stirred for 4 h at room temperature. The reaction was followed by analytical RP-HPLC and analyzed by ESI-mass spectrometry to confirm that the HBD2 was present in the oxidized form (elution at 40 mins). The final yield of oxidized β-HBD2 is 3-6 mg from 3 litres of *E. coli* culture (based on 10 preparations).

Western Blot Analysis

Peptides were separated on a 12% Bis-Tris gel as described by the manufacturer (Invitrogen) followed by electroblotting using a Trans blot SD Semi-Dry Transfer cell (Bio-Rad) onto a Hybond-ECL nitrocellulose membrane (GE Healthcare). HBD2 was detected with a HBD2-specific antibody (Autogen Bioclear) and electrochemiluminescence plus (ECL$^+$) using a Streptavidin-HRP antibody according to the manufacturer's instructions (GE Healthcare).

Disulfide Bond Connectivity

The disulfide bond connectivity of the oxidized HBD2 was determined by trypsin/chymotrypsin digest, Edman degradation and mass spectrometry analysis as described previously [40,44].

1D ^{1}H NMR Spectrum

1 mg of oxidized HBD2 was dissolved in 20 mM sodium acetate buffer, pH 4.0 at 25 °C and 10% D_2O (v:v) was added to give to a final peptide concentration of 0.46 mM. The ^{1}H NMR spectrum was recorded on a Bruker AVANCE spectrometer equipped with a cryoprobe operating at 600 MHz and 25 °C. 128 scans were taken with a sweep width of 15 ppm and 8000 complex points. For water suppression double-pulsed gradient spin echo was used.

Antimicrobial Activity Assay

The purified, oxidized HBD2 was dissolved into 0.01% acetic acid and centrifuged (13000 rpm for 10 minutes, 25 °C) to remove precipitate. The HBD2 was concentrated (Vivaspin 0.5 mL concentrator, 3000 MWCO PES) to 1 mg/mL and stock HBD2 solutions of concentrations 15, 30, 60, 125, 250 and 500 μg/mL were prepared. Antimicrobial assays were carried out according to the method set out in our previous study [25,40,45]. Briefly, a laboratory strain of *E. coli* K-12 MG1655 was grown to midlogarithmic phase (OD at 600nm = 1.0). From this 90 μl *E. coli* (~1.0 x 10⁵ cells) was incubated with 10 μl of each stock HBD2 solution and as a negative control 90 μl *E. coli* was incubated 10 μl 0.01% acetic acid. These samples were incubated at 37°C for 2 hours. Then 10-fold serial dilutions of the incubation mixture were plated on Iso-Sensitest plates, incubated at 37 °C, and the CFU was determined the following day. Colonies were counted and the LD_{50}, LD_{90} (Lethal Dose: amount of peptide required to kill 50 % and 90% of viable cells) and the $MBC_{99.99}$ (Minimum Bactericidal Concentration at 99.99 %) values were calculated from the resulting killing curve. The same antimicrobial assays were performed with *Pseudomonas aeruginosa* (PAO1), a Gram-positive strain *Staphylococcus aureus* (ATCC 25923) and a fungus, *Candida albicans* (J2922) [45]. In parallel, the same strains were used with the antimicrobial agent Polymyxin B (PMB) as a control. All the killing assays were performed at least 3 times for each strain and the values were obtained by taking the mean of each 3 experiments.

High Resolution FT-ICR Mass Spectrometry

The oxidized HBD2 was diluted to a final concentration of 1 μM in electrospray buffer, consisting of 50:50 methanol:H_2O with 0.2 % formic acid. Data was acquired on a 12 Tesla Apex Qe FT-ICR (Bruker Daltonics, Billerica, MA) equipped with mass resolving quadrupole, coupled to a nano-electrospray ionization (nESI) enabled TriVersa Nanomate (Advion Bioscience, Ithaca, NY). Samples were infused at a flow rate of 50 nanolitres per minute. Desolvated ions were transmitted to a 6 cm Infinity cell® penning trap. Trapped ions were excited (frequency chirp 48-500 kHZ at 100 steps of 25 μs) and detected between *m/z* 600 and 2000 for 1 s to yield broadband 1 Mword time-domain data. Each spectrum was the sum of 64 mass analyses. Typical chamber base pressure was ~9 x 10⁻¹¹ mbar. Time-domain FT-ICR data was acquired using an AQS console and the aquisition rate was typically ~1 scan/2 s. Fast Fourier Transforms and subsequent analyses were performed using DataAnalysis (Bruker Daltonics, Billerica, MA).

Chemotaxis Assay

The chemotaxis activity analysis was carried out against HEK293 cells expressing CCR6 as we have previously reported [25]. The migration of CCR6-transfected human embryonic kidney HEK293 cells was assessed with a micro-chemotaxis chamber technique. Chemotactic activity was measured as the optimal concentration of test compound at which the highest chemotactic index value was obtained. Experiments were carried out three times. CCL20 (also known as MIP3-α) was from Peprotech (London, UK).

RESULTS AND DISCUSSION

Synthesis of HBD2 Gene by Recursive PCR

Our goal was to produce mature, untagged HBD2 as a single β-defensin isoform. Our strategy to enhance the expression of the toxic human antimicrobial peptide HBD2 in the host *E. coli* was to fuse it to the highly insoluble ketosteroid isomerase (KSI) tag using a commercially available plasmid. Six overlapping primers (Table 1) with codons optimized for expression in *E. coli* were designed to synthesise the HBD2 gene in a one step recursive PCR reaction [43] (Fig. 1B). An ATG Met codon was incorporated at the 5' end of the HBD2 gene to enable cleavage of the peptide from the KSI tag by cyanogen bromide (CNBr) (Fig. 1B). A similar chemical cleavage strategy had been used by Ganz and coworkers to produce active HBD2 expressed in baculovirus-infected insect cells [29]. Restriction sites for *Alw*NI, flanking the HBD2 sequence, were engineered into the gene to enable cloning into the KSI expression plasmid, pET-31b and a stop codon was engineered upstream of the 3' *Alw*NI site to avoid generation of a homoserine lactone HBD2 derivative after cleavage. Initial PCR gave a gene product at the expected size of the HBD2 target (144bp, Fig. 2A) and a second PCR amplification using this template with the 5' and 3' terminal primers gave a gene that was cloned firstly into plasmid pGem-T Easy then into the expression plasmid pET-31b digested with the same enzyme. To utilize His-tag purification technology, the KSI-HBD2 fusion gene was excised from pET-31b and ligated into pET-28a downstream of a 6xHis-tag. To improve the efficiency of the chemical

cleavage and generate a single CNBr cleavage site within the KSI-HBD2 fusion, the Met1 and Met126 residues within the KSI gene were converted to Ala by site-directed mutagenesis to generate the expression plasmid pET-28a/His-KSI-HBD2 which was used for all further studies (Fig. 1A).

Expression of His-KSI-HBD2

Plasmid pET-28a/His-KSI-HBD2 was used to transform BL21 (DE3) cells and on a small scale (10ml) induction with IPTG, a strong band corresponding to His-KSI-HBD2 at 20.2 kDa was observed by SDS-PAGE in agreement with the predicted molecular weight of the KSI-HBD2 fusion protein of 189aa (Fig. 2B). This expression was scaled up to 3 litres of culture medium and yielded ~9 g wet weight cell paste that was frozen at -20°C.

Purification of His-KSI-HBD2 and Cleavage of HBD2

The His-KSI-HBD2 fusion was isolated from the bacterial pellet by a series washing and centrifugation steps. Aliquots were removed throughout the purification protocol and analysed by SDS-PAGE to monitor the increased purity and yield of His-KSI-HBD2. We engineered a methionine residue at the N-terminus of the HBD2 protein to allow cleavage from the KSI tag by CNBr. This non-enzymatic cleavage is efficient and less expensive than using proteolytic enzymes such as enterokinase. After a one-step Ni-NTA affinity purification, the His-KSI-HBD2 was sufficiently pure for CNBr cleavage (Fig. 3A). After 18-22 h, the cleavage was complete and separation of the fusion protein from HBD2 was carried out by dialysis against buffer (25 mM Tris, pH 8.0) followed by centrifugation (10,000 r.p.m.) to remove any precipitate. Cleaved HBD2 was shown to be in the soluble fraction by SDS-PAGE (Fig. 3A).

Characterisation of Oxidized, Folded β-Defensin HBD2

Soluble HBD2 was purified by preparative RP-HPLC and mass spectrometry showed that it was a mixture of reduced and oxidized forms. This HBD2 mixture was completely reduced using TCEP then purified by RP-HPLC. The recovered HBD2 was oxidized at room temperature using a
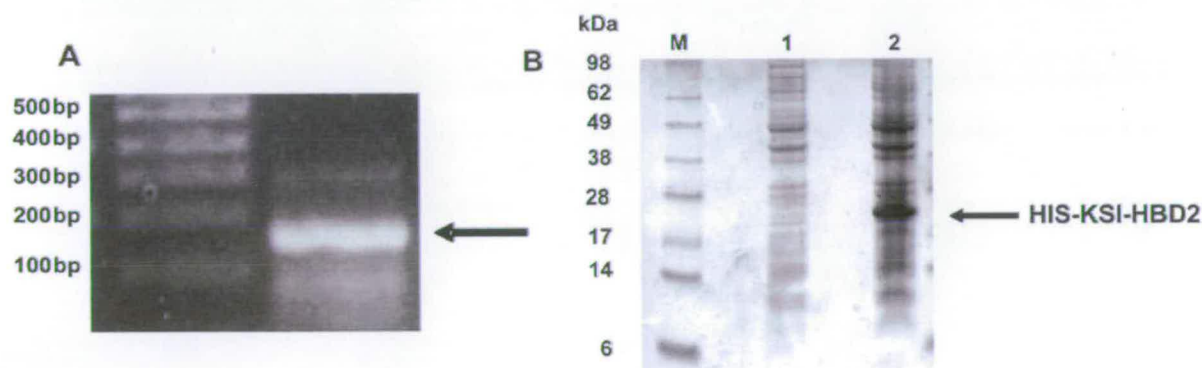

Figure 2. A. Synthesis of optimised HBD2 gene by recursive PCR. Lane 1, 1kb DNA Hyperladder I (Bioline); lane 2, recursive HBD2 PCR product. The band indicated by arrow is the 147bp codon-optimised HBD2 gene product. **B.** Expression of HIS-KSI-HBD2 in pET-28/HisKSI. 12 % Bis-Tris acrylamide gel analysis before and after induction with IPTG. Lane M, SeeBlue 2 protein marker (Invitrogen); lane 1, total bacterial lysate before induction; lane 2 insoluble fraction after induction (His-KSI-HBD2, Mr 20.2 kDa).
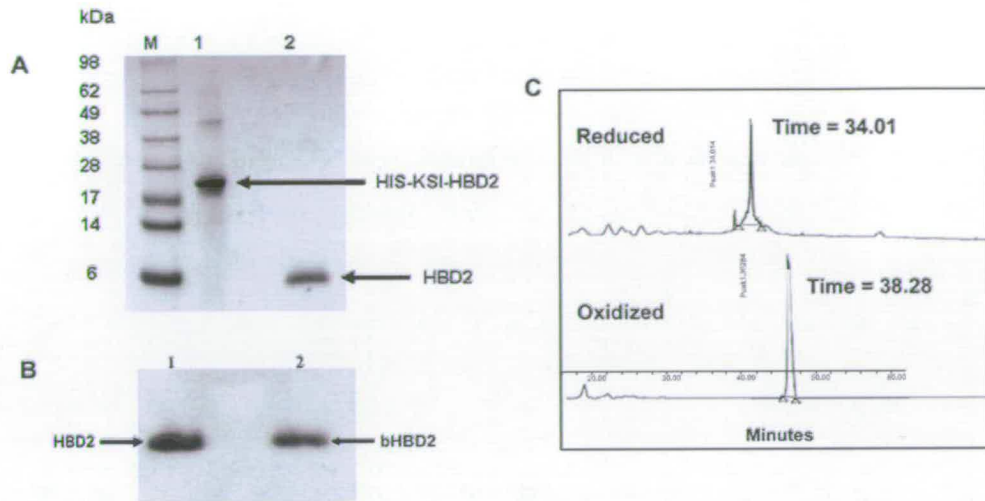
Figure 3. Purification of recombinant HBD2 **A.** 12 % Bis-Tris acrylamide gel analysis of HIS-KSI-HBD2 fusion (lane 1) and recovered, soluble HBD2 after CNBr cleavage (lane 2) (M, SeeBlue 2 marker (Invitrogen)). **B.** Western blot of oxidized HBD2 probed with anti-HBD2 antibody (Lane 1, Oxidised HBD2 (2.5 µg); lane 2, Synthetic biotinylated bHBD2 (1 µg)). **C.** Reverse-phase HPLC chromatograms of reduced HBD2 (upper trace, ~34 mins) and oxidized HBD2 (lower trace, ~38 mins).

cysteine/cystine redox buffer. The fully oxidized form has a longer retention time (~4 minutes) compared to the reduced form (Fig. **3C**) in agreement with previously published data [44]. This peptide was reactive in a Western blot assay with anti-HBD2 antibody that confirms the identity of the purified HBD2 (Fig. **3B**). High resolution FT-ICR mass spectrometry was used to determine the accurate mass of HBD2 and confirm its oxidation state. The HBD2 ionized efficiently displaying three charge states [$(M+3H)^{3+}$, $(M+4H)^{4+}$ and $(M+5H)^{5+}$) and the isotopic distribution for the +4 charge state and mass fit to those predicted for fully oxidised HBD2 with an elemental composition ($C_{188}H_{305}N_{55}O_{50}S_6$) and average mass of 4328.23 Da (Fig. **4**). After purification and freeze drying, ~3-6 mg of fully oxidised β-HBD2 was obtained. The 1D ^{1}H NMR spectrum shows sharp, well-dispersed peaks in the amide region, which is indicative of a folded structure (Fig. **5**). Furthermore, it was important to carry out trypsin/chymotrypsin digest and Edman degradation analysis which showed that the peptide displayed the β-defensin (1-5, 2-4, 3-6) connectivity (data not shown).

Antimicrobial and Chemotactic Activity of Recombinant HBD2

Fully oxidised HBD2 was dissolved in 0.01% acetic acid and the sample was concentrated to 500 µg/mL for the assay. We analysed the activity of the fully oxidised HBD2 against *E. coli* K-12 MG1655, *P. aeruginosa* PAO1, *S. aureus* ATCC 25923 and *C. albicans* J2922 using a previously published assay [25,40,45]. Values of LD_{50}, LD_{90} and $MBC_{99.99}$ values against 1 x 10^5 cells were determined (Table **2**). HBD2 was found to be effective in killing Gram-negative bacteria (*E. coli* and *P. aeruginosa*) and yeast *C. albicans* in the µM range, but showed a lower bactericidal effect toward Gram-positive *S. aureus*. These results are in good agreement with that of the natural sample[23], the recombinant HBD2 preparations from other groups [29,46] and peptide prepared by solid-phase peptide synthesis [47] (Table **2**).
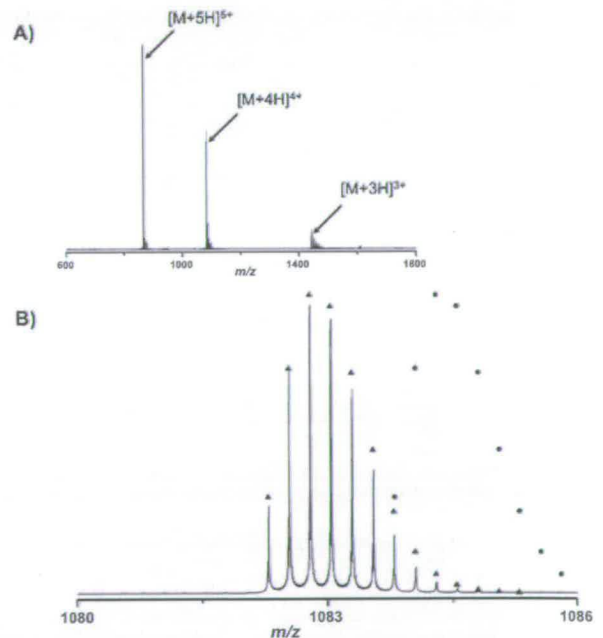

Figure 4. FT-ICR high resolution mass spectrometry analysis of recombinant HBD2. **A.** The ion envelope for nanospray FT-ICR analysis of oxidized HBD2 showing the +5 to +3 charge states. **B.** The isotopic envelope of the +4 charge state of oxidized HBD2. Closed circles represent the theoretical envelope expected from a HBD2 monomer with all cysteines reduced and the closed triangles represent that expected from a fully oxidized HBD2 with 3 S-S bonds.
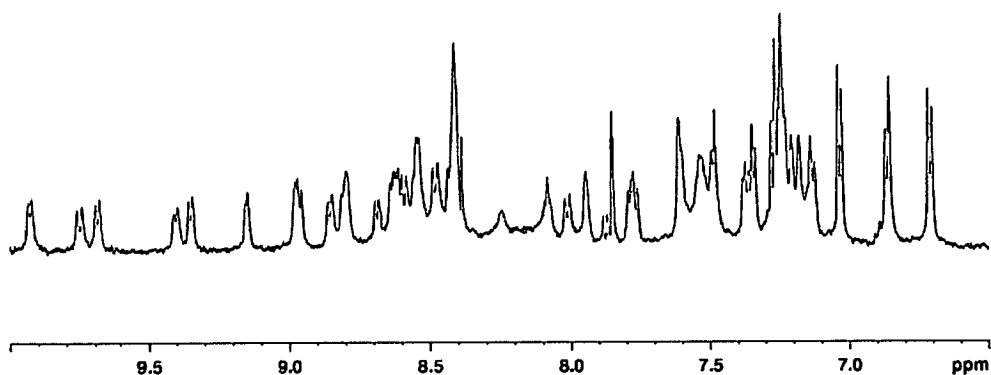
Figure 5. 1D ^{1}H NMR spectrum of oxidized HBD2 in 20 mM sodium acetate buffer pH 4.0 and 10 % D_2O on a Bruker AVANCE spectrometer equipped with a cryoprobe operating at 600MHz and 25 °C. Only the amide proton region is shown for clarity.

Table 2. Comparison of Antimicrobial Activity of HBD2 with Previous Studies (Values are in μg/mL, PMB: Polymyxin B as Control AMP)

Strain	Source	MBC$_{99.99}$[a]/MIC[b]	LD90[c]	LD50[d]
E. coli K12-MG1655	This paper	MBC$_{99.99}$<20 [a] (<1.5[a], PMB)	3-6	<1.5
E. coli ML-35	47	17 [b]		
E. coli	23		~10	
E. coli ML35p	29		4.25-12.25[f]	
P. aeruginosa PAO1	This paper	<25[a] (<1.5[a], PMB)	<3	<1.5
P. aeruginosa ATCC 27853	47	17[b]		
P. aeruginosa	23		~10	
P. aeruginosa ATCC 9027	29		4.25-12.25[f]	
C. albicans J2922	This paper	>50[a] (<3[a], PMB)	>6	>1.5
C. albicans	47	70[b]		
C. albicans	23		25	
C. albicans 820	29		4.25-12.25[f]	
S. aureus ATCC 25923	This paper	>50[a] (6[a], PMB)	>12	>3
S. aureus 710A	47	35-70[b]		
S. aureus	23	100[e]		
S. aureus ATCC 6341	29	N.D.[e]		

[a] MBC$_{99.99}$ values are the minimum concentration of peptide required to kill 99.99% of initial inoculum.
[b] MIC values are the lowest concentration of peptide that will inhibit the visible growth of a microorganism.
[c] LD90 values are the concentration of peptide required to kill 90% of initial inoculum.
[d] LD50 values are the concentration required to kill 50% of initial inoculum.
[e] Bacteriostatic effect.
[f] Bactericidal effect.

Yang and colleagues discovered that many defensins are potent chemotactic agents against a range of cells from the mammalian immune system including dendritic cells and T cells [26]. The exact nature of the molecular interactions between HBD2 and the CCR6 receptor are presently unknown but a recent analysis of HBD1/CCR6 has begun to explore the residues involved [22]. It was shown that HBD2 was active in chemotaxis assays against CCR6, a GPCR previously been shown to be activated by the chemokine CCL20 (MIP3-α). We tested our recombinant HBD2 against HEK 293 cells expressing CCR6 in an assay we have used in our laboratory [25] and found that it had optimal activity at 100 ng/ml (Fig. 6).

CONCLUSION

The method described in this paper is straight forward and low-cost, allowing for the production of milligram amounts of β-defensin HBD2 in a commonly-used *E. coli* host. The mature form of HBD2 was isolated as a single, homogenous, oxidized isoform with β-defensin S-S bond connectivity. This HBD2 was an active chemokine for cells expressing the GPCR receptor CCR6 and a potent antimicrobial peptide against a range of microbes. It displayed excellent structural properties (NMR spectroscopy and high resolution mass spectrometry) and is suitable for future analysis of HBD2 in complex with a range of biological tar-

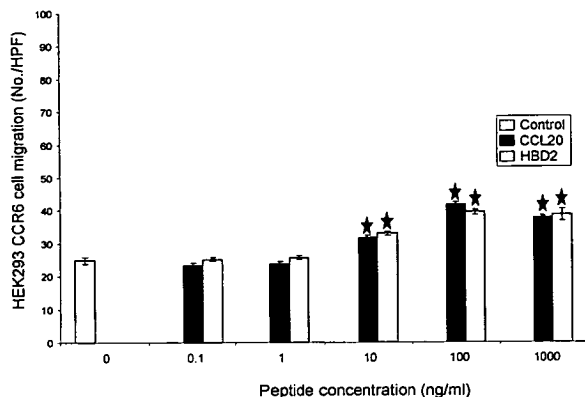gets. The expression clone is also suitable for generation of a range of mutant defensins.

Figure 6. Chemotactic activity of HBD2. The graph shows the number of HEK293 cells expressing the human chemokine receptor CCR6 that migrate towards the peptides. The number of cells per high power field (No./HPF) under the microscope is given. Chemotaxis medium is the control, CCL20 (also known as MIP-3α) is the known chemokine ligand of CCR6. Each assay was repeated three times, numerical data are means ± S.D. and columns with an asterisk indicate peptide with significant activity ($p<0.05$) above culture medium.

ACKNOWLEDGEMENTS

REFERENCES

[1]　Zasloff, M. Antimicrobial peptides of multicellular organisms. *Nature*, 2002, *415*, 389-395.

[2]　Crovella, S.; Antcheva, N.; Zelezetsky, I.; Boniotto, M.; Pacor, S.; Verga, F.M.V.; Tossi, A. Primate beta-defensins--structure, function and evolution. *Curr. Protein Pept. Sci.*, 2005, *6*, 7-21.

[3]　Ganz, T. Defensins: antimicrobial peptides of innate immunity. *Nat. Rev. Immunol.*, 2003, *3*, 710-720.

[4]　Lehrer, R.I. Primate defensins. *Nat. Rev. Microbiol.*, 2004, *2*, 727-738.

[5]　Pazgier, M.; Hoover, D.M.; Yang, D.; Lu, W. Lubkowski, J. Human beta-defensins. *Cell. Mol. Life Sci.*, 2006, *63*, 1294-1313.

[6]　Selsted, M.E.; Ouellette, A.J. Mammalian defensins in the antimicrobial immune response. *Nat. Immunol.*, 2005, *6*, 551-557.

[7]　Ganz, T.; Selsted, M.E.; Szklarek, D.; Harwig, S.S.L.; Daher, K.; Bainton, D.F.; Lehrer, R.I. Defensins. Natural peptide antibiotics of human neutrophils. *J. Clin. Invest.*, 1985, *76*, 1427-1435.

[8]　Schutte, B.C.; Mitros, J.P.; Bartlett, J.A.; Walters, J.D.; Jia, H.P.; Welsh, M.J.; Casavant, T.L.; McCray, P.B.; Jr. Discovery of five conserved beta -defensin gene clusters using a computational search strategy. *Proc. Natl Acad. Sci. USA*, 2002, *99*, 2129-2133.

[9]　Patil, A.; Hughes, A.L.; Zhang, G. Rapid evolution and diversification of mammalian a-defensins as revealed by comparative analysis of rodent and primate genes. *Physiol. Genomics*, 2004, *20*, 1-11.

[10]　de Leeuw, E.; Burks, S.R.; Li, X.; Kao, J.P.Y. Lu, W. Structure-dependent functional properties of human defensin 5. *FEBS Letters*, 2007, *581*, 515-520.

[11]　Lehrer, R.I.; Selsted, M.E.; Szklarek, D. Fleischmann, J. Antibacterial activity of microbicidal cationic proteins 1 and 2, natural peptide antibiotics of rabbit lung macrophages. *Infect. Immun.*, 1983, *42*, 10-14.

[12]　Szyk, A.; Wu, Z.; Tucker, K.; Yang, D.; Lu, W.; Lubkowski, J. Crystal structures of human a-defensins HNP4, HD5, and HD6. *Protein Sci.*, 2006, *15*, 2749-2760.

[13]　Wu, Z.; Ericksen, B.; Tucker, K.; Lubkowski, J.; Lu, W. Synthesis and characterization of human a-defensins 4-6. *J. Peptide Res.*, 2004, *64*, 118-125.

[14]　Yang, D.; Chen, Q.; Chertov, O.; Oppenheim, J.J. Human neutrophil defensins selectively chemoattract naive T and immature dendritic cells. *J. Leukoc. Biol.*, 2000, *68*, 9-14.

[15]　Bauer, F.; Schweimer, K.; Kluver, E.; Conejo-Garcia, J.R.; Forssmann, W.G.; Rosch, P.; Adermann, K.; Sticht, H. Structure determination of human and murine beta-defensins reveals structural conservation in the absence of significant sequence similarity. *Protein Sci.*, 2001, *10*, 2470-2479.

[16]　Hoover, D.M.; Chertov, O.; Lubkowski, J. The structure of human beta-defensin-1: new insights into structural properties of beta-defensins. *J. Biol. Chem.*, 2001, *276*, 39021-39026.

[17]　Hoover, D.M.; Rajashankar, K.R.; Blumenthal, R.; Puri, A.; Oppenheim, J.J.; Chertov, O.; Lubkowski, J. The structure of human beta-defensin-2 shows evidence of higher order oligomerization. *J. Biol. Chem.*, 2000, *275*, 32911-32918.

[18]　Landon, C.; Thouzeau, C.; Labbe, H.; Bulet, P.; Vovelle, F. Solution structure of spheniscin, a beta-defensin from the penguin stomach. *J. Biol. Chem.*, 2004, *279*, 30433-30439.

[19]　Sawai, M.V.; Jia, H.P.; Liu, L.; Aseyev, V.; Wiencek, J.M.; McCray, P.B., Jr.; Ganz, T.; Kearney, W.R.; Tack, B.F. The NMR structure of human beta-defensin-2 reveals a novel alpha-helical segment. *Biochemistry*, 2001, *40*, 3810-3816.

[20]　Schibli, D.J.; Hunter, H.N.; Aseyev, V.; Starner, T.D.; Wiencek, J.M.; McCray, P.B., Jr.; Tack, B.F.; Vogel, H.J. The solution structures of the human beta-defensins lead to a better understanding of the potent bactericidal activity of HBD3 against Staphylococcus aureus. *J. Biol. Chem.*, 2002, *277*, 8279-8289.

[21]　Zimmermann, G.R.; Legault, P.; Selsted, M.E.; Pardi, A. Solution structure of bovine neutrophil beta-defensin-12: the peptide fold of the beta-defensins is identical to that of the classical defensins. *Biochemistry*, 1995, *34*, 13663-13671.

[22]　Pazgier, M.; Prahl, A.; Hoover, D.M.; Lubkowski, J. Studies of the biological properties of human b-defensin 1. *J. Biol. Chem.*, 2007, *282*, 1819-1829.

[23]　Harder, J.; Bartels, J.; Christophers, J.; Schroder, J.M. A peptide antibiotic from human skin. *Nature*, 1997, *387*, 861.

[24]　Shai, Y. Mode of action of membrane active antimicrobial peptides. *Biopolymers*, 2002, *66*, 236-248.

[25]　Taylor, K.; Clarke, D.J.; McCullough, B.; Chin, W.; Seo, E.; Yand, D.; Oppenheim, J.J.; Uhrin, D.; Govan, J.R.W.; Campopiano, D.J.; MacMillan, D.; Barran, P.; Dorin, J.R. Analysis and separation of residues important for the chemoattractant and antimicrobial activities of beta-defensin 3. *J. Biol. Chem.*, 2008, *283*, 6631-6639.

[26]　Yang, D.; Chertov, O.; Bykovskaia, S.; Chen, Q.; Buffo, M.; Shogan, J.; Anderson, M.; Schroder, J.; Wang, J.; Howard, O.; Oppenheim, J. Beta-defensins: linking innate and adaptive immunity through dendritic and T cell CCR6. *Science*, 1999, *286*, 525-528.

[27]　Raj, P.A.; Antonyraj, K.J.; Karunakaran, T. Large-scale synthesis and functional elements for the antimicrobial activity of defensins. *Biochem. J.*, 2000, *347 Pt 3*, 633-641.

[28]　Kluver, E.; Adermann, K.; Schulz, A. Synthesis and structure-activity relationship of b-defensins, multi-functional peptides of the immune system. *J. Pept. Sci.*, 2006, *12*, 243-257.

[29]　Liu, A.Y.; Destoumieux, D.; Wong, A.; Park, C.H.; Valore, E.V.; Liu, L.; Ganz, T. Human b-defensin-2 production in keratinocytes is regulated by interleukin-1, bacteria, and the state of differentiation. *J. Invest. Dermatol.*, 2002, *118*, 275-281.

[30]　Porter, E.M.; van Dam, E.; Valore, E.V.; Ganz, T. Broad-spectrum antimicrobial activity of human intestinal defensin 5. *Infect. Immun.*, 1997, *65*, 2396-2401.

[31]　Valore, E.V.; Martin, E.; Harwig, S.S.; Ganz, T. Intramolecular inhibition of human defensin HNP-1 by its propiece. *J. Clin. Invest.*, 1996, *97*, 1624-1629.

[32]　Valore, E.V.; Park, C.H.; Quayle, A.J.; Wiles, K.R.; McCray Jr., P.B.; Ganz, T. Human b-Defensin-1: an antimicrobial peptide of urogenital tissues. *J. Clin. Invest.*, 1998, *101*, 1633-1642.

[33]   Fang, X.; Peng, L.; Xu, Z.; Wu, J.; Cen, P. Cloning and expression of human beta-defensin-2 gene in *Escherichia coli. Protein Pept. Lett.*, **2002**, *9*, 31-37.

[34]   Pazgier, M.; Lubkowski, J. Expression and purification of recombinant human a-defensins in *Escherichia coli. Protein Expr. Purif.*, **2006**, *49*, 1-8.

[35]   Xu, Z.; Peng, L.; Zhong, Z.; Fang, X.; Cen, P. High-level expression of a soluble functional antimicrobial peptide, human beta-defensin 2, in *Escherichia coli. Biotechnol. Prog.*, **2006**, *22*, 382-386.

[36]   Zhong, Z.; Xu, Z.; Peng, L.; Huang, L.; Fang, X.; Cen, P. Tandem repeat mhBD2 gene enhance the soluble fusion expression of hBD2 in *Escherichia coli. Appl. Microbiol. Biotechnol.*, **2006**, *71*, 661-667.

[37]   Chen, H.; Xu, Z.; Xu, N.; Cen, P. Efficient production of a soluble fusion protein containing human beta-defensin-2 in *E. coli* cell-free system. *J. Biotechnol.*, **2005**, *115*, 307-315.

[38]   Cipakova, I.; Hostinova, E. Production of the human-beta-defensin using *Saccharomyces cerevisiae* as a host. *Protein Pept. Lett.*, **2005**, *12*, 551-554.

[39]   Boniotto, M.; Antcheva, N.; Zelezetsky, I.; Tossi, A.; Palumbo, V.; Verga, F.M.V.; Sgubin, S.; Braida, L.; Amoroso, A. Crovella, S. A study of host defence peptide b-defensin 3 in primates. *Biochem. J.*, **2003**, *374*, 707-714.

[40]   Campopiano, D.J.; Clarke, D.J.; Polfer, N.C.; Barran, P.E.; Langley, R.J.; Govan, J.R.; Maxwell, A.; Dorin, J.R. Structure-activity relationships in defensin dimers: a novel link between beta-defensin tertiary structure and antimicrobial activity. *J. Biol. Chem.*, **2004**, *279*, 48671-48679.

[41]   Clarke, D.J.; Campopiano, D.J. Structural and functional studies of defensin-inspired peptides. *Biochem. Soc. Trans.*, **2006**, *34*, 251-256.

[42]   Maemoto, A.; Qu, X.; Rosengren, K.J.; Tanabe, H.; Henschen-Edman, A.; Craik, D.J. Ouellette, A.J. Functional analysis of the a-defensin disulfide array in mouse cryptdin-4. *J. Biol. Chem.*, **2004**, *279*, 44188-44196.

[43]   Stemmer, W.P.; Crameri, A.; Ha, K.D.; Brennan, T.M.; Heyneker, H.L. Single-step assembly of a gene and entire plasmid from large numbers of oligodeoxyribonucleotides. *Gene*, **1995**, *164*, 49-53.

[44]   Wu, Z.; Hoover, D.M.; Yang, D.; Boulegue, C.; Santamaria, F.; Oppenheim, J.J.; Lubkowski, J.; Lu, W. Engineering disulfide bridges to dissect antimicrobial and chemotactic activities of human beta-defensin 3. *Proc. Natl Acad. Sci. USA*, **2003**, *100*, 8880-8885.

[45]   Taylor, K.; McCullough, B.; Clarke, D.J.; Langley, R.J.; Pechenick, T.; Hill, A.; Campopiano, D.J.; Barran, P.E.; Dorin, J.R.; Govan, J.R. Covalent dimer species of beta-defensin Defr1 display potent antimicrobial activity against multidrug-resistant bacterial pathogens. *Antimicrobiol. Agents Chemother.*, **2007**, *51*, 1719-1724.

[46]   Feng, Z.; Jiang, B.; Chandra, J.; Ghannoum, M.; Nelson, S.; Weinberg, A. Human beta-defensins: differential activity against candidal species and regulation by *Candida albicans. J. Dent. Res.*, **2005**, *84*, 445-450.

[47]   Antcheva, N.; Boniotto, M.; Zelezetsky, I.; Pacor, S.; Verga Falzacappa, M.V.; Crovella, S. Tossi, A. Effects of positively selected sequence variations in human and *Macaca fascicularis* beta-defensins 2 on antimicrobial activity. *Antimicrob. Agents Chemother.*, **2004**, *48*, 685-688.